Contract No:

This document was prepared in conjunction with work accomplished under Contract No. DE-AC09-08SR22470 with the U.S. Department of Energy (DOE) Office of Environmental Management (EM).

Disclaimer:

Savannah River National Laboratory™

OPERATED BY SAVANNAH RIVER NUCLEAR SOLUTIONS

Savannah River National Laboratory

2016 LDRD

Laboratory Directed Research and Development Program

Environmental Stewardship and Nuclear Materials Management

Non-Proliferation and Nuclear Deterrent

Clean Energy

ANNUAL REPORT

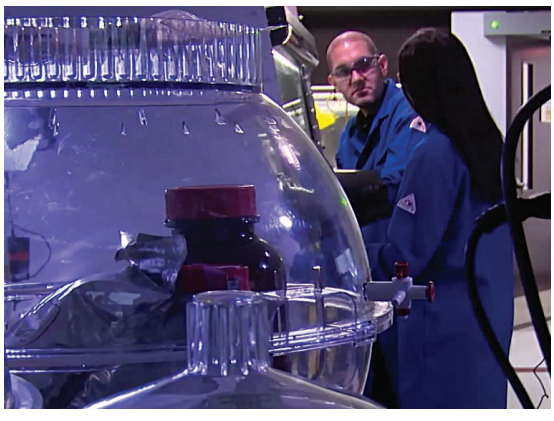

DISCLAIMER:

"This report was prepared by Savannah River Nuclear Solutions, LLC (SRNS) for the United States Department of Energy under Contract No. DE-AC09-08SR22470 and is an account of work performed under that contract. Neither the United States Government nor any agency thereof, nor any of their employees, not any of their contractors, subcontractors or their employees assume any legal liability or responsibility for any third party's use of the results of such use of any information, apparatus, product, or process disclosed, or represent that its use would not infringe privately owned rights. Reference herein to any specific commercial product, process or services by trademark, name, manufacturer or otherwise does not necessarily constitute or imply endorsement recommendation, or favoring of same by SRNS or the United States Government or any agency thereof."

SRNL-MS-2017-00048

Table of Contents

Message
From the Laboratory Director

An innovative and effective Laboratory Directed Research and Development (LDRD) program is the lifeblood of a National Laboratory, positioning it for future growth in key mission areas. For Savannah River National Laboratory (SRNL), the LDRD program provides an avenue for early exploration and exploitation of creative ideas that will enhance the ability of the lab to support the critical DOE missions in environmental stewardship, national security, clean energy, and nuclear materials management.

Additionally, LDRD activities sustain staff excellence by providing the opportunity to nurture existing and grow emerging core competencies. The LDRD program also provides an avenue to forge strategic partnerships with not only other national labs, but also universities and commercial companies. SRNL's university partnerships are especially valuable as they not only allow for fruitful collaborations, but also allow us to connect with the next generation of scientists and engineers as students and post-doctoral researchers working on cutting-edge R&D programs. I am enthusiastic about the growth and opportunities that the SRNL LDRD program is creating for the laboratory and the nation. The program continues to demonstrate advancements in the scientific underpinnings that reveal the quality of SRNL's research and open new doors for technology deployment.

This report reflects the execution of our LDRD program within the objectives and guidelines outlined by the DOE through the DOE Order 413.2C. The projects described herein reflect the innovation required to fulfill SRNL's strategic vision and program plans, and they provide great value to the DOE and the nation. The diversity exhibited in the research and development projects underscores the DOE Office of Environmental Management (DOE-EM) mission and enhances that mission by developing the technical capabilities and human capital necessary to support future DOE-EM national needs.

On behalf of the SRNL Senior Management team, I would like to congratulate those members of the SRNL staff, and their collaborators, for their accomplishments and the quality of their work. Their efforts create a product that continues to be a critical mechanism to demonstrate the importance of SRNL's competencies to the nation. ■

Dr. Terry A. Michalske
Laboratory Director
Savannah River National Laboratory

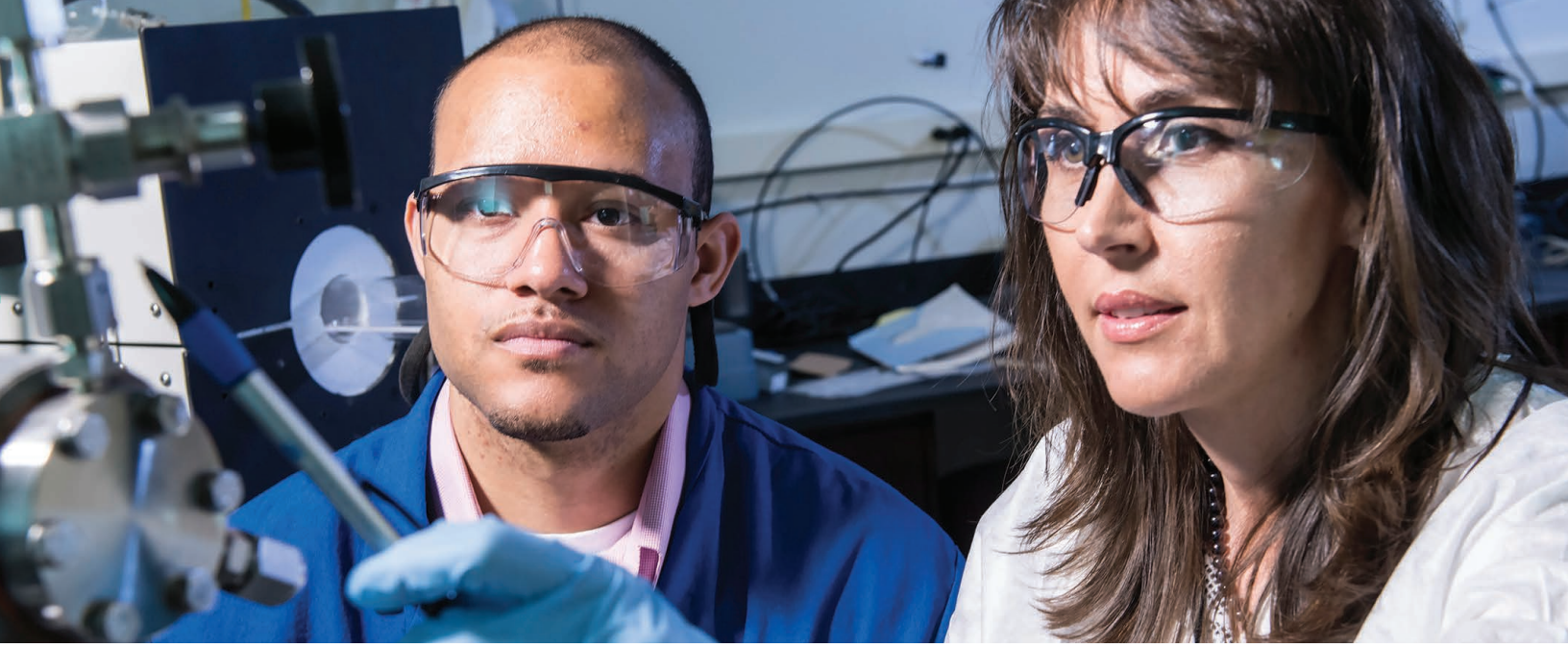

2016 Overview

Laboratory Directed Research and Development Program

Savannah River National Laboratory's (SRNL) Laboratory Directed Research and Development (LDRD) program is focused on advancing the technical capabilities needed for the future success of the Department of Energy's (DOE) critical missions for environmental stewardship, national security, clean energy, and nuclear materials management. As the only discretionary funding available to SRNL, the LDRD program enables programmatic growth through early exploration and exploitation of creative ideas that will enhance SRNL's ability to execute current and future strategic initiatives and to sustain staff excellence via involvement of post-doctoral and student researchers, as well as strategic hires. The LDRD program leverages the unique capabilities of SRNL to yield foundational scientific research and development (R&D) essential to our core business areas, while aligning optimally and continuously with SRNL's Strategic Plan and providing long-term benefits to DOE and the National Nuclear Security Administration (NNSA), other customers, and stakeholders.

The LDRD program also fosters new science and technology ideas that will nurture cross-cutting core competencies and discipline-level capabilities deemed critical to supporting SRNL's emerging priorities and transforming technologies to meet customers' mission requirements. SRNL's four Core Competencies are (1) Environmental Remediation and Risk Reduction; (2) Tritium Processing, Storage, and Transfer Systems; (3) Nuclear Materials Processing and Disposition; and (4) Nuclear Materials Detection, Characterization and Assessment.

The FY16 LDRD Program included focus areas in each of our three main business areas. Specific focus areas were as follows:

Nuclear Materials Management and Environmental Stewardship: Unique concepts that lead to new approaches and options for critical EM risk reduction challenges and also reduce the life cycle in processing high activity liquid waste and nuclear materials, remediating contaminated soil, groundwater and facilities, as well as validating long-term remediation strategies.

Non-Proliferation and Nuclear Deterrent: Unique concepts that address national security mission area needs that are currently underserved by the DOE Lab system. Game-changing innovations and tools that advance the national security agenda for the United States Government, including monitoring, nonproliferation, and deterrence.

Clean Energy: Advanced research in the development, demonstration, and deployment of clean energy technologies; innovative technologies to assure the future utilization of clean, reliable energy that dramatically improves the energy efficiency of industrial, manufacturing, transportation, and/or building technologies, and strengthens SRNL's Core Capabilities.

By The Numbers

$7.5 M
TOTAL PROGRAM COST

34
TOTAL NUMBER OF PROJECTS

220 K
AVERAGE PROJECT COST

FY2016 LDRD Metrics

FY 16 Scientific Productivity:

Research efforts supported by the LDRD program led to securing intellectual property and peer reviewed publications.

- **7** Invention Disclosures Were Submitted During FY16
- **2** Patents Being Granted Related to Prior Year LDRD Efforts
- **7** Publications In Peer Reviewed Journals

Post-Doctoral and Student Involvement:

13 Post-doctoral Researchers were members of **11** LDRD supported Research Teams

12 Researchers Performed Research at SRNL

This represents half of all SRNL post-docs being supported by LDRD projects

16 Graduate

8 Undergraduate

Students who performed research, both on and off-site for LDRD projects

Sustaining Staff Excellence

4 New hires in FY16 were attributed to the LDRD program

10% Percent of hours charged to LDRD projects in FY16 were by new staff (< 2 years of service)

59% Percent of FY16 projects involved post-docs or early career professionals (terminal degree within the past 10 years)

39% Percent of the FY16 projects were led by early career staff (terminal degree within the past 10 years)

2016 Total Collaborations: 25

This includes 10 different universities, 2 companies and 1 national lab.

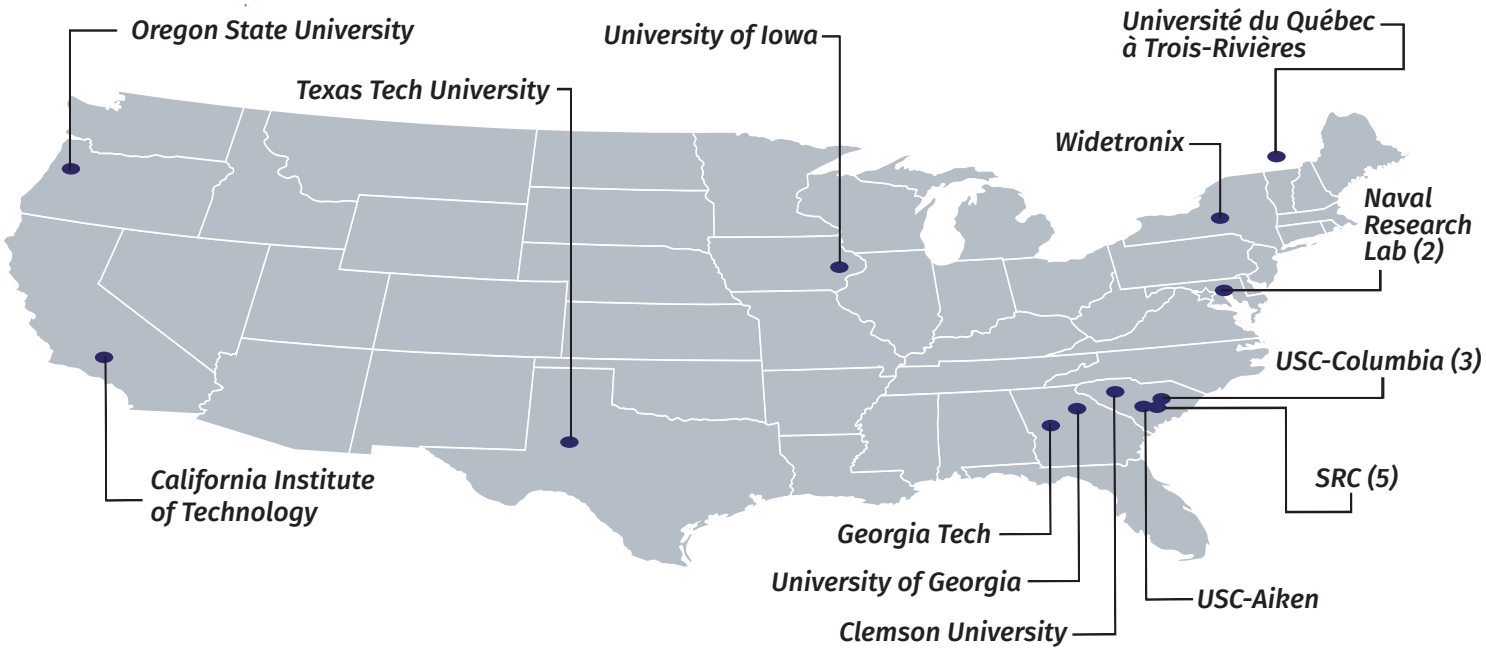

Environmental Stewardship and Nuclear Materials Management

Smart Manufacturing: Replacing Analytical Sample Control with Model Predictive Control

Project Team: M.B. Gorensek (Primary), D.P. Lambert, T.B. Edwards, and M. Luther (Summer Intern)
Subcontractor: C.-C. Chen (Texas Tech University)
Thrust Area: Smart Manufacturing
Project Type: Standard (continuation of FY2015 project extension)
Project Start Date: February 11, 2014
Project End Date: September 30, 2016

Liquid waste operations at SRS rely on sampling and analysis for product quality control, dictating long wait times and round-the-clock analytical staffing. We are building a detailed model of Sludge Receipt and Adjustment Tank (SRAT) and Slurry Mix Evaporator (SME) operations that could be used instead of sampling and analysis to control Defense Waste Processing Facility (DWPF) operations. Since the model's predictions need to be at least as reliable as the analyses it is intended to replace, we have teamed with a world-class electrolyte properties expert to equip it with a new electrolyte-NRTL properties package that accurately and efficiently simulates sludge properties. Our team also includes one of the DWPF Product Composition and Control System (PCCS) developers who knows the uncertainties in the sludge sample analyses and their impact on product quality requirements. The work to date has focused on demonstrating this capability with bench scale sludge simulant experiments.

FY2016 OBJECTIVES

- Finish adding glycolic acid flowsheet process chemistry to the formic acid flowsheet electrolyte-NRTL properties package
- Build dynamic model of lab-scale SRAT/SME sludge batch simulant experiments for the glycolic acid flowsheet
- Demonstrate uncertainty of predicted sludge batch compositions equal to or less than those of sample analyses
- Quantify potential cost savings for DWPF due to reduced analytical support requirement and accelerated production schedule

INTRODUCTION

Nuclear materials processes across the DOE complex use traditional analytical sample control, relying on hold points at critical steps to verify by analysis that composition/properties meet product acceptability criteria. Waiting for analyses accounts for much of the processing time. Analyses also add cost and require round-the-clock laboratory staffing. We see radiochemical processes of the future as highly automated systems that take advantage of SM concepts, using advanced automation, process control, and information technology to optimize performance.

We are developing a model of the DWPF sludge treatment process that provides material balances with sufficient detail to replace analytical sampling hold points. This includes an electrolyte properties model tailored to DWPF compositions, capturing only those components needed for process control. The model is robust and should be fast enough to serve as the basis for a truly predictive control system. The immediate significance is that this has the potential to reduce batch processing times up to 40%, increasing DWPF capacity by up to 67%. Fewer analyses would be needed, and could be scheduled during normal working hours (as confirmation), reducing analytical costs and staffing needs. Finally, this represents a first step toward implementation of SM concepts at SRS, leading the way toward similar improvements in other SRS facilities.

When fully implemented, SM will have the potential to allow global optimization of SRS operations, enabling rapid, effective response to any changes in manufacturing conditions (e.g., funding, mission, staffing, priorities, etc.). This requires good real-time models of SRS processes. SRNL has the opportunity to establish technical leadership in SM since it has direct access to actual nuclear waste operations and the requisite modeling expertise. The significant cost savings that could be demonstrated by application of this technology to DWPF operations should open up other funding opportunities.

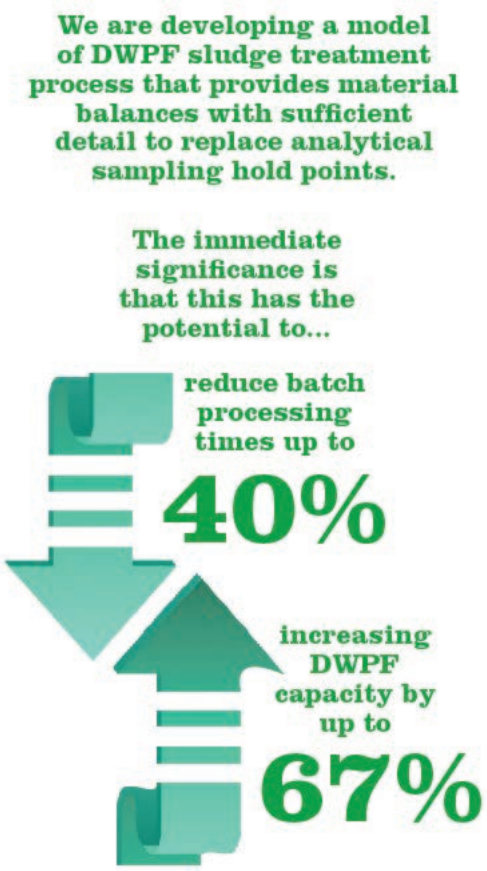

APPROACH

The main focus of the project was the SRAT/SME process model. The plan is to demonstrate that this method can be used to predict the results of lab-scale SRAT/SME simulant runs with equal or better confidence than analytical measurements, first for the formic acid flowsheet, and then for the glycolic acid flowsheet.

A major thrust of the project was to custom fit (to all available data) electrolyte-NRTL properties packages (speciation and parameter sets) for use with the Aspen Plus™ properties model to simulate sludge processing streams. This gives phase equilibrium and energy balance calculations the kind of accuracy that is essential if the process model will ever replace grab sampling and analysis. Prof. Chau-Chyun Chen of Texas Tech University (TTU), the author of the Chen electrolyte-NRTL properties model had primary responsibility for this aspect of the project. The work had two parts: the first, completed in FY 2014, was a properties package for the formic acid flowsheet model, while the second, originally slated for FY 2015 but deferred to FY 2016, was an expanded package for the glycolic acid flowsheet model that takes into account the more complicated chemistry of glycolic acid in sludge streams. After agreement was reached on which components needed to be included in the properties packages, Prof. Chen and his graduate students at TTU were to search for available data, establish relevant speciation, and regress the requisite pure component property and binary interaction parameters. The final product in both cases was to be a complete properties package that could be imported into an aspenONE® simulation file along with a report describing the package in detail and demonstrating the properties models' fit to the available data.

The main focus of the project was on the SRAT/SME process model. The initial intent was to build a dynamic process model in Aspen Custom Modeler (ACM). However, the process chemistry includes reactions that yield gaseous products, making it necessary to use true compositions instead of apparent components, which ACM cannot easily accommodate. After trying unsuccessfully (in FY 2015) to build a dynamic model in ACM using the true composition basis, the decision was made to switch to a pseudo-dynamic Aspen Plus™ model in which time intervals are simulated as consecutive steady-state operations. Figure 1 shows the first three steps in the Aspen Plus™ simulation of a lab-scale experiment with sludge batch simulant SB6-H (Flowsheet Development Run GF-21). The plan is to demonstrate that this method can be used to predict the results of lab-scale SRAT/SME simulant runs with equal or better confidence than analytical measurements, first for the formic acid flowsheet, and then for the glycolic acid flowsheet.

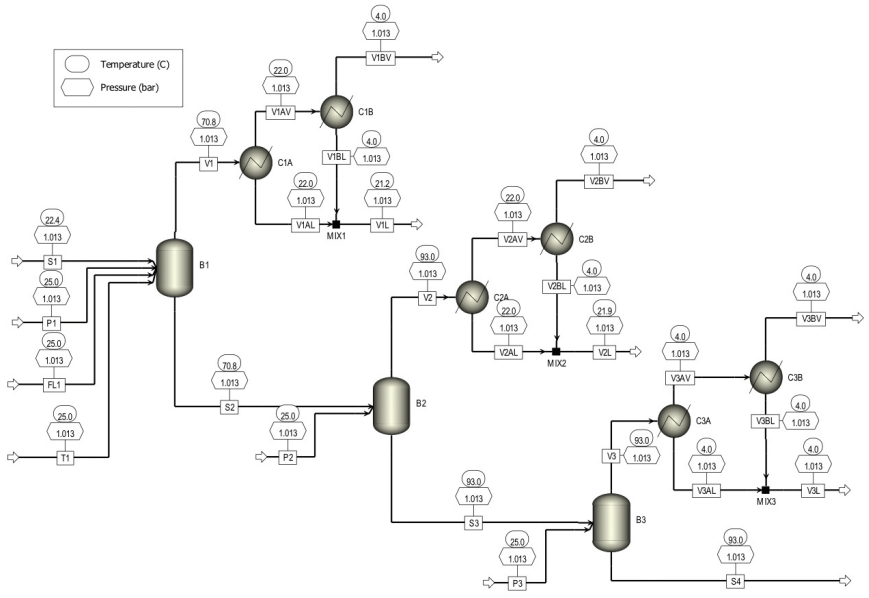

Figure 1. Excerpt (first three time steps) from Aspen Plus™ flowsheet model used to simulate bench scale SRAT/SME tests with sludge batch simulant

RESULTS / DISCUSSION

The major effort in FY 2016 was on completing the addition of glycolic acid chemistry to the properties model and on completing and validating the SRAT/SME process model. The originally planned dynamic ACM model had been abandoned in FY 2015 in favor of a less elegant yet effective "pseudo-dynamic" Aspen Plus™ model, which treats time intervals as consecutive steady-state operations. Figure 2 compares the results of an Aspen Plus simulation of Flowsheet Development Run GF-21 using sludge batch simulant SB6-H. As can be seen from the plot, the match between experimental data and the model is good for most variables.

Figure 2. Comparison between results of Aspen Plus™ simulation of Flowsheet Development Run GF-21 for sludge batch simulant SB6-H with experimental data

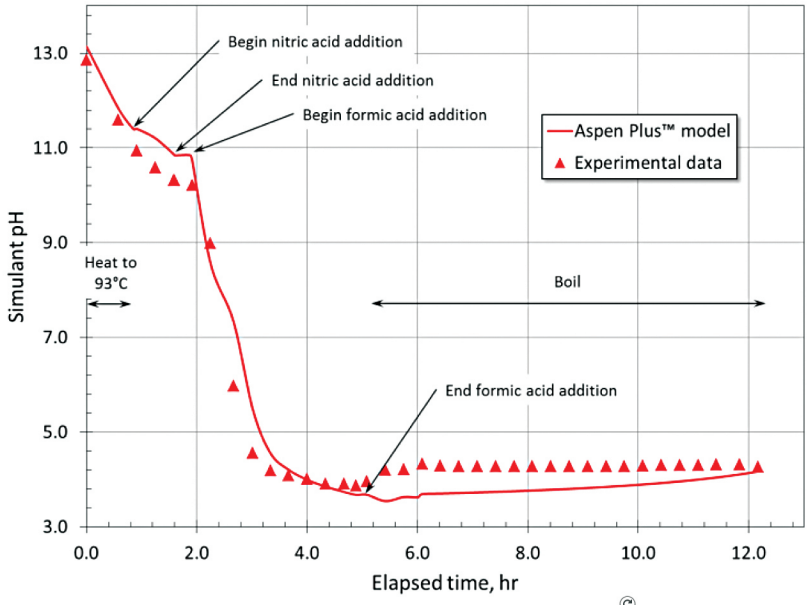

The formic acid flowsheet properties package completed in FY 2015 was revised to account for glycolic acid chemistry. It now includes solubility equilibria for $Al(OH)_3$, $Ca(OH)_2$, $Fe(OH)_3$, $Mn(OH)_2$, $Mg(OH)_2$, and $Ni(OH)_2$, as well as interaction parameters for the water-glycolic acid and water-sodium glycolate binaries.

Flowsheet Development Run GN-74 using sludge batch simulant SB8 was selected as the test case for the glycolic acid flowsheet model. Progress on this model was impeded by unplanned absence of the PI, who was on leave for nearly the entire 4th quarter of FY 2016. A summer intern was available to work on the flowsheet model for several weeks instead. While the intern was not able to finish the model, enough progress was made to show that this approach should work. Figure 3 compares the results of an Aspen Plus simulation of the first few hours of Run GN-74 with experimental data. The calculated CO_2 evolution rate is similar to that measured by the gas chromatograph.

Figure 3. Comparison between results of Aspen Plus™ simulation of Flowsheet Development Run GN-74 for sludge batch simulant SB8 with experimental data

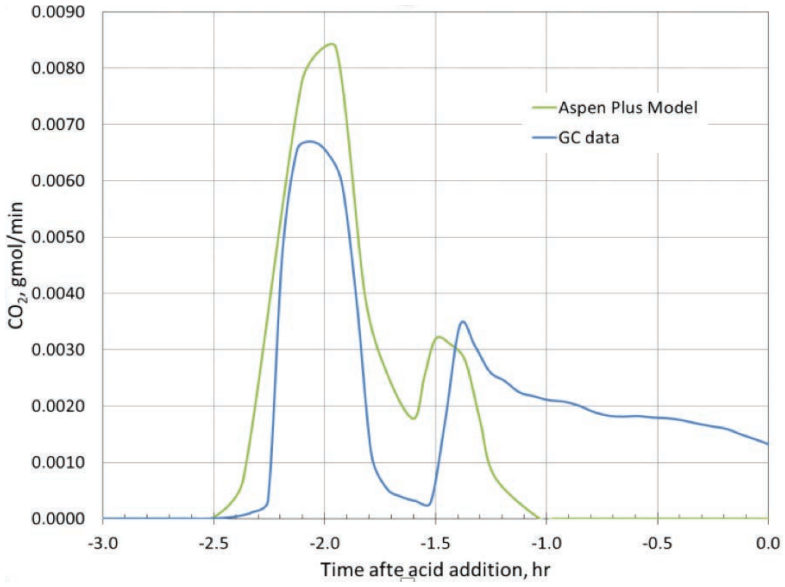

FY2016 ACCOMPLISHMENTS

Completed 87-component glycolic acid flowsheet properties package with 16 electrolyte equilibrium and 22 dissociation reactions

Presented paper on the solution thermodynamics and phase equilibria of the H_2O-HNO_3-$NaNO_3$ ternary at the 2015 AIChE Annual Meeting in Salt Lake City November 9, 2015

Began work on pseudo-dynamic model of lab-scale SRAT/SME experiments, successfully simulating the first four hours, including the acid addition steps and the start of boiling

FUTURE DIRECTIONS

- Present results to DWPF Flowsheet Development and Facility Integration to explore potential interest in continuing the work to completion and in using the properties models developed for this project in their process models
- Explore possibility of funding the summer intern to return in December 2016-January 2017 for four weeks to complete the pseudo-dynamic simulation of Test Run GN-74
- Look for other funding sources in SRNS or SRR to complete this work

References

1. **Meng Wang, Maximilian B. Gorensek, Chau-Chyun Chen.** Comparison between the OLI-MSE and eNRTL Models in Predicting Thermodynamic Properties of the NaN_{O3}-HN_{O3}-H_2O Ternary System. manuscript in preparation for submission in 2016.
2. **Meng Wang, Chau-Chyun Chen, Maximilian B. Gorensek.** Comparison between the OLI-MSE and eNRTL models in calculating thermodynamic properties of NaN_{O3}- HN_{O3}-H_2O ternary system. Paper 457b, to be presented at the 2016 AIChE Annual Meeting, San Francisco, CA, November 16, 2016.

Acronyms

ACM	Aspen Custom Modeler
DOE	Department of Energy
DWPF	Defense Waste Processing Facility
FY	Fiscal Year
NRTL	Non Random Two-Liquid
PCCS	Product Composition and Control System
SM	Smart Manufacturing
SME	Slurry Mix Evaporator
SRAT	Sludge Receipt and Adjustment Tank
SRNL	Savannah River National Laboratory
SRNS	Savannah River Nuclear Solutions, LLC
SRR	Savannah River Remediation, LLC
SRS	Savannah River Site
TTU	Texas Tech University

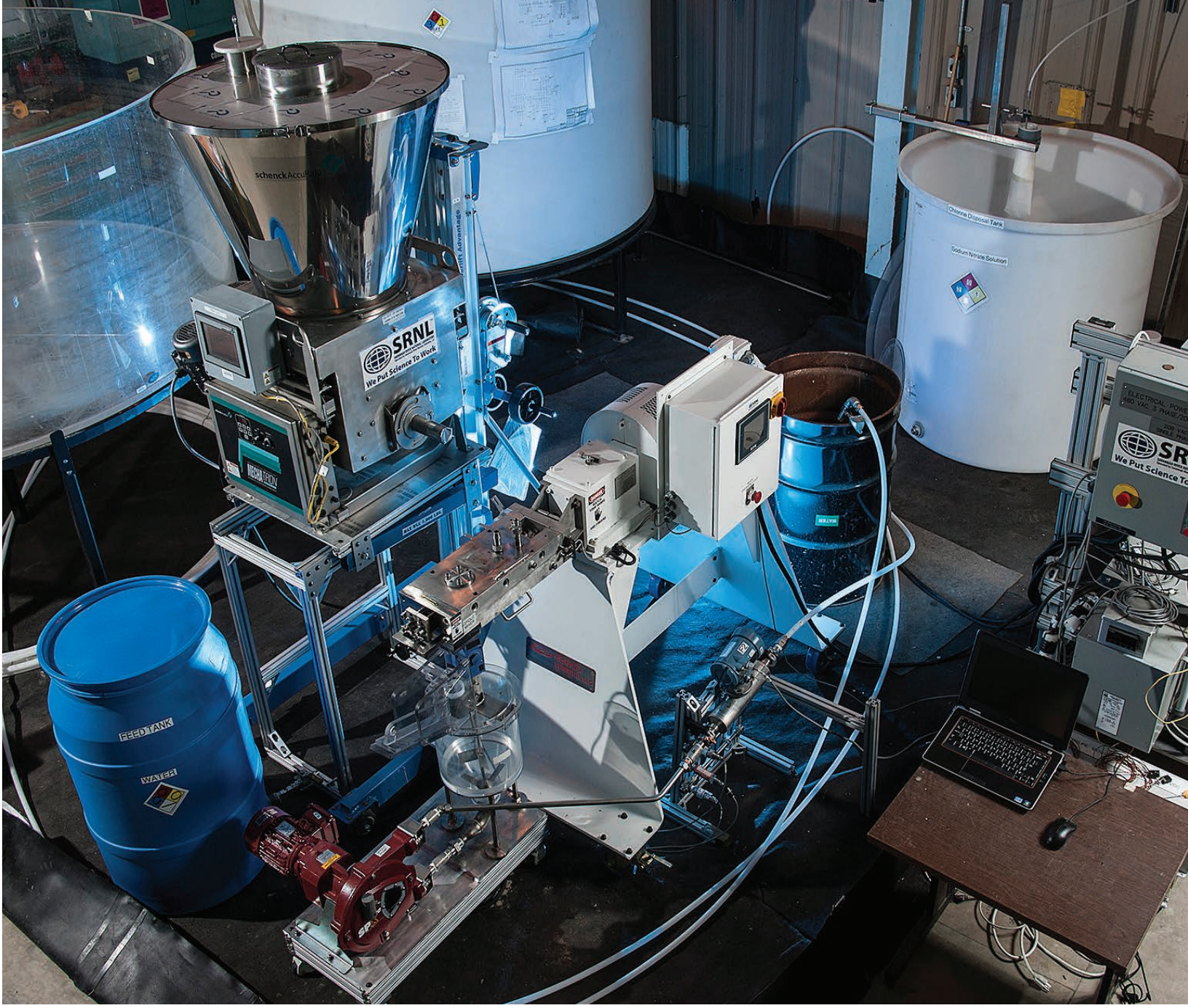

Low Temperature Waste Form Process Intensification

Project Team: D. L. McClane, K. M. Fox, A. D. Cozzi, K. A. Hill, E. K. Hansen
Thrust Area: Process Intensification and Smart Manufacturing
Project Type: Continuation
Project Start Date: February 1, 2014
Project End Date: September 30, 2016

Cementitious waste forms fabricated at low temperature are considered viable for immobilizing Low Activity Waste (LAW). These waste forms can be easily produced by mixing blast furnace slag, Class F fly ash, and ordinary portland cement with LAW salt solutions. Formulation at higher waste concentrations is of particular interest, since a significant reduction in the necessary volume of the waste form and the subsequent disposal costs could be achieved. The current work focuses on how increasing the waste loading (by approximately 60%), and how additions of alternative pozzolans— metakaolin and zeolite—influence various properties that relate to the production, disposal, and performance of the material.

FY2016 OBJECTIVES

- Develop an improved understanding of the retention of contaminants in low temperature, cementitious waste forms such that a step-change reduction in waste form volume can be achieved
- Identify potential processing issues when waste concentration is increased
- Measure waste form performance when formulated at high waste concentrations
- Identify changes to dry blend composition that improve waste form performance

INTRODUCTION

The objective of this study was to develop an improved understanding of the retention of contaminants in low temperature, cementitious waste forms such that a step-change reduction in waste form volume can be achieved. Figure 1 demonstrates this potential reduction in waste form volume.

As shown in Figure 1, concentrating a low activity waste (LAW) salt solution feed from 5M sodium to 8M sodium would reduce the volume of the waste form by approximately 50%, and would reduce mission life cycle costs by a similar percentage.

The study reported here continued to investigate the properties and performance of low temperature forms fabricated with high sodium concentration simulated LAW solutions, along with the addition of dry blend (or premix) components at a W/P ratio of 0.5. It was hypothesized that a reduced W/P ratio, as well as the addition of geopolymer materials, could offer improved retention of contaminants of concern, while continuing to meet other material processing and performance requirements.

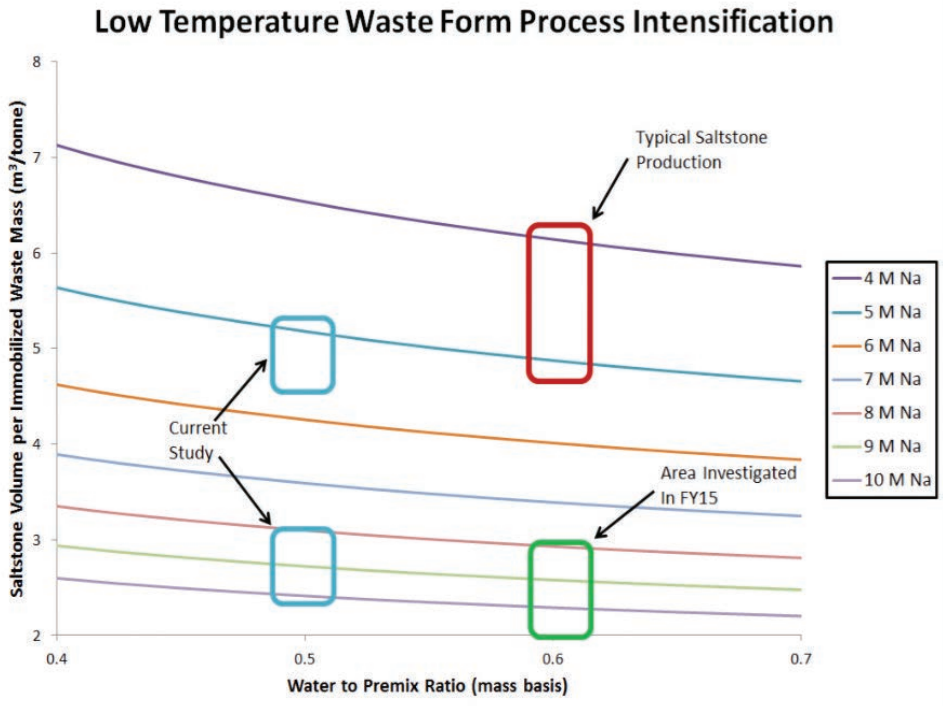

Figure 1. Calculated waste form volume as a function of sodium molarity and water to premix ratio

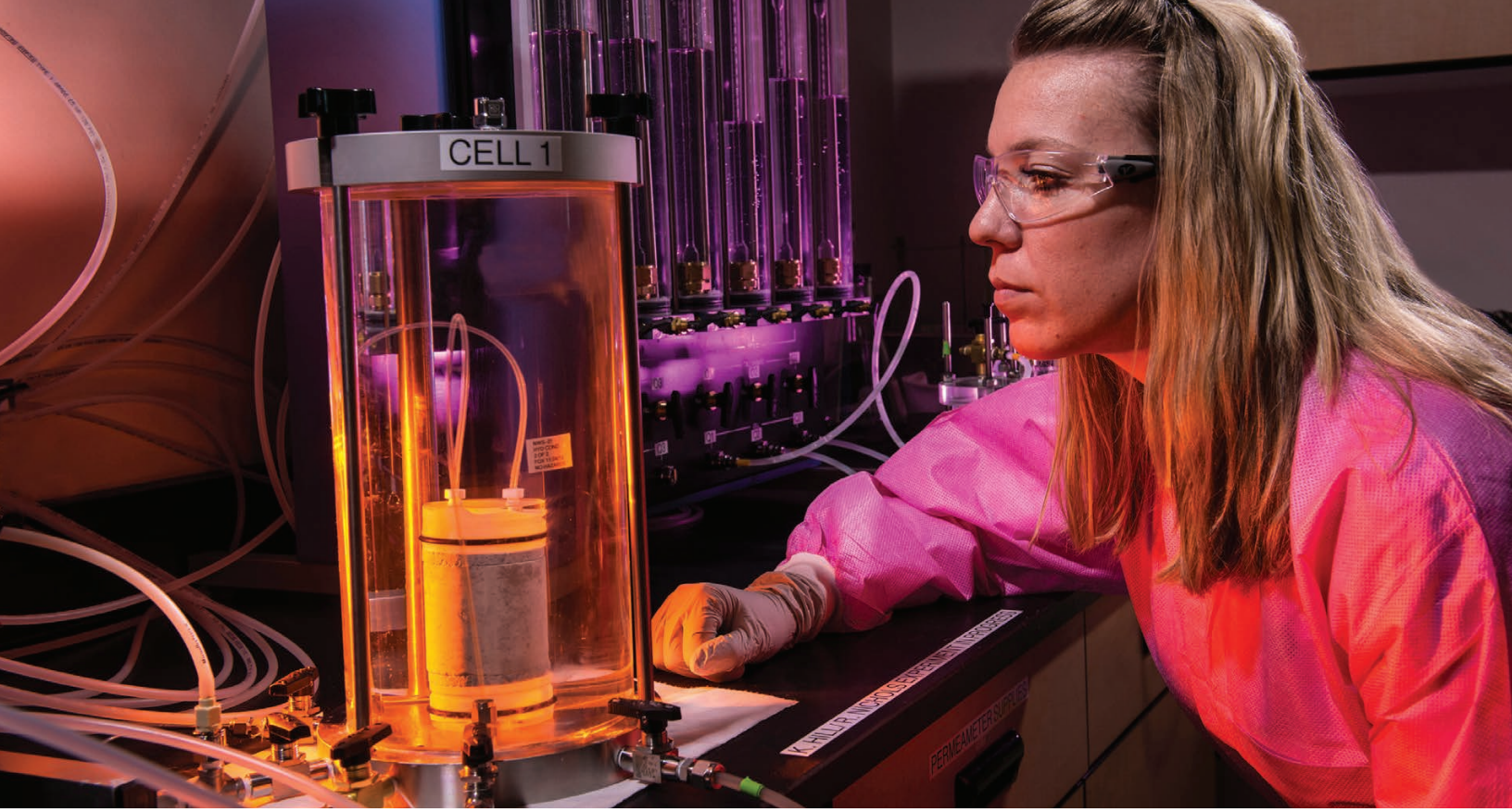

APPROACH

A series of low temperature waste form test mixes was developed for this study utilizing a salt solution simulant that represents the overall average LAW composition expected to be processed at the Hanford Site. The baseline composition was prepared with a 5.25 M Na simulant so that comparison could be made to a typical SRS saltstone, and to allow for investigation of the individual influence of a decreased W/P ratio. The same baseline composition was also prepared with an 8.5 M Na simulant so that comparison could be made to results from FY15 [1]. This mix also allowed for investigation of the individual influence of increased waste loading. Finally, based on results from FY15 [1], zeolite and metakaolin substitutions were made for Class F fly ash. These additions were investigated in an attempt to further improve cementitious waste form performance.

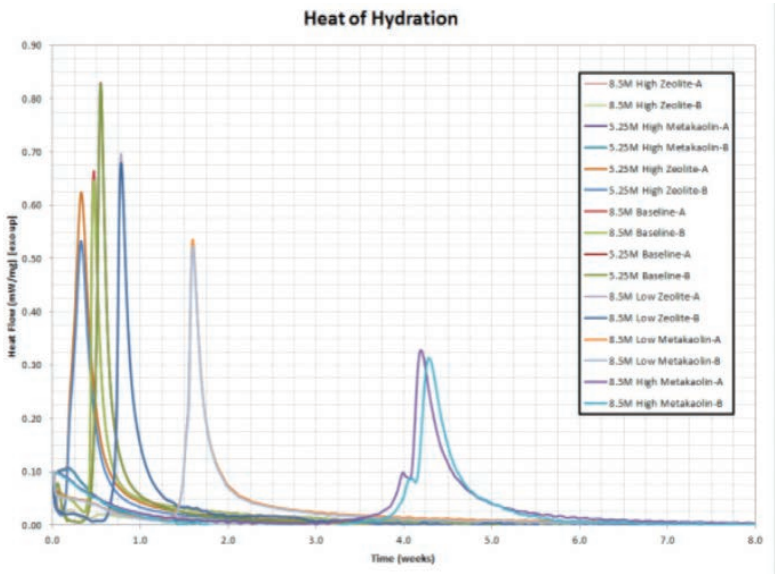

Figure 2. Measured heat of hydration

After preparation in the laboratory, the fresh properties of the mixes were measured. Fresh properties, including density, flowability, gel time, set time, plastic viscosity, yield stress, bleed water, and heat of hydration, determine the processability of the slurry. The intent was to develop formulations that can be processed using existing equipment and facilities, thus minimizing the need for any capital expenditures to process the waste form at higher waste concentrations. The experimental mixes were then cured for at least 28 days in preparation for cured properties measurements. Cured properties, including compressive strength and leachability, are indicative of the performance of the waste form in the disposal environment.

One potential issue with increased waste loading mixes is the observed delay in set time caused by a delay in the hydration reactions. This was especially obvious for mixes prepared with metakaolin and zeolite substituted for fly ash.

RESULTS / DISCUSSION

The fresh (processing) properties appeared to be largely influenced by the W/P ratio and simulant concentration, while being minimally influenced by premix composition. Processing of lower W/P ratios, regardless of composition, at the current waste loading appears that it could present more difficulty due to the higher observed densities and rheologies, as well as quicker gel times. These changes would require a facility to ensure the prepared mixes were constantly flowing, and that the pump lines be immediately flushed if an issue was to arise. Contradictory to compositions prepared with the 5.25 M sodium simulant, mixes prepared with the increased simulant concentration (8.5 M sodium) exhibited lower rheology/greater flow, and longer gel times. These results indicate that not only does the use of an increased simulant concentration increase waste loading, but it also appears to help offset the processing issues that arise as a result of decreasing the W/P ratio. One potential issue with increased waste loading mixes is the observed delay in set time caused by a delay in the hydration reactions. This was especially obvious for mixes prepared with metakaolin and zeolite substituted for fly ash.

The cured (performance) properties appeared to be largely controlled by the phases formed as a result of hydration reactions (a function of premix composition and illustrated by the total heat flow shown in Figure 2). The 8.5 M High Zeolite and 5.25 M High metakaolin mixes that did not produce an observable heat of hydration peak performed worse in all areas compared to every other composition. When these two compositions are excluded, there appears to be another trend associated with mix composition. Both the 28-day and 91-day compressive strength decreased with increasing simulant concentration and increased with fly ash substitution (although all compositions that exhibited an exothermic peak displayed strengths in excess of 1,000 psi after 28 days and 2,000 psi after 91 days). Additionally, the reduced 0.5 W/P greatly increased the strength of the tested compositions, compared to a typical SRS saltstone [1]. Since previous studies had shown that increased waste loading hindered this mechanical property [1,2], demonstrating that this can be addressed by decreasing the W/P ratio and/or partially replacing fly ash is promising. While leaching behavior tracks closely with porosity, it is interesting to note that the samples that displayed lesser (or no) observable hydration reactions exhibited higher porosity.

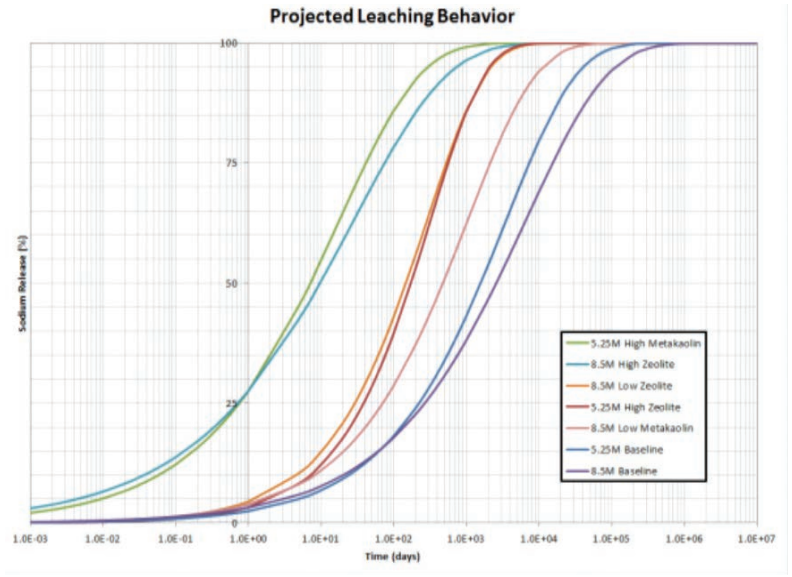

Figure 3. Projected leaching behavior based on Avrami fit to sodium release.

Additionally, the projected sodium release based on Avrami fits to the data collected following EPA 1315 [3], shown in Figure 3, appears to be segregated by pre-mix composition. These results also revealed that while fly ash did not aid in improving strength, it may play a critical role in decreasing waste release.

FY2016 ACCOMPLISHMENTS

Demonstrated successful immobilization of wastes concentrated to 8.5 M sodium

Fresh properties, which dictate the ability to produce the waste form in an economical facility, have been measured and many tested compositions demonstrated the ability to be processed with existing equipment

Cured properties, including compressive strength and leach-ability, demonstrated acceptable performance for several of the waste forms, including those with increased waste concentration

Measurement results were correlated to compositions to further understanding of material parameters

FUTURE DIRECTIONS

- Seek direct funding from Hanford and SRS site contractors

Publications/Presentations

1. **"Low Temperature Waste Form Process Intensification,"** MS&T 2016, Salt Lake City UT.
2. **D. L. McClane, A. D. Cozzi, K. A. Hill,** Low Temperature Waste Form Process Intensification: FY2016 Progress Report. Savannah River National Laboratory, Aiken, SC (2016).
3. **K. M. Fox, A. D. Cozzi, E. K. Hansen, K. A. Hill,** Low Temperature Waste Form Process Intensification: FY2015 Progress Report. SRNL-STI-2015-00448, Savannah River National Laboratory, Aiken, SC (2015).

References

1. **K. M. Fox, A. D. Cozzi, E. K. Hanson, K. A. Hill,** Low Temperature Waste Form Process Intensification: FY2015 Progress Report. SRNL-STI-2015-00448, 2015: Savannah River National Laboratory, Aiken, SC.
2. **K. M. Fox, K. A. Roberts, T. B. Edwards,** Cast Stone Formulation at Higher Sodium Concentrations. SRNL-STI-2013-00499, 2014: Savannah River National Laboratory, Aiken, SC.
3. **EPA 1315,** Mass transfer rates of constituents in monolithhic or compacted granular materials using a semi-dynamic tank leaching procedure, 2013.

Acronyms

LAW	Low Activity Waste
SRNL	Savannah River National Laboratory
SRS	Savannah River Site

Electrodialysis for Intensification of Aqueous Polishing and Other Separations

Project Team: Roderick Fuentes, Brenda L. Garcia-Diaz, Steve Serkiz
Subcontractor: Joseph Mannion, Mary Ann Williford, Brian A. Powell, and Scott Husson (Clemson University)
Project Start Date: October 1, 2013
Project End Date: September 30, 2016

Aqueous polishing is the preferred method for separating and purifying Pu that is used in the fabrication of MOX fuel as well as other separation activities at SRS. Aqueous polishing is performed using an ion exchange resin that selectively absorbs Pu complexes and allows them to be separated from other fission products. HB-line can perform at SRS in a batch process, but the facility safety basis prevents adding a second resin bed that could make the process semi-continuous. This project investigates the creation of an electrodialysis process that will allow aqueous polishing to be carried out in a continuous operation. Membrane materials have been synthesized and tested for Pu uptake selectivity and cells have been designed and fabricated for the process.

FY2016 OBJECTIVES

- **Develop poly(4-vinyl pyridine)-based membranes with medium and high iodohexane conversion**
- **Measure the conductivity of poly(4-vinyl pyridine)-based membranes for plutonium nitrate anionic complexes using cerium nitrate as surrogate**
- **Quantification of cerium nitrate surrogate**

INTRODUCTION

Aqueous polishing is a process where plutonium nitrate anionic complexes $Pu(NO_3)_x^{6-x}$ are selectively absorbed onto an ion exchange resin such as Reillex HPQ in order to separate them from other fission products and solution components. Aqueous polishing processes have been developed by LANL, AREVA, and others using ion exchange resins. Typically an acidic solution with a nitric acid concentration of at least 5 M containing Pu complexes is passed over the resin and they absorb. The resin is then washed with 5-8 M nitric acid to remove all remaining impurities. The Pu is then eluted using a mildly acidic nitric acid solution.

Electrodialysis is a method commonly used for deionizing water that uses a combination of anion and cation exchange membranes coupled with electrochemical reactions to drive separation. Electrodialysis techniques can be coupled with ion selective membranes to create a process that will separate specific components of a solution. Additional couples of anionic and cationic membranes can be added to a stack to increase the processing rate.

The process that is being developed will use anion exchange membranes that are selective for $Pu(NO_3)_x^{6-x}$ along with a proton exchange membrane such as Nafion to make an electrodialysis cell that creates a continuous aqueous polishing process. The creation of an electrodialysis cell based on the existing Reillex HPQ polymers is not straight-forward because the anion exchange membranes are not as available as membranes and the ionic conductivity of nitrate complexes through membranes of these polymers is not known.

APPROACH

Figure 1 outlines the electrodialysis process for aqueous polishing. The mixed fission product inlet streams are fed in from the bottom in alternating streams. The polished outlet come out in the outlet streams that alternate with the inlet streams. There are also reductant and oxidant inlets that are for sacrificial solutions that enable the electrode reactions. The electrode reaction forces an ionic current between the anode and cathode. This ionic current carries the anions across the anionic exchange membranes and the cations across the cationic exchange membranes. The plutonium concentration that will typically be in the inlet solution is 10 g_{Pu}/L and the nitric acid concentration is 5-8 M. The outlet solution typically has a nitric acid concentration of 0.35 M. The residence time of the fluids in the bed in the batch process is typically 11.5 min. [1]. These design parameters are used as a starting point for cell design and operation. Quarternized Poly(4-Vinylpyridine) (P4VP), the main polymer component of Reillex HPQ, is used as the preferred polymer for the separation due to its high selectivity for $Pu(NO_3)_x^{6-x}$. In FY15 an aminated polypropylene oxide (PPO) membrane had been studied, but did not have high enough selective conductivity of cerium nitrate surrogate for use as a separation membrane. For studies in FY16, quarternized P4VP membranes that have much higher base selectivity for Pu were chosen for modification. Traditional quarternized P4VP polymer is hard and brittle and needed modification to have membrane-like properties. The tests in FY16 focused on a hexyl quarternized version of the polymer having medium- and high- iodohexane conversion (membrane thickness 0.17 and 0.16 mm, respectively) that were identified during initial synthesis in FY15 to be more flexible and less brittle.

The tests in FY16 focused on a hexyl quarternized version of the polymer having medium- and high- iodohexane conversion (membrane thickness 0.17 and 0.16 mm, respectively) that were identified during initial synthesis in FY15 to be more flexible and less brittle.

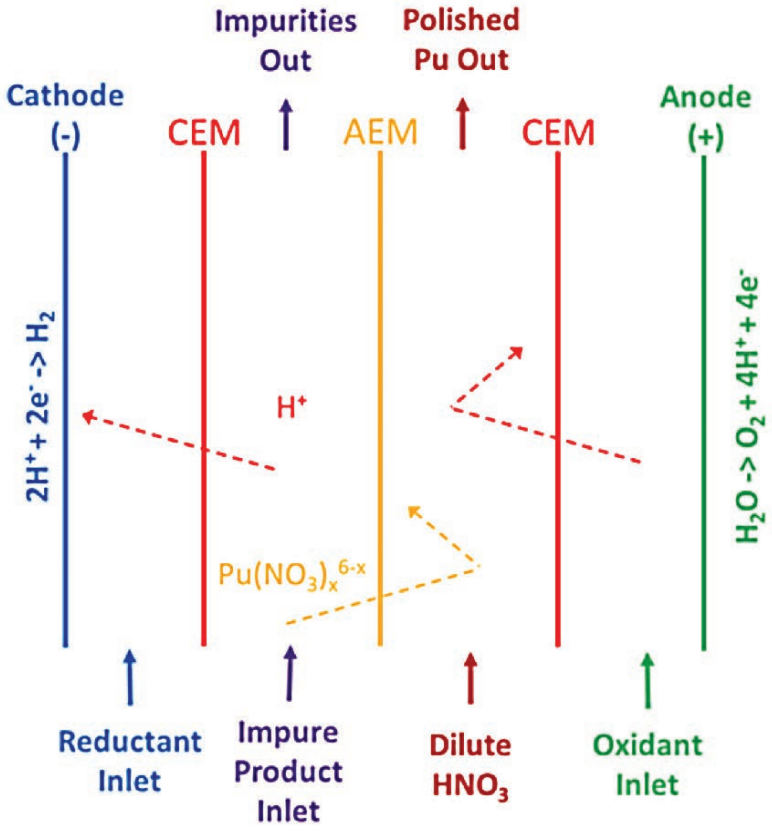

Figure 1. Schematic of an electrodialysis cell for Pu purification

RESULTS / DISCUSSION

Development of poly(4-vinylpyridine) membrane with medium- and high Iodohexane conversion

P4VP was fully dissolved in chloroform (10 wt%). Iodohexane was added to this solution (0.375 g iodohexane/g P4VP) and allowed to mix at room temperature for 24 hours. Dibromohexane, diluted with chloroform, was then added and allow to mix for ~10 seconds before pouring into stainless steel molds (0.33 g dibromohexane/g P4VP). Casting solution is approximately 6.5 wt% P4VP and membrane thickness is determined by the amount of casting solution placed in molds. Films were allowed to dry while covered overnight before baking at 80°C for 24 h. Schematic of P4VP membrane synthesis is shown in Figure 2. The water uptake and linear expansion ratio of P4VP membrane are 38 ± 0.5 % and 9.7 ± 2 %, respectively.

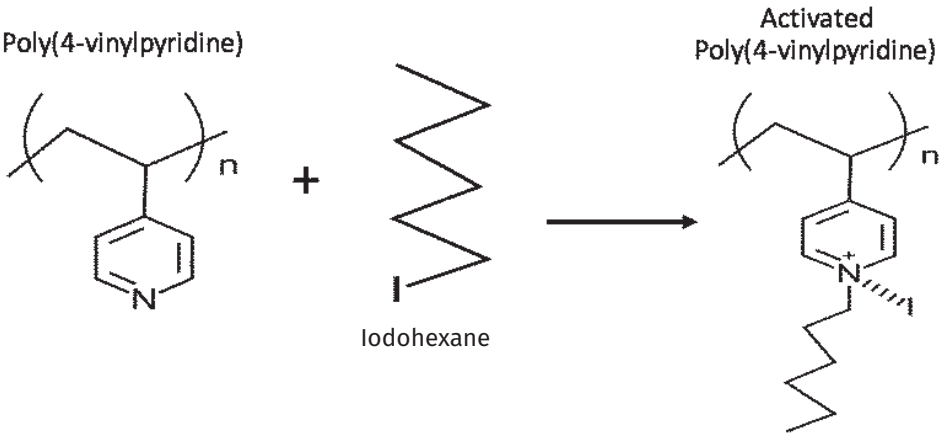

Figure 2. Poly(4-vinylpyridine) activation reaction with iodohexane

Figure 3. (a) Photograph of four probe conductivity cell, **(b)** schematic of P4VP membrane assembled under Pt wires in the conductivity cell, and **(c)** EIS spectra of P4VP membrane

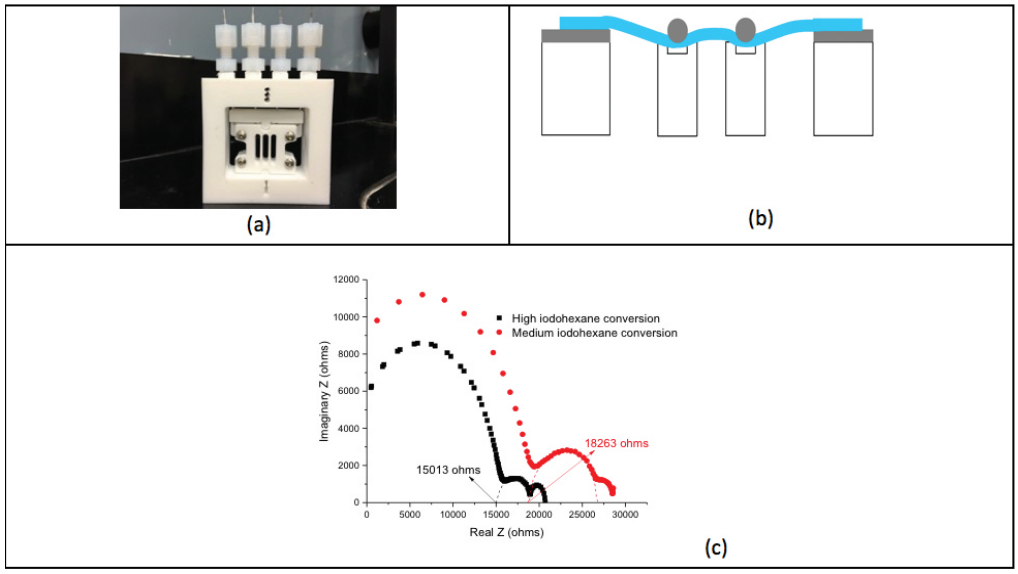

Membrane Conductivity Studies

Tests of P4VP membrane conductivity were performed in DI water followed by immersion in cerium nitrate solution (25g in 8M HNO_3). Conductivity measurements were performed with a four electrode conductivity cell (Fig. 3 a & b) on membranes where excess surface moisture had been absorbed right before placing the sample in the conductivity cell.

Electrochemical impedance spectroscopy (EIS) was used to measure the membrane conductivity in the frequency range 100 kHz-100 mHz. Representative EIS spectra obtained in DI water of P4VP membranes having medium- and high- iodohexane conversion are shown in Fig. 3c. The conductivities of medium and high iodohexane conversion membranes are 2.7 and 3.5 mS/cm, respectively.

Figure 4 shows the conductivity of the hexyl-quarternized P4VP membranes compared to the aminated PPO membranes that previously had been synthesized. The conductivity of these membranes was nearly 3 orders of magnitude higher that the aminated PPO membranes with no cerium nitrate added to the solution. This indicates that poly 4-vinylpyridine membranes have a high ability to conduct ions and indicates that they could be very good options for electrochemical separation of plutonium. The hexyl-quarternized poly-4-vinylpyridine membranes exhibited unexpected curling and brittleness when exposed to cerium nitrate solutions. This indicated that the hexyl-quarternization requires varying degrees of cross-linking to help maintain the mechanical integrity of the membranes. It is believed that a scope of work that focuses on further development of these membranes has promise given the high conductivity for the P4VP hexyl quarternized base polymer in DI water.

Figure 4. Electrodialysis stack integrated with P4VP membrane

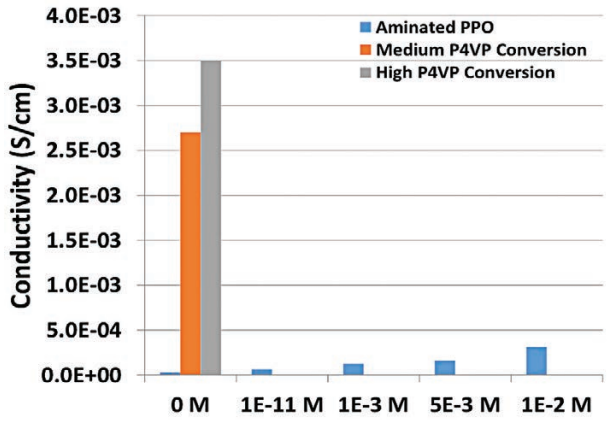

FY2016 ACCOMPLISHMENTS

Poly(4-vinylpyridine)-based membranes having medium and high degree of iodohexane conversion was synthesized

The ionic conductivity of P4VP membranes was measured to be 2.7 and 3.5 mS/cm for medium and high iodohexane conversion samples

P4VP membranes were integrated into the electrodialysis cell stack for proof-of-concept testing

FUTURE DIRECTIONS

- Increase the mechanical stability of P4VP membranes
- Stabilize the hydrophilic polymer in aqueous media through cross-linking reaction
- Measure the ionic conductivity of P4VP membrane with dibromohexane
- Measure the Pu and Ce uptake of developed P4VP membranes having iodohexane/dibromohexane conversions
- Integrate developed P4VP membranes having iodohexane/dibromohexane conversions into the electrodialysis stack and characterize the change in transport of cerium nitrate

References: [1] **E. Kyser,** WSRC-TR-2000-00372.

Development of Liquid Phase Water Detritiation Technology

Project Team: Steve Xiao, Tommy Sessions, Jim Klein, Bob Rabun
R&D Team: Lucas Angelette, Paul Beaumont, Ben Randall, Michael Brown, Donna Allison
SRNS Support (Tritium Study): Jay Hutchison, Jim Collin, Tommy Young, Linda Youmans, Karl Damon
Subcontractor: Clemson University
Thrust Area: Environmental Stewardship
Project Type: Strategic
Project Start Date: October 1, 2014
Project End Date: September 30, 2017

An innovative 3-step SRNL concept is being developed, leveraging the SRNL expertise in isotope separation. In FY16, material screening and process variable study were complete. Wet column performance was verified. Further tritium data were collected with confirmed tritium removal. Tritium study is beginning in SRNL to incorporate catalytic isotope exchange. The subcontract with Clemson University has confirmed no isotope separation from the Nafion membrane bithermal process.

The innovative water detritiation process, if fully developed, could have broad impacts to heavy water from SRS legacy moderator, TVA (Tennessee Valley Authority) cooling water, nuclear power industry, and environmental remediation, etc. The continuation of this project is critical to develop this discovery.

FY2016 OBJECTIVES

Complete parameter study for process optimization	Fundamental studies on isotope separation	Follow up Clemson subcontract

INTRODUCTION

An efficient water detritiation process, if fully developed, could have broad impacts to heavy water from SRS legacy moderator, TVA (Tennessee Valley Authority) cooling water, nuclear power industry, and environmental remediation, etc. Over the past four decades no breakthrough technologies have been developed to process tritium-contaminated water efficiently and economically [1-5] despite continuing interest and efforts. A number of materials/processes have been reported to have isotopic effects with water molecules [6-8], including a SRS patent [9] by Dr. Myung Lee (inventor of TCAP—Thermal Cycling Absorption Process). The potential for a direct isotope separation of water molecules is of considerable interest. This project achieved direct HDO/H_2O separation experimentally as a surrogate for HTO/H_2O separation. Further fundamental studies on isotope separation factor and separation mechanisms would augment this breakthrough development. Until now, no technology existed to remove low levels of tritium contamination economically.

APPROACH

A novel three-step engineering concept is illustrated in Figure 1 as an example configuration.

>> Scalable 3-Step Concept Water Detritiation Process

- WIE (Water Isotope Exchange): discharge majority clean water and develop tritium concentration profile along the column
- CIE (Catalytic Isotope Exchange) to regenerate the column and to convert HTO into HT gas
- TCAP to separate HT/H_2

>> Collaboration between the SRNL Environmental & Waste Management and National Security directories in this area (between DOE EM and NNSA)

Figure 1. Conceptual 3-step process cleans up tritiated water with no secondary contaminated streams

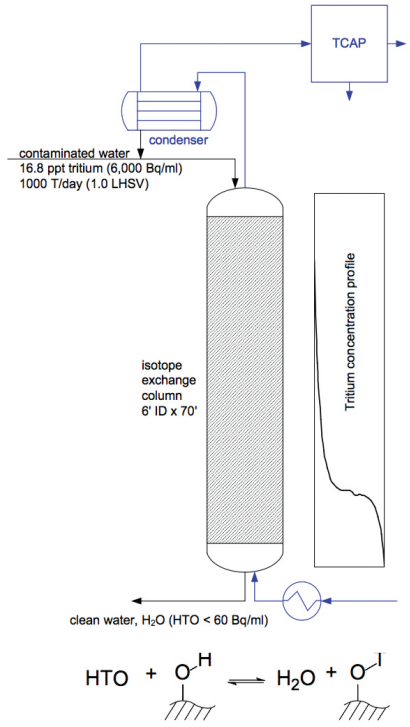

a) Water Isotope Exchange for Cleaning

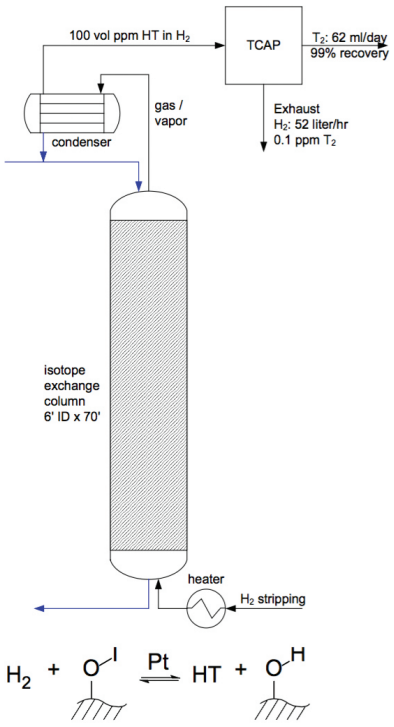

b) Catalytic Isotope Exchange for Regeneration

Effective treatment of low-level tritiated water is technically very challenging due to the large volume of water that needs processing. However, the extremely low concentration also provides ample capacity for a column to remove tritiated water if the isotopic separation factor is adequate to establish a concentration profile. In the SRNL 3-step concept, TCAP is a mature technology for elemental hydrogen isotope separation. CIE has been demonstrated at SRS with 1,000 DF (decontamination factor) and 99.9% tritium recovery [10]. The development of WIE is critical for the success of the SRNL concept and herein the focus of this project.

RESULTS / DISCUSSION

In FY16, material screening and process variable study were complete. Wet column performance was verified. Tritium data were collected with confirmed tritium removal. Because of promising results, a demonstration plan has been developed and there has been continuous discussion with NNSA NA-123, NA-197, and TVA. Table 1 lists the R&D progression that has achieved 45 times improvement since initial breakthrough experiment. Preliminary tritium data in Table 2 demonstrated removal of pCi tritium from water. Work is commencing to begin a tritium study in SRNL that will combine the WIE and CIE.

Progression with HDO/H_2O study	Amount of deuterium removal per pass relative to early results
Early results	100
Material screening	296
Dry column, chilled	1554
Wet column, ambient	4580

Table 1. Results from process optimization

		Feed	Uncertainty	Effluent	Uncertainty
		pCi/g	pCi/g	pCi/g	pCi/g
Material 1	Dry	1935	5.4	1624	5.1
	Repeat	1947	5.7	1616	5.0
Material 2	Dry	1840	5.9	1461	6.1
	Repeat	1738	6.2	1524	5.5
Material 1	Wet	1802	5.4	22	1.0
	Wet	1802	5.4	647	4.7
Repeat	Wet	1800	5.4	40	1.2
	Wet	1800	5.4	573	4.6
Material 2	Wet	1670	4.9	2.0	0.8
	Wet	1670	4.9	112	1.9
Repeat	Wet	1756	4.9	3.2	0.7
	Wet	1756	4.9	288	2.8

** 1940 pCi/g tritium = 0.6 ppt T/H ratio*

Table 2. Preliminary tritium data

Due to challenge of natural background deuterium, two ways of testing hydrogen stripping (catalytic isotope exchange) were identified:

- **Tritiated water with hydrogen stripping**
- **Natural water with protium stripping**

Figure 2. Clemson bithermal Nafion test cell

Figure 3. Illustration of quantum tunneling by solving schrödinger equation

$$\frac{d^2\psi}{dx^2} = \frac{2m}{\hbar^2}[V(x) - E]\psi = [\alpha(x)]^2\psi$$

$$\alpha(x) = \sqrt{\frac{2m}{\hbar^2}[V(x) - E]}$$

$$T = \left|\frac{D}{A_0}\right|^2 \approx 16\left(\frac{E}{V_0}\right)\left(1 - \frac{E}{V_0}\right)e^{-2\alpha L}$$

The subcontract with Clemson University has confirmed no isotope separation from the Nafion membrane bithermal process based on a SRNL patent by Dr. Myung W. Lee [9]. It was identified that the permeation of water molecules was too high for any meaningful isotope separation, if there are any. Figure 2 shows the Clemson bithermal Nafion test cell. Clemson and SRNL have submitted a joint funding proposal "Hydrogen isotope fractionation using graphene and related 2-D materials" to DOE Office of Nuclear Physics, during which SRNL has developed a quantum tunneling explanation for hydrogen isotope selectivity over graphene membrane based on recent science discovery by University of Manchester [11]. Figure 3 illustrates quantum tunneling by one dimensional Schrödinger equation.

FY2016 ACCOMPLISHMENTS

- Complete parameter study for process optimization
- Fundamental studies on isotope separation
- Follow up Clemson University subcontract for HDO/H_2O separation using Nafion membrane
- Collected initial tritium data (not in milestone, exceeding expectations)

FUTURE DIRECTIONS

- Material development for further improvement
- Fundamental study in mechanisms
- Demonstrate the process in a sizable column (pilot plant)
- Seek external funding source to continue the development
  >> Joint proposal submitted with Clemson for DOE-SC funding has been selected for FY18 and FY19 funding

References

1. **K. H. Lin,** "Tritium Enrichment by Isotope Separation Technique", ORNL-TM-3976, Oak Ridge National Laboratory, 1972.
2. **H. K. RAE,** "Selecting Heavy Water Processes" in Separation of Hydrogen isotopes, ACS Symposium Series 68, Washington D.C., (1978), Chalk River Nuclear Laboratories, Atomic Energy of Canada, Ontario, Canada.
3. **C. M. King, V. V. Brunt, R. B. King, A. R. Garber,** "Concepts for Detritiation of Waste Liquids", WSRC- MS-91-027, Savannah River Site, 1991.
4. **H. H. Fulbright, A. L. Schwirian-Spann, B. B. Looney, K. M. Jerome, V. Van Brunt,** "Status and Practicality of Detritiation and Tritium Production Strategies for Environmental Remediation", Savannah River Site, WSRC-RP-96-0075, 1996.
5. **D.J. Geniesse, G.E. Stegen,** "2009 Evaluation of Tritium Removal and Mitigation Technologies for Wastewater Treatment", DOE/RL-2009-18, Hanford.
6. **Y. Iwai, T. Yamanishi,** "Isotopic Distribution Coefficient of Tritiated Water Adsorbed on Faujasite - Type Zeolite", Fusion Science and Technology, Vol 56, 158, 2009.
7. **S. Tanaka, F. Ono, Y. Takahashi, R. Kiyose,** "Removal of Tritiated Water Vapor by Adsorption on Molecular Sieves - Effects of Co-Existing H2O", Fusion Technol. 8 (1985) 2196.
8. **X. Cao, G. Cheng,** "Reemission of Tritium from Tritium-Sorbed Molecular Sieve", Fusion Sci. Technol. 48 (2005) 593.
9. **Myung W. Lee,** "Method and Apparatus for Separation of Heavy and Tritiated Water", US Patent 6,332,914 (2001).
10. **L.K. Heung, G.W. Gibson, M.S. Ortman,** "Tritium Stripping by a Catalytic Exchange Stripper", Fusion Technology, Vol. 21, 588, 1992.
11. **Lozada-Hidalgo,** M., **et al.,** Sieving hydrogen isotopes through two-dimensional crystals. Science, 2016. 351(6268): p. 68-70

Acronyms

CIE	Catalytic Isotope Exchange
DF	Decontamination Factor
EM	Environmental Management
FTIR	Fourier Transform Infrared Spectroscopy
LDRD	Laboratory Directed Research and Development
NNSA	National Nuclear Security Administration
RGA	Residue Gas Analyzer (mass spectrometer)
SF	Separation Factor
SRS	Savannah River Site
SRNL	Savannah River National Laboratory
SRNS	Savannah River National Solutions, LLC.
TCAP	Thermal Cycling Absorption Process
TVA	Tennessee Valley Authority
WIE	Water Isotope Exchange

Post-Doctoral Researchers

2

Functionalized Magnetic Mesoporous Silica Nanoparticles (MMSNs) for U and Tc Removal: Defining Capacities and Engineering Parameters for Applications

Project Team: Dien Li (Primary), D. I. Kaplan, S.M. Serkiz
Subcontractor: Dr. Sarah C. Larsen, University of Iowa
Thrust Area: Nuclear Materials Management & Environmental Stewardship
Project Type: Standard
Project Start Date: February 1, 2014
Project End Date: September 30, 2016

U(VI) species display limited adsorption onto sediment minerals and synthetic sorbents in pH < 4 or pH > 8 groundwater. This project demonstrated that functionalized magnetic mesoporous silica nanoparticle (MMSNs) were effective for U removal from pH 3.5 and 9.6 artificial groundwater (AGW). The removal capacities of these functionalized MMSNs were as high as 38 mg/g from the pH 3.5 AGW, 133 mg/g from the pH 9.6 AGW, and 54 mg/g from seawater simulant. The adsorbed uranyl species from different aqueous media were bound with functional groups of the MMSN surfaces. Seven new functionalized mesoporous silica nanoparticles (MSNs) were developed using post or direct synthesis. Polyethyleneimine-functionalized MSNs was the best performer for Tc removal from pH < 7 groundwater with K_d up to 400 mL/g. In addition, a granular activated carbon and two organoclays have been demonstrated to have high adsorption capacities of > 3.2 mg/g and K_d values >20,000 L/kg for pertechnetate (TcO_4^-) removal from groundwater under a wide range of pH conditions, and synchrotron- XAS analyses confirmed that the Tc species adsorbed onto these sorbents remained was TcO_4^-, rather than reduced Tc(IV). The implications of the materials sorbing TcO_4^- is that it can be deployed in most waste stream, waste disposal, or environmental remediation sites without having to first create an artificial low redox environment.

FY2016 OBJECTIVES

- Conduct batch experiments evaluating capacity of the developed functionalized MMSNs for uranium removal from artificial groundwater and seawater simulant, complete U L3-edge XAFS measurement and data analysis, and complete the submission of inventory disclosure, and manuscripts for uranium work
- Develop and evaluate seven new mesoporous silica nanoparticles (MSNs) functionalized with Sn^{2+}, quaternary ammonium (direct and post-synthesis), monomethylated polyethylene glycol (PEG), polyethyleneimine (PEI), and dihydroimidazole (direct and post synthesis) for Tc removal from groundwater
- Quantify the adsorption capacity of granular activated carbon (GAC 830) and two organoclays (OCB and OCM) for pertechnetate removal from groundwater
- Determine technetium speciation and binding chemistry on these sorbents using Tc K-edge XAFS spectroscopy, and to evaluate desorption/extraction behavior of the adsorbed Tc species from these sorbent materials

INTRODUCTION

Uranium is the most common radioactive contaminant in the DOE complex [1], and also at U mine / processing sites, and fuel cell rod storage basins. There are two common oxidation states of U in natural environments and waste streams, U(IV) and U(VI). U(VI) is normally more mobile, bioavailable and toxic than its counterpart, U(IV). The aqueous U(VI) species exists commonly in extremely acidic (pH < 4) or naturally-occurring basic carbonate (pH > 8) conditions. It has little or no adsorption to sediments under pH < 4 or pH > 8 aqueous conditions due to repulsive surface charges between U species and sediment minerals, [2] which leads to severe difficulties in its remediation. Existing technologies for U contaminant treatment include various biotic and abiotic reduction processes. [3, 4] However, these processes have several application shortcomings, of which the most important is that U readily becomes remobilized if a reduction processes undergoes oxidation. There is, therefore, a great need to address this knowledge gap and to develop novel and cost-effective technologies for remediation of acid/base U contaminated systems. In addition, seawater appears as a potentially promising and less environmentally damaging source for uranium, but additional technology development is necessary.

Tc is a key risk driver at the Savannah River Site (SRS) and other DOE environmental management sites (most notably the Hanford Site, Paducah Gaseous Diffusion Plant, and Oak Ridge National Laboratory). [1] The anionic TcO_4^- is mobile and difficult to immobilize with sorbents.[5] For waste streams with a high content of TcO_4^-, reductant materials (Fe_3S_4, soluble or structural Fe(II), zero-valence iron) and reducing bacteria can reduce Tc(VII) to Tc(IV) and remove Tc effectively. [6, 7] But like U(IV), the reduced Tc form (e.g., $TcO_2 \cdot nH_2O$) is susceptible to re-oxidation under most natural environmental conditions and the mobile TcO_4^- will be released to the environments. [8] There are currently no demonstrated technologies that are highly efficient and cost-effective for separation of Tc-containing nuclear waste streams and remediation of aqueous Tc in the contaminated sites.

Building on the progress made in FY15, during FY16, we developed seven new functionalized mesoporous silica nanoparticles (MSNs) with Sn^{2+}, quaternary ammonium, monomethylated polyethylene glycol (PEG), polyethyleneimine (PEI), and dihydroimidazole using post- or direct synthesis methods. We evaluated these new functionalized MSNs for their Tc adsorption coefficient, as well as granular activated carbon and organoclays for their Tc removal capacity, from groundwater under a wide range of pH conditions. We conducted Tc K-edge XAFS spectroscopy experiments to determine Tc chemical speciation and bonding chemistry with activated carbon and two organoclays that exhibited high capacity for Tc removal.

APPROACH

MSNs were synthesized using surfactant- template self-assembling methods, as we did for MMSNs in FY15 (Figure 1A).[9, 10] Functionalized MSNs for Tc removal were made using post- or direct synthesis (Figure 1B). [11, 12] All functionalized MSNs, as well as granular activated carbon and organoclays, were evaluated for Tc removal from pH = 3.5, 6.5 and 9.5 groundwater. Adsorption coefficient (K_d, mL/g) and the equilibrium adsorption capacity (q_e, mg/g) were calculated using formula 1 and 2, respectively where C_0 and C_e were U or Tc concentrations before and after adsorption, respectively, V was the total volume of liquid phase (i.e., groundwater), and M was the mass of nanoparticle sorbent. Oxidation state and chemical bonding of Tc species onto activated carbon and two organoclays were investigated using synchrotron radiation X-ray absorption Fine Structure (XAFS) spectroscopy.

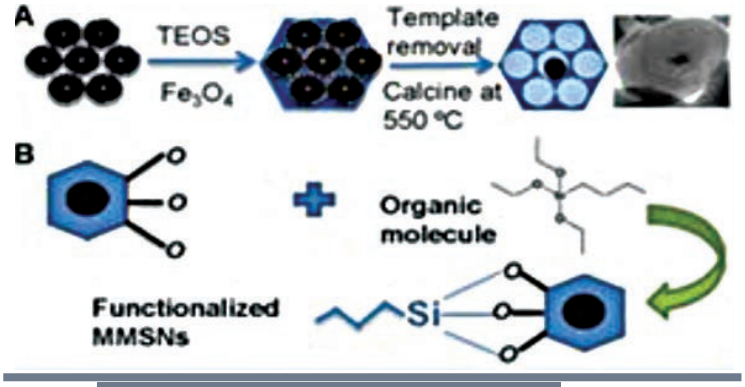

Figure 1. Synthesis of functionalized MMSNs

(1) $$K_d = \frac{C_0 - C_e}{C_e} \times \frac{V}{M}$$

(2) $$q_e = \frac{(C_0 - C_e) \times V}{M}$$

RESULTS / DISCUSSION

1. Adsorption capacity of functionalized MMSNs for U removal

The U isotherm data (U sorbed onto sorbent vs U remained in solution) from batch experiments were analyzed using Langmuir isotherm model (see equation 3 below) where q_{max} is the saturation adsorption capacity, and K_L is the Langmuir constant that is directly related to the binding site affinity. Values for q_{max}, K_L and coefficient of correlation (R^2) that measures how well the Langmuir model fits to the experimental data were obtained by plotting C_e/q_e versus C_e. The U saturation adsorption capacity data of functionalized MMSNs from pH 3.5 and 9.6 artificial groundwater, and seawater simulant are summarized in Table 1. The U removal capacity of the functionalized MMSNs was as high as 38 mg/g from pH 3.5 groundwater, 133 mg/g from pH 9.6 groundwater, and 54 mg/g from seawater simulant. X-ray absorption fine structure (XAFS) data indicated that U speciation sorbed onto the functionalized MMSNs remained as various uranyl (UO_2^{2+})-type species and were bound with functional groups on the MMSNs surfaces.

(3) $$\frac{C_e}{q_e} = \frac{1}{q_{max}} C_e + \frac{1}{K_L q_{max}}$$

2. Tc removal of new functionalized MSNs from groundwater

The K_d values of new functionalized MSNs for Tc removal from pH 3.2, 6.5 and 9.5 artificial groundwater are given in Table 1. PEI-functionalized MSNs is the best performer among these MSNs with K_d values of 400 mL/g at pH < 7.

Table 1. U saturation adsorption capacity of functionalized MMSNs from pH 3.5 and 9.6 artificial groundwater, and seawater simulant

Samples	pH 3.5 AGW		pH 9.6 AGW		Seawater simulant	
	q_{max} (mg/g)	R^2	q_{max} (mg/g)	R^2	q_{max} (mg/g)	R^2
MMSNs-BT			32.5 ± 1.6	0.993		
MMSNs-DIM	24.9 ± 3.0	0.957	109.9 ± 8.5	0.982	34.1 ± 1.9	0.992
MMSNs-AD	30.6 ± 4.9	0.951	125.0 ± 10.9	0.980	45.6 ± 8.3	0.912
MMSNs-PP	37.5 ± 0.8	0.998	55.0 ± 5.1	0.976	45.3 ± 4.9	0.967
MMSNs-PPA	20.6 ± 2.7	0.952	108.7 ± 3.6	0.997	51.6 ± 7.7	0.918
MMSNs-PPI	9.5 ± 1.0	0.965	133.3 ± 6.2	0.933	52.1 ± 4.9	0.967
MMSNs-PAMAM			29.4 ± 0.4	0.999	53.8 ± 10.4	0.868

Table 2. Adsorption coefficient (K_d) of Tc onto functionalized MSNs in groundwater

Samples	Synthesis methods	K_d (mL/g)		
		pH = 3.2	pH = 6.5	pH = 9.5
MSNs-PEG	Post	40.5	0.5	0.2
MSNs-PEI	Post	436.6	400.6	21.6
MSNs-QAM-D	Direct	39.6	0	21.3
MSNs-QAM-P	Post	36.2	4.0	0
MSNs-DIM-D	Direct	55.8	0.1	0
MSNs-DIM-P	Post	59.4	11.1	0
MMSNs-Sn	Post	157.7	13.6	2.8

PEG = Monomethylated polyethylene glycol PEI = Polyethyleneimine QAM = Quaternary ammonium DIM = Dihydroimidazole

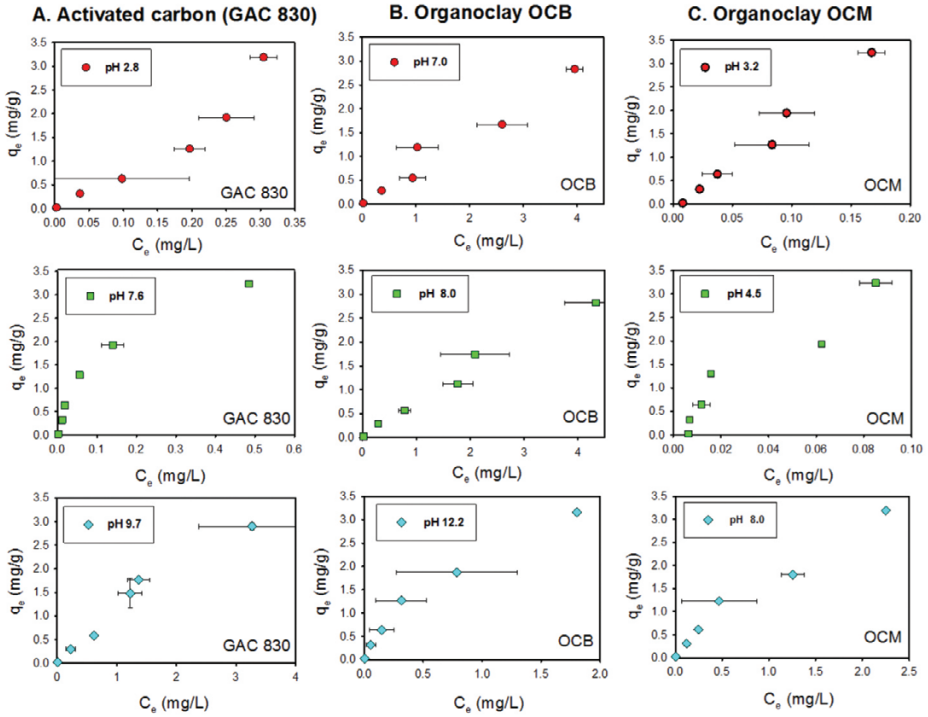

3. Adsorption capacity of activated carbon and organoclays for Tc removal

The isotherm curves for activated carbon (GAC 830) and two organoclays (OCB and OCM) for Tc removal from groundwater under a wide range of pH conditions are shown in Figure 2. GAC 830 and two organoclays (OCB and OCM) can quantitatively remove pertechnetate from groundwater with a wide range of pHs (nearly 100% for most of the cases). The adsorption capacities of these materials were as high as 3.2 mg/g, which could be higher because it can be seen that the isotherm curves have not reached the saturation plateau for most of these cases.

Figure 2. Isotherm curves of activated carbon (panel A), organoclay OCB (panel B) and organoclay OCM (panel C) for Tc removal from artificial groundwater with varying pHs. qe is the mass of Tc bound to the sorbent and Ce is the aqueous Tc concentration at equilibrium (*Note that while the y-axes were kept constant, the x-axes varied between plots)*

4. Tc speciation and chemical binding on activated carbon and organoclays

Tc K-edge X-ray absorption near-edge structure (XANES) of activated carbon (GAC 830) and two organoclays (OCB and OCM) after Tc adsorption are shown in Figure 3, in comparison with model compounds (ammonia pertechnetate and Tc(IV) oxide). The results indicated that the adsorbed Tc species remained as $Tc(VII)O_4^-$, rather than reduced Tc(IV).

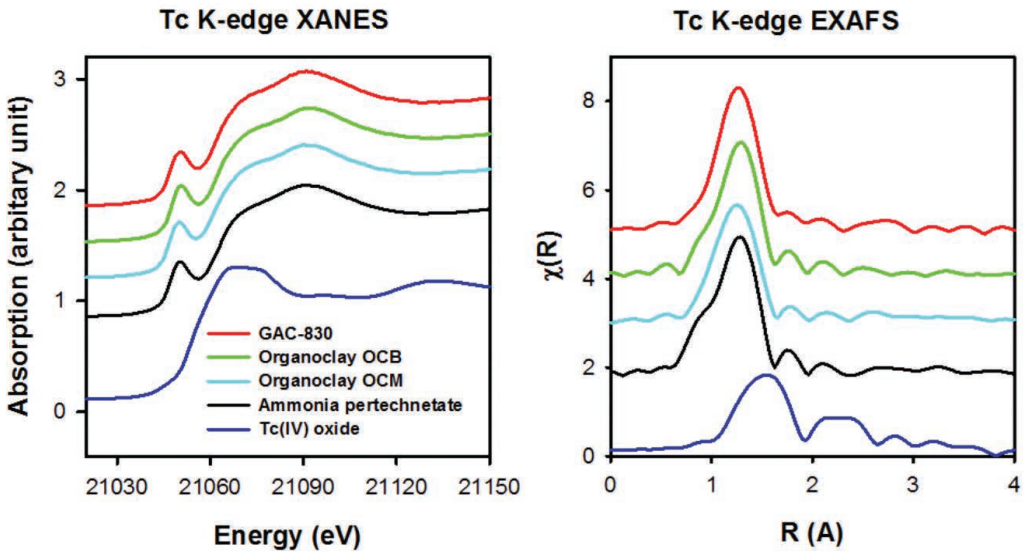

Figure 3. Tc K-edge XAFS of activated carbon (GAC 830) and two organoclays (OCB and OCM), in comparison with model compounds [ammonia pertechnetate and Tc(IV) oxide] (*Note that the spectra of the three sorbents are similar to the ammonia pertechnetate standard, indicating Tc is bound to these sorbents as* TcO_4^-)

FY2016 ACCOMPLISHMENTS

- Functionalized magnetic mesoporous silica nanoparticles (MMSNs) had uranium adsorption capacities as high as 38 mg/g from pH 3.5 artificial groundwater (AGW), 133 mg/g from pH 9.6 AGW, and 54 mg/g from seawater simulant
- U L_3-edge XAFS data demonstrated that various uranyl species in different aqueous media were bound with functional groups of the MMSN surfaces
- Seven new functionalized mesoporous silica nanoparticles (MSNs) were developed using post or direct synthesis; Polyethyleneimine (PEI)-functionalized MSNs was the best performe for Tc removal from pH < groundwater with Kd up to 400 mL/g
- One activated carbon and two organoclays have been demonstrated to have high adsorption capacities of >3.2 mg/g for pertechnetate removal from groundwater under a wide range of pH conditions
- Tc K-edge XAFS data indicated that Tc species adsorbed onto activated carbon and two organoclays remained as pertechnetate (TcO_4^-), rather than reduced Tc forms (Tc(IV))

FUTURE DIRECTIONS

- Continue to complete U L_3-edge XAFS data analysis of functionalized MMSNs and prepare two manuscripts for journal publication
- Continue to complete Tc K-edge XAFS data analysis and desorption or extraction experiments of activated carbon and organoclays to determine chemical bonding and stability of Tc species sorbed on these sorbent materials, and prepare one or two manuscripts for journal publication
- Develop and evaluate new types of novel materials (e.g., porous iron) for enhanced attenuation of pertechnetate contaminant in groundwater or for separation of Tc species from liquid nuclear wastes
- Field demonstration of activated carbon and organoclays at SRS and other sites
- Proposals to DOE EM Soil & Groundwater Remediation Program, International Program and DOE Nuclear Energy Programs

Publications/Presentations

1. **Functionalized magnetic mesoporous silica nanoparticles for Uremoval from low and high pH groundwater,** Dien Li, Shani Egodawatte, Daniel I. Kaplan, Sarah C. Larsen, Steven M. Serkiz, John C. Seaman, Journal of Hazardous Materials 317 (2016) 494–502.
2. **Removal of uranium from artificial groundwater and seawater by functionalized magnetic mesoporous silica nanoparticles: Capacity and XAFS study,** Dien Li, Shani Egodawatte, Daniel I. Kaplan, Sarah C. Larsen, Steven M. Serkiz, John C. Seaman, Kirk G. Scheckel, Advanced Photo Source (APS) User's Meeting, Chicago, IL, May 9-12, 2016.
3. **Uranium speciation and bonding mechanisms on functionalized mesoporous silica nanoparticles (MMSNs) in low and high pH groundwater,** Dien Li, Shani Egodawatte, Daniel I. Kaplan, Sarah C. Larsen, Steven M. Serkiz, John C. Seaman, Kirk G. Scheckel, In preparation.
4. **Extraction of uranium from seawater by functionalized mesoporous silica nanoparticles (MMSNs): Capacity and XAFS study,** Dien Li, Shani Egodawatte, Daniel I. Kaplan, Sarah C. Larsen, Steven M. Serkiz, John C. Seaman, Kirk G. Scheckel, In preparation.

References

1. **Riley, R.G., M. M. Zachara,** Chemical Contaminants on DOE Lands and Selection of Contaminants Mixtures for Subsurface Science Research, 1992, DOE: Washington, DC.
2. **Pabalan, R.T.,** et al., Uranium(VI) sorption onto selected mineral surfaces, in Adsorption of Metals by Geomedia: Variable, Mechanisms, and Model Applications, E.A. Jenne, Editor 1998, Academic Press: San Diego, USA. p. 99-130.
3. **Wu, W.M.,** et al., In situ bioreduction of uranium (VI) to submicromolar levels and reoxidation by dissolved oxygen. Environmental Science & Technology, 2007. 41(16): p. 5716-5723.
4. **Gu, B.,** et al., Reductive precipitation of uranium(VI) by zero-valent iron. Environmental Science & Technology, 1998. 32(21): p. 3366-3373.
5. **Icenhower, J.P.,** et al., THE BIOGEOCHEMISTRY OF TECHNETIUM: A REVIEW OF THE BEHAVIOR OF AN ARTIFICIAL ELEMENT IN THE NATURAL ENVIRONMENT. American Journal of Science, 2010. 310(8): p. 721-752.
6. **Fredrickson, J.K.,** et al., Reduction of TcO4- by sediment-associated biogenic Fe(II). Geochimica Et Cosmochimica Acta, 2004. 68(15): p. 3171-3187.
7. **Liang, L.Y., B.H. Gu, and X.P. Yin,** Removal of technetium-99 from contaminated groundwater with sorbents and reductive materials. Separations Technology, 1996. 6(2): p. 111-122.

References Continued:

8. **Morris, K.,** et al., An X-ray absorption study of the fate of technetium in reduced and reoxidised sediments and mineral phases. Applied Geochemistry, 2008. 23(4): p. 603-617.
9. **Feng, X.,** et al., Functionalized monolayers on ordered mesoporous supports. Science, 1997. 276(5314): p. 923-926.
10. **Wu, P.G., J.H. Zhu, and Z.H. Xu,** Template-assisted synthesis of mesoporous magnetic nanocomposite particles. Advanced Functional Materials, 2004. 14(4): p. 345-351.
11. **Barquist, K. and S.C. Larsen,** Chromate adsorption on amine-functionalized nanocrystalline silicalite-1. Microporous and Mesoporous Materials, 2008. 116(1-3): p. 365-369.
12. **Fryxell, G.E.,** et al., Design and synthesis of self-assembled monolayers on mesoporous supports (SAMMS): The importance of ligand posture in functional nanomaterials. Journal of Materials Chemistry, 2007. 17(28): p. 2863-2874.

Acronyms

AD	Polyaryloamidoxime
AGW	Artificial Groundwater
BT	Benzoylthiourea
DIM	Dihydroimidazole
DOE	Department of Energy
EFRC	Energy Frontier Research Center
EM	Environmental Management
EXAFS	Extended X-ray Absorption Fine Structure
MMSNs	Magnetic Mesoporous Silica Nanoparticles
MSNs	Mesoporous Silica Nanoparticles
NEUP	Nuclear Energy University Program
PAMAM	Poly(amidoamine) Dendrimer
PEG	Monomethylated Polyethylene Glycol
PEI	Polyethyleneimine
PP	Phosphonate
PPA	Phosphonate-amino
PPI	Poly(propylenimine) Dendrimer
QAM	Quaternary Ammonium
SRNL	Savannah River National Laboratory
XAFS	X-ray Absorption Fine Structure
XANES	X-ray Absorption Near-edge Structure

Intellectual Property

1. **Functionalized magnetic mesoporous silica nanoparticles for binding uranium from aqueous media,** Dien Li, Daniel I. Kaplan, Steven M. Serkiz, Sarah C. Larsen, Shani Egodawatte, SRS-15-004, Submitted on Jan. 18, 2016.

Total Number of Post-Doctoral Researchers

One Ph.D. Candidate researcher involved this project through our subcontractor, University of Iowa, and she is now a postdoc at University of South Carolina working for a DOE EFRC project.

Pu Anion Exchange Process Intensification

Project Team: K. M. L. Taylor-Pashow (Primary), T. C. Shehee, D. T. Hobbs, J. G. Pribyl (USC graduate student), B. C. Benicewicz (USC), W. P. Steckle (USC), M. Y. Coblyn (OSU)
Subcontractor: University of SC
Thrust Area: Nuclear Materials
Project Type: Standard
Project Start Date: October 1, 2015
Project End Date: September 30, 2017

This research is focused on improving the efficiency of the anion exchange process for purifying plutonium. While initially focused on plutonium, the technology could also be applied to other ion-exchange processes. The technology involves the use of open-celled polymeric foams, which have large surface areas available for solute sorption. The fluid passes through the large open pores of this material, allowing convection to be the dominant mechanism by which mass transport takes place. The materials are prepared from a high internal phase emulsion (HIPE) process and are then functionalized with poly(4-vinylpyridine) (PVP) through either a photoinitiated or thermally initiated polymerization method. The porous foam column provides advantages over the typical porous resin beads by eliminating the slow diffusion through the beads, making the anion-exchange sites easily accessible on the foam surfaces. Eliminating the diffusive mass transport increases the ion-exchange rate, and also results in much sharper elution profiles.

FY2016 OBJECTIVES

- **Preparation of polymeric foam materials containing poly(4-vinylpyridine) by University of South Carolina**
- **Column testing of new materials with Pu and comparison of uptake and elution to Reillex® HPQ resin**
- **Fabrication of microchannel array prototype device from poly(4-vinylpyridine)**

INTRODUCTION

The Pu anion-exchange process currently performed at the Savannah River Site for purification of Pu involves the use of a commercial poly(4-vinylpyridine) resin, Reillex® HPQ, in a packed bed column. This step in the Pu purification process represents a bottleneck due to the limited volume and flow rate which can be processed. Conventional ion-exchange resins are limited by mass transfer at the solution-particle interface and diffusion through the large granular resin particles. Convective mass transport through the packed bed is much faster than diffusive mass transport inside of the resin beads (Figure 1).

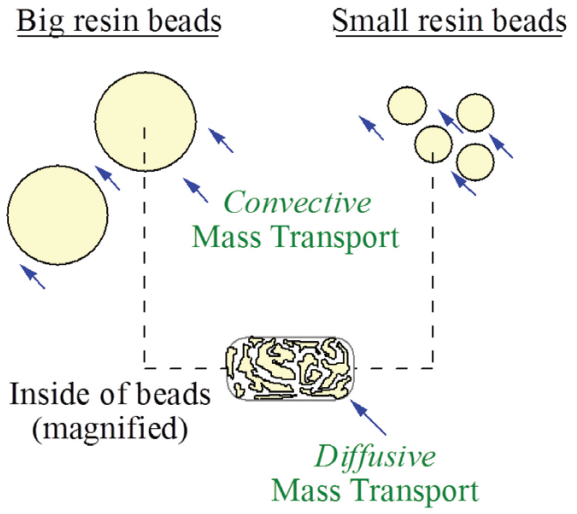

Figure 1. Convective versus diffusive mass transport

The initial focus of the project is on the Pu anion-exchange process, but once the technology is demonstrated for this application it is envisioned that it could be modified for other ion-exchange applications.

The diffusive mass transport can be somewhat reduced by reducing the size of the resin particles, however, this is limited by the increase in pressure drop across a column, which increases as the particle size of the resin decreases. This project seeks to overcome these limits through the use of a novel ion-exchange configuration, either an inverse column or a microchannel array. Both of these configurations overcome the slow diffusion through conventional granular resin particles. The inverse column, which is a porous foam monolith of material, has the advantage that it can be prepared in the appropriate size and shape to be a direct replacement for the granular resin in the current facility configuration. The microchannel arrays would allow for increased throughput by simply increasing the number of arrays deployed in order to reach the desired throughput. The initial focus of the project is on the Pu anion-exchange process, but once the technology is demonstrated for this application it is envisioned that it could be modified for other ion-exchange applications.

SRNL established collaborations with the University of South Carolina (USC) and Oregon State University (OSU) during the course of this project. USC provided the polymer synthesis expertise, and prepared foam monoliths grafted with poly(4-vinylpyridine) (PVP) chains to introduce quaternary amine functional groups as the anion-exchange sites. In high nitric acid concentrations (i.e., 7-8 M) the Pu is present as the hexanitrato anionic complex $[Pu(NO_3)_6]^{2-}$ which binds to the quaternary amine groups on the resin. This is the same chemistry utilized by the Reillex® HPQ commercial resin, which is a PVP resin, also containing quaternary amine groups. In addition, USC attempted to prepare plaques of crosslinked PVP that could be machined by collaborators at the OSU Microproducts Breakthrough Institute to prepare a microchannel array prototype including the same quaternary amine functional groups.

APPROACH

High internal phase emulsions (HIPE) are used as templates for the formation of the porous polymeric foam monoliths. HIPEs are water-in-oil emulsions in which the water phase comprises at least 76% of the emulsion by volume. The oil phase consists of the monomers used to prepare the polymer, crosslinking agents, and a surfactant. After polymerization and drying the resulting crosslinked polymer is an open-celled isotropic foam. The foam monoliths in this work are prepared from styrene crosslinked using divinylbenzene (DVB). Varying percentages of two different co-monomers were incorporated to allow for later grafting of poly(4-vinylpyridine) chains through either a photoinitiated polymerization or a thermally initiated polymerization. For the photoinitiated polymerizations vinylbenzyl chloride was included as the co-monomer. These foams were then subsequently treated with sodium thiosulfate to introduce free-radical initiation sites on the vinylbenzyl chloride sites.[1] The 4-vinylpyridine was then polymerized from these sites upon exposure to UV light, resulting in grafted polymer chains extending into the foam. For the thermally initiated polymerizations a monomer containing a thermal initiating group was prepared and incorporated into the foam synthesis. The 4-vinylpyridine was then polymerized onto the foam through a thermally initiated polymerization. The final PVP content of the foams can be tuned by varying the content of the initiating co-monomer in the foam preparation (graft density) as well as by varying the reaction conditions for the PVP grafting reaction (chain length).

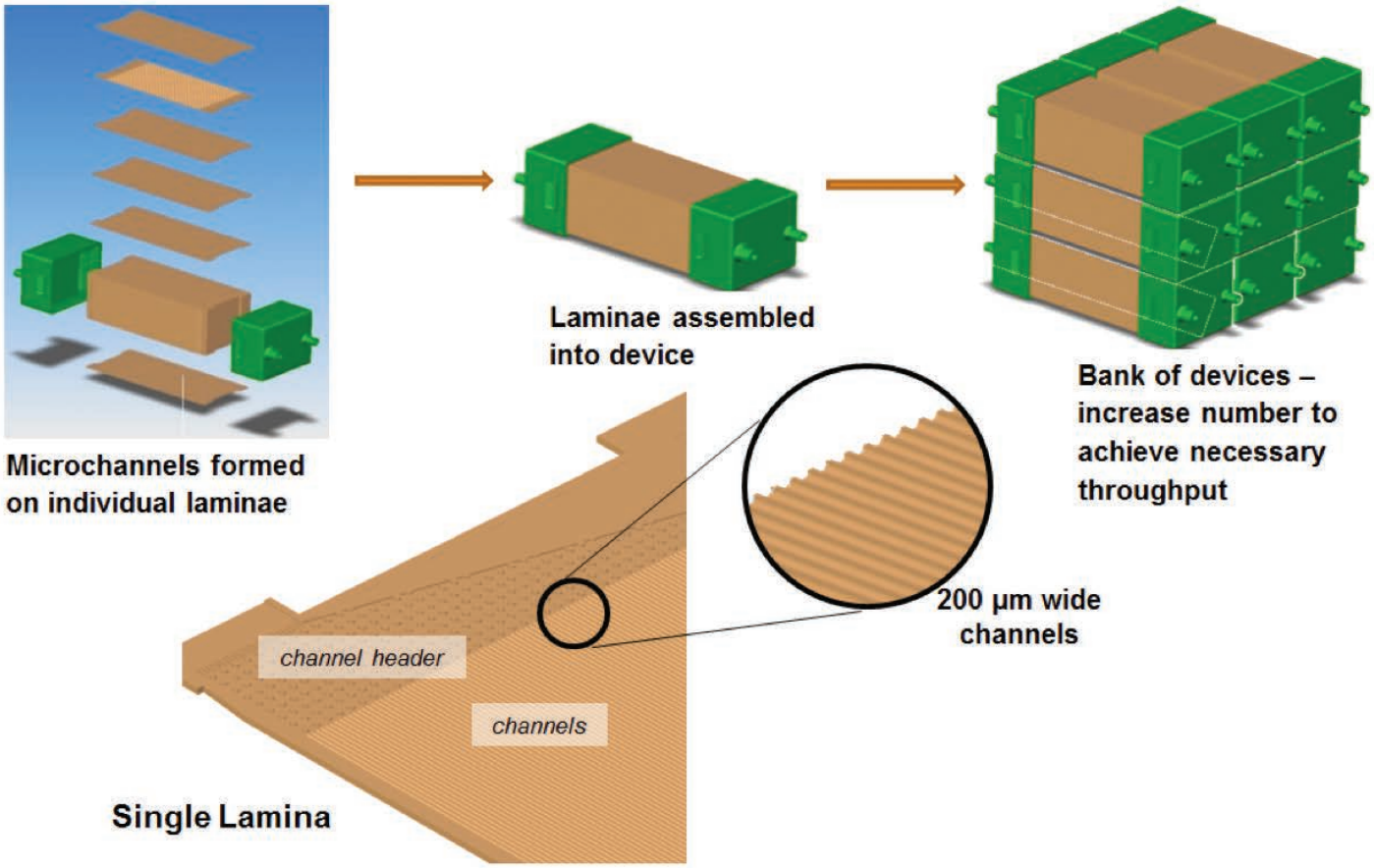

Figure 2. Example of a microchannel array device

In addition to the porous foam columns, we also attempted preparation of a microchannel array device. The approach taken for the microchannel array was to prepare the individual laminae from crosslinked PVP, which would then already contain the quaternary amine functional groups necessary for the Pu anion exchange process. Figure 2 provides a schematic of a microchannel array device. USC attempted preparation of plaques of PVP prepared using varying amounts of DVB as a crosslinker. Later attempts also included varying percentages of styrene co-monomer to reduce the amount of swelling observed when exposed to 8 M nitric acid. OSU attempted micromilling techniques to form the microchannels on the plaques provided by USC.

Figure 3. Plaque prepared from 30% VP, 50% styrene, and 20% DVB

RESULTS / DISCUSSION

Attempts at preparing plaques of crosslinked PVP for microchannel preparation were largely unsuccessful. It was found difficult to prepare a continuous plaque of material with no cracking or voids generated during the curing. Incorporation of the styrene co-monomer improved the properties of the plaque somewhat, but attempts at machining were largely unsuccessful due to existing cracks and additional cracking during the machining process. Figure 3 shows a photograph of a typical plaque.

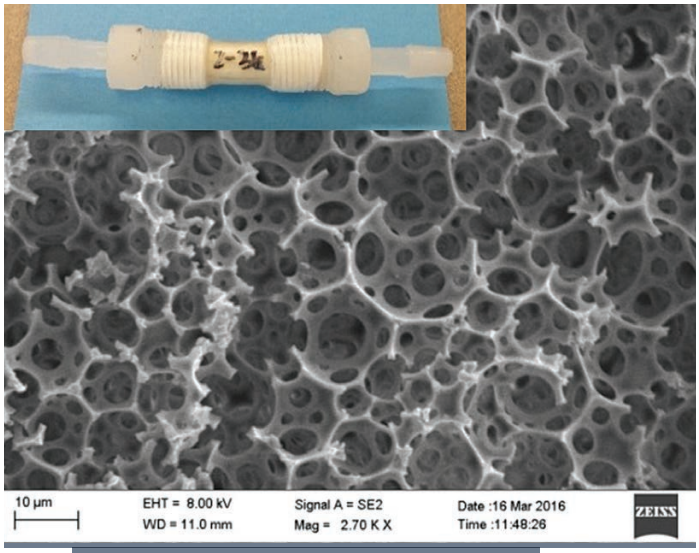

Figure 4. Photo of foam test column (inset) and SEM of foam pore structure

The preparation of porous foam columns was quite successful. Conditions for the HIPE polymerization to generate the porous foam were adjusted to obtain foams with large open voids to improve flow of solution through the materials. Several foam columns were prepared using the photoinitiated grafting of PVP. In order to improve penetration of the UV light though the entire foam for even grafting, the diameter of the columns was reduced. Table 1 (next page) provides a summary of characterization data for the columns prepared via the photoinitiated method. As can be seen, the N content varied from ~3.5 wt% to ~8.3 wt%. The N content correlates directly with the amount of PVP on the foam. The PVP grafting increased with increased reaction time, but results were not consistently reproducible. For comparison, the theoretical N content of the commercially available Reillex® HPQ resin is 8.75 wt%.

Several samples of foam columns prepared using the thermally initiated PVP grafting method were also characterized and evaluated. The thermally initiated method provides several advantages over the photoinitiated, mainly the fact that there is not an issue with penetration of UV light, and also, that it is a controlled polymerization, which should result in more predictable and reproducible amounts of grafted PVP with reaction time. A summary of relevant data for the thermally initiated samples is also included in Table 1. The N content in these samples is reported as "Net N Content", as the starting foam contains some N due to the co-monomer. The "net" N content shows the N content attributed to the grafted PVP.

Table 1. P Summary of Foam Column Data

Photoinitiated Samples				
Sample ID	**N Content (%)**	**Weight Gain (%)**	**Reaction Time (h)**	**Pu Capacity (g Pu/g)**
JP-1-270 Unmod.	0	0	0	0.0003
JP-1-270	3.5	34	6	0.019
JP-1-282A	5.4	70	10.5	0.044
JP-1-282B	7.0	77.2	10.5	0.060
JP-2-6	8.32	87	21.5	0.056
JP-2-24	6.85	92	23.5	0.035
Thermally Initiated Samples				
Sample ID	**Net N Content (%)**	**Weight Gain (%)**	**Reaction Time (h)**	**Pu Capacity (g Pu/g)**
JP-1-297	9.59	265	21.5	NM
JP-2-31	9.65	318	22	NM
JP-2-36	9.81	366	25	0.185
JP-2-55	10.33	455	25	Results Pending
JP-2-68	10.20	433	25	
JP-2-73	10.54	419	25	

Samples of both types of columns were tested for Pu uptake and elution, and the Pu capacities were determined based on the amount of Pu that was eluted from the columns. A sample of Reillex® HPQ was also tested in parallel for comparison. For the Reillex® testing, a small glass column was packed with Reillex® HPQ resin. The gravimetric Pu capacities are included for each column tested in Table 1. For comparison the Reillex® HPQ Pu capacity as measured in our testing was 0.038 g Pu/g resin. Many of the columns outperformed the Reillex® on a gravimetric basis, partly due to the extremely low densities of the porous foams (average of 0.091 g/cm^3 pre-functionalization). On a volumetric basis, the highest performing foam column (JP-2-36) had a capacity of 0.028 g Pu/mL, compared to 0.034 g Pu/mL for the Reillex® HPQ. Although we did not exceed the volumetric capacity of the Reillex® HPQ, we came close with our first sample of material prepared using the thermally initiated method, indicating there is still room for improvement. In addition to the Pu capacities of the materials, another important feature, and improvement of the foams over typical resin beads, is the elution profile, which is much sharper in the foam material due to the lack of diffusion of Pu from large resin beads during elution. The elution profiles for several samples are shown in Figure 5. As can be seen in the figure, the elution is much sharper from the foam columns, as they do not exhibit the "tail" that is seen in the Reillex® HPQ elution. The elution for the foam columns was essentially complete in less than 2.5 bed volumes; whereas the tail from the Reillex® HPQ elution extended past 4 bed volumes. The best performing column (JP-2-36) reached a Pu concentration of greater than 40 g/L in the hearts cut; which represents concentration by greater than 10x from the feed solution.

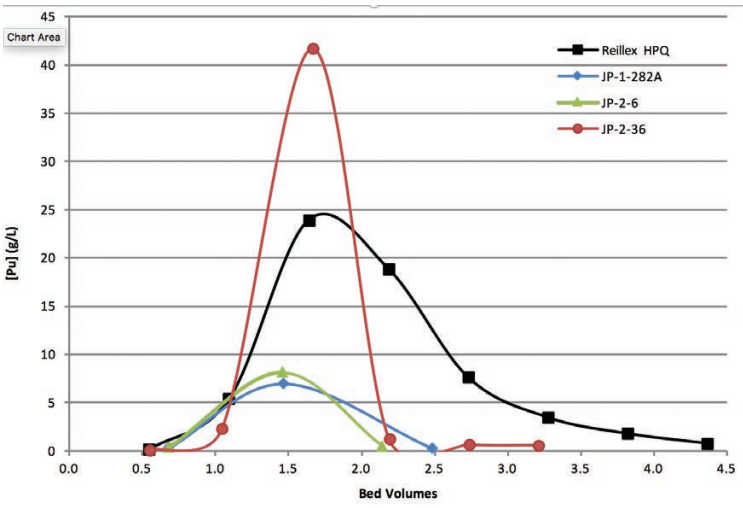

Figure 5. Elution profiles of select foam column samples compared to Reillex® HPQ

FY2016 ACCOMPLISHMENTS

- **Successfully prepared samples of PVP modified porous foam columns using 2 different polymerization techniques for grafting of the PVP**
- **Demonstrated improved gravimetric Pu capacities over the commercial Reillex® HPQ resin**
- **Approached the Pu volumetric capacity of the commercial Reillex® HPQ resin with the best performing foam sample**
- **Demonstrated sharper elution profiles with the foam columns when compared to Reillex® HPQ**

FUTURE DIRECTIONS

- Optimization of the thermally initiated method for preparing PVP functionalized foam columns
- Scale-up of foam column preparation
- Investigate alternative approach to microchannel array device preparation utilizing photochemically etched stainless steel as the lamina material

Publications/Presentations

1. **"High-internal phase emulsion foams with surface-grafted poly(4-vinyl pyridine) for plutonium sorption"** J. Pribyl, B. Fletcher, W. Steckle, K. Taylor-Pashow, T. Shehee, and B. Benicewicz, presented at the 252nd ACS National Meeting, Philadelphia, PA, August 21, 2016.
2. **"Porous Foam Columns for Plutonium Anion Exchange"** K. M. L. Taylor-Pashow, T. C. Shehee, D. T. Hobbs, J. G. Pribyl, and B. C. Benicewicz, to be presented at the Nineteenth Symposium on Separation Science and Technology for Energy Applications, Gatlinburg, TN, October 11, 2016.

References

1. **B. C. Benicewicz, G. D. Jarvinen, D. J. Kathios, and B. S. Jorgensen, J. Radioanal.** Nucl. Chem. 1998, 235, 31-35.

Acronyms

DVB	Divinyl Benzene
HIPE	High Internal Phase Emulsion
NM	Not Measured
OSU	Oregon State University
PVP	Poly(4-vinylpyridine)
USC	University of South Carolina
UV	Ultraviolet

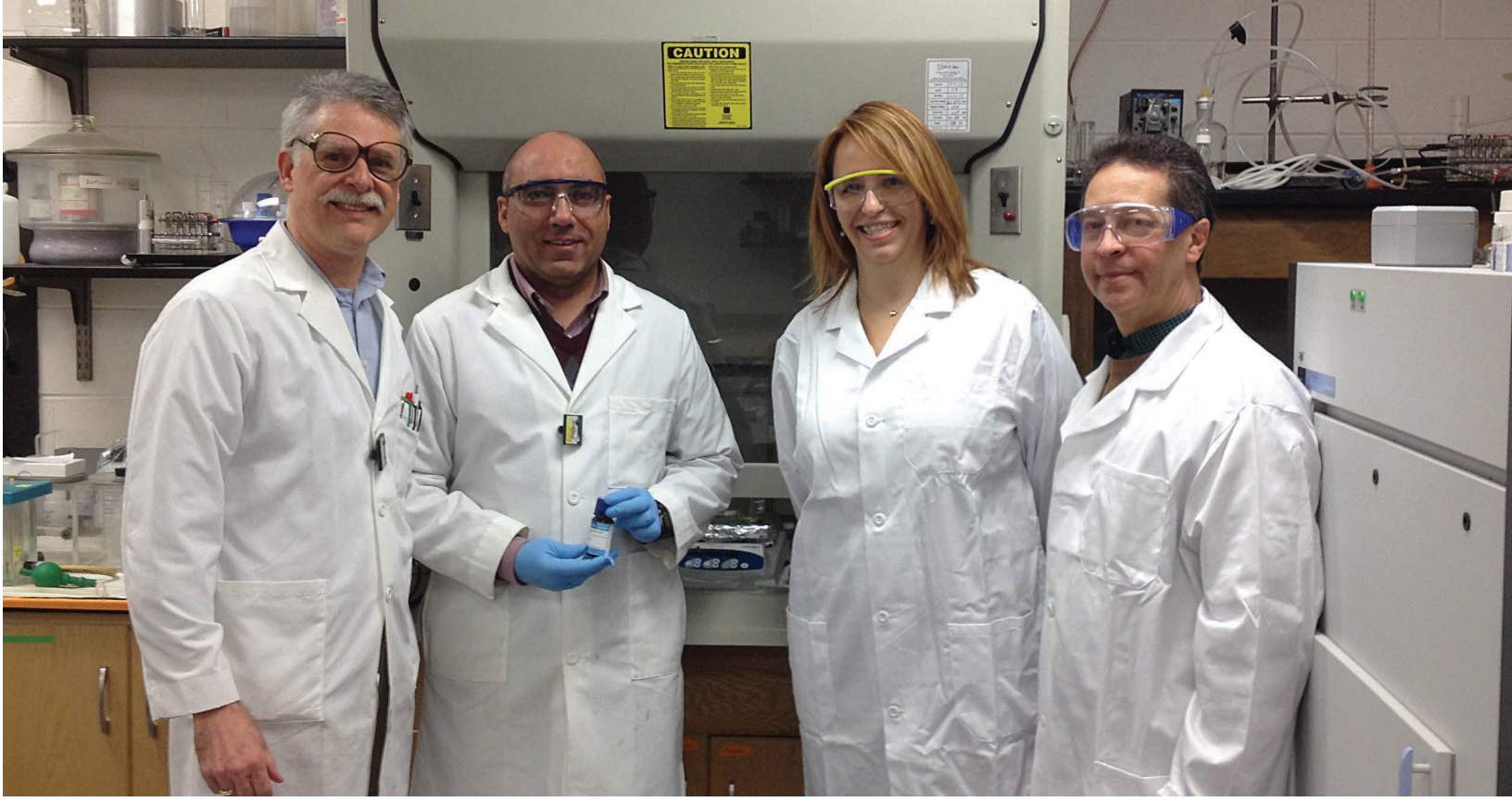

Problematic Contaminants (Tc-99, Hg) For Tank Waste Treatment and Disposal

Project Team: M. M. Reigel (Primary), T. B. Peters, S. H. Reboul, D. P. DiPrete, and T. A. DeVol
Subcontractor: Clemson University (T. A. DeVol)
Thrust Area: Environmental Stewardship
Project Type: Standard
Project Start Date: October 26, 2015
Project End Date: September 30, 2017

Processing and retention of problematic contaminants (Tc-99, Hg) in high-level tank waste has been an issue throughout the DOE complex, due to the inherent mobility of these contaminants in environmental media and the associated environmental risks. The goal of this project is to design improved processes for removing the contaminants from tank waste and/or retaining the contaminants in the final wasteform (such as in the Saltstone wasteform at SRS). Synthesis, evaluation and testing of two novel extractant media for removing technetium from salt tank waste was performed in FY16, with one new technetium extractant (methyldioctylamine resin) showing promise for outperforming the current established technetium removal champion (Eichrom TEVA). Completion of the technetium removal testing will occur in FY17, along with evaluation of a new silica-based MDOA fixing agent to increase retention of technetium in the Saltstone wasteform. Plans for addressing removal/retention of mercury will also be developed in FY17.

FY2016 OBJECTIVES

Synthesis of methyldioctylamine (MDOA) and triethylamine (TEA) technetium removal polystyrene resins

Batch contact decontamination testing of Tc-99 removal and kinetics under salt simulant conditions (comparing MDOA & TEA resins to commercially-available resins)

Synthesis of MDOA technetium retention silica fixing agent for application in Saltstone wasteform

Decontamination of SRS/Hanford aqueous waste streams, improved binding of technetium within SRS Saltstone grout, and remediation of contaminated saltwater near the Fukushima reactor are examples of promising applications.

INTRODUCTION

At DOE waste sites, ^{99}Tc is typically a primary environmental risk driver owing to its high fission yield, high mobility, and long half-life. Performance Assessments performed at the Savannah River Site identified ^{99}Tc as a principal radionuclide contributing potential long-term beta-dose, both from stabilized waste residue remaining after tank cleaning and from stabilized salt waste immobilized in the cement-based wasteform (Saltstone). At the Hanford reservation, research has proceeded in the area of technetium removal, in an effort to reduce concentrations of ^{99}Tc in existing waste, and ultimately to reduce potential releases of ^{99}Tc into the environment after disposition and closure.

Most of the tested technetium extraction agents are either eluted or back-extracted after capture, with the objective of regenerating the extraction medium for further repeated use. An alternative is to use an extraction agent that has such high affinity for technetium that it retains it over the long-term and can double as a binding agent within the final stable wasteform. Recent research[1] has identified two tertiary amines that hold promise for such potential use—methyldioctylamine (MDOA) and triethylamine (TEA). Initial results suggest that the extraction efficiencies of the MDOA and TEA are high relative to other established extractants, and that moderately high concentrations of acid and base (4 M nitric acid and 4 M sodium hydroxide) have little impact on the holding power of the extractant. The proposed LDRD project will quantify the removal/retention efficiencies of the MDOA and TEA, using simulated and real-waste solutions.

The science being investigated in this project has potential applications to multiple DOE waste sites and to environmental remediation efforts associated with damaged nuclear reactor facilities such as those at Fukushima and Chernobyl. Development of a superior technetium removal strategy (and/or wasteform retention strategy) utilizing MDOA and/or TEA would be potentially marketable to such applications. Following successful demonstration of the strategy, external funding would be targeted via facility- specific proposals. Decontamination of SRS/Hanford aqueous waste streams, improved binding of technetium within SRS Saltstone grout, and remediation of contaminated saltwater near the Fukushima reactor are examples of promising applications.

APPROACH

MDOA and TEA were incorporated into polystyrene resins via amination, to facilitate solid-liquid phase extraction testing. Alkaline salt simulant containing Tc-99 and other common radionuclides (I-129, Cs- 137, uranium isotopes, Np-237, and plutonium isotopes) was prepared and used to evaluate the technetium decontamination efficacies of the MDOA and TEA resins against those of TEVA resin (the “gold standard” of technetium removal resins) and conventional anion exchange resin. Batch contact decontamination tests were conducted over a 24 hour period, with sampling and analysis performed on salt simulant aliquots removed at times of 1, 4, 8, and 24 hours. The salt simulant aliquots were analyzed for Tc-99 and other key constituents, to quantify constituent decontamination factors as a function of time.

MDOA was also incorporated into a silica support via amination, for use in future wasteform technetium retention tests.

RESULTS / DISCUSSION

Technetium decontamination factors (DFs) for the salt simulant tests are plotted as a function of contact time in Figure 1. As shown in the figure, at contact times greater than or equal to four hours, the MDOA resin removed significantly more technetium than the other resins, including the "gold standard" TEVA resin. At a contact time of twenty-four hours, the DF for the MDOA resin (DF=50) was about twice that of the TEVA resin (DF=26), about three times that of the TEA resin (DF=15), and about seven times that of the conventional anion exchange resin (DF=7.3). As shown in Figure 1, the kinetics of the MDOA resin reactions were slower than those of the other resins, as evidenced by the fact that the MDOA DF was highest at twenty-four hours and lowest at one hour, while the DFs of the other resins were relatively constant over the range from one to twenty-four hours. To better understand the kinetics of the MDOA resin, future technetium removal testing should be performed: a) at contact times greater than twenty-four hours (this will identify the equilibrium time of the MDOA resin; and b) using a methacrylate-based MDOA resin (which has the potential to improve kinetics due to the higher porosity).

In contrast to the measurable technetium DFs identified for each of the resins, none of the resins removed significant amounts of the other salt waste constituents, including iodine, cesium, uranium, neptunium, and plutonium.

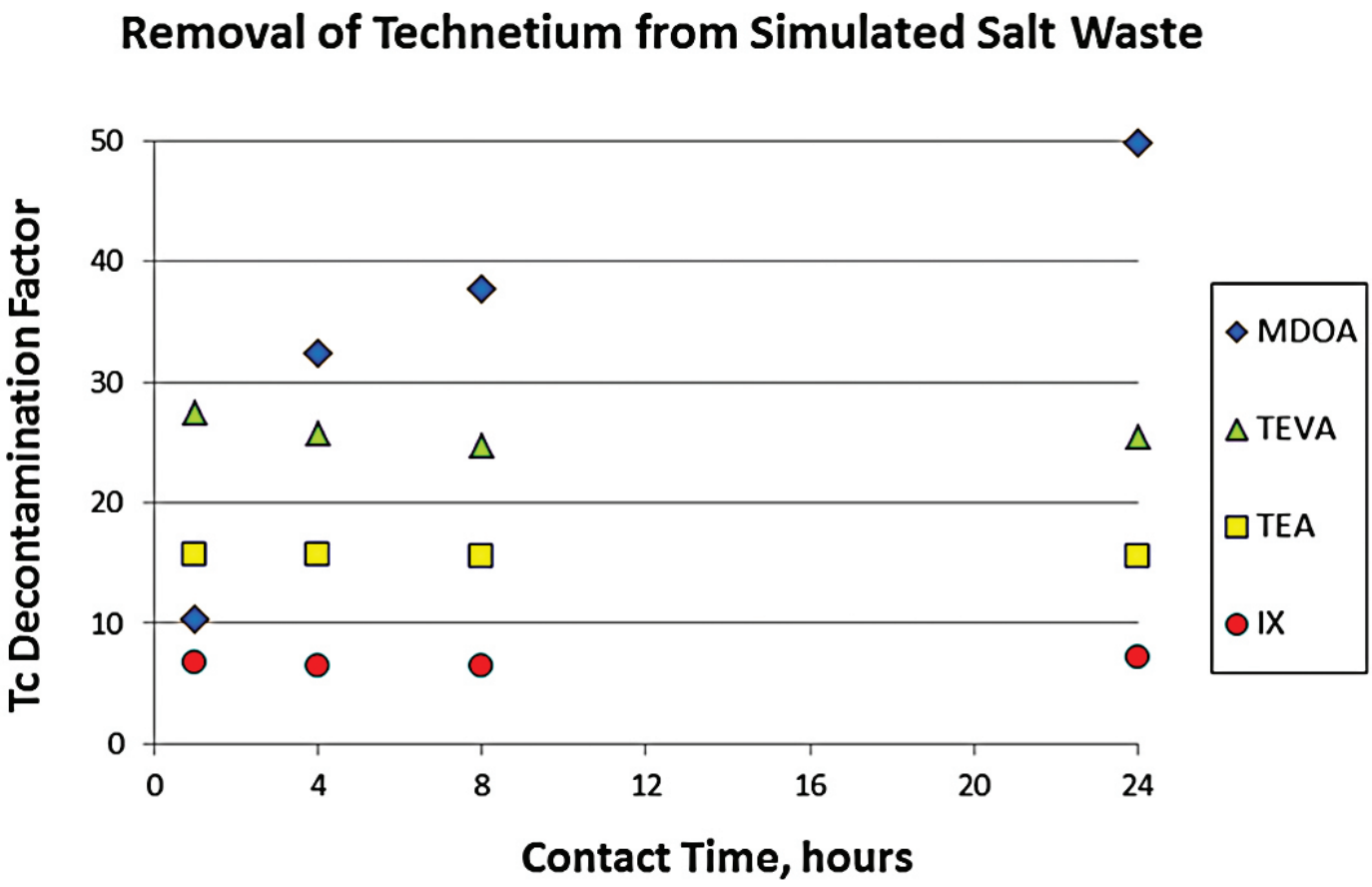

Figure 1. Technetium Decontamination Factors as a Function of Resin Contact Time

FY2016 ACCOMPLISHMENTS

Successfully synthesized two new technetium removal resins (MDOA styrene resin and TEA styrene resin), and completed initial caustic side testing of them in comparison to two commercially-available removal resins

Demonstrated that the MDOA styrene resin removes significantly more technetium from simulated caustic salt waste than the reigning commercially-available technetium extraction resin (Eichrom TEV A)

Successfully synthesized a new technetium wasteform fixing agent (MDOA silica medium) for evaluation in FY17 technetium wasteform retention testing

FUTURE DIRECTIONS

- Complete salt simulant kinetics testing of MDOA resin to determine maximum Tc decontamination factor, time requirements, and the corresponding Tc distribution coefficient
- Perform Saltstone wasteform Tc retention testing using silica-based MDOA fixing agent
  >> Quantify retention aid effectiveness
  >> Determine optimal usage conditions and impact of condition variability on effectivenes
- Pursue methacrylate-based MDOA resin to accelerate Tc removal equilibrium
  >> Perform kinetics and effectiveness testing
- Develop plan for pursuing development/testing of Hg removal/retention technologies

References

1. **Sleiman, A. F., A. Samadhi, S. M. Hasson, E. H. Bora, and T. A. Devall,** "Preparation of Polymer-Coated, Scintillating Ion-Exchange Resins for Monitoring of 99Tc in Groundwater," Anal. Chem. 83, 4759-4766, 2011.

Acronyms

MDOA	Methyldioctylamine
TEA	Triethylamine
DF	Decontamination Factor

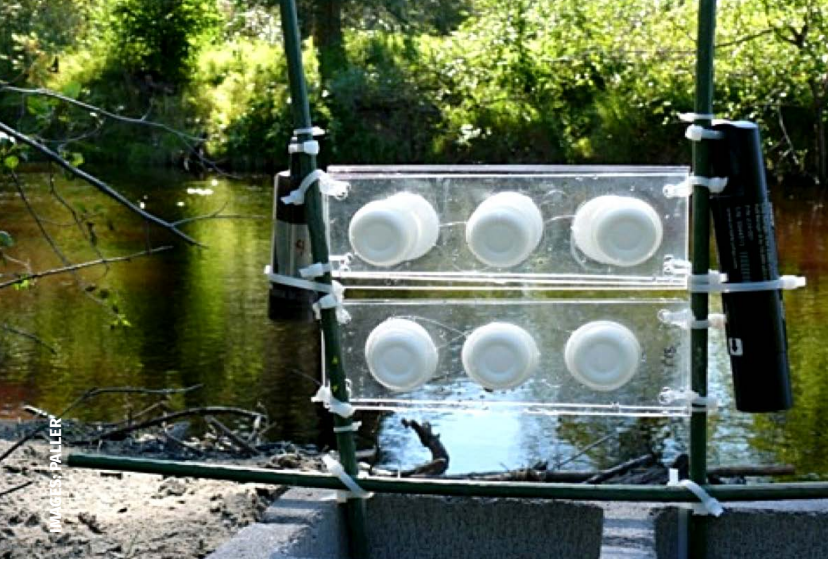

IMAGES: PALLER

IMAGES: PALLER

Use of Diffusive Gradients in Thin Films (DGT) As an Alternative Monitoring Tool for Inorganic Environmental Contaminants

Project Team: Michael Paller (SRNL), Anna Knox (SRNL), Wendy Kuhne (SRNL), Nancy Halverson (SRNL), Michele Harmon (USCA)
Subcontractor: University of Georgia
Thrust Area: Environmental Stewardship
Project Type: Standard
Project Start Date: October 1, 2015
Project End Date: September 30, 2017

DGT is a type of passive sampler that consists of a gel-layer that selectively binds to contaminants and a diffusion gel that admits molecules that are available and toxic to organisms. DGT has potential to improve and modernize environmental monitoring of surface and ground water on DOE sites by reducing labor and analytical costs and providing better data for calculating risks. Our research included laboratory studies that explored the relationships between DGT results and the bioaccumulation and toxicity of metals to aquatic organisms and field studies that investigated the performance of DGT in a wetland environment. Results show that DGT can mimic contaminant uptake by aquatic organisms and help establish a basis for the refinement of DGT methods for cost-effective environmental monitoring. Planned work includes the development of DGT methods for the measurement of toxic methylmercury in aquatic ecosystems and the measurement of radionuclides of interest on DOE sites.

FY2016 OBJECTIVES

- **Measure environmental metal concentrations with DGT passive samplers and verify these measurements by comparing them with contaminant uptake by fish and other biota**
- **Compare DGT measurements with measurements made by conventional methods**
- **Compare DGT measurements with biological uptake by organisms**
- **Determine how differences in water chemistry affect the performance of DGT**

INTRODUCTION

Traditional environmental monitoring programs for surface and ground water require collecting, processing, and analyzing samples from a variety of environmental media. Data interpretation can be difficult because of differences in sample size, heterogeneity within and among media, and failure to measure the chemical species that are bioavailable and toxic. Recently, passive samplers are being investigated as efficient and cost-effective alternatives to traditional methods. Passive samplers rely on the unassisted molecular diffusion of analytes through a diffusive surface onto an adsorbent as a result of differences in concentration between the two media. They require no electricity, have no moving parts, and are simple to use. The adsorbed analytes are desorbed off the adsorbent and analyzed; e.g., by inductively coupled plasma mass spectrometry. Diffusive Gradients in Thin Films (DGT) is a type of passive sampler that consists of an absorbent gel that selectively binds to specific contaminants and a diffusion gel that selectively admits analyte molecules (Davison and Zhang 1994, Van der Veeken et al. 2010) (Figure 1). Frick's law is used to calculate the environmental concentrations of elements based on the concentration of the element in the absorbent gel, device configuration, analyte diffusion coefficients, deployment time, and other factors. DGT can be deployed in surface water, ground water, submerged sediments, and saturated soils to measure metals and radionuclides. It tends to measure dissolved and labile chemical forms of contaminants that are available to organisms and, in some respects, can be viewed as "virtual organisms" that absorb contaminants in a manner analogous to fish and other aquatic organisms.

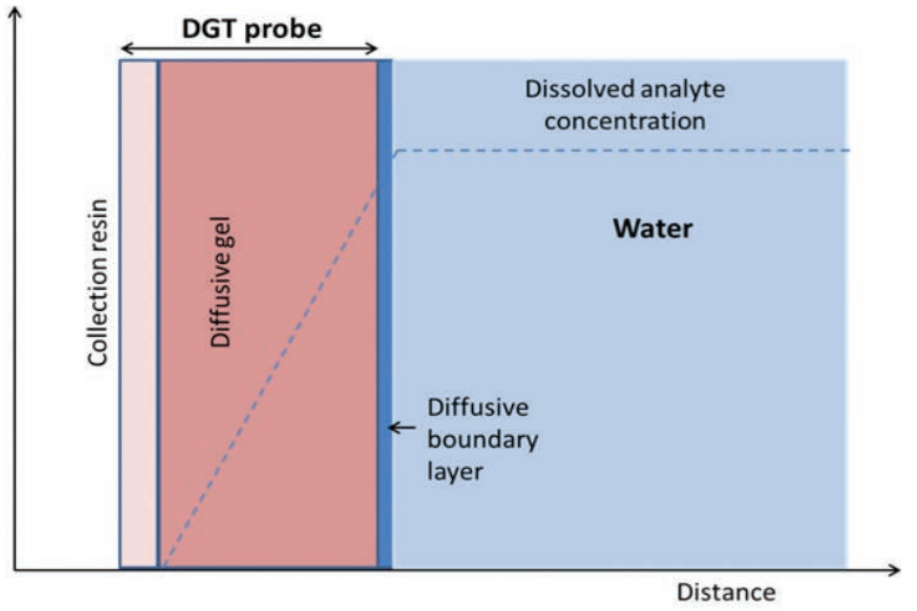

Figure 1. Schematic cross-section through a DGT probe showing a steady state concentration gradient between an analyte in solution and a collection resin

Potential advantages of DGT include:

>> **Cost Savings.** Passive samplers can reduce costs because they combine sampling, sample processing, selective analyte isolation, and analyte pre-concentration.

>> **Realism.** Passive samplers theoretically measure the dissolved and labile chemical species that are available and toxic to organisms (the bioavailable fraction).

>> **Sensitivity.** Passive samplers make it possible to measure very low but significant levels of contaminants because they pre-concentrate and maximize the amount of analyte sampled.

>> **Representativeness.** Passive samplers yield a time-integrated average concentration that is more representative of prevailing contaminant levels than the "snapshot" typically produced by grab samples.

>> **Quality Assurance.** Data from passive samplers are consistent and comparable, which facilitates spatial comparisons, trend assessment, and adequate replication for robust statistical testing.

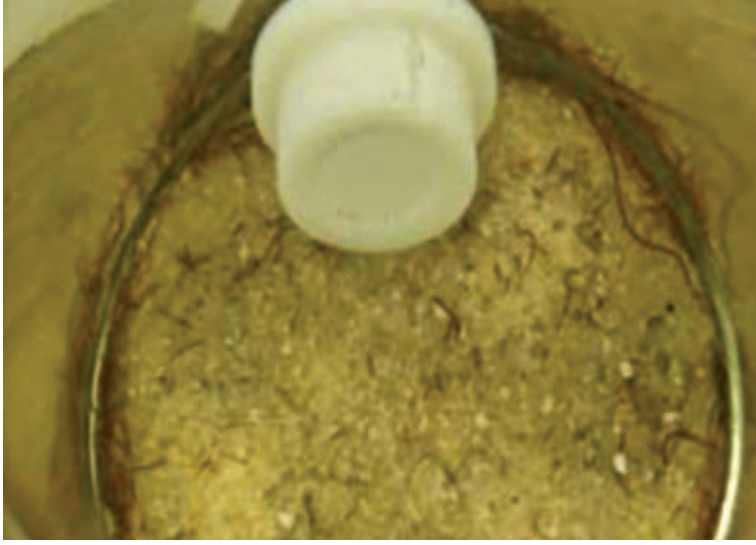

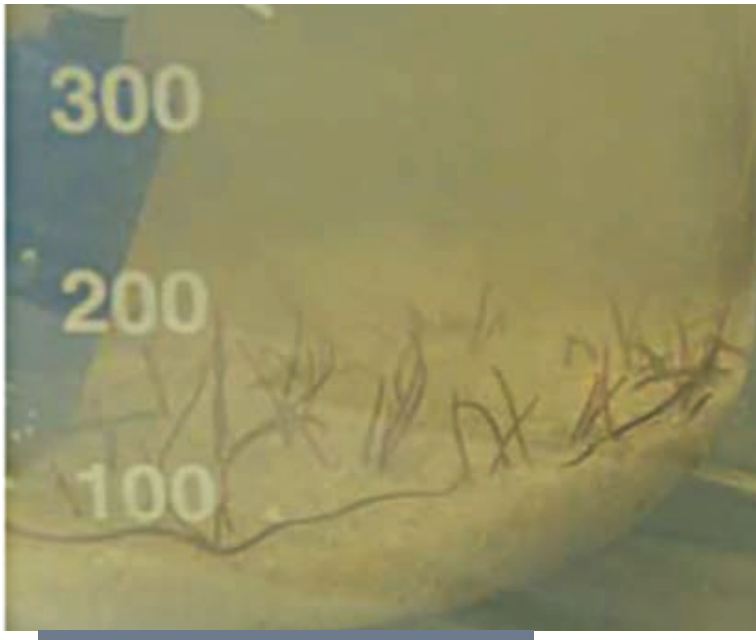

Figure 2. Experimental setup (left). DGT probe (top right). Lumbriculus (bottom right)

APPROACH

Task 1: Laboratory study designed to assess the ability of DGT to measure the bioaccumulation of metals in the aquatic invertebrate Lumbriculus variegatus.

Hypothesis: The uptake of metals by DGT probes will mimic the uptake of metals by an aquatic invertebrate.

Surface water was collected from two sources and spiked with heavy metals to produce different levels of contamination. Experiments were conducted with dissolved copper alone and with combinations of dissolved metals (cadmium, chromium, cobalt, copper, lead, nickel, and zinc). Multiple individuals of Lumbriculus variegatus, an aquatic worm, were added to beakers with different concentrations of metals (Figure 2). Metal levels were measured with DGT probes placed in the beakers and with conventional methods of water analysis. Other water chemistry variables included pH, hardness, alkalinity,etc. were also measured. After 10 days of exposure, Lumbriculus variegatus were harvested and analyzed for body burdens of metals, and the data were analyzed to answer the following questions: 1) how do DGT measurements compare with measurements made by established methods, 2) how do metal measurements made by both methods compare with biological uptake by aquatic organisms?

Task 2: Wetland field study—using DGT to measure bioavailable metals in A-01 Wetland Treatment System (WTS).

Hypothesis: DGT probes will accurately measure a known contamination gradient and provide an accurate estimate of the bioavailable metal fraction.

The A-01 WTS is designed to remove copper and other metals from the A-01 effluent. Effluent passes from the A cell to the B cell resulting in a gradient of decreasing metal contamination along the effluent flow path (Knox et al. 2006) (Figure 3). DGT probes were placed at intervals along the gradient and compared with water, sediment, and fish samples collected at the same locations:

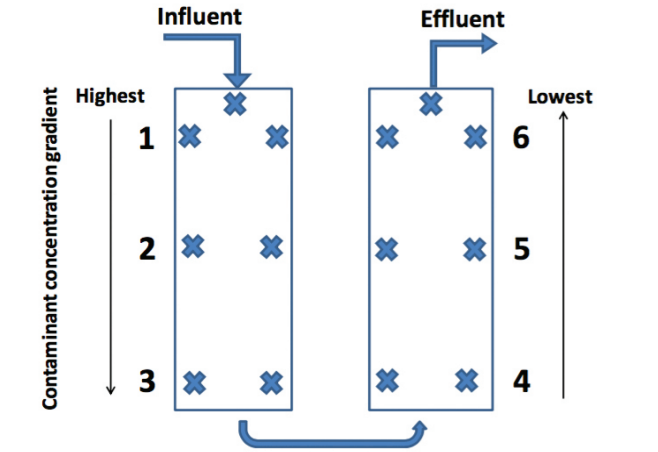

Figure 3. Wetland cells 4A and 4B. Sample locations are marked with an "X"

Samples included

>> DGT water probes (for Cu, Pb, Zn, Cd) suspended in water for 24 & 168 hrs
>> DGT sediment probes embedded in sediments for 24 hrs
>> Sediment cores – one inch diameter cores to a depth of 3 inches
>> Water samples – surface water grab samples measured for total metals
>> Indigenous fish collected from wetland.

DGT results were analyzed to see if they conformed to the expected contamination gradient, were comparable to samples collected by other methods, and appeared to measure bioavailable metals fractions within the WTS.

Task 3: Laboratory toxicity study: assessing effects of water quality on DGT measurements of bioavailable metals (Copper and Zinc)

Hypothesis: DGT measurements of metal toxicity in different types of water will be more similar than measurements based on conventional methods because DGT measurements exclude metal species that are not bioavailable.

Figure 4. Toxicity testing in climate controlled test chamber at the University of South Carolina (Aiken)

Metal toxicity is known to be affected by water hardness and the amount of dissolved organic matter in the water.

The toxicity of copper and zinc to *Ceriodaphnia dubia* was calculated for the following:

>> Simulated SRS water with low hardness and low dissolved organic carbon (DOC)
>> Simulated SRS water with low hardness and added DOC
>> High hardness water with low DOC
>> High hardness water with added DOC

Lethal metal concentrations (48 hr LC50s) were calculated using 1) conventional methods (based on total metal levels measured in the water) and 2) DGT measurements of bioavailable metals (Figure 4).

RESULTS / DISCUSSION

Task 1: Laboratory study designed to assess the ability of DGT to measure the bioaccumulation of metals in the aquatic invertebrate *Lumbriculus variegatus.*

Copper concentrations measured by DGT probes were strongly correlated with copper uptake by *Lumbriculus* held in the beakers for 10 days (Figure 5). This relationship persisted over dissolved copper concentrations ranging from several parts per billion (ppb) to 800 ppb and occurred in relatively hard Savannah River water as well as soft, acidic Tinker Creek water. Copper accumulated in the DGT probes over time paralleling the accumulation in copper over time that occurred in *Lumbriculus* (Figure 6). Copper concentrations measured by DGT were strongly correlated with copper concentrations in water measured by traditional methods of analysis.

Results with mixtures of seven dissolved metals were generally similar to those reported for copper: Pearson correlations between metal uptake by *Lumbriculus* and metal concentrations measured by DGT probes were strong and statistically significant, ranging from 0.68 to 0.94 ($p<0.05$). DGT probes and *Lumbriculus* exhibited similar affinities for different metals, with the exceptions of cobalt and nickel, which were taken up more strongly by the DGT probes than by *Lumbriculus.*

These results show that the metal concentrations measured by DGT are strongly correlated with metal uptake by the aquatic invertebrate, *Lumbriculus,* and that metals accumulate in DGT probes over time paralleling their accumulation in aquatic organisms. This supports the use of DGT as a biomimetic monitoring tool.

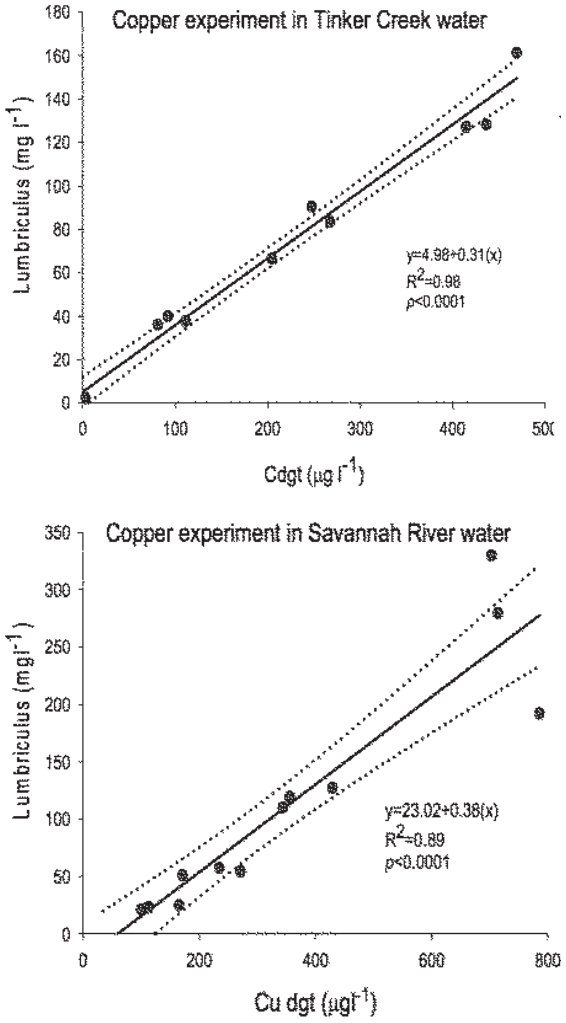

Figure 5. Copper levels in *Lumbriculus* vs. copper levels measured by DGT (Cu dgt)

Figure 6. Uptake of copper over time in *Lumbriculus* and DGT probes.

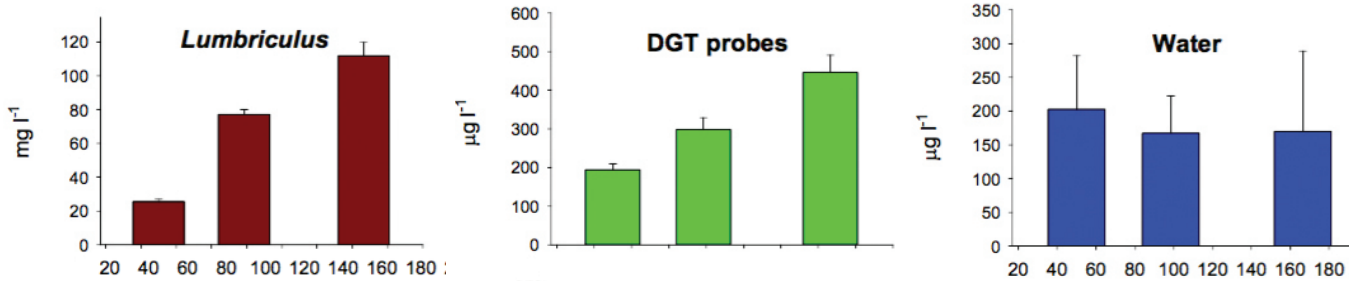

Task 2: Wetland field study—using DGT to measure bioavailable metals in A-01 Wetland Treatment System (WTS).

Copper (Cu), lead (Pb), and zinc (Zn) concentrations measured by DGT water probes generally declined as influent traveled from the beginning of the effluent flow path (indicated by 1 in Figure 7) to the end of the effluent flow path (indicated by 6 in Figure 7). In contrast, metal concentrations measured by conventional water samples exhibited this pattern only for copper. These results suggest that metal concentration measurements derived from DGT water probes were better than metal concentration measurements derived from conventional water samples at reflecting the contamination gradient previously shown to be present in the WTS (Knox et al., 2006). Metal concentrations measured by DGT probes were lower than metal concentrations measured in water for Cu and Zn, likely reflecting reduced bioavailability of these metals in the wetland and pointing out the potential ability of DGT to measure potentially toxic metal species while excluding metal species unlikely to have biological effects. These results will be verified when metal concentration data for fish and sediments are obtained from our contract laboratory and analyzed in October 2016.

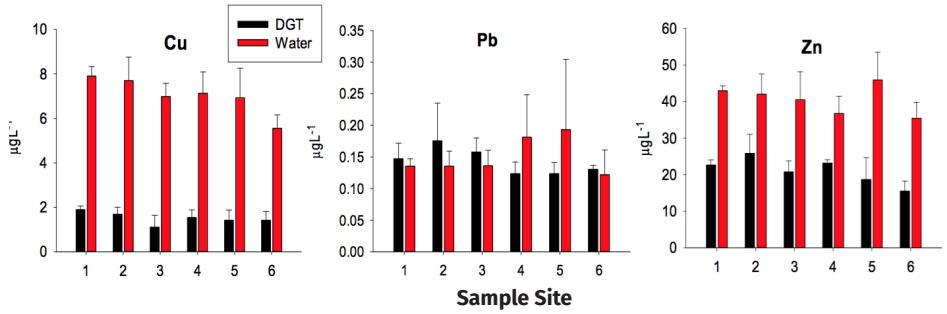

Figure 7. Metal concentration data in the A-O1 WTS measured by DGT water probes and by water grab samples analyzed for total metals

Task 3: Laboratory toxicity study: assessing effects of water quality on DGT measurements of bioavailable metals (Copper and Zinc)

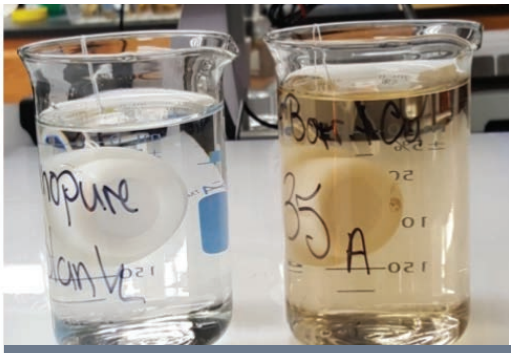

Figure 8. Water with (right) and without (left) the addition of humic acids. DGT probes are suspended in the beakers.

Lethal concentrations (LC50s) for copper were far higher in water with humic acids (dissolved organic matter) than in water without humic acids (Figures 8 and 9). The effects of hardness were weaker than the effects of humic acids; however, the LC50 for copper was higher in hard water without humic acids than in soft water without humic acids (Figure 9). The lowest LC50 was in water that was low in hardness and lacked humic acids, reflecting a lack of ligands of any type that could bind with copper and reduce its bioavailability and toxicity. In contrast, the effects of humic acids and hardness on zinc toxicity were much weaker than observed with copper suggesting that dissolved ligands have less influence on the toxicity of this element.

The presence of ligands that affect metal bioavailablity can result in large variations in apparent toxicity. We hypothesize that LC50s based on DGT results will be more consistent than LC50s based on water measurements because DGT measures only bioavailable forms of Cu. In contrast, LC50s based on measurements of total copper in water include both available and unavailable forms of metals, the latter of which do not contribute to toxicity but influence the results of conventional toxicity tests. When DGT results from our contract laboratory become available (mid-October 2016) we will be able to complete the testing of our hypothesis.

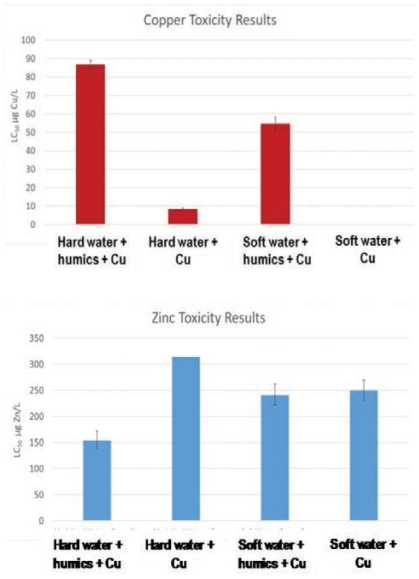

Figure 9. Relationship between the toxicity of metals and water quality for copper and zinc

FY2016 ACCOMPLISHMENTS

- Metal concentrations measured by DGT water probes were strongly related to metal uptake by an aquatic invertebrate
- Metal uptake over time by DGT probes paralleled metal uptake over time by an aquatic invertebrate
- DGT measurements in a wetland treatment system corresponded with expected gradients of contamination and appeared to measure bio available contaminant fractions more accurately than conventional sampling methods
- Laboratory bioassay studies show distinct influences of water chemistry on copper toxicity; Data under analysis will demonstrate whether these influences are accurately reflected by DGT results

FUTURE DIRECTIONS

- Complete the final stages of Tasks 2 and 3 (described previously)
- Development of a method for measuring mercury (Hg) species using Hg-Diffusive Gradients in Thin film (Hg-DGT) technology
- Adapt an extraction method developed by Gao et al. (2014) for 3-mercaptoproply silica so that it can be used for Spheron-Thiol resin, thus providing a new, cost effective method for measuring methylmercury and mercury speciation
- Development and application of DGT for assessment of environmental contamination by radionuclides; The application of DGT to radionuclides is experimental and has not seen widespread use. DGT probes could be developed for the cost-effective measurement of environmental contamination with radionuclides

References

1. **Davison, W., Zhang, H. 1994. I**n situ speciation measurements of trace components in natural waters using thin-film gels. Nature 367: 546-548.
2. **Gao, Y. S.De Craemer, W. Baeyens. 2014.** A novel method for the determination of dissolved methylmercury concentrations using diffusive gradients in thin films technique. Talanta 120: 470– 474.
3. **Knox, A.S., M.H. Paller, E.A. Nelson, W.L. Specht, N.V. Halverson, and J.B. Gladden. 2006.** Metal distribution and stability in constructed wetland sediment. Journal of Environmental Quality 35:1948-1959.
4. **Van der Veeken, P.L.R., Van Leeuwen, H.P., 2010.** DGT/DET gel partition features of humic acid/metal species. Environ. Sci. Technol., 44: 4253-4257.

Acronyms

DGT	Diffusive Gradients in Thin Films
DOE	Department of Energy
Hg	Mercury
Hg-DGT	Mercury-Diffusive Gradients in Thin Films
SRS	Savannah River Site

Microencapsulation of Solid Radioactive Waste in Cement Matrices

Project Team: C. A. Langton, K. P. Crapse, J. M. Duffey, L. N. Oji, C. L. Crawford
Subcontractor: Clemson University Advanced Microscopy Laboratory
Thrust Area: Nuclear Materials Management
Project Type: Standard
Project Start Date: October 1, 2015
Project End Date: September 30, 2017

The objective of this work is to design and test cement-based waste forms for microencapsulation of radioactive oxide waste currently stored at the SRS. A waste form / process will be developed which supports higher waste loadings. Also data will be generated to update the engineering calculations for radiolysis of cement materials. Existing data are overly conservative and limiting.

Processing cement matrices with low water contents has been demonstrated using resonant acoustic mixing technology. This type of mixing does not generate secondary waste, results in excellent dispersion, and supports rigorous material accountability. Six different low-water cement matrices were prepared with surrogate oxide, HfO_2.

Microencapsulation was demonstrated and matrices characterized. The lowest evaporable water mix was selected for the initial radioactive waste form preparation and H_2 generation rate measurements (FY17 scope). Hydrogen generation rates will also be measured for the other matrices to update data for engineering calculations.

FY2016 OBJECTIVES

- Design/prepare low-water cement waste forms that microencapsulates 1 wt. % HfO_2 (surrogate for actual waste oxide)
- Identify/develop waste form processing method which does not generate secondary waste and which facilitates material control and accountability
- Calculate the H_2 generation resulting from radiolysis of water using literature data
- Demonstrate microencapsulation of oxide waste using surrogate material
- Select the most promising waste forms for radioactive waste testing in year 2 of this project
- Prepare R&D directions for preparing radioactive samples
- Identify actual oxide for initial H_2 generation rate testing
- Assemble pressure vessels and equipment necessary to conduct H_2 generation rate measurements

A key objective of this effort is to determine H_2 g-values for several of the most promising microencapsulated waste forms to support more realistic estimates of H_2 generation rates for these materials.

INTRODUCTION

Microencapsulation in a cementitious matrix was identified as a treatment for waste oxide that would support higher waste loadings. However, alpha radiolysis of water in cementitious materials is known to generate H_2, which can result in exceeding flammability limits under certain conditions such as extended storage in unvented containers. For the purpose of estimating maximum H_2 generation rates due to alpha radiolysis of cementitious materials during transportation and storage, bounding H_2 g-values of 0.4 – 0.6 molecules of H_2 per 100 eV absorbed dose are typically cited along with assumed water contents of at least 30 wt. % [3, 4]. However, although somewhat limited, literature data on radiolysis of hydrated cement materials are available that indicate H_2 g-values are significantly lower for cementitious materials that have lower water contents or that contain appreciable nitrate [2, 5]. A key objective of this effort is to determine H_2 g-values for several of the most promising microencapsulated waste forms to support more realistic estimates of H_2 generation rates for these materials.

APPROACH

Six cements and cement blends were identified for testing. Each type of cement resulted in a different hydrated phase assemblage and microstructure. Hydrogen getter chemistry was reviewed and a soluble getter was identified for evaluation. Resonance acoustic mixing (RAM) technology was selected as the waste form processing method that best addressed two needs: no secondary waste and support easily implementation material accountability. HfO_2 was identified as a surrogate oxide for non rad demonstration of solid particulate waste microencapsulation.

An existing SRNL RAM mixer was used for non- radioactive screening studies. A second SRNL RAM mixer was transferred from a non rad lab to a rad lab at SRNL in preparation for 2nd year testing using actual radioactive oxide material. This material was purified at SRNL and partially characterized. It will be used to measure effects of alpha radiolysis on hydrated cement waste forms in year 2 of this project.

Figure 1. RAM mixer, waste form components, and example of final surrogate waste form

RESULTS / DISCUSSION

Cement microencapsulation offers ambient temperature, low cost, high throughput processing. Technical challenges include: minimizing radiolytic H_2 generation, minimizing moisture sorption during vented storage, achieving uniform dispersion of the waste oxide in the matrix, and smart processing which does not generate secondary waste and supports rigorous material accountability.

Testing was performed to identify the lowest mass ratio of water to cement which could be processed using RAM processing and to demonstrate microencapsulation of surrogate oxide. This was completed for 6 different cement types which correspond to six different hydrated mineral assemblages and chemistries. Surrogate waste forms were characterized to determine evaporable, chemisorbed, and bound water using DTA/TGA. See Figure 2. Mineralogy, microstructure, 105° C evaporable water, bound water, and density were characterized for each matrix.

Mineralogy was determined using x-ray diffraction. Scanning electron microscopy was used to confirm good distribution of the surrogate oxide in the cement matrix and to demonstrate microencapsulation of the oxide waste. See Figure 3.

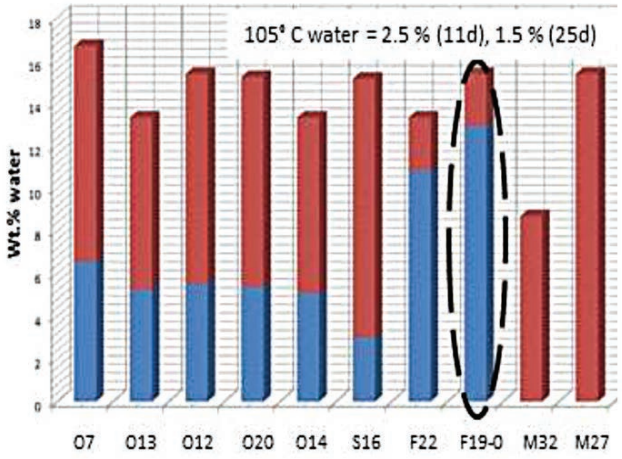

Figure 2. Evaporable H_2O vs total H_2O; Sum of 22 chemically bound water (blue) and evaporable water (red) at 105° C for matrices with a water to cement ratio of 0.20

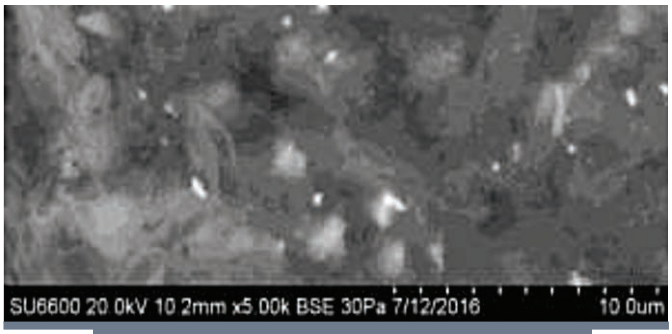

Figure 3. Surrogate oxide microencapsulation; Bright spots are particles of HfO_2

FY2016 ACCOMPLISHMENTS

- RAM mixer relocated to Rad Lab - Figure 4 (following page)
- Rad Con and IH evaluations and approvals for rad mixing location completed
- Run Plan finalized for first 8 rad waste forms (H_2 generation and characterization)
- Rad mixing and handling work instructions drafted
- RAM mixer operability evaluation and practice in rad lab underway
- Purified oxide (25 g) relocated to work area
- Oxide characterization plan and schedule drafted and accepted
- Micro GC upgrades and gas standards obtained
- New seals for pressure vessels ordered
- Pressure vessel integrity evaluation underway — Figure 4 (following page)
- USQs: Two USQs drafted; (1) rad mixing (2) H_2 generation measurements

Figure 4. RAM mixer relocated in Rad Lab (left); Pressure vessel and sample container for radiolysis measurements (right)

FUTURE DIRECTIONS

- Prepare and characterize cement waste forms containing radioactive oxide waste
- Complete preparation for radioactive waste form mixing and H_2 generation measurements
- Prepare radioactive waste forms that contain 1 wt. % purified radioactive oxide
- Initial cement matrix selection based on 105 °C moisture loss
- Up to 6 matrices for free vs. chemisorbed vs. crystalline water evaluation
- Measure H_2 generation rate over ~ 2 to 4 months
- If successful, evaluate processing larger (1-10 kg) non rad samples using Resonance Acoustic Mixing
- Characterize SRNL prepared rad samples and non rad (scale-up) samples for homogeneity
- Optimize waste form and processing

References

1. **N. E. Bibler,** "Radiolytic Gas Generation in Concrete Made with Incinerator Ash Containing Transuranium Nuclides," in Scientific Basis for Nuclear Waste Management, Vol. 2 (1980); C. J. M. Northrup, Jr., Ed.; Plenum Publishing, New York; pp 585 – 592.
2. **U.S. Nuclear Regulatory Commission,** CH-TRU Payload Appendices, Rev. 3, December 2007, www.nrc.gov/docs/ML1103/ML110330353.pdf.
3. **NUREG/CR-6673,** "Hydrogen Generation in TRU Waste Transportation Packages," prepared by B. L. Anderson, M. K. Sheaffer, L. E. Fischer, Lawrence Livermore National Laboratory, May 2000.
4. **J. M. Duffey and R. R. Livingston,** "Hydrogen Generation Scoping Study of Surrogate WSB Concrete Waste Forms," WSRC-TR-2003-00350, Rev. 0, August 2003.

Acronyms

R&D	Research and Development
RAM	Resonant Acoustic Mixer
RPM	Revolutions Per Minute
USQ	Unresolved Safety Question

Mercury Removal & Stabilization in the Subsurface Using Vapor Phase Sulfur

Project Team: Dennis G. Jackson (Primary), Miles E. Denham, and Carol Eddy-Dilek
Thrust Area: Environmental Stewardship
Project Type: Standard
Project Start Date: October 26, 2015
Project End Date: September 30, 2017

We have evaluated operational strategies that couple in-situ thermal heating with a stabilization mechanism to address elemental mercury present in the subsurface. Following the initial subsurface heating, which removes a significant mass fraction, the treatment approach uses the residual heat in the system to aid in the delivery of elemental sulfur that acts as a sequestering agent for residual elemental mercury. In the vapor phase, sulfur readily combines with mercury to form mercury sulfide compounds, a more stable, less leachable form of mercury. Under this operating paradigm, thermal mass removal is coupled with a process that stabilizes residual contamination in place. We applied geochemical modeling analysis to develop an implementation strategy and identified operational conditions that allow for formation of the desired recalcitrant mercury species.

FY2016 OBJECTIVES

Utilize Geochemical Modeling to evaluate formation of Mercury Sulfides at Equilibrium Temperatures in the subsurface to develop thermal remediation strategy for elemental mercury in the subsurface

INTRODUCTION

The Oak Ridge Y-12 National Security Complex (Y-12) used large amounts of elemental mercury from the early 1950's through the 1970's. This mercury serves as a source of contamination to groundwater and surface waters that exit the reservation. Remediation of mercury contaminated soils and building materials is a high priority technical challenge that needs to be resolved to support decommissioning activities within the Y-12 complex. In this research our team is evaluating the remediation of elemental mercury from the subsurface using *in-situ* thermal remediation coupled with a novel *in-situ* stabilization mechanism.

Thermal remediation is a mature technology that has been used for 2-decades in the remediation of organic contaminants such as benzene, toluene, trichloroethylene and tetrachloroethylene from soils. All of these compounds have boiling points on the order of (80 to 125°C). In thermal remediation, heat is used to increase the vapor pressure of the contaminant allowing removal using soil vapor extraction. Conventional thermal remediation involves heating the subsurface to temperatures near the boiling point of the target contaminant (357°C for elemental mercury). Our team is exploring the unique properties of elemental mercury to evaluate and develop a remediation strategy at operating temperatures consistent with current in-situ remediation technology. For large-scale applications that involve thermal removal of elemental mercury, the use of lower treatment temperatures will translate directly to lower implementation and operational costs compared to baseline costs.

To ensure long-term compliance with the treatment standards, our remediation strategy incorporates a sequestration mechanism to address residual mercury that remains after the heating campaign. This research develops an SRNL technology (US #8,770,891) designed to stabilize elemental mercury in the subsurface. The technology uses residual heat present following thermal treatment to deliver elemental sulfur vapor as a sequestering agent. Sulfur combines with mercury to form mercury sulfide compounds, a more stable, less leachable form of mercury. Our goal is to establish an operating paradigm that couples thermal mass removal with this process to stabilize residual contamination in place.

APPROACH

The basis for our treatment paradigm exploits the unique behavior of mercury volatilization from soils during heating to develop a thermal remediation strategy specific to elemental mercury. This strategy is based upon the "thermograms" for various species of mercury that are presented in Figure 1. These thermograms illustrate the volatilization (removal) of various mercury species from soils during controlled pyrolysis. Our team is using the unique temperature window of each of the different mercury species and compounds to develop remediation strategy technologies specific to elemental mercury. The results from these controlled pyrolysis studies indicate that relatively low temperatures (80 to 125°C) are sufficient to liberate elemental mercury from soils. These observations are being used to identify and develop specific technologies for the remediation of elemental mercury.

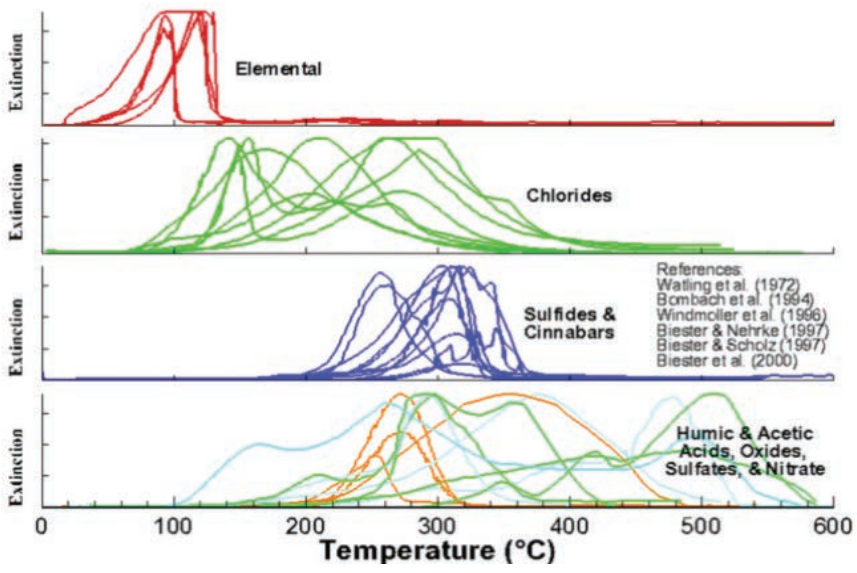

Figure 1 "*Thermograms*" depicting the removal of mercury species during controlled pyrolysis

Since elemental mercury is so reactive with very low environmental thresholds, any in-situ remedy will need to provide a stabilization component to address any residual material left in the subsurface following thermal extraction. SRNL technology (US #8,770,891) provides a mechanism to stabilize elemental mercury in the subsurface. The patented technology uses residual heat present in the subsurface following thermal treatment to aid in the delivery of elemental sulfur for use as a sequestering agent. Our approach is to evaluate mercury and sulfur reactions in the subsurface as a function of temperature. We note that in the thermograms, mercury sulfides require temperatures in the 200 to 350°C range to decompose. This indicates a more recalcitrant species versus the more soluble elemental mercury and the chloride species. Chemical equilibrium modeling was used to evaluate effectiveness of the treatment and assess secondary reactions associated with formation of stable mercury compounds.

RESULTS / DISCUSSION

Geochemist Workbench reaction path modeling was used to evaluate the formation of mercury sulfides under various temperatures representative of subsurface cooling following the deployment of in-situ thermal remediation. Previous large-scale field investigations following the use of thermal remediation indicate that subsurface temperatures decrease at a rate on the order of 1°C per month. Multiple scenarios were evaluated to identify subsurface conditions that promoted the formation of recalcitrant mercury sulfides species. In the vapor phase sulfur readily combines with mercury to form mercury sulfide compounds (Figure 2.1), a more stable, less leachable form of mercury. In the subsurface a number of factors regarding secondary reactions were evaluated heuristically. These reactions include the oxidation of sulfur causing potential soil acidification (Figure 2.2) and the likely interactions with primary soil constituents that will increase sulfur requirements (Figure 2.3). These evaluations have enabled us to develop an implementation strategy using an inert carrier gas for deployment of this innovative approach (Figure 2.4).

Figure 2. Mechanisms effecting the formation of stabile mercury complexes in the subsurface using gas-phase sulfur as an amendment

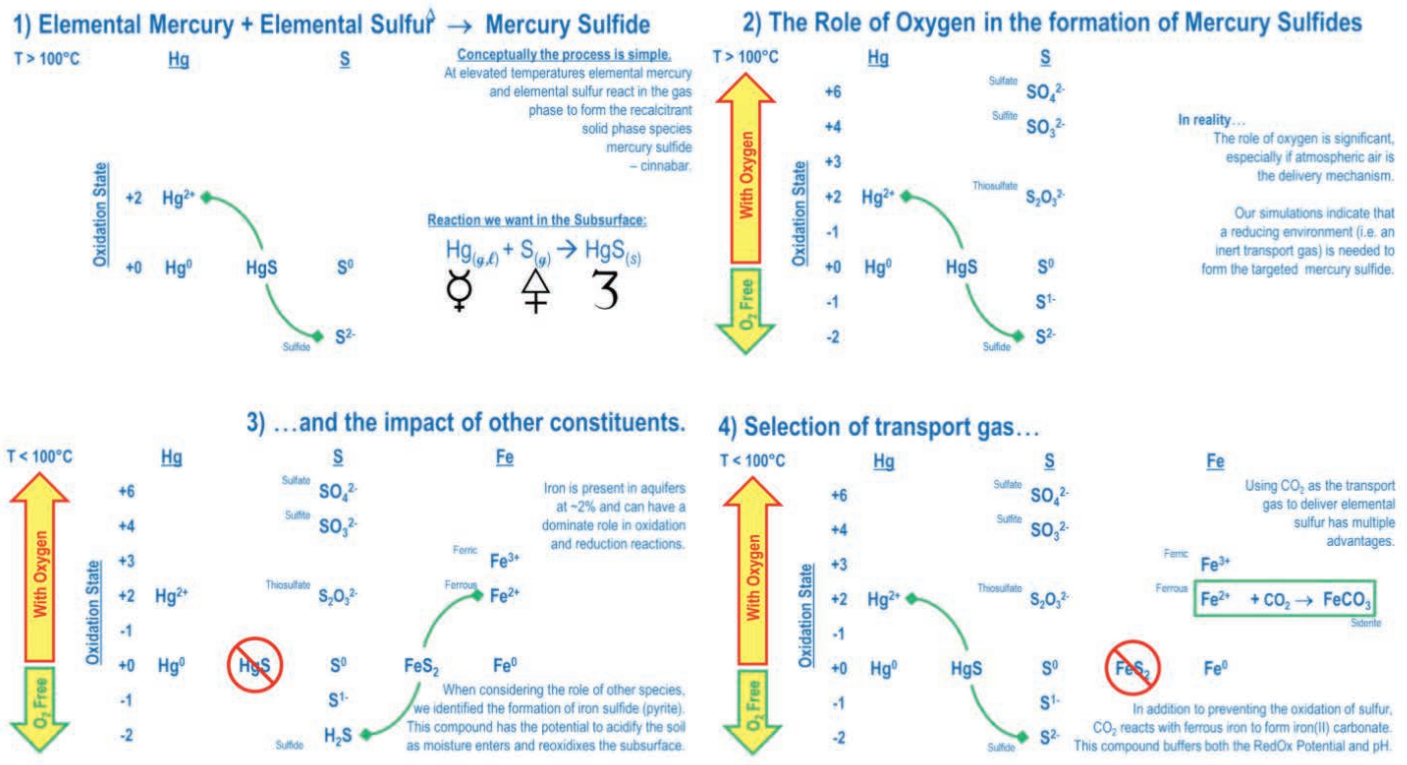

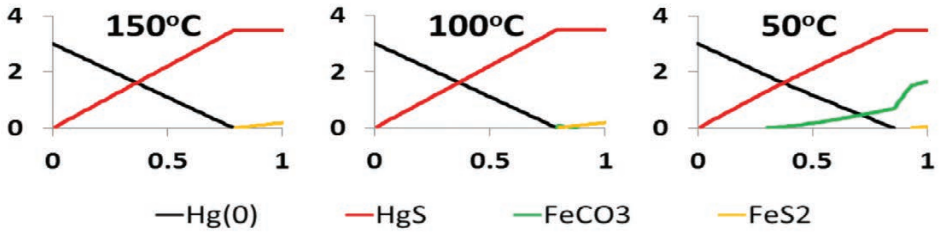

Figure 3. Role of temperature on the formation of stabile mercury species (HgS) from elemental mercury under a carbon dioxide and sulfur atmosphere; The formation of the buffering compound siderite ($FeCO_3$) below 100°C prevents formation of iron sulfides which would cause soil acidification

In this implementation, following a thermal treatment deployment the vapor extraction infrastructure would be used to flush the subsurface with carbon dioxide. This has two advantages, both related to the natural presence of iron in most soils. The carbon dioxide would displace any oxygen in the subsurface preventing the formation of iron sulfides and would also sequester the available iron by the formation of siderite (an iron carbonate). This compound will act as a buffer to control both the pH and redox potential of the subsurface allowing the formation of the recalcitrant mercury sulfide. As indicated in Figure 3 the formation of the buffering compound (siderite) begins once subsurface temperatures cool to approximately 100°C. Adding the sequestering amendment when subsurface temperatures are above this threshold allows the formation of the buffering compound siderite ($FeCO_3$) and the formation of stabile mercury species (HgS) from elemental mercury under a carbon dioxide and sulfur atmosphere.

FY2016 ACCOMPLISHMENTS

Determined conditions that gas-phase sulfur can be used as an amendment to sequester elemental mercury in the subsurface at elevated temperatures

Established that oxygen prevents formation of target species & that interactions w/ natural soil constituents impact the formation of desired recalcitrant mercury species

Developed implementation strategy and identified operational conditions that allow for formation of recalcitrant mercury species

FUTURE DIRECTIONS

- Partner with Clemson University and perform chemically reactive geochemical modeling of the multiphase processes that occur during heating, cooling, and injection of the sequestering agent and cover gas mixture into the porous media

Publications/Presentations

Poster Presentation: "Thermal Strategies for Subsurface Mercury Characterization, Extraction, and Stabilization," Clemson University. **EXTERNAL REVIEW OF SRNL SELECT COMPETENCIES:** Environmental Science and Engineering, Chemistry and Radiochemistry, Materials Science and Engineering, & Separations Science and Engineering , SRNL Ellenton Room.

Platform Presentation: "Thermal Strategies for Mercury Removal and Vapor Phase Sulfur Stabilization," 10th Tenth International Conference of Chlorinated & Recalcitrant Compounds, SRNL-STI-2016-00277, Palm Springs, California.

Intellectual Property

July 2011: Invention disclosure for described technology submitted; strategic endeavor to position SRNL in an position to garner future research funding. **July 2014:** US Patent (#8,770,891) issued. *LDRD funds are being used to develop the existing IP so data beyond simple proof of concept is available.*

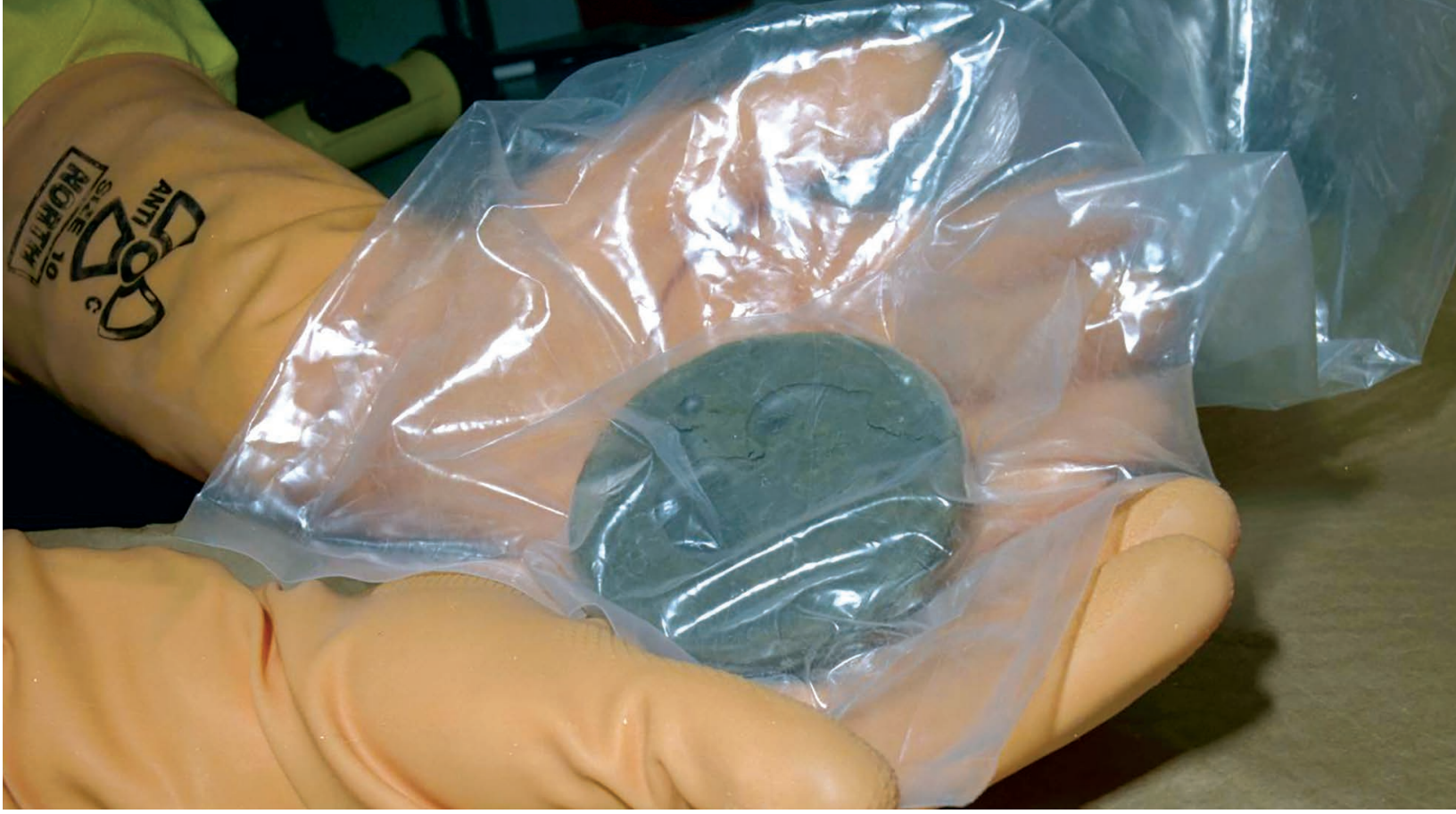

Development of Advanced Processing Technologies for Plutonium Oxide Production

Project Team: L. Roy (Primary), T. Shehee, J. Bobbitt, M. Kesterson, and T. Smith
Thrust Area: Environmental Stewardship
Project Type: Standard
Project Start Date: October 1, 2015
Project End Date: September 30, 2016

Alternative options for Pu disposition are being sought that lower the technical risk and cost currently associated with the MOX disposition path. The most attractive option is "downblending and disposal" using direct metal oxidation (DMO) to convert Pu metal to PuO_2. While DMO has some advantages, several disadvantages of the method also exist. This project funded the development of alternative technologies for Pu oxidation utilizing nitration gases as oxidants with an optimized furnace design for metal oxidation. The program explored chemical reactions involving NO and NO_2 gases with Pu metal utilizing a reactor design that is strategically tailored to optimize reactor conditions. The goals were to: 1) have complete metal oxidation occur at a lower temperature and higher reaction rate than the benchmark process and 2) design, model, and optimize a reactor a priori *for process-driven designs.*

FY2016 OBJECTIVES

To develop alternative technologies for Pu metal oxidation utilizing nitration gases as oxidants with optimized furnace designs

INTRODUCTION

Plutonium disposition is a multi-faceted problem within the DOE complex and there are several disposition options for the 34 metric tons of weapons-grade Pu at SRS. Alternatives to the current MOX program are being sought that lower technical risk and cost. Recent focus is on "downblending and disposal" using direct metal oxidation (DMO) to convert Pu metal to PuO_2. This method was developed by LANL and also has disadvantages; the product does not meet the technical requirements for MOX feed material (necessitating the MOX aqueous polishing process), residual metal particulates from incomplete oxidation at low T, potential pyrophoric intermediaries, calcination temperatures @ 950°C prevent dissolution. Hence, there is a need to simplify the disposition path to reduce the processing and waste disposal costs. In an attempt to develop a Pu process that has more favorable characteristics for dry processing, this project set out to develop alternative technologies for Pu oxidation with *simultaneous design and optimization* of chemical processes and reactor design for complete metal oxidation. Oxidation reactions focused on nitration gases to convert metal to metal oxide. Utilizing process-driven designs allowed for advancement in new technologies concepts for radiochemical processing across the entire nuclear enterprise.

APPROACH

This project set out to explore chemical reactions involving NO and NO_2 gases with Pu metal utilizing a reactor design that is strategically tailored to optimize reactor conditions.

The use of nitration oxidants is common in the nuclear industry. Interaction of NO, NO_2, and N_2O gases on a uranium surface has been investigated previously.[1] The oxidants such as NO_2, and N_2O_5 are compatible with stainless steel and nickel, making the reactions a prime candidate for a process-driven design using additive manufacturing. Therefore, reaction conditions could be translated and optimized for direct conversion of Pu metal into oxide. The key to translation is simultaneous product and process design by integrating both science and engineering aspects throughout process development. This project set out to explore chemical reactions involving NO and NO_2 gases with Pu metal utilizing a reactor design that is strategically tailored to optimize reactor conditions.

Our research approach consists of two main steps:

Step 1: Reactor design and chemical reaction engineering simulations. The first step in this project was to design and simulate the chemical reactions of the system using a basic system. By setting up a model and studying the results from the simulations, the team could understand what further optimizations are required to move forward in the design process for ultimate optimization and control the process' variables and parameters. These 'virtual' experiments are run to adapt the process to various operating conditions. The modeling effort serves two functions in this project: 1) It will support chemical processing at lower temperature and/or higher reaction rates compared with DMO process and 2) The reactor geometries will be converted into a format for 3D metal printing.

Step 2: Chemical Synthesis. Synthesis of the desired product was to be based on chemical modeling results used in reactor design. The first prototype was to demonstrate reactor performance and reactor stability in an oxidizing environment. Following completion of an experiment, further optimization of the reactor for was to occur. As described above, the use of modeling and simulation allows for more focused experiments so that fewer, more targeted experiments can be conducted. Also, deeper level of understanding is achieved, thereby increasing the chance for success.

RESULTS / DISCUSSION

A prototype reactor was designed and printed that is loosely based on vortex reactors (Figure 1). The complicated design consists of placing a metal coupon inside a small chamber wherein the reactant gases, in addition to reacting with the metal surface, also remove the PuO_2 product from the coupon. The resulting PuO_2 product would then be picked up by the high gas flow and moved into the larger chamber for an expansion separation. Aside from several design issues, other issues specific to additive manufacturing became apparent. While a considerable amount of time and effort is needed for application design and setting process parameters, the surface finish and dimensional accuracy may be of lower quality than other traditional manufacturing methods. In our printed pieces, the surface finish is described as coarse and a considerable amount of post-processing will be required especially when considering material accountability. Therefore, additive manufacturing may not be the best choice for a project involving reactor design using powdered radioactive materials. Therefore, a COMSOL Multiphysics model was developed using a simplified glass reactor design to predict temperature profiles and species concentrations for the laboratory scale plutonium oxidation reactor. This model includes heat transport, fluid transport, and multicomponent chemical reactions. The predicted heat generated by the oxidation of plutonium metal by NO_2 is 942.8 KJ/mol.

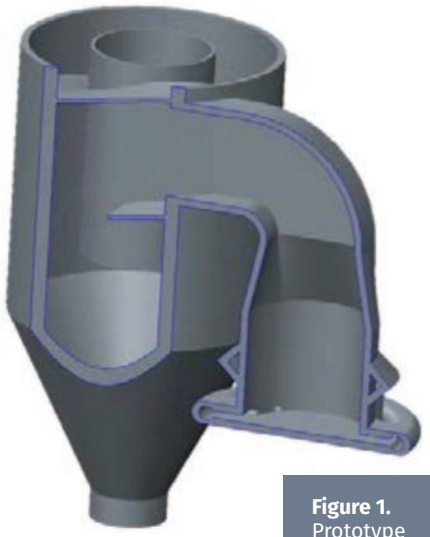

Figure 1. Prototype reactor

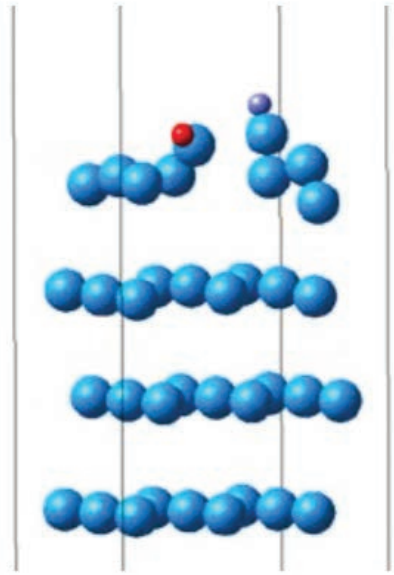

Figure2. DFT calculation of NO gas on Pu metal surface

The synthetic portion of the project had several setbacks affecting execution, namely in obtaining gas cylinders of NO or NO_2 gas. Therefore, a gas mixture was generated by reacting concentrated HNO_3 with graphite rods. The gas was collected in polyethylene bags and transported for the reaction. Two experiments were performed at room temperature. Pu metal was either washed with HNO_3 solution or filed to expose the metal surface. Once cleaned, the metal was placed in the bottom of the reaction vessel and the vessel was clamped to prevent tipping. To convert the NO to NO_2, in house compressed air was pumped into the bag containing the NO/NO_2 to roughly double the volume of the gas in the bag. The bag was attached to the reaction vessel via Tygon tubing. To introduce the gas to the reaction vessel, the bag was compressed until gas was observed at the exit port of the vessel. After a period of time, compressed air was directed through the reaction vessel in an attempt to dislodge any oxide forming at the surface of the metal. The introduction of gas and purge cycles were repeated for ~3 hours. Both experiments showed negligible mass change and it is assumed that no reaction took place.

Additional density functional (DFT) calculations were performed to understand the extent of oxidation and reactions of NO and NO_2 gases on a Pu metal surface. The oxide calculations show that Pu metal oxidation cannot be defined by distinct layers of $PuO_2/Pu_2O_3/PuO$ on the metal surface. Each of the oxide species contains crystallographic elements that relate their structures. Therefore, the oxidative layers are better described as a gradual transition between the oxide species. Calculations of NO and NO_2 on the Pu metal surface show that reaction occurs with both nitrogen and oxygen adsorbing on the surface. In the NO reactions, the Pu metal surface is disrupted and the structure is reminiscent of the coordination environment found in PuN and PuO_2 (Figure 2). Therefore, it is expected that both nitrogen and oxygen would adsorb dissociatively onto the surface, similar to reactions of U metal with nitrogen oxides.

FY2016 ACCOMPLISHMENTS

Performed literature search and found NO_2 favorably reacts with uranium metal vs other NOx gases	Designed and printed a prototype reactor based on concepts from vortex reactors	Critically analyzed additive manufacturing for this application and the lower quality surface finish of the printed reactor is not the best choice when using powdered radioactive materials	Calculated the thermodynamic reactions of Pu and NOx gases and performed finite element modeling calculations; Identified NO_2 as the optimal reactant gas	Performed reactions of Pu metal with NO/NO_2 gas at room temperature; No reaction was observed and discrepancies could be the result of a lack of pure gas used for the experiment and temperature	Demonstrated using DFT calculation that both nitrogen and oxygen would adsorb dissociatively onto the Pu metal surface

FUTURE DIRECTIONS

- This work is of strong interest to SRNS senior personnel for the development of alternative technologies for Pu metal conversion. Our business development plan is to present results to SRNS senior personnel and NNSA for further funding. More broadly, the principles could be extended to other problems in the DOE complex for novel approaches into the design of complex chemical reactors. Areas that focus on reactors of all types (fuel cell, batteries, microreactors, biochemical reactors, etc.), reactor design in general, and design and control of all systems associated with energy from renewable sources have a high priority for funding.

References

1. **Albert F. Carley, Paul Nevitt, Paul Roussel,** "The Interaction of Uranium Metal with Nitrogen Oxides: The Formation of An Oxynitride Surface Layer", Journal of Alloys and Compounds 448 (2008) 355–362.

Acronyms

DFT	Density Functional Theory
DMO	Direct Metal Oxidation
MOX	Mixed Oxide Fuel
N_2O	Nitrous Oxide
N_2O_5	Dinitrogen Pentoxide
NO	Nitric Oxide
NO_2	Nitrogen Dioxide
NOx	Generic Term—Mono-Niitrogen Oxides NO and NO_2
Pu_2O_3	Plutonium (III) Sesquioxide
PuO	Plutonium (II) Oxide PuO2 – Plutonium (IV) Dioxide

Non-Proliferation and Nuclear Deterrent

Direct LiT Electrolysis in a Metallic Fusion Blanket

Project Team: Luke Olson, Brenda Garcia-Diaz, Hector Colon-Mercado, Joe Teprovich, Dave Babineau
Subcontractor: Greenway Energy, LLC
Thrust Area: Non-Proliferation and Nuclear Deterrent
Project Type: Strategic
Project Start Date: October 1, 2013
Project End Date: September 30, 2016

A process that simplifies the extraction of tritium from molten lithium based breeding blankets was developed. The process is based on the direct electrolysis of LiT using a ceramic Li ion conductor that replaces the molten salt extraction step. Extraction of T_2 from LiT in the blankets/targets of fusion/fission reactors is critical in order to maintain low concentrations. This is needed to decrease the potential T permeation to the surroundings and large releases from unforeseen accident scenarios. Extraction is complicated due to the low concentrations required and because of the high affinity of T to the blanket. This work identified, developed and tested the use of ceramic lithium ion conductors capable of sustaining LiT electrolysis at high temperatures. Multiple electrochemical cells were designed, fabricated, and used to test the proposed process. Successful electrolysis of LiH was confirmed with a residual gas analyzer and electrochemical measurements at the LiH concentrations tested. Additional work scope was added in FY16 to test the electrolytes in a Li immersion cell to better simulate expected operating conditions in reactor, and positive results indicating the stability of the electrolyte in molten Li at 300 °C were obtained.

FY2016 OBJECTIVES

- Design immersion cell and experiments for cell characterization
- Fabricate immersion cell, solid electrolyte contactor and balance of experimental setup
- Demonstrate LiT electrolysis in bench-scale test with molten Li immersed solid electrolyte
- Analysis of reaction products and reaction characterization (Quantify selectivity toward LiT decomposition)
- Optimize solid electrolyte for improved performance during lithium immersion

INTRODUCTION

Liquid tritium breeder materials, such as lithium and Pb-Li eutectic, are attractive as their breeding potential is very high and separate neutron multipliers are not necessarily required. Because it is a liquid, the tritium recovery system can be designed outside the neutron environment and will not incur radiation damage. Blanket designs are simplified when the breeding material is also used as a coolant because nuclear heating also occurs in the breeding material. However, there are a number of engineering design difficulties such as magneto-hydrodynamic pressure drops, corrosion due to liquid metal, efficient tritium recovery and containment from the liquid metal breeder. [1, 2]

In most applications, the tritium inventory in the blanket has to be kept low (~1 appm) for reliable and safe operation. The extraction of tritium can be problematic from the blanket since the tritium exists bound to lithium in the form of LiT. Extraction from liquid Li is considered more challenging due to the high solubility of LiT in the melt. On the other hand, the solubility of LiT in Pb-Li eutectic is several orders of magnitude lower, making extraction somewhat less challenging. Nevertheless the state of the art extraction approaches are essentially similar. Among the considered extraction technologies are molten salt extraction followed by electrolysis (Maroni Process), “gettering”, permeation followed by molten liquid extraction, fractional distillation, cold trapping and a combination of all. However, all of the proposed extraction technologies require a series of complex mechanical steps (expensive mechanical parts with limited lifetimes) in order to carry out the separation and prevent the buildup of impurities in the extraction process [1]. This work simplifies or eliminates many of the problems associated with the current extraction technologies.

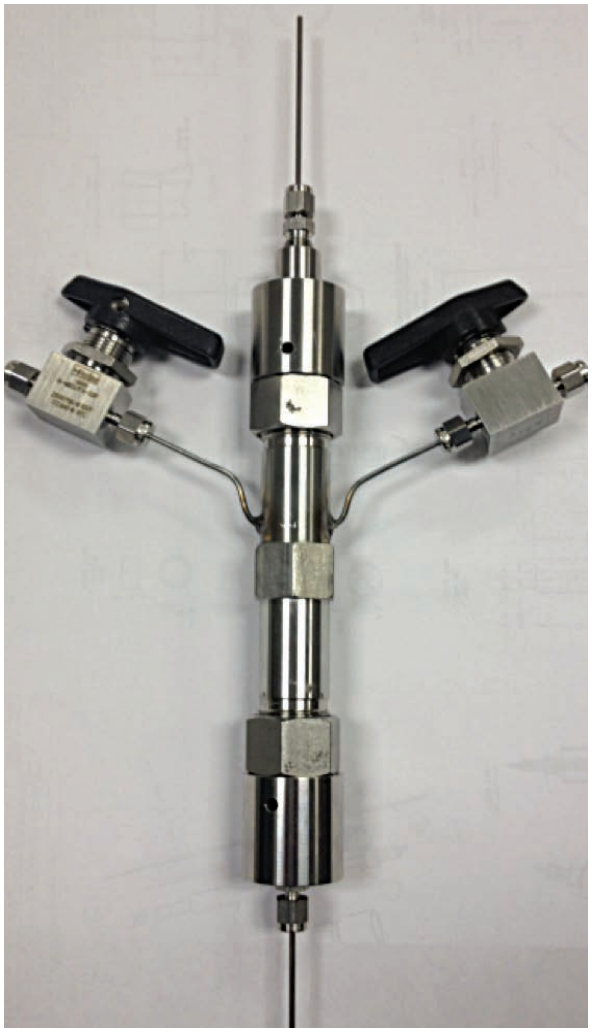

Figure 1. Electrochemical cell design for LiH electrolysis

APPROACH

In the typical Maroni process, molten Li is mixed with a molten salt in order to extract the LiT. Afterwards, the LiT undergoes electrolysis and the hydrogen is extracted. Our approach simplifies the process by incorporating a solid Li ion conductor to eliminate many of the mechanical steps in the extraction section, Figure 2.

In FY16 a Li immersion cell was designed to more effectively simulate conditions expected to be encountered in plant operation, Figure 3. This new cell allowed for the solid electrolyte to be submerged in molten Li at 300 °C, and for stirring of the molten Li/LiH mixture. This cell allowed for better simulation of conditions expected for use in a plant, and to explore and begin to address challenges that would be encountered during such operations.

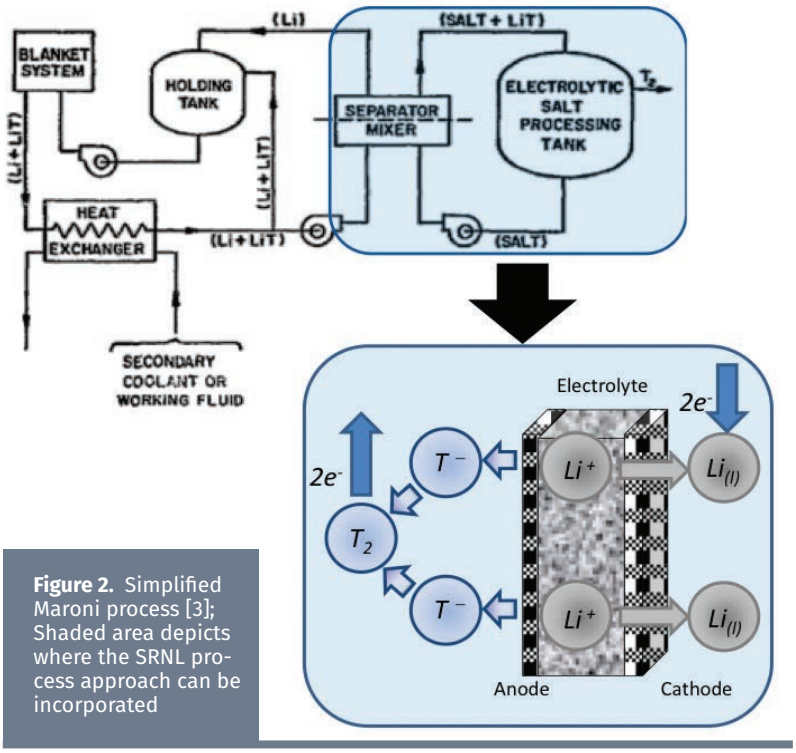

Figure 2. Simplified Maroni process [3]; Shaded area depicts where the SRNL process approach can be incorporated

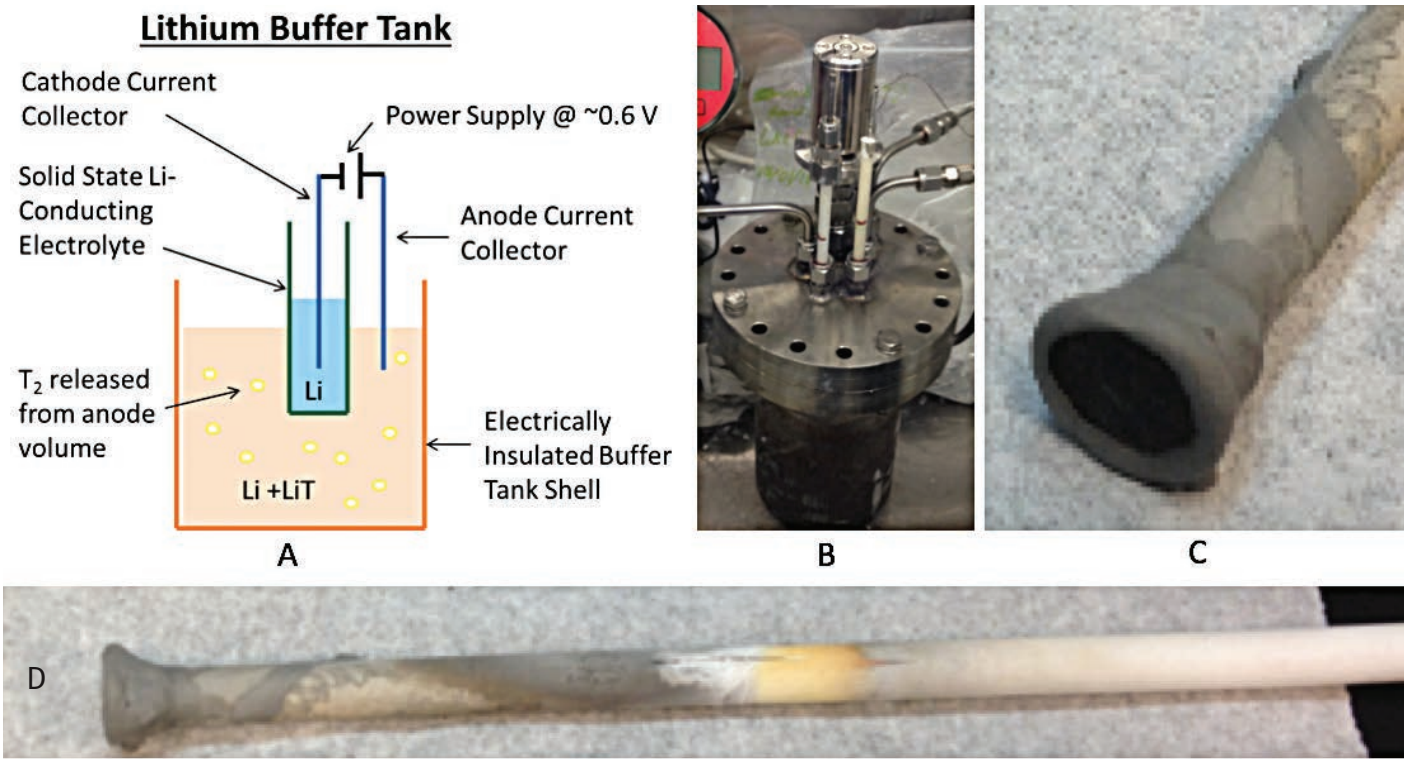

Figure 3. A) Immersion Cell Concept, B) immersion reactor vessel showing gas and cooling ports, electrodes, and stirring mechanism, c) solid electrolyte immersion electrode, note black circular region is the electrolyte that is attached to an alumina tube using boron nitride paint, inside the electrode is a tungsten wire contacting a small pool of molten Li, D) the electrode is sealed from atmosphere, but can exchange gas within the vessel through a slit in the side so that the vessel can be evacuated without breaking the electrolyte electrode

RESULTS / DISCUSSION

Two main versions of the electrochemical cell from Figure 1 were designed, fabricated and used to test the initial electrolyte materials. Typically the electrolyte consisted of $Li_7La_3Zr_2O_{12}$ (LLZO) that has been pressed and sintered into a pellet. LLZO has been shown to have among the highest conductivities at the temperatures of interest. Once prepared, the pellet was characterized using X-ray Diffraction (XRD) to confirm cubic phase formation. The cubic phase in LLZO has the highest conductivity of the potential phases present. Heat treatments and mixing conditions were explored to determine the optimal synthesis methodology for the cubic phase formation and development of mechanically stable pellet.

Figure 4. XRD ***(Top)*** and ionic conductivity ***(Bottom)*** examination of the LLZO solid electrolyte

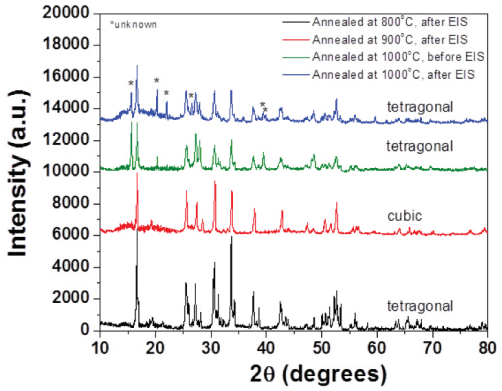

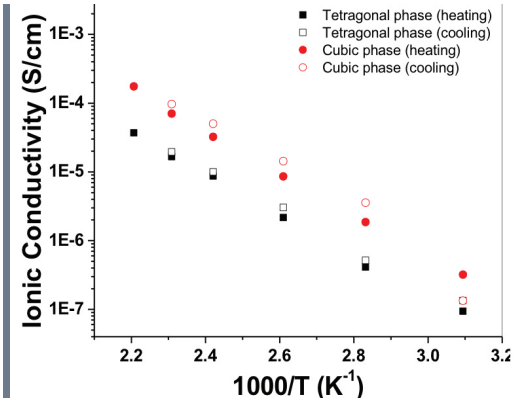

Figure 4 shows the XRD confirmation of the cubic and tetragonal phases during synthesis optimization. Ionic conductivity was evaluated as well to confirm high conductivity phase formation.

The electrolysis cell in Figure 1 (page 64) consisted of a Li/LiH electrode, the LLZO electrolyte and a gold contact counter electrode. The evolution of H_2 was monitored in-situ with a residual gas analyzer (RGA) during cell operation. Figure 5 shows the validation run of the proposed process at 350 °C as well as a picture of the prepared electrode. The results show a direct correlation between the point when the potential is applied and the point when H_2 is released from the Li/LiH electrode. The H_2 signal slowly decays as the LiH closest to the electrolyte is consumed. Figure 5 (right) shows the Tafel polarization for the LiH electrolysis at 350 °C. An exchange current density of 3.06 mA/cm^2 and limited current density of 20.4 mA/cm^2 was observed. Improvements such as operation at higher temperatures and fluidization of the working electrode should result in higher current densities.

The electrolysis cell in Figure 1 (page 64) consisted of a tungsten wire current collector that contacted a Li droplet that sat on the top of the LLZO electrolyte, with the electrolyte, attached to an insulating alumina rod with BN and/or alumina, which was submerged into molten Li-LiH mixture at 300 °C. An RGA was used to monitor H_2 evolution during electrolysis tests. A total of 11 trials were made using the immersion cell in FY16, during which electrolyte fabrication methods were improved to give an electrolyte without the carburization observed post testing shown in C of Figure 3 (previous page), and improved functionality and survivability of the electrolyte/Li contactor.

Figure 5. ***(Left)*** Electrolysis at 350 °C using LLZO electrolyte, gold counter electrode and Li/LiH as a working electrode. Inset shows LLZO pellet; ***(Right)*** Tafel polarization for the electrolysis of LiH

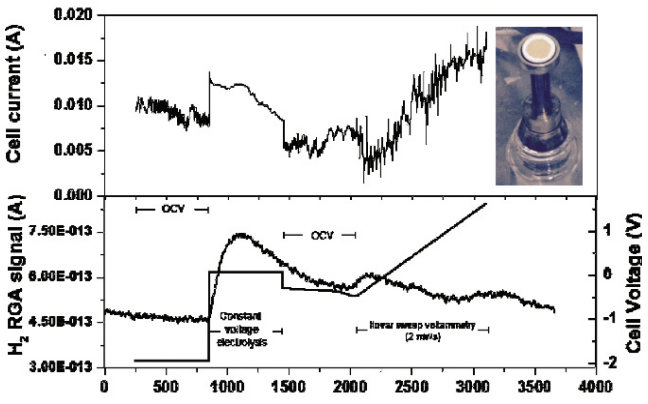

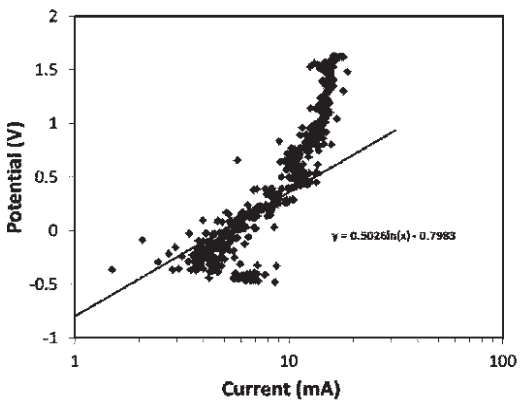

FY2016 ACCOMPLISHMENTS

Designed, fabricated, demonstrated, and characterized an electrochemical reactor that immersed a Li conducting electrolyte in molten Li to electrolyze LiH into Li and H

Characterized the LiH electrolysis reaction in molten Li and analyzed reaction products

Successfully synthesized and evaluated Li-ion conducting materials for molten Li immersion and improved processing techniques partially reducing carburization at solid electrolyte surface

FUTURE DIRECTIONS

- Improve electrode/electrolyte cell design geometry to delay shorting and allow for longer experiment durations
- Perform experiments using low concentration of hydrogen isotopes
- Engage with researchers at national laboratories to discuss how to incorporate the modified extraction process in projects requiring hydrogen extraction
- Improve hydrogen gas collection system in Li immersion cell to improve RGA signal collection from electrolysis
- Further improve processing techniques to make a higher conductivity, thinner walled electrolyte microstructure for improved electrolytic efficiency
- Investigation of electrolyte fabrication using slip casting to more easily enable closed end tubes that could be bundled

Publications/Presentations

1. **"Electrolytic Tritium Extraction in Molten Li-LiT,"** L.C. Olson, B.L. Garcia-Diaz, H. Colon-Mercado, J. Teprovich, D. Babineau, SRNL-STI-2015-00605, Fall 2015 Tritium Focus Group Meeting, November 3-5, 2015, Los Alamos National Laboratory.

References

1. **H. Moriyama, S. Tanaka, D.K. Sze, J. Reimann, A. Terlain**. Fusion Engineering and Design, 28 (1995) 226-239

2. **S. Malang, R. Mattas.** Fusion Engineering and Design, 27 (1995) 399-406

3. **V. Maroni, R. Wolson, G. Staahl.** Nuclear Technology, 25 (1975) 83-91.

Acronyms

appm	Atomic Parts per Million
LiH	Lithium Hydride
LiT	Tritium Tritide
LLZO	Lithium Lanthanum Zirconium Oxide
T	Tritium
XRD	X-ray diffraction

Intellectual Property

U.S. Provisional Application: SRS-14-014—Recovery of Tritium from Molten Lithium Blanket

Total Number of Post-Doctoral Researchers

One postdoctoral student half time

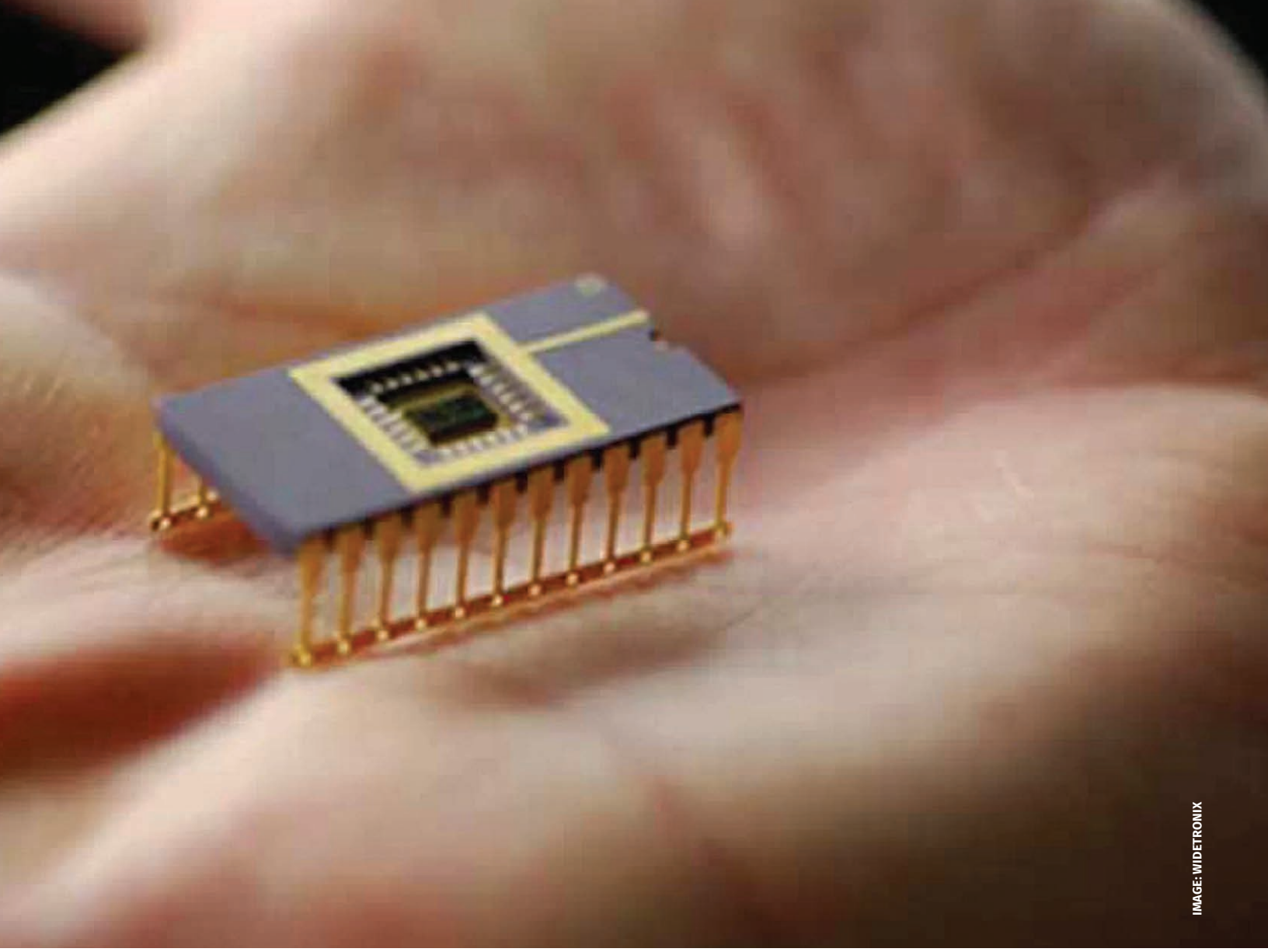

IMAGE: WIDETRONIX

Advancement of Tritium Powered Betavoltaic Battery Systems

Project Team: Greg Staack (PI), Jay Gaillard (PI), Jeff Coughlin, Kipp Neikirk, Chip Fisher, Dale Hitchcock, Ian Demass, Brent Peters, Hector Colon-Mercado, Joseph Teprovich, and Timothy Krentz
Collaborators: Dr. Chris Thomas at Widetronix.
Thrust Area: National Security
Project Type: Strategic
Project Start Date: February 16, 2015
Project End Date: September 30, 2016

Due to their decades-long service life and reliable power output under extreme conditions, betavoltaic batteries offer distinct advantages over traditional chemical batteries, especially in applications where frequent battery replacement is hazardous, or cost prohibitive.

Although many beta emitting isotopes exist, tritium is considered ideal in betavoltaic applications for several reasons: 1) it is a "pure" beta emitter, 2) the beta is not energetic enough to damage the semiconductor, 3) it has a moderately long half-life, and 4) it is readily available. Unfortunately, the widespread application of tritium powered betavoltaics is limited, in part, by their low power output. This research targets improving the power output of betavoltaics by increasing the flux of beta particles to the energy conversion device (the p-n junction) through the use of low Z structured tritium trapping materials.

FY2016 OBJECTIVES

- Complete fabrication and documentation of tritium charging equipment (This includes assembly, pressure, and leak testing of the remaining tritium exposure vessels, cabling for glovebox feedthroughs, and an instrumentation rack to be used in the Tritium facilities)
- Obtain and prepare energy conversion devces (Obtain energy conversiorn devices from Widetronix, deposit tritium trapping films, wire bond, and install the devices in the tritium exposure vessels; Bake out under vacuum and leak check the vessels at temperature)
- Characterize energy conversion devices (Perform scanning electron microscopy [SEM] and energy dispersive spectroscopy [EDS] on films deposited. Measure current voltage [IV] responses for the films with tritium trapping materials deposited)
- Tritium exposure of films while monitoring resistivity and power output (Tritium load films while measuring real-time changes in their resistivity to confirm tritium loading. Monitor the power output of the devices after loading is complete)

INTRODUCTION

Conversion of the energy from the beta decay of a radioactive source was initially proposed in the early 1950s.

Like all nuclear batteries, betavoltaics convert energy from the decay of a radioactive material into electricity. Unlike other nuclear batteries, however, betavoltaics rely on the kinetic energy of a beta decay rather than the thermal energy (heat) generated by the decay as in thermionics and thermoelectrics. Betavoltaics generate electricity when a semiconducting *p-n* junction is exposed to a beta-particle which in turn excites an electron-hole pair(s) thereby generating an electric current. Conversion of the energy from the beta decay of a radioactive source was initially proposed in the early 1950s. Testing by Rappaport using $^{90}Sr \rightarrow ^{90}Y \rightarrow ^{90}Zr$ not only proved the concept of betavoltaics, but also provided basic theory behind their operation. Unfortunately, the high energy beta emitted by ^{90}Y decay (2.28 MeV) damaged the semiconductor, resulting in a decrease in power output of ~90% over a period of one week. More recent efforts have focused on the use of lower-energy beta emitting materials to minimize long-term damage to the energy collection device. Furthermore, recent research has shown large bandgap semiconducting materials to increase the conversion efficiency of betavoltaic devices [1].

More recent research with tritium has addressed the needs for a low energy beta emitter and for large bandgap semiconductors in the form of SiC *p-n* junctions. However, the flux of beta particles inside the device is still a pressing issue. In the case of tritium betavoltaics this issue has partially been overcome through the use of tritiated thin films due to their ability to store significantly more tritium per unit volume when compared to gaseous tritium as shown in Figure 1.

Isotope	Decay Mode	$T_{1/2}$ (years)	E_{max} (keV)	Activity (Ci/cc)
^{3}H	beta	12.3	18.6	4.53E+06
^{63}Ni	beta	101	66.9	6.30
^{90}Sr	beta	28.8	546	52.2
^{147}Pm	beta	2.6	224	128.8

Figure 1. Potential radionuclides for betavoltaic batteries

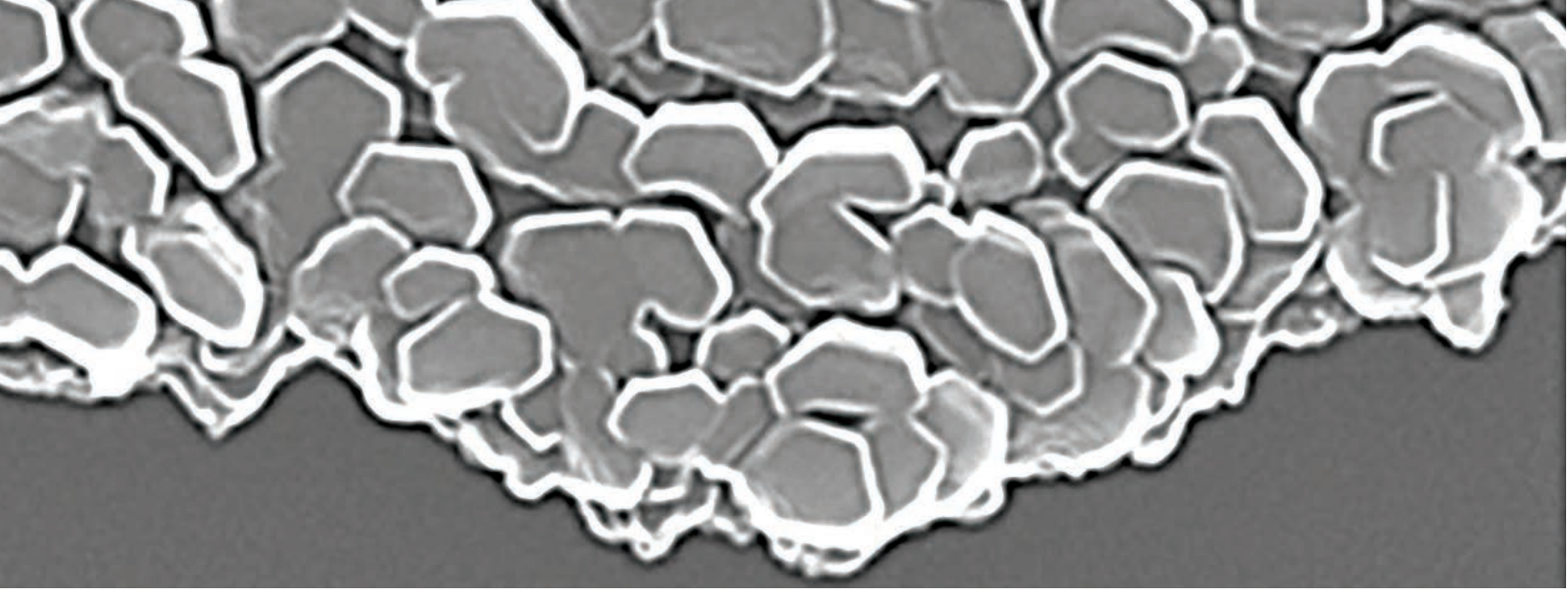

Figure 2. Structured magnesium film

APPROACH

As mentioned above, increasing the beta flux to the p-n junction will increase the power and applicability of betavoltaic devices. The goal of this research is to increase this flux through two avenues: 1) the use of structured tritium trapping materials to increase the amount of tritium stored in the film, and 2) the use of low Z tritium trapping materials to decrease self-absorption of the beta particles before they reach the *p-n* junction. Deposition and hydrogenation of structured magnesium films were investigated earlier in the course of this project. An image of a structured magnesium film is shown in Figure 2. Tritium loading of magnesium films was not performed.

Traditionally, pressure, volume, and temperature (PVT) measurements have been used to verify and monitor the hydrogenation/tritiation of a hydride under a given set of conditions. Because only minute amounts of gas are absorbed by the thin films used in betavoltaics, an alternate method was needed. The test cell shown in Figure 3 is equipped to monitor the resistivity of the film in real-time during the loading process. The films transition from metallic conductors to insulators as hydrogen is absorbed. Additionally, the tritium loading cell provides the capability to monitor the power output of an experimental device without removal from the cell.

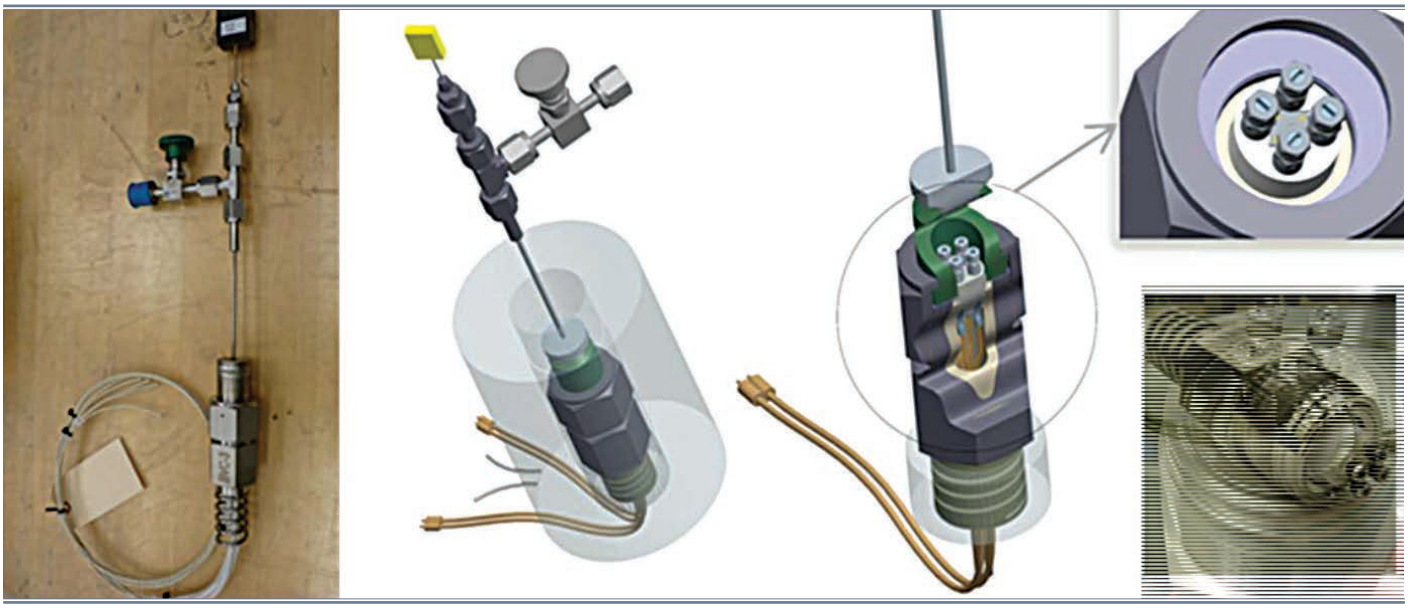

Figure 3. ATritium loading cell designed and fabricated at SRNL

RESULTS / DISCUSSION

Betavoltaics received exploratory funding in February of FY16 to complete tritium loading. Final pressure and leak testing of 8 test vessels were performed (including rework) as well as completion of the data acquisition system and associated cabling. Energy conversion devices were received from Widetronix, a betavoltaic manufacturing firm based in Ithaca, NY. The devices had been produced to deposit gold contacts for power measurements. Once the contacts were deposited, photoresist was applied, exposed to UV light. The films were then shipped to SRNL where the photoresist was developed to expose a fresh surface to deposit tritium trapping films. Thin films of titanium were then deposited on the device and capped with palladium. Gold contacts were deposited in the corners of the films before the remaining photoresist was removed. These steps are shown graphically in Figure 4.

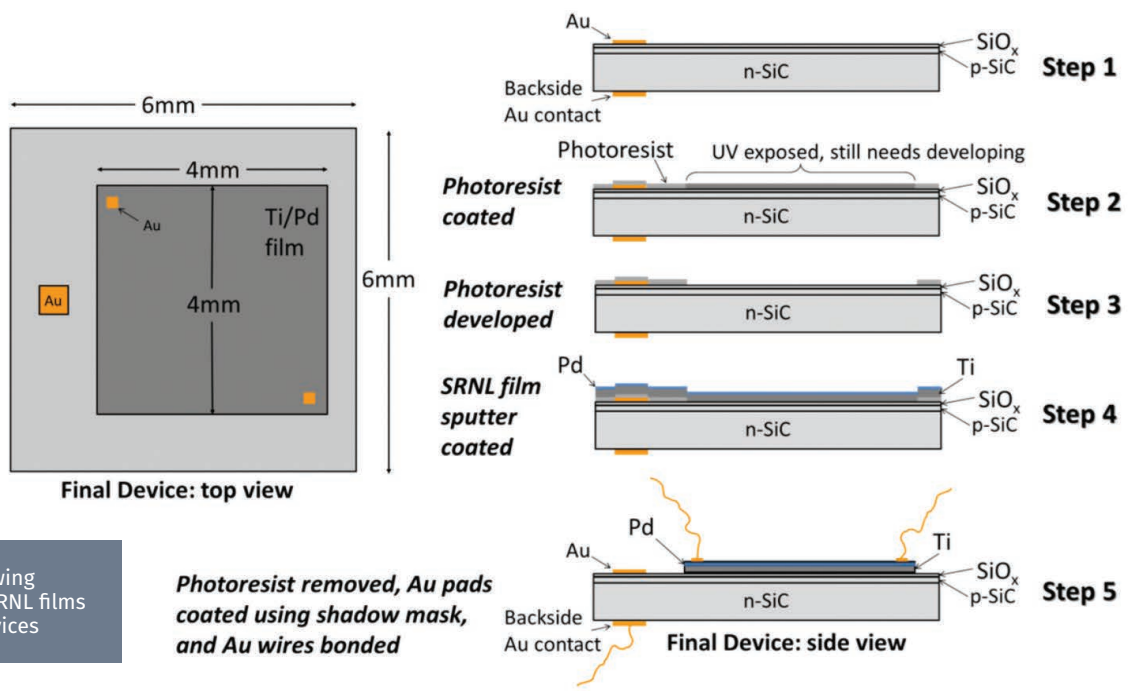

Figure 4. Schematic showing steps taken to deposit SRNL films on top of Widetronix devices

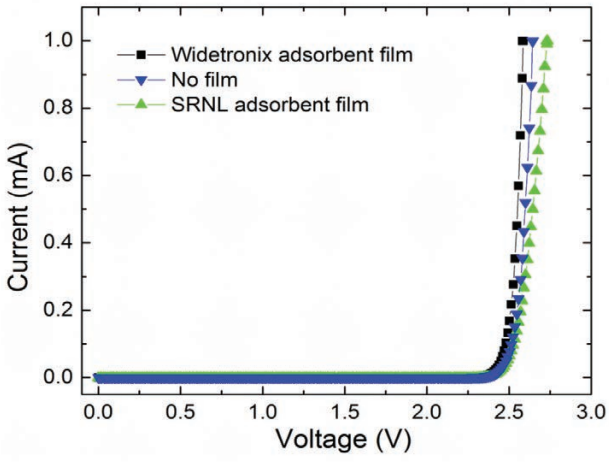

Figure 5. IV curve for Widetronix device measured in SRNL load cell.

Removal of the remaining photoresist exposed the goldpower contacts, which were wire bonded, installed in the test cells, and IV (current-voltage) curves were measured. The cells were then baked-out under vacuum and leak checked at temperature to reduce the chances of tritium leaks during loading. Following the bake-out, the IV curves were re-checked to verify no internal wires were compromised, and the cells were delivered to Tritium. Figure 5 shows a representative graph of the Widetronix device measured after mounted in the load cell and bake out. The figure shown to the right is the data for devices currently in Tritium Facilities for future resistance and power measurements. The data was taken using the electronics that will be utilized for the betavoltaic measurements in Tritium. The software written for the electronics was tested with a commercially available solar cell.

Figure 6 displays a representative data set for the solar cell and includes the power versus time plots from four simultaneously measured solar cells in real time. A power drop is seen in the SMU2B channel after covering part of the associated solar cell. The identified open circuit voltage (V_{oc}) is the maximum voltage of the solar cell at which the net current is zero.

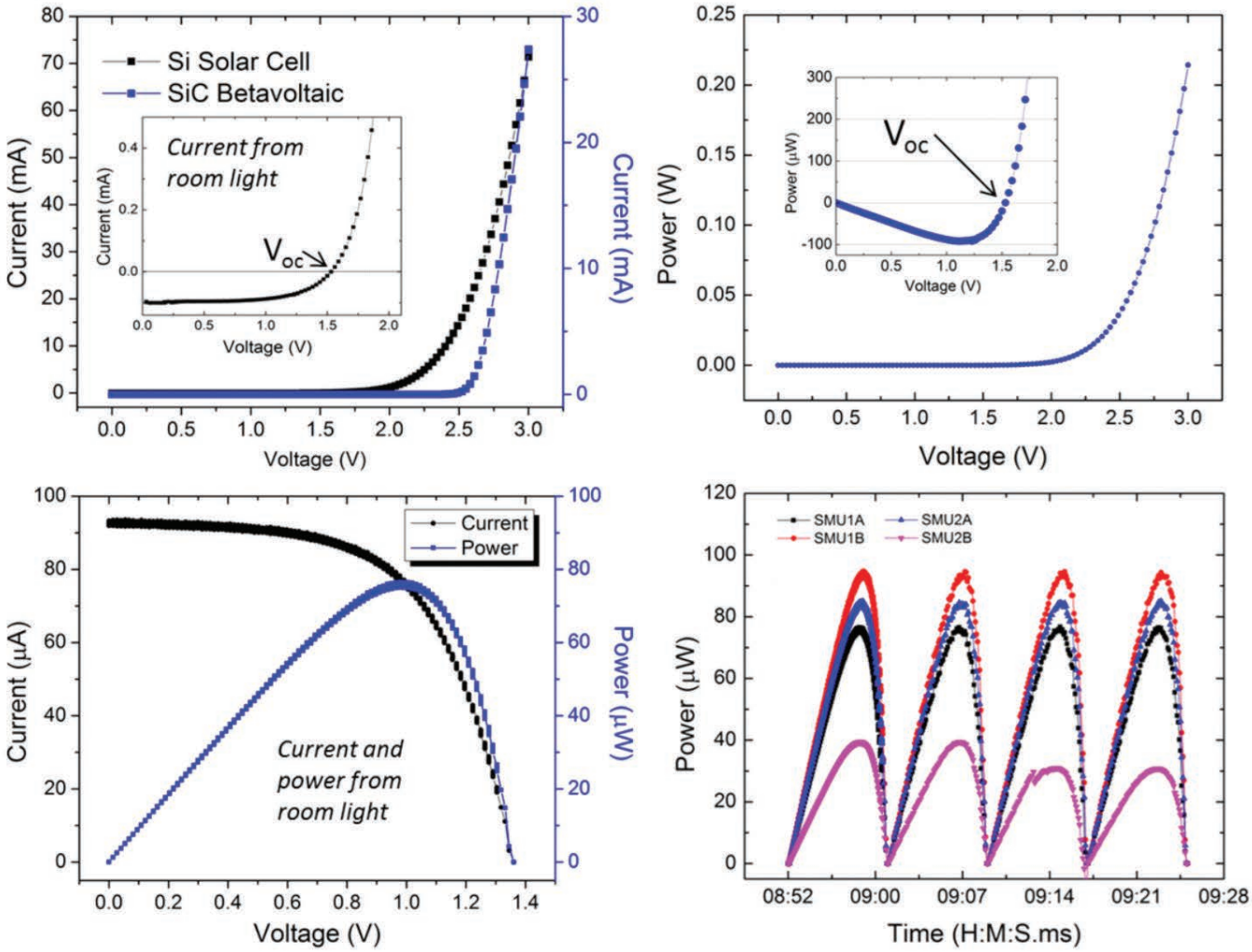

Figure 6. Solar cell data taken with electronics built for real time testing of betavoltaic devices during tritium uptake

Tritium loading of the betavoltaic devices did not occur this fiscal year. This is primarily due to three reasons: competing facility priorities, delays associated with fabrication of cabling feedthroughs, and rupture disc challenges. Loading of the first four samples is currently scheduled for this October. Once loading of the first sample set has been achieved and capabilities have been demonstrated, additional funding may be pursued.

FY2016 ACCOMPLISHMENTS

- Completed Task Technical Plan permitting loading in the SRTE
- Completed pressure and leak testing on nine loading cells (included rework)
- Completed fabrication of cabling needed for tritium loading
- Received energy conversion devices from our corporate partner, Widetronix
- Deposited Pd capped Ti films using OAD in a sputtering chamber at SRNL
- Leak checked and baked out films installed in loading cells
- Verified loading cell functionality by obtained IV curves on films deposited in loading cells
- Delivered loading cells and all needed equipment to SRTE for tritium loading

FUTURE DIRECTIONS

- Tritium loading of films is anticipated in FY17
- Verification of tritium load results and cell measurement capability will allow pursuit of additional funding

References

1. **L. C. Olsen,** "Review of Betavoltaic Energy Conversion," in Proc. 12th Space Photovolt. Res. Technol. Conf, 1993, p. 256.

Acronyms

HRTL Hydrogen Research and Technology Lab
OAD Oblique Angle Deposition
PVT Pressure, Volume, and Temperature
SRNL Savannah River National Laboratory
SRTE Savannah River Tritium Enterprise

Intellectual Property

Invention disclosure has been drafted

Total Number of Post-Doctoral Researchers

1. Postdoctoral Researcher, Timothy Krentz
2. Summer Intern, Ian Demass, Clemson

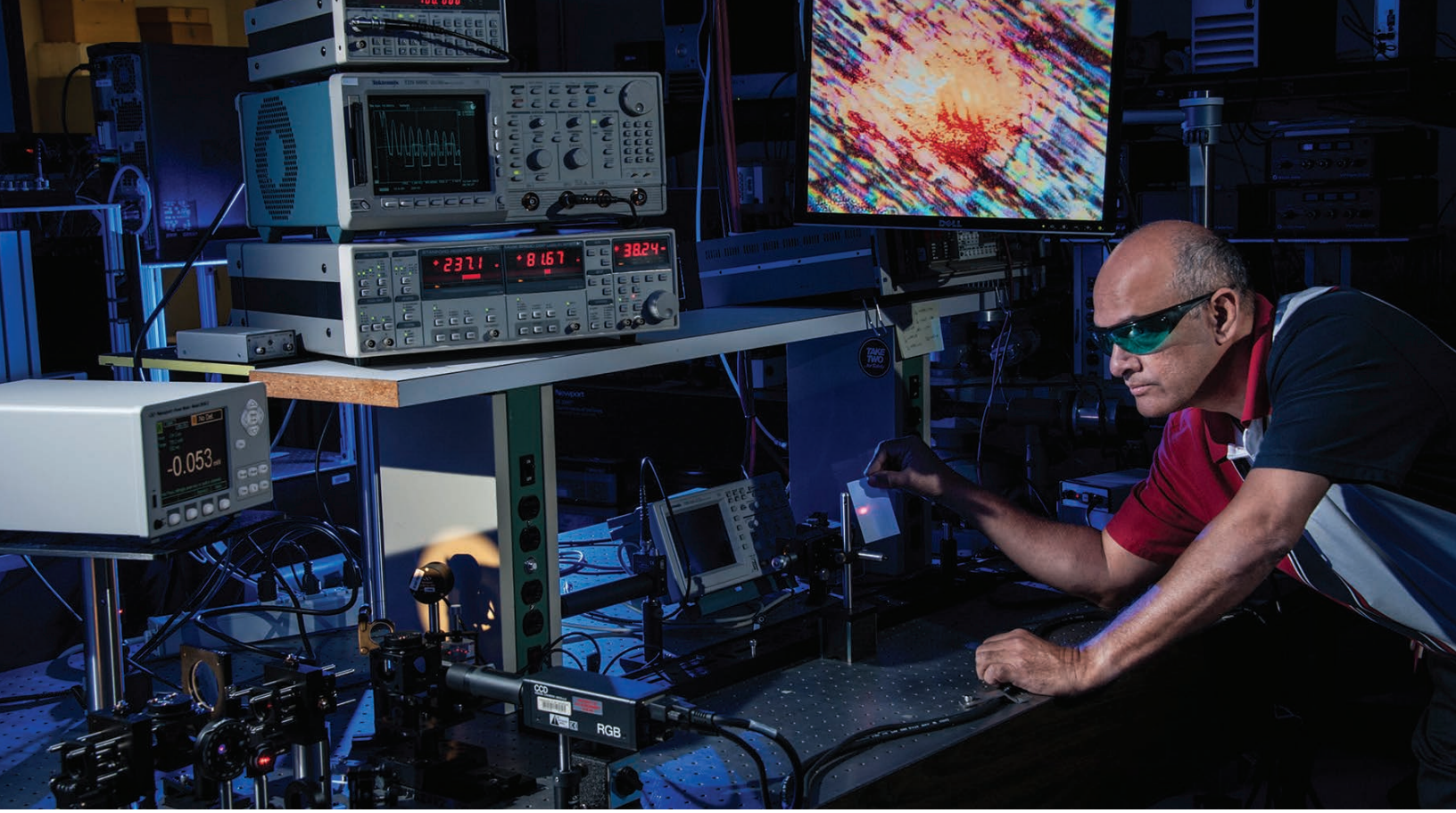

Characterization of High Explosive Detonations Via Laser-Induced Plasmas

Project Team: E. Villa-Aleman (Primary), A. L. Houk, and W. A. Spencer
Subcontractor: A. L. Houk
Thrust Area: Non-Proliferation and Nuclear Deterrent
Project Type: Strategic
Project Start Date: October 1, 2014
Project End Date: September 30, 2016

SRNL has collected and analyzed particulates from the detonation of devices with high explosives (HE) since 2004. SRNL developed passive and electrostatic precipitator-based collectors (such as rockets) to collect particulates near and far away from the plumes created by the detonation of HE devices. The temporal formation of particulates and the correlation with radiant emissions are not well understood. Large field-scale experiments are expensive and infrequent. On-demand simulated laboratory-scale experiments are needed to further our knowledge of the chemistry and particle formation. Our goal is to develop a laboratory experimental test bed to develop new optical measurement and particle collection concepts and methodologies that can be used to correlate the particle formation process with the optical observables of the detonation fireball. Since handling small quantities of explosives in the laboratory is challenging, laser-induced plasmas can be used to simulate micro-explosions, with the intent to study the temporal behavior of the fireball observed in field tests. The temporal evolution of the plasma, generated with a Nd:YAG laser and conducted with different atmospheric conditions, will be probed with a variety of lasers including ultrafast lasers. These experiments will help design future equipment for large-scale HE tests to measure unique signatures of the device. Concurrently with laser probes, temporal and spectral emissions of the plasma and laser light scattering will be analyzed with high speed thermal and visible cameras.

FY2016 OBJECTIVES

- Develop an HE simulation experimental test bed for particulate collection and diagnostic equipment
- Develop a better understanding of plasma phenomena and characterization of transient and stable products
- Track generated species in plasmas from atoms to molecules to particulates
- Develop and test a gated high rate imager (HRI) with a camera and a spectrograph for a laser operating at 76 MHz and with a 200 ps temporal window
- Test and apply a high speed visible camera (Phantom) to image temporal events on the order of 1 microsecond
- Test and apply a high speed infrared camera for short temporal imaging of fast phenomena
- Develop a particle charge counter to detect charged particulates from laser ablation
- Develop spectroscopic techniques to characterize soot and nanodiamonds related to HE experiments
- Characterize carbon content in U-bearing particulates collected from HE experiments

INTRODUCTION

The nuclear program status of a country can be defined, in part, by the types of tests conducted at different facilities. High explosives (HE) tests are required for nuclear weapons development programs and are used to explore properties of materials that will be used in nuclear devices, such as understanding the materials and components of a device when under high temperatures and pressures. These HE tests also release effluents into the environment, which are characteristic of a typical experiment.

SRNL has conducted particulate matter (PM) collection campaigns during cold hydrodynamic tests since 2004. Analysis of the PM collected during the detonation can provide a traceable path to the unique construction of the device. Optical spectroscopic methods can help characterize materials from these detonations through the determination of the particulate elemental composition (uranium, aluminum, iron and carbon), which can provide information about the device construction and field tests.

Laser ablation plasmas have been used for over 20 years to introduce material into a carrier gas for elemental analysis with mass spectrometry. Coating deposition is another application for plasmas produced with lasers. Depending on the laser power density at the target, temperatures of several thousand degrees are common. Laser ablation plasmas can be used to simulate detonations with HE. Our goal is to use the laser generated plasma approach to understand potential observables in HE experiments. Significant progress was made in FY15 to create an experimental plan, assemble two experimental test beds, procure materials and equipment, repair instrumentation, design and fabricate fiber optics assemblies required to conduct highly advanced characterization experiments. In FY16 additional accomplishments include characterizing uranium- and carbon-bearing materials, designing, building and testing a new concept in spectral characterization for fast events, completing the assembly of a HRI gater/detector to be used in conjunction with a femtosecond laser to characterize repetitive transient phenomena and Raman spectroscopy, and demonstrating the use of high speed cameras (visible and infrared) to characterize fast phenomena.

APPROACH

The proposed approach develops test platforms to characterize atomic, molecular emissions and particulates formed from the laser ablation of several targets. During the course of this research, several tasks will be completed: 1) design and build a test bed for instrument development, 2) characterize "simulated explosions" using spectroscopy techniques and particle collection methodologies and 3) correlate particulate formation with other observable phenomena like optical emission.

Test beds

Two laser ablation test bed systems will be assembled to characterize laser ablation plumes. One test bed will be used to conduct ultraviolet–visible–near-infrared experiments and the other test bed will be used to characterize the thermal/molecular emission and absorption in the infrared spectral region. Nd:YAG lasers, with energies up to 1 Joule, will be used to create an ablation plume from a target of a selected material. A stage with a set angular velocity will be used to provide new surface material for ablation/plasma creation.

Spectral and Particulate Characterization

The spectral emission of the plasma will be characterized with an Intensified Charge Coupled Display (ICCD) detector. Other spectroscopies such as absorption, laser induced luminescence and Raman spectroscopy will be used to study atomic, molecular and particle characterization. New technologies (picosecond laser with a fast gated imager) will be used for Raman characterization in the presence of high intensity luminescence. Picosecond and femtosecond lasers will be used as probe lasers of the plume.

New concepts in particulate collections will be evaluated to acquire temporal information during the coalescence of gaseous molecular species to particle formation. High speed schlieren, shadowgraphy and infrared imaging techniques will be pursued to capture fast phenomena. Particle collectors with deflectors for ionized particulates will be considered in this research. In these experiments, aluminum, steel, carbon and soil will be used to evaluate particle formation. Ablation of a depleted uranium metal target will be considered as a possible source of nanograms of material for reactions with aluminum. Several experiments will be conducted to explore the different aspects of plasma attributes. The particle research falls closely in the field of particle archaeology, in the sense that we would like to find how particle formation takes place in an explosion and how to identify its temporal evolution in order to improve our collections in the field.

The particle research falls closely in the field of particle archaeology in the sense that we would like to find how particle formation takes place in an explosion and how to identify its temporal evolution in order to improve our collections in the field.

These experiments conducted in the laboratory will help us evaluate future technologies that will be deployed in the field during HE experiments enabling SRNL to continue its presence in these campaigns.

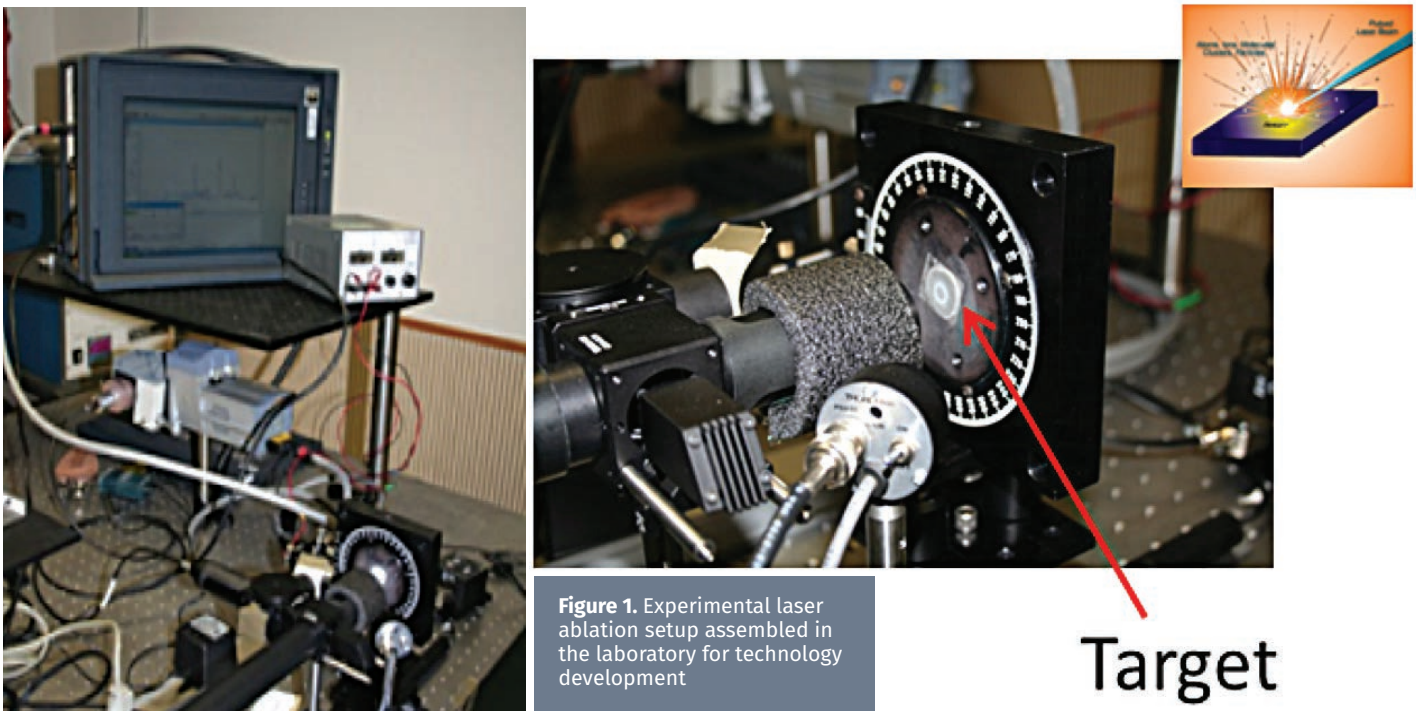

Figure 1. Experimental laser ablation setup assembled in the laboratory for technology development

RESULTS / DISCUSSION

The goal of this two year LDRD strategic project is to develop new technologies and methodologies to characterize the detonation of HE via laser-induced plasmas in the laboratory. Since solids, gases and ionized matter are present in any explosion/implosion, this research focused on the characterization of materials that might be present in these devices. The scientific literature was reviewed to develop an experimental plan in order to identify measurable phenomena. Spectral emission from elemental and molecular species is critical in the analysis of laser plasmas. Spectral information might be obtained through fluorescence, laser-induced fluorescence, Raman and absorption spectroscopy. Particulates generated in a detonation have different sources which include spallation and particle growth from molecular gases. Temperature is also an important aspect of any given detonation. Shockwaves provide information on energy propagation. The requirements suggest developing a system that can simulate an explosion via laser-induced ablation of a target and characterization of light emission from the ultraviolet through the infrared region of the electromagnetic spectrum. Since spectral information is highly dependent on the temporal behavior, technologies are required to investigate the dependence of spectra on the temporal scale. The path forward for this project requires the assembling of a test bed system capable to produce “explosions on demand” and use the system to measure observables in laser ablation plasma to compare (emulate) to real world detonations. The following information captures some of the work conducted in FY15, followed by the work completed in FY16.

1. Two laser ablation experimental setups were assembled to study laser generated plumes in the ultraviolet-visible-near infrared spectral region and in the mid to long-infrared spectral region.
   a. One laser ablation system was assembled with a step-scan Fourier transform infrared (SS-FTIR) spectrometer to monitor surface and gaseous molecular species with a temporal resolution of 50 ns, shown in Figure 1. The performance of the ablation system was good but the SS-FTIR performed below expectations. The problem was identified as a bad connector within the spectrometer. The compartment of the FTIR was modified allowing for several experiments to be conducted. The SS-FTIR will enable us to study the temporal evolution of surface species and the oxidation of material followed by the generation of particulates.

b. A second laser ablation experimental setup was built to study laser-induced fluorescence, particle collection and shock waves. The system performance was demonstrated with an Al target. The primary ICCD developed timing problems and the detector with the spectrograph was sent for repairs. A more limited spectrograph was used to further demonstrate ablation and thermal emission.

2. Laser ablation of aluminum and copper targets was demonstrated with both laser ablation systems.

3. An infrared diffuse accessory was modified to study the effect of laser ablation on an IR diffuse beam accessory.

4. A new infrared emission setup was assembled to study surface spectroscopy.

5. Developed a microscope system to observe temporal phenomena with picosecond and femtosecond lasers.

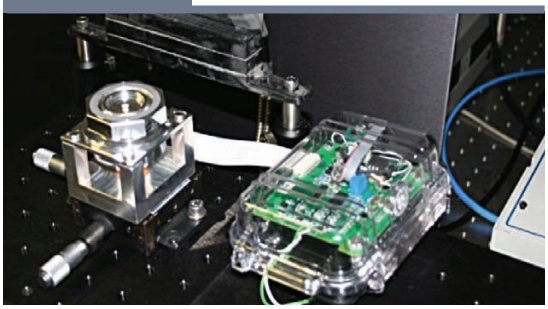

Figure 2. Experimental breadboard for temporal and spectral separation of fast phenomena

6. A picosecond gate imager was procured and the gated HRI was successfully tested with a camera and spectrograph at 76 MHz and with a 200 ps window.

7. An ion lens kit was procured to collect particulates from a laser ablation pulse.

8. A new device to measure spectral information from fast phenomena was designed, built and tested in the laboratory, shown in Figure 2. The concept will enable observation of the spectral evolution of an explosion or any transient phenomenon into microsecond segment intervals. First tests of the system were successful and we are currently working on a patent.

9. Developed a platform for Coherent anti-Stokes Raman spectroscopy (CARS) to be used with plumes and particles.

10. Developed a system that enables the measurement of optical spectra from high speed phenomena.

a. Tested and applied a high speed visible camera (Phantom) to image temporal events on the order of 1 microsecond, including using Schlieren and shadowgraphy imaging techniques, example shown in Figure 3.

b. Tested and applied a high speed infrared camera for short temporal imaging of fast phenomena, example shown in Figure 4.

11. Measured the Raman spectrum of nanodiamonds from carbon-bearing materials that are related to HE.

12. Characterized soot with deep UV light (244 nm).

13. Measured carbon entrapment in uranium samples from HE experiments.

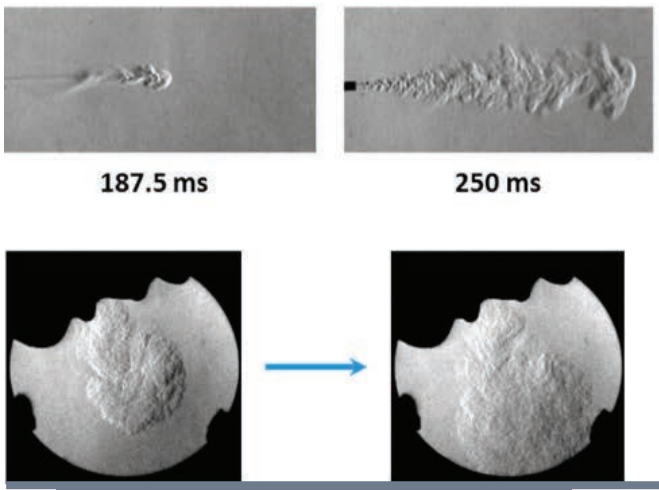

Figure 3. High speed Schlieren analysis of an air duster plume and a person coughing

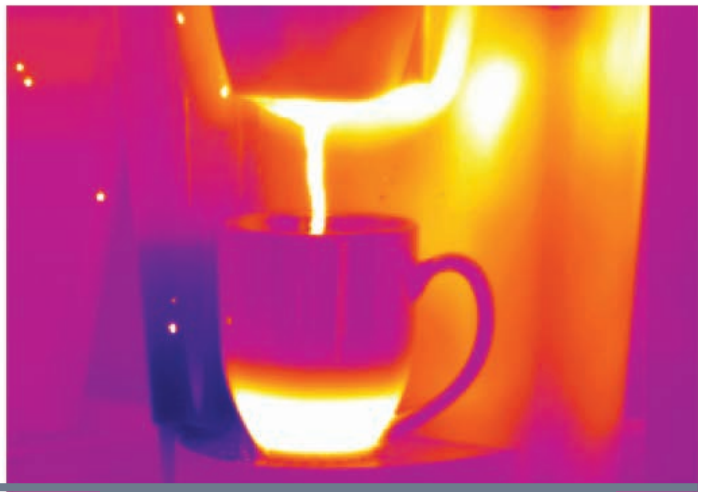

Figure 4. High speed infrared imagery of a coffee maker with liquid droplets

FY2016 ACCOMPLISHMENTS

- Assembled and tested two laser ablation systems
- Demonstrated temporal detection of light pulses with SS-FTIR
- Designed and fabricated a unique fiber optic assembly for multi-point emission characterization
- Designed, built and tested a new concept in spectral characterization from fast events
- Completed the assembly of a HRI gater/detector to work with a femtosecond laser to characterize repetitive transient phenomena and Raman spectroscopy
- Demonstrated the use of high speed cameras (visible and infrared) to characterize fast phenomena
- Characterized uranium and carbon-bearing materials

FUTURE DIRECTIONS

- The temporal analysis of transient phenomena will be demonstrated with the HRI gater/picosecond laser
- The HRI gater with a high repetition rate laser (Ti:Sapphire laser at 76 MHz) will be used to measure the Raman spectrum from uranium-bearing compounds in soil samples with high luminescence.
- Future studies will be conducted to see the temporal growth of particulates with a high speed camera
- Soot samples will be characterized with CARS

Acronyms

CARS	Coherent Anti-Stokes Raman Scattering
HE	High Explosive
HRI	High Rate Imager
ICCD	Intensified Charge Coupled Display Detector
nm	Nanometer
ns	Nanosecond
PM	Particulate Matter
SS-FTIR	Step-Scan Fourier Transform Infrared Spectrometer

Intellectual Property

An invention disclosure on the temporal/spectral measurement of a transient phenomenon is being written

Total Number of Post-Doctoral Researchers

1. Amanda L. Houk, Oak Ridge Associated Universities
2. Kimberly Fessler, Oak Ridge Associated Universities

Magnetically Induced Heat Generation For Controlled Hydrogen Isotope Release From Nano-Hydrides

Project Team: S. Hunyadi Murph (Primary), K. Coopersmith, H. Sessions, M. Brown, G. Larsen, R. Lascola
Subcontractor: Greenway/ARC
Thrust Area: Non-proliferation and Nuclear Deterrent
Project Type: Strategic
Project Start Date: October 1, 2014
Project End Date: September 30, 2016

This project is directly related to the Tritium Production and Readiness Mission but can be used in fields of separations to remotely load/unload environmental analytes, sensing, manipulation and photothermal destruction of analytes, catalytic processes, biological imaging and magnetic manipulation, hyperthermia applications, energy storage materials among others. The ultimate goal of this project is to generate heat wirelessly, targeted, on demand ("flip of a switch") from a plasmonic (light) or alternating electromagnetic field for the targeted release of hydrogen gas that will eradicate the use of hot/cold nitrogen (HCN) processes. Multifunctional hydride-magnetic materials were used for magnetically induced hydrogen release. The rate and amount of hydrogen release was controlled by varying the magnetic field strength by varying the current. This controlled release (significant results) can be employed to selectively release different hydrogen isotopes by varying the magnetic field strength as well as the size of the coil. This new proposed design demonstrates that plasmonically or magnetically induced heat generation for controlled isotope release from hydride beds is a viable and simple alternative. It is easy to implement and will eliminate the use of bulky HCN systems. With a very small footprint, the proposed technology will also provide a safer method of handling radioactive materials.

FY2016 OBJECTIVES

Evaluation and optimization of heat-responsive magnetic-hydride materials with hydrogen analogues from a controlled oscillating electromagnetic field

Optimize the heating efficiency from a controlled oscillating electromagnetic field or plasmonic field as function of material and magnetic field property data

Demonstrate controlled release of hydrogen from Pd-Fe_2O_3 materials when exposed to an alternating magnetic field

INTRODUCTION

A hot/cold nitrogen (HCN) circulation system is currently being used in the Tritium facility for heating and cooling of hydride storage beds, hydrogen isotope separation through TCAP units, and flow- through beds for inert gas species separation. While operational, the hot/cold nitrogen system requires the use of large compressors, heat exchanges, valves and piping that is bulky and maintenance intensive. Therefore, one of the top priorities of the Tritium Facility is eliminating HCN system. A new technology is sought that will eradicate the use of hot/cold nitrogen to adequately perform the aforementioned processes. We propose to develop heat-responsive magnetic nanomaterials for the controlled release of hydrogen gas. The triggered release of hydrogen gas molecules will be achieved via localized heating induced from a controlled oscillating electromagnetic or plasmonic field.

In an oscillating magnetic field system, the magnetic nanoparticles act as a local "hot-spot" to heat up the surrounding environment by hysteresis loss or relaxation mechanisms. This occurs because the magnetic moment of the nanoparticle changes direction to line up with the external field, which can cause local heating. This change of direction can take place two different ways: Brownian relaxation, where the nanoparticle physically rotates so the moment lines up with the external field, and Neel relaxation, where the particle is stationary, but the magnetic moment rotates in the fixed lattice.

Utilizing magnetic nanoparticles for heat generation has a range of advantages over conventional heating methods:

- >> Energy input is noncontact, selective, localized and targeted.
- >> Heat generation occurs wirelessly, remotely and the resultant heat is also targeted.
- >> Heat delivered can be modulated by suitable selection of alternating electromagnetic or plasmonic field, such as amplitude and frequency of the alternating magnetic field, shape of the magnetization curve, VIS-near IR, as well as material's type, size, shape and crystallinity.
- >> The magnetic/plasmonic nanoparticles can be selectively placed in regions where heat is necessary and stimulated to generate the desired amount of heat in a controlled manner.
- >> Heating can be self-controlling based on the Curie temperature of the material.

APPROACH

Multifunctional nanoparticles with a magnetic (Fe_2O_3) or a plasmonic domain (Au) and a hydrogen storage domain (Pd) have been synthesized for the controlled and localized heating with light or an alternating magnetic field. Using nano-metal hydrides to process tritium would lead to a reduced footprint and lower costs by allowing for localized temperature control and employing smaller storage beds.

The magnetic heating of multifunctional nanoparticles has been controlled by altering the nanoparticle composition, size, shape and concentration. The heating efficiency of the Fe_2O_3 nanoparticles was not dependent on the growth of another metallic domain. Unlike bulk heating, magnetic heating locally targets the species that interacts with the field, thus, the temperature at the surface is expected to be higher than the surroundings. This will lead to a rapid and localized heating within the hydride beds without significantly heating the entire vessel. To measure this temperature difference, the nanoparticles have been functionalized with fluorescent DNA to map the surface temperature via the DNA melting temperature. Hydrogen sorption studies have also demonstrated the ability of solid Fe_2O_3-Pd and Pd nanoparticles to adsorb and release hydrogen as a function of temperature.

RESULTS / DISCUSSION

Magnetic and metallic nanoparticles (NPs) can absorb magnetic or electromagnetic energy and release it as heat.[1-4] This heating method is highly localized, controlled and non contact, so it has been exploited for targeted drug delivery, tumor ablation, MRI imaging agents, among others. In this project, magnetic nanoparticles were functionalized with hydrogen absorbing metal domains to control the absorption and release of hydrogen. Fe_2O_3 nanoparticles were-functionalized with gold (for plasmonic heating) and palladium through metal reduction in the presence of the Fe_2O_3 nanoparticle seeds.[5, 6] SEM and EDX imaging was used to image the growth of the metal domains as shown in Figure 1.

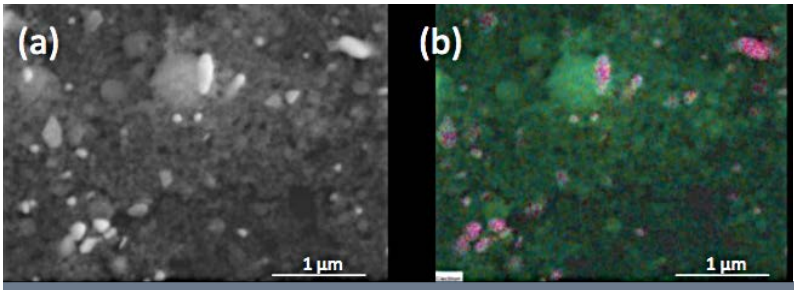

Figure 1. (a) SEM and (b) EDX mapping of Fe_2O_3-Au conjugates

The effect of concentration, metal domain growth and NP shape on magnetic hyperthermia was investigated. In Figure 2a, higher concentrations of Fe_2O_3 led to higher final temperature of the magnetic solution; however, it did not have an effect on the specific loss power, or the amount of power achievable per gram of Fe_2O_3 (Figure 2b). The growth of a metal domain didn't affect the temperature, indicating the preservation of the magnetic properties after functionalization. Comparing different shapes of Fe_2O_3 NPs, nanotubes, nanorings and nanowires didn't create any heat in the alternating magnetic field. As shown in figure 2d, the nanospheres responded to the magnetic field; therefore all experiments were carried out with the Fe_2O_3 spheres.

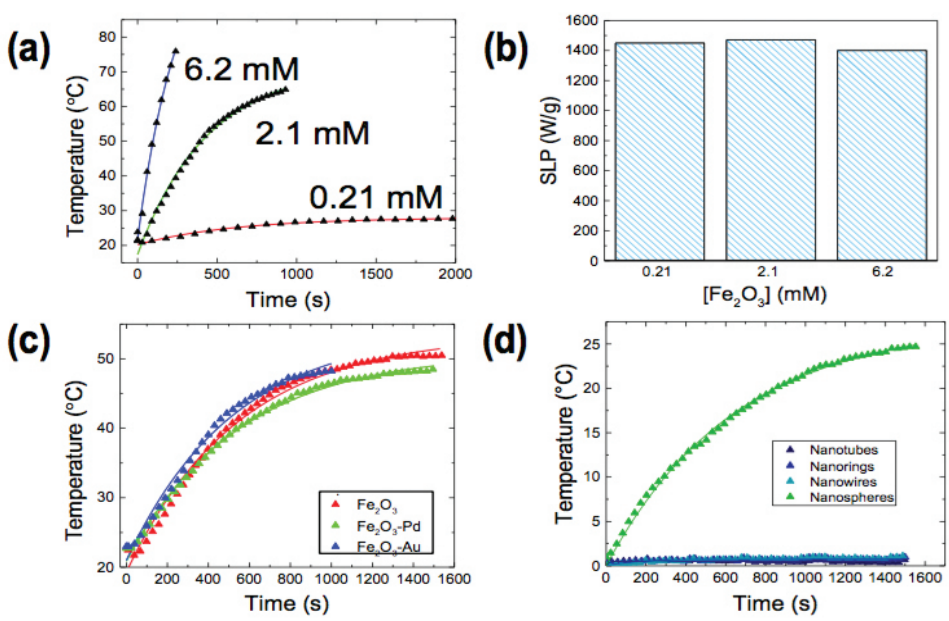

Figure 2. Magnetic hyperthermia effects of (a-b) different concentrations of Fe_2O_3 NPs; (c) metal domain growth and (d) NP shape

Hydrogen was loaded onto Fe_2O_3-Pd particles supported inside of a capillary tube as seen in Figure 3a. The hydrogen was loaded when the capillary was cooled using dry ice. The larger pressure decrease during the cooling for the Fe_2O_3-Pd capillary compared to the control Fe_2O_3 capillary is an effect of hydrogen absorption by the palladium, which is a known hydride material (Figure 3b).[7,8] Once the capillaries were loaded with hydrogen and were brought back to room temperature, they were exposed to an alternating magnetic field. As shown in Figure 3c, there was an immediate increase in pressure for the Fe_2O_3-Pd NPs but not for the Fe_2O_3, demonstrating the release of hydrogen due to the interactions of the Fe_2O_3-Pd NPs with the magnetic field.

To determine if the hydrogen release could be controlled, the pressure was measured for the Fe_2O_3-Pd capillary with different magnetic field strengths by altering the power output of the magnetic induction heater. As shown in Figure 4, the pressure maximum and the initial slope both increased with increasing current and magnetic field strength. The increase in the initial slope indicates the increase in the kinetics of hydrogen release from the Pd hydride. This data demonstrates that the rate of hydrogen release from Fe_2O_3-Pd hydride materials can be controlled through an alternating magnetic field. For future studies, the effect of magnetic field strength and the controlled and selective release of the different isotopes will be investigated.

In this report, multifunctional hydride-magnetic materials were used for magnetically induced hydrogen and magnetic field strengths for the hydrogen release. The rate and amount of hydrogen release was controlled by varying the magnetic field strength by varying the current. This controlled release can be employed to selectively release different hydrogen isotopes by varying the magnetic field strength as well as the size of the coil.

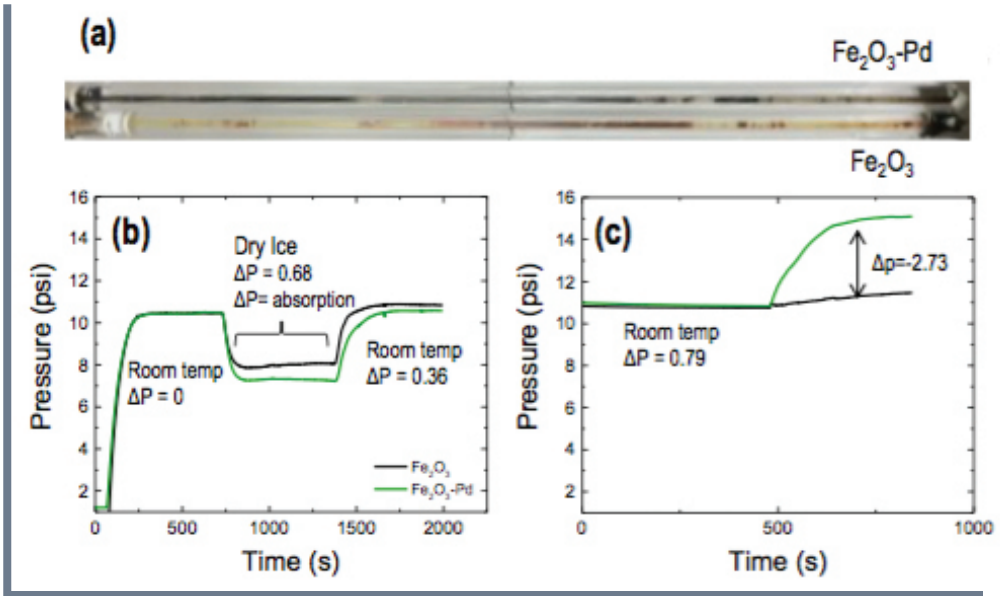

Figure 3. (a) Fe_2O_3 (control) and Fe_2O_3-Pd capillaries; Change in pressure of Fe_2O_3 and Fe_2O_3-Pd loaded capillaries during (b) absorption and (c) magnetically induced release of H_2

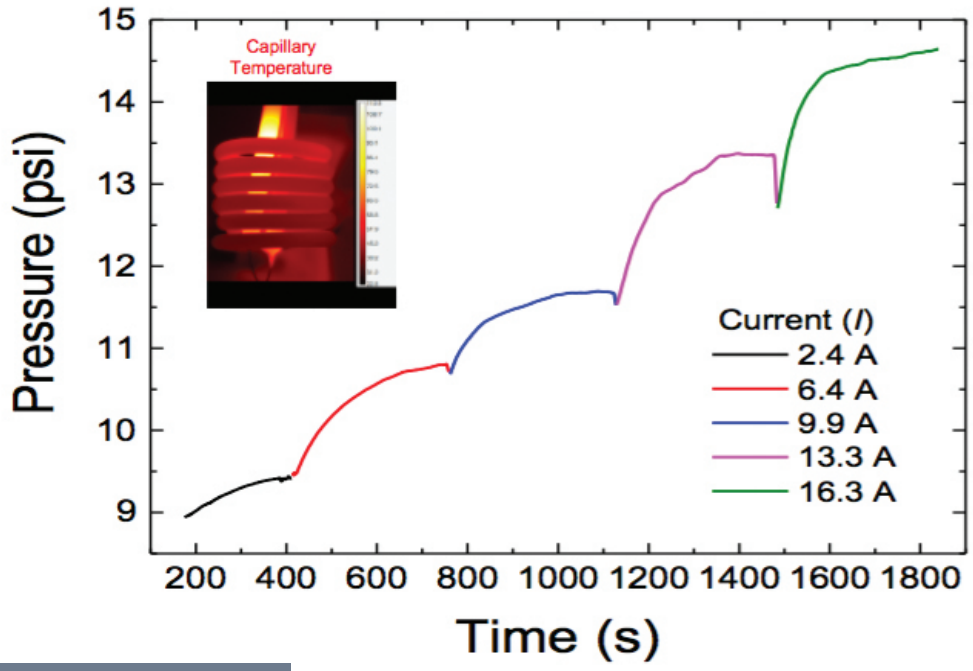

Figure 4. Change in pressure for different current and magnetic field strengths for the hydrogen loaded Fe_2O_3-Pd capillary; ***Inset:*** Capillary temperature imaged using an infrared thermal imaging camera

FY2016 ACCOMPLISHMENTS

Nano-materials fabrication & characterization

INCLUDED:

>> Prepared and characterized a library of multi-functional nanoparticles (Nps) of different size, shape, composition and properties: Fe_2O_3-Au-Pd

Generate targeted heat wirelessly and on demand via alternating magnetic field

INCLUDED:

>> The heating rate of the Fe_2O_3 Nps is not significantly affected by the growth of metal (Au/Pd) domains on the surface; *Ex. 75 °C ≈ 3 min for 1 mg material.*

>> Reproducible results; Variables: Np shape, concentration, composition, sample volume & coil size

>> Nanothermometry: Functionalized Nps with fluorescent molecular beacons (DNAs) for mapping temperature profiles on the NP surface; Ex: NPs surface temperatures is ≈ 1.5x higher than bulk temp

Hydrogen gas absorption studies

INCLUDED:

>> Demonstrate hydrogen sorption onto Pd and Pd-Fe_2O_3 Nps (Nps in solution and solid Nps);
Ex. A reversible storage capacity of≈ [H (mol) / Pd (mol)] = 0.45 from the nanoparticle isotherms → 11 grams of nanoPd will store 1 liter of H_2

>> Reproducible results after several sorption/desorption processes

>> Magnetically induced heating: hydrogen gas is released upon magnetically induced heating of hydride/magnetic Nps in solution

>> Theoretical/modelistic studies: a thermal energy balance model was generated which provides an accurate calculation of the heating rate of the nanoparticles; the theoretical results are in agreement with the experimental results.

>> Multifunctional hydride-magnetic materials were used for magnetically induced hydrogen release (The rate and amount of hydrogen release was controlled by varying the magnetic field strength by varying the current; This controlled release can be employed to selectively release different hydrogen isotopes by varying the magnetic field strength as well as the size of the coil)

FUTURE DIRECTIONS

- Evaluation and optimization of heat-responsive LANA materials with hydrogen analogues

Publications/Presentations

1. **"Multifunctional Fe2O3-Au Nanoparticles with Different Shapes: Enhanced Catalysis, Photothermal Effects, and Magnetic Recyclability",** J. Phys. Chem. C, 2016, 120, 15162- 15172.
2. **"Porous Iron Oxide Nanorods and Their Photothermal Applications",** SPIE Proceeding, Nanophotonic Materials XIII, 2016.
3. **"Multifunctional Hybrid Fe2O3-Au Nanoparticles for Efficient Plasmonic Heating",** J. Visual Experiments (JOVE), 2016, (108), e53598, doi:10.3791/53598.
4. **"Fe2O3/TiO2 Core-Shell Nanorod Array for Visible Light Photocatalysis",** Catalysis Today, special issue C1 Catalytic Chemistry, 2016, 270, 51-58. Undergraduate student publications—conference proceedings.
5. **"Synthesis and Characterization of Novel Nanothermometers",** National Conference on Undergraduate Research (NCUR) 2016.
6. **"Synthesis and Characterization of Novel Nanothermometers",** Phi Kappa Phi (PKP) - Augusta University, 2016.
7. **"DNA Functionalized Gold Nanoparticles for Thermometry Applications",** SERMACS, 2016.

References

1. **Keblinski, P., Cahill, D. G., Bodapati, A., Sullivan, C. R., Taton, T. A., "**Limits of Localized Heating by Electromagnetically Excited Nanoparticles" J. Appl. Phys. 2006, 100, 054305.
2. **Coral, D. F., Zelis, P. M., Marciello, M., del Puerto Morales, M., Craievich, A., Sanchez, F. H., Fernandez van Raap, M. B.** "Effect of Nanoclustering and Dipolar Interactions in Heat Generation for Magnetic Hyperthermia". Langmuir 2016, 32, 1201-1213.
3. **Laurent, S., Dutz, S., Hafeli, U. O., Mahmoudi, M.,** "Magnetic Fluid Hyperthermia: Focus on Superparamagnetic Iron Oxide Nanoparticles", Adv. Colloid Interface Sci. 2011, 166, 8-23.
4. **Jiang, K., Smith, D. A., Pinchuk, A.** "Size-Dependent Photothermal Conversion Efficiencies of Plasmonically Heated Gold Nanoparticles". J. Phys. Chem. C 2013, 117, 27073-27080.
5. **Carbone, L., Cozzoli, P. D. .** "Colloidal Heterostructured Nanocrystals: Synthesis and Growth Mechanisms", Nano Today 2010, 5, 449-493.
6. **Zhang, H., Ding, J., Chow, G., Dong, Z.,** "Engineering Inorganic Hybrid Nanoparticles: Tuning Combination Fashions of Gold, Platinum and Iron Oxide", Langmuir 2008, 24, 13197-13202.
7. **Konda, S. K., Chen, A. "**Palladium Based Nanomaterials for Enhanced Hydrogen Spillover and Storage", Mater. Today 2016, 19, 100-108.
8. **Griessen, R., Strohfeldt, N., Giessen, H.** "Thermodynamics of the Hybrid Interaction of Hydrogen with Palladium Nanoparticles",. Nat. Mater. 2016, 15, 311-317.

Acronyms

Nps Nanoparticles

Intellectual Property

Four invention disclosures submitted

2016 SRS-16-033 "Controlled Release of Hydrogen Gas from Nano Hydrides via Induced Magnetic Field"
2016 SRS-17-003 "Targeted release of nanoparticle sequestered analytes via plasmonic or magnetic field"
2016 SRS-16-016 "Plasmonic Distillation Separation of Hydrogen Isotopes in the Liquid Phase.
2016 SRS-15-016 "Multifunctional Nanomaterials for Efficient Plasmonic Heating and Catalytic Applications"

Total Number of Post-Doctoral Researchers

Two Post-Doctoral Researchers

Graphene-Based Gas Separation Membranes

Project Team: D. Hitchcock, S. Serkiz, J. Velten, M. Townsend (SRNL), A. Rao, S. Bhattacharya (Clemson University)
Subcontractor: Clemson University
Project Type: Strategic
Project Start Date: October 1, 2014
Project End Date: September 30, 2016

Gas separation is wide spread in industrial and commercial processes. Thin membranes are highly suitable for the role of selective separation membranes, but are limited by their mechanical strength, chemical compatibility, and target molecule selectivity. In this work, we focused on developing graphene-based gas separation systems. By introducing suitable and controlled defects (i.e., pores) in continuous graphene sheets, the properties of this otherwise impermeable one atomic-layer thick membrane can be tuned to selectively separate gaseous species. Based on this principle, our primary goal was to achieve efficient separation of trace gases (H_2S, He, Ar, N_2, H_2O, and CO_2) from natural gas streams and impurities (NH_3, H_2O, and He) from tritium process streams. The results from the work are expected to improve both portable and large-scale gas-separation processes.

FY2016 OBJECTIVES

- Synthesize graphene and graphene oxide films
- Introduce controlled defects in the membranes by B and N doping, and neutron irradiation
- Characterize "as-prepared" and "defects-induced" membranes by Raman, FTIR, XPS, and HRTEM
- Characterize the permeability of membranes for target gas analytes

INTRODUCTION

Membrane-based gas separation systems have gathered tremendous interest owing to their high efficiency and low energy consumption. In principle, these membranes should be as thin as possible to maximize flux [1]. However, thin membranes often suffer from poor mechanical strength which poses a major hindrance to their effective application. Graphene, a two-dimensional (2-D) carbon allotrope, has emerged as a single-layer material possessing ultra-high mechanical strength, chemical inertness, and thermal stability. These properties meet the requisite characteristics of suitable gas-separation membranes.

In their pristine form (i.e., continuous sheet with no defects), graphene membranes are impermeable to all gases, including hydrogen. This property is attributed to the overlapping π-orbitals that form a dense delocalized electron cloud that block the passage of all gaseous species. However, their permeability can be tuned by introducing defects into the continuous graphene sheet [2]. These defects disrupt the orbital structure rendering it permeable to specific molecules. This project was aimed at developing methods to engineer the permeability of graphene membranes via the introduction of defects by either the removal of carbon atoms or the addition of dopant atoms.

To reach our intended goals, we have fabricated suspended graphene membranes with induced lattice defects for the purpose of investigating their permeation properties. In our preliminary experiments, we used a high-energy electron beam (e-beam) and reactive ion etching (RIE) processes to introduce lattice defects in the suspended graphene sheets. This e-beam approach, however, is not amenable to scalable membrane systems, and RIE was not controllable in terms of the quality and quantity of lattice defects emplaced. Later experiments have focused on introducing defects through neutron exposures of graphene membranes, and in-situ doping of B and N in the graphene lattice. These graphene membranes, both pristine and defect-induced, were then spectroscopically characterized and imaged at the atomic level using aberration-corrected High Resolution Transmission Electron Microscopy (HR-TEM) at the Center for Nanophase Materials Science (CNMS) at Oak Ridge National Lab (ORNL). Besides developing these defect engineering processes, a sensitive gas permeation characterization system based on mass spectrometry was designed and assembled.

APPROACH

The experimental approach was to take advantage of the unique properties of graphene to design and fabricate membranes for highly selective gas separation processes by manipulating their chemical functionality, surface charge, and the number and character of defect sites (holes or nitrogen/ boron dopants in the graphene lattice structure). From an engineering standpoint, stacked platelet (Figures 1A & B) and porous continuous-sheet membrane (Figure 1C) designs were candidates as modified graphene membranes for subsequent evaluation.

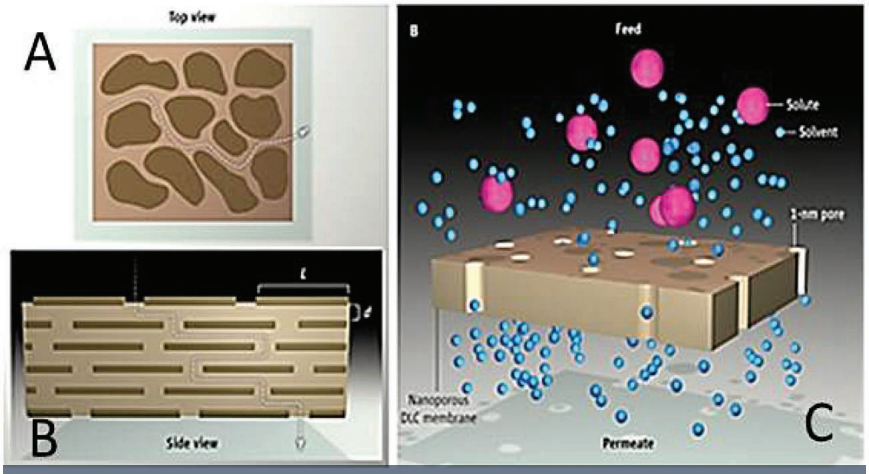

Figure 1. (A) top view of dispersed nanoplatelets of graphene; (B) side view of intercalated nanoplatelet design; (C) schematic of continuous sheet design and process (note: pink spheres represent solute and blue spheres solvent) [3]

The proposed work leverages ongoing NSF-funded work in the area of scalable production of carbon nanotubes (Clemson) and the development of permeation barriers and radiation resistant polymers (SRNL) funded by the PDRD program.

RESULTS / DISCUSSION

Both pristine- and doped-graphene samples have been grown using the Chemical Vapor Deposition (CVD) method. Defects have been emplaced in-situ by B and N doping during synthesis on a number of different substrates. These samples have been characterized by Raman spectroscopy, Fourier Transform Infrared (FTIR) spectroscopy, x-ray photoelectron (XPS) spectroscopy, and High Resolution Transmission Electron Microscopy (HRTEM). The XPS results confirmed the existence of the N-doping in the graphene. Furthermore, this doping was observed as defect structures in the aberration corrected HRTEM (Figure 2).

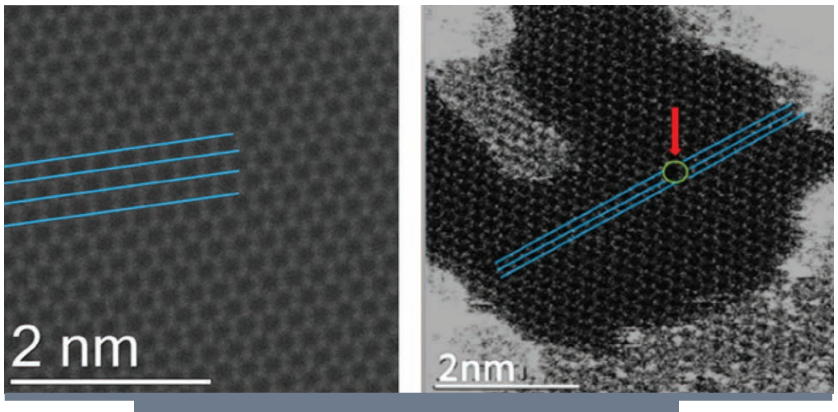

Figure 2. Atomic level HRTEM of (L) pristine graphene and (R) N-doped graphene with Pyridinic defects

A representative Raman spectrum of pristine graphene, collected using a 514.5 nm laser excitation, exhibits the characteristic D (disorder), G band (graphitic) and G' band at ~1350, 1582 and ~2700 cm^{-1} as shown in Figure 3. Furthermore, control of the growth parameters allowed for the selective production of bi-layer graphene, as indicated by the similar intensities of the G and G' bands (Figure 3). Fitting of the G' band to a single Lorentzian peak can be deconvolved into four Lorentzian peaks (Figure 3) also indicated the presence of bi-layer graphene [4].

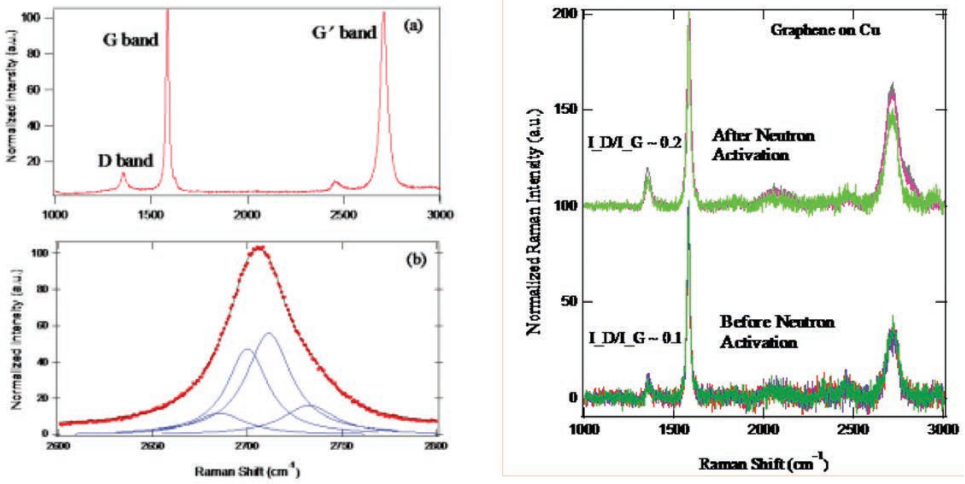

Figure 3. ***(upper left)*** Raman spectra and ***(lower left)*** Lorentzian fit of bilayer graphene. ***(right)*** Raman spectra of graphene before and after exposure to neutron irradiation

In an attempt to introduce controlled defects in the graphene lattice, pristine graphene samples grown on copper and nickel substrates were exposed to neutrons at SRNL. The Raman spectra of graphene grown on copper, before and after neutron exposure, are shown in Figure 3. Surprisingly, the D-band (arising from disorder) of graphene did not increase after neutron exposure. The ratio of the intensities of the D and G-bands of graphene changed slightly from ~0.1 to ~0.2 indicating that the graphene was mostly unaffected by neutron exposure. The aberration corrected TEM image of the neutron-exposed graphene also showed no visible defects. This may indicate that a longer neutron exposure would be necessary to produce the desired defects in graphene. Further investigation on the effect of neutron exposure on graphene is necessary to arrive at better understood conclusions.

When transferred to a substrate, graphene membranes are very delicate and, therefore, did not survive our initial permeation measurements. For this reason, a parallel-pass permeation measurement system was designed and built in order to avoid dislodging the membranes during testing. The new design, uses a Residual Gas Analyzer (RGA) as the detector, and an Ar sweep gas, and allows for very small differential pressures across the membrane, which can be controlled by adjusting the back pressure on the exhaust lines.

Figure 4 is the schematic of the fabrication scheme of graphene membranes for gas permeability measurements: i) Graphene Membrane-1 grown on copper and nickel substrates and transferred with Poly(methyl methacrylate) (PMMA) to Swagelok VCR gaskets with the graphene layer facing the VCR, ii) Graphene Membrane-2 grown on copper and nickel substrates and transferred with PMMA on to VCR MGFS with a prior layer of graphene, iii) graphene grown on compressed nickel foam substrates that exhibited micron sized holes. Due to time constraints, however, permeation measurements on graphene membranes were not completed.

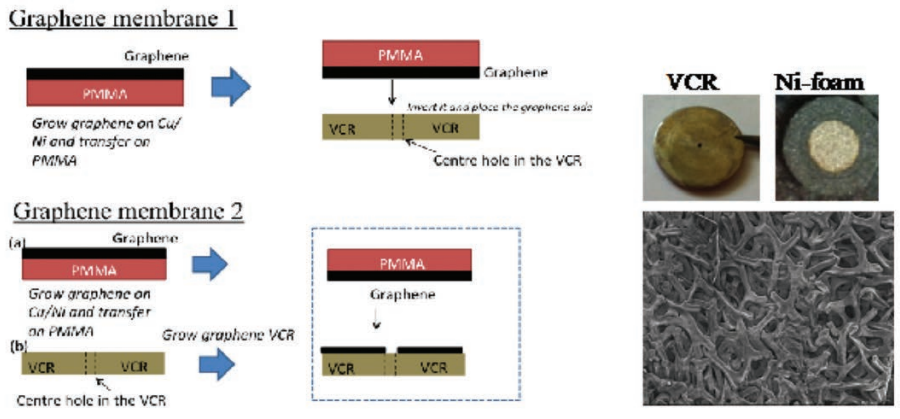

Figure 4. Left panel shows the schematic of two types of graphene membranes ***(described above)*** fabricated for gas permeability measurements; The top right panels show a commercial VCR with ~450 μm bore and a compressed Ni foam substrate for graphene growth and membrane testing (The panel on the right ***(bottom)*** is the SEM image of a compressed Ni-foam substrate with numerous micron-sized bores)

FY2016 ACCOMPLISHMENTS

Produced & characterized graphene films (Both pristine and doped graphene samples have been grown using the CVD method; Defects have been emplaced by B and N doping during synthesis on a number of different substrates)	Samples have been characterized by Raman, FTIR, XPS, and HRTEM	Pristine undoped graphene samples have been exposed to neutron irradiation at SRNL	Boron-coated graphene samples are scheduled for neutron exposures at SRNL	Designed and assembled parallel pass gas permeation test setup

FUTURE DIRECTIONS

- Neutron irradiation of boron coated graphene samples are currently scheduled at SRNL; The (n,alpha) reaction of the B with incident neutrons offers a way to control the momentum of the incident radiation on the graphene

Publications/Presentations

S. S. K. Mallineni, D. W. Boukhvalov, I. S. Zhidkov, A. I. Kukharenko, A. I. Slesarev, A. F. Zatsepin, S. O. Cholakh, A. M. Rao, S. M. Serkiz, S. Bhattacharya, E. Z. Kurmaev, and R. Podila "Influence of dopants on the impermeability of graphene" Submitted to Nanoscale

References

1. **Koenig et al. Nature Nanotechnology,** Vol 7, 2012, p 728
2. **Sun et al. Langmuir** 2014, 30, pp 675–682
3. **Paul, Science 2012,** 335 (6067) pp. 413-414
4. **Malard et al. Phys. Rep.** 2009, 473, 51-87

Acronyms

CNMS	Center for Nanophase Materials Science
CVD	Chemical Vapor Deposition
e-beam	Electron Beam
FTIR	Fourier Transform Infrared Spectroscopy
HRTEM	High Resolution Transmission Electron Microscopy
ORNL	Oak Ridge National Lab
PMMA	Poly(methyl methacrylate)
RIE	Reactive Ion Etching
RGA	Residual Gas Analyzer
XPS	X-ray photoelectron spectroscopy

Intellectual Property

An invention disclosure has been submitted, **SRS-15-009**

Total Number of Post-Doctoral Researchers

1. Josef Velton, postdoctoral researcher

2. Katie Townsend, intern (a doctoral student in the materials science department at GA Tech)

Advanced Ultrafast Spectroscopy for Chemical Detection of Nuclear Fuel Cycle Materials

Project Team: E. Villa-Aleman (Primary), W. A. Spencer, and A. L. Houk
Subcontractor: A. L. Houk
Thrust Area: Non-proliferation and Nuclear Deterrent
Project Type: Strategic
Project Start Date: October 1, 2015
Project End Date: September 30, 2017

The development of new signatures and observables from processes related to proliferation activities are often related to technological advancements. In our physical world, the intensity of observables is linearly related to the input drivers (light, current, voltage, etc.). Ultrafast lasers with high peak energies, opens the door to a new regime where the intensity of the observables is not necessarily linear with laser energy. Potential non-linear spectroscopic applications include chemical detection via remote sensing, material characterization and processing, surface phenomena modifications, nuclear fusion, etc. Currently, we can achieve laser energies in the 5 nano-Joule range, preventing the study of non-linear phenomena. To advance our non-proliferation research into the non-linear regime we require laser pulses in the milli-Joule (mJ) energy range. We have procured a 35 fs-7 mJ laser, operating at one kilohertz repetition rate, to investigate elemental and molecular detection of materials in the laboratory with potential applications in remote sensing. The spectral and temporal behavior of the laser pulses will be modified with a spatial light modulator allowing for quantum coherent control of the studied material.

FY2016 OBJECTIVES

Develop non-linear spectroscopic detection tools and techniques to characterize materials related to the nuclear fuel cycle using Raman, fluorescence and infrared spectroscopy

Demonstrate detection of particles of interest in soil samples that are at a distance of up to 5 meters away

INTRODUCTION

The National Security Directorate (NSD) has supported the DOE NA-22 Uranium Program via characterization of UO_2F_2 particulates and aged products with Raman, luminescence and infrared spectroscopic techniques. These techniques were used to study the behavior of particulates in the laboratory under different humidity and lighting conditions. Other U-bearing compounds (UO_2, U_3O_8 and UO_3) were also studied in order to understand the oxidation process of uranyl samples in the environment. NSD has also conducted particulate matter collection campaigns from different U-based sources. Particulate collections were made during campaigns dedicated to the detonation of devices with depleted uranium, U-bearing compounds from conversion and enrichment plants and other facilities dedicated to the production of materials from the nuclear fuel cycle. Our collections have resulted in the identification of unique signatures from different processes.

Similarly, pre-screening of environmental samples for anthropogenic uranium and fluoride compounds is important in order to identify proliferation activities. The hydrolysis of UF_6 results in the formation of UO_2F_2 and its aged products. Luminescence of the environmental soil matrix overwhelms the spectroscopic signals of interest originating from the anthropogenic compounds. The weak spontaneous Raman scattering signal requires long integration times for analysis and is one of the major limiting factors of large-scale sample analysis. Ultrafast lasers have opened new doors in research to enhance detection sensitivity. The expected several orders of signal enhancement (i.e. up to 10^6 orders of magnitude)[1] with non-linear spectroscopic techniques are a game changer for detection of chemical species related to proliferation activities.

The recent acquisition of femtosecond and picosecond lasers, a deep ultraviolet laser and an ultrafast gate imager for picosecond Raman spectroscopy has opened the door to conduct advanced linear and non-linear spectroscopic research. Currently, the laser systems helped to secure additional funding from DOE NA-22 to study plutonium particulates. The laser systems are also being used in different research projects funded by DOE NA-22 and LDRD programs. One goal of the current LDRD project is to demonstrate remote detection of U-bearing compounds in soil samples using Stimulated Raman Scattering (SRS) or Coherent Anti-Stokes Raman Scattering (CARS) in a stand-off configuration, which has successfully been shown in literature for the detection of explosive residues.[2] Data from this project will be used to write new work with NA-22 for improved detection sensitivity for U and Pu. In another project, a gated imager will be used to gate Raman scattering from particulates generated from laser ablation of targets within a 300 picosecond window, therefore eliminating/reducing the strong luminescent background interfering with the signal of interest. We are also exploring CARS to identify microscopic particles embedded in bulk material and in airborne material. These projects are providing technological seeds to grow a core capability within the DOE weapons complex that will facilitate increased ROI through future proposals to other government agencies.

APPROACH

Our research approach for this LDRD includes procuring an ultrafast laser, assembling the ultrafast laser in the laboratory and testing the laser performance. Additionally, procuring a spatial light modulator (SLM) and writing software to manipulate the energy and temporal properties of the femtosecond laser pulses with the SLM, shown in Figure 1.[3] Following installation of the ultrafast laser, a single laser Stimulated Raman Scattering (SRS) and CARS experimental setup will be assembled to analyze particulates of interest (i.e. nuclear fuel cycle materials). We will then demonstrate detection of particles of interest in soil samples, as well as detection of samples up to 5 meters away. Other spectroscopic and material processing applications will also be conducted and demonstrated, including surface modification through laser desorption and ablation, chemical characterization within the desorbed material pulse, hydrogen and deuterium detection, etc.

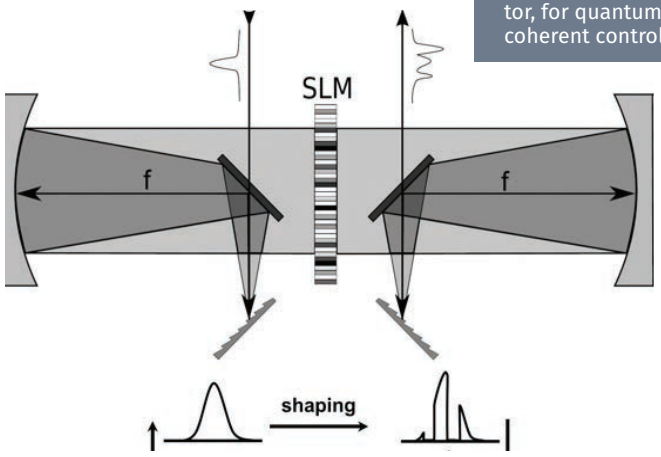

Figure 1. Modification of temporal and spectral information of a femtosecond laser pulse using a spatial light modulator, for quantum coherent control

RESULTS / DISCUSSION

Several ultrafast lasers from different manufactures were evaluated and an ultrafast laser system was selected and procured from Coherent. The ultrafast laser system chosen was the Astrella ultrafast Ti:Sapphire amplifier that produces <35 fs pulses at >7 mJ/pulse at a repetition rate of 1 kHz. An optical parametric amplifier (OPA), the OPerA Solo from Coherent was also chosen for use with the Astrella amplifier, which extends the wavelength range from 190 nm to 20 µm. The ultrafast laser and the OPA were delivered to the National Security Directorate laser laboratory on September 7, 2016 and are currently awaiting installation by the laser vendor, Coherent.

Various spatial light modulators (SLM) from several companies were considered and a transmissive SLM was chosen and procured from Meadowlark Optics. The SLM chosen was the CRi SLM-128-D-VN, which has a dual-mask configuration for simultaneous phase and amplitude pulse shaping in the range of 488-900 nm. The SLM was delivered to the laboratory on September 1, 2016. We have also completed the design of the microscope and optical components that are required to couple laser light to the sample.

FY2016 ACCOMPLISHMENTS

Several manufacturers of ultrafast lasers were evaluated in FY16; Coherent was chosen to provide the Astrella laser (<35 fs at >7 mJ/pulse and 1 kHz) and an optical parametric amplifier (OPA) covering the 190 nm to 20 µm spectral range (The ultrafast laser and OPA were delivered on September 7, 2016 and will be installed by Coherent)

Various SLM designs were assessed from different companies and a transmissive SLM was selected and procured from Meadowlark Optics (The SLM [CRi SLM-128-D-VN] has a dual-mask configuration for simultaneous phase and amplitude pulse shaping [spectral range of 488-900 nm]. The SLM was delivered on September 1, 2016)

Design of microscope and optical components required to couple laser light to the sample has been completed

FUTURE DIRECTIONS

- Demonstrate soft laser desorption and ablation of surfaces for analyses
- Setup and demonstrate Stimulated Raman Scattering (SRS) experiment with a single laser
- Demonstrate detection of several U-bearing compounds in the presence of luminescence materials, as in a soil sample
- Demonstrate detection of samples up to 5 meters away
- New technologies developed during this project have the potential to lead to applications in the fields of chemical detection via remote sensing, material characterization, surface decomposition, isotropic composition, etc.

References

1. **D. W. McCamant, P. Kukura and R. A. Mathies,** "Femtosecond Broadband Stimulated Raman: A New Approach for High-Performance Vibrational Spectroscopy," Appl. Spectrosc., vol. 57, pp. 1317-1323, 2003.
2. **M. T. Bremer and M. Dantus,** "Standoff Explosives Trace Detection and Imaging by Selective Stimulated Raman Scattering," Appl. Phys. Lett., vol. 103, pp. 061119, 2013.
3. **Y. Silberberg,** "Quantum Coherent Control for Nonlinear Spectroscopy and Microscopy," Annu. Rev. Phys. Chem., vol. 60, pp. 277-292, 2009.

Acronyms

CARS	Coherent Anti-Stokes Raman Scattering
fs	Femtosecond
mJ	Milli-Joule
NSD	National Security Directorate
OPA	Optical Parametric Amplifier
ROI	Return on Investment
SLM	Spatial Light Modulator
SRS	Stimulated Raman Scattering
U	Uranium

Total Number of Post-Doctoral Researchers

1. Amanda L. Houk, Oak Ridge Associated Universities

Synthesis of Zeolite Materials For Noble Gas Separation

Project Team: Randall Achey, Omar Rivera-Betancourt, Matthew Wellons, Douglas Hunter (SRNL), Christopher Klug (NRL)
Subcontractor: MPO interagency agreement (IAA) with NRL
Thrust Area: Non-Proliferation & Nuclear Deterrent
Project Type: Standard
Project Start Date: October 1, 2015
Project End Date: September 30, 2017

Microporous zeolite adsorbent materials are widely used as a medium for separating gases(1-3). Adsorbent gas separation systems can run at ambient temperature and require minimal pressure to flow the input gas stream across the adsorbent bed. This allows for low energy consumption relative to other types of separation systems. SRNL currently is the leader in using zeolites for noble gas sampling for non-proliferation detection platforms. However, there is a constant costumer need for improved noble gas sampling capabilities. This project will improve the understanding of how non-reactive gases adsorb to the surfaces and diffuse through the pore structure of zeolites. The zeolites that are currently used for noble gas separation have been characterized to understand which properties are most important for noble gas separation. This knowledge is being used to develop improved zeolites which will allow the building of a new generation of noble gas samplers.

FY2016 OBJECTIVES

- Currently used zeolites will be characterized using gas sorption analysis, SEM, XRD and Raman spectroscopy
- Microwave-assisted and conventional hydrothermal synthesis will be used to make a variety of zeolites tailored for noble gas separation
- Candidate materials will be down-selected based on highest available surface area, maximum overall capacity for gas adsorption and best selectivity for noble gases (or optimum exclusion of noble gases)
- Boronation and/or silanation modifications will be tested on commercial materials and new materials for fine-tuning of pore size and adsorption properties

INTRODUCTION

Advances in analytical techniques and the science of zeolites since the development of zeolites that are currently used at SRNL for noble gas sampling give the opportunity to improve the understanding of how zeolites separate noble gases from air and open the door to the synthesis of better zeolites. Data collected in the first year of this two-year strategic LDRD will be used to help guide the synthesis of these new materials. Microwave-assisted and conventional hydrothermal synthesis has been tested in initial trial syntheses in the first year, and will be used to make a variety of zeolites tailored for noble gas separation in the final year of the project. A thorough understanding of the properties of the existing zeolites has been gained through characterization of the materials with XRD, SEM, and gas sorption analysis. Such characterization has revealed which properties of our zeolite materials are most important for separating noble gases from air. Correlation of the performance of existing zeolite with these properties will allow intelligent design of new custom engineered zeolite materials with advantageous properties. Custom engineered zeolites will be synthesized from raw materials with chemistry designed to give optimal adsorption characteristics and pore structure that are best for noble gas separations while maintaining robust mechanical properties and hydrothermal stability[4]. If necessary, post-synthesis modification of the zeolites will be performed with boronation, silanation and/or ion exchange to fine tune the sorption characteristics. Full characterization of the synthesized materials will be used to determine the suitability of the synthesized zeolites for noble gas separation as well as compare their properties with the existing materials.

APPROACH

There are several zeolite materials that are currently used at SRNL for noble gas sampling. These zeolites were developed many years ago. They have a proven record of consistent and reliable performance. These zeolites are used in two different ways: one time grab sampling and continuous concentration. The grab sampling method relies on capture of the noble gas by the zeolite, while the continuous concentration method uses zeolites that exclude noble gases and adsorb the other gases in air. As part of this project, zeolites will be synthesized and/or modified to give improved performance in both sampling methods. For the continuous concentration sampling zeolite, materials will be synthesized that give better size exclusion of noble gases from the pores, and the composition of the zeolite surface will be designed to increase the heat of adsorption for nitrogen and oxygen to give better separation and higher capacity[1-3]. Two avenues are being pursued for material development. The first method is microwave assisted hydrothermal synthesis of zeolites from raw materials[4-6]. The use of a microwave oven to heat the mixture of reactants does greatly speed up the synthesis of zeolites as compared to traditional hydrothermal synthesis in conventional ovens. The second method of material development is modification of commercial zeolites using boronation, silanation and/or ion exchange.

Zeolite synthesis was performed at SRNL. Microwave synthesis equipment was used for the project, including the oven and synthesis vessels, to synthesize mordenite and Linde type L as initial trial syntheses for the project. Powder x-ray crystallography, electron microscopy and Raman spectroscopy were used for zeolite characterization. SEM has revealed crystal morphology for the different types of mordenites we have synthesized so far. X-Ray crystallography can determine the type of zeolite synthesized based on comparing the diffraction pattern of the powder sample with a reference library of diffraction pattern for the zeolite materials. For FY17, solid-state NMR analysis will give information on bonding environments of various elements in the crystal lattice. This will provide information on the newly synthesized samples' amorphous phases that cannot be detected by x-ray crystallography. Candidate materials will be down-selected based on highest available surface area, maximum overall capacity for gas adsorption and best selectivity for noble gases (or optimum exclusion of noble gases).

RESULTS / DISCUSSION

Initially we attempted variations on a mordenite synthesis performed at 190ºC for five days in a Teflon lined pressure vessel within a conventional heating oven. To improve the synthesis, we employed microwave heating technology in order to reduce the time of the reaction and increase sample purity. We performed this reaction by transferring a batch sample of synthetic mordenite into a Teflon lined vessel and then heating in a microwave at a temperature of 220 ºC. The purpose of this first set of syntheses was to study how long it takes to obtain a pure product tailored for our purposes. We performed the microwave heating experiments at time lapses of five hours[5]. After one lapse had passed we removed an aliquot of the sample to be characterized by p-XRD. As seen on the left panel of Figure 1, we performed the reaction up to 30 hours. At the five hour stage, the mordenite sample shows complete amorphous character.

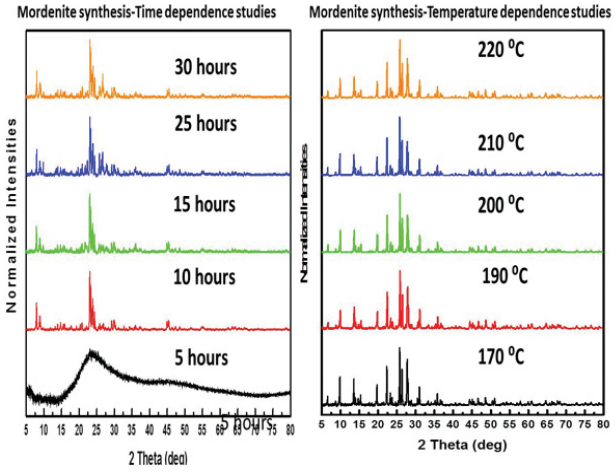

Figure 1. XRD scans of mordenite synthesized in a microwave reaction oven for a range of times and temperatures

For every five hour interval the amorphous character starts to disappear around the 2theta/theta angle of 20-30°. From the diffraction pattern results, a reaction time of 25 hours produced the highest intensities. The top left panel of Figure 1 shows this pattern matched with a known mordenite powder pattern from the ICDD database. This confirmed the presence of mordenite in our synthesized samples. All diffraction patterns showed interfering patterns of other minerals such as analcime and gismondine.

The right panel of Figure 1 shows another study performed to obtain synthetic mordenite[6]. For this study we focused on different microwave reaction temperatures ranging from 170-220 ºC. All reactions were completed in under 3 hours. We added a few milligrams of mordenite powder as a seed, CBV10ADS from Zeolyst corporation, to catalyze the rate of growth of the synthesized mordenite. Reactions carried out from 170 to 190ºC showed some characteristic XRD patterns for a positive identification of mordenite, but some amorphous character was present in these samples. This is not shown in Figure 1 as all the diffraction patterns have been baseline corrected. Diffraction patterns for the samples synthesized at 200-220ºC showed the highest rate of crystallinity, with little to no amorphous character present in the samples. The sample synthesized at 210ºC gave us the highest signal intensity. As seen in the bottom panel of Figure 2, this pattern matched a known mordenite powder pattern from the ICDD database. This helped us confirm the presence of mordenite in our synthewsized samples, with no presence of interfering patterns.

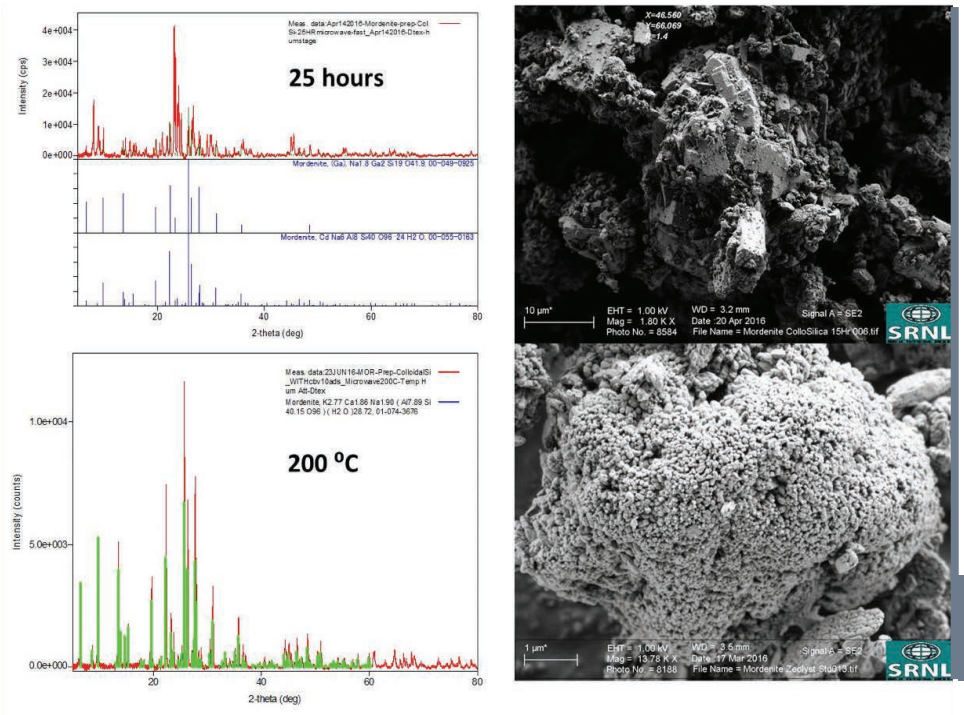

Figure 2. XRD scans of mordenite syntheized in a microwave compared with reference pattern

For trial syntheses of zeolites, the initial gas sorption analysis has shown that the samples have the expected microporous structure. We are still in the process of analyzing the synthesized zeolite samples.

We have performed gas sorption experiments since the start of the fiscal year 2016. Adsorption isotherms for the existing zeolite materials currently used in noble gas samplers have been completed. For trial syntheses of zeolites, the initial gas sorption analysis has shown that the samples have the expected microporous structure. We are still in the process of analyzing the synthesized zeolite samples. We found that mill grinding the samples prior to experimentation led to more available surface area. We employed Raman spectroscopy as a tool to characterize our samples. We used a 532 nm Ti Sapphire laser as our irradiation source and CCD detector to capture our signal. The left panel of Figure 3 shows the Raman spectroscopy results for several of the samples we have synthesized. The right panel of Figure 3 displays a representative spectral study of synthetic mordenite prepared at microwave reaction temperatures ranging from 170-220 ºC. These reactions were performed at reaction times of less than three hours using CBV10ADS seeds. All spectra showed characteristic Raman shifts corresponding to mordenite[7-10]. A wavenumber shift range of 390-460cm^{-1} corresponds to the movement of the five membered ring of the tetrahedron in the mordenite structural network. The band at 490cm^{-1} is due to metal-O-Si bending and symmetric stretching of the framework. The band close to 400cm^{-1} belongs to a five-fold ring stretch. Around the 950-1250cm^{-1} region we can find the Si-O-Al chain asymmetric stretching modes.

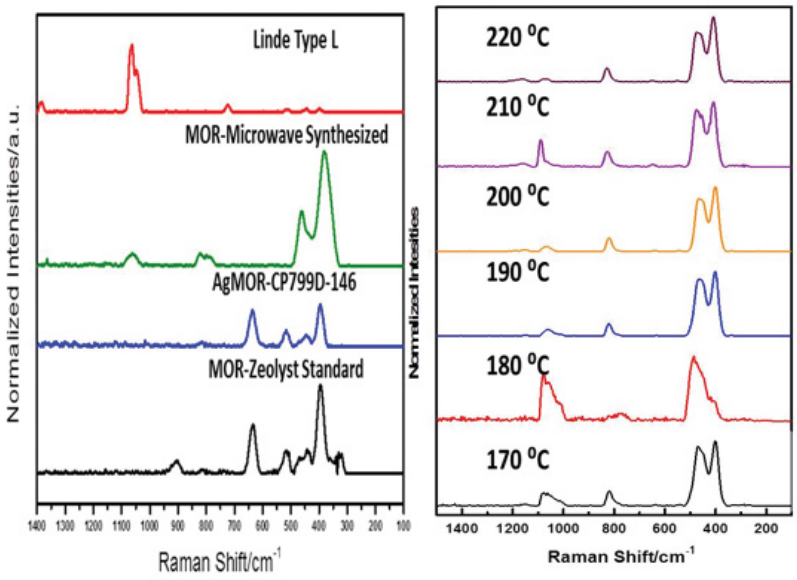

Figure 3. Raman spectra of commercial and synthesized zeolites

FY2016 ACCOMPLISHMENTS

Trial syntheses of known zeolites such as mordenite (MOR) and Linde type L (LTL) have been performed using microwave and conventional oven hydrothermal synthesis

Variations in reaction conditions for known mordenite recipes such as time, temperature, and crystallization rate have been tested for improvements in separation characteristics

Currently used zeolites have been characterized using gas sorption analysis, SEM, XRD and Raman spectroscopy

FY2016 ACCOMPLISHMENTS

CONTINUED

Characterization and trial modifications of commercial zeolites have been performed

Improved pre-treatment of samples prior to gas sorption analysis using ball milling. This method has greatly improved the available surface area of the synthesized mordenite and LTL

An MPO interagency agreement (IAA) has been approved for subcontract for NMR analysis by NRL >> First use of DoD agency for "subcontract" work under LDRD

FUTURE DIRECTIONS

- Characterization of synthesized zeolites to improve understanding of the physical/chemical properties of zeolites and how non-reactive gases interact with the surfaces and pores (Oct 2016 - Aug 2017)
- Synthesis and testing of new zeolite materials (Oct 2016 - Aug 2017)
- Down select 3-5 candidate zeolites; Pelletize, test and optimize recipes for candidates

Publications/Presentations

An abstract has been accepted for the "2016 Southeast Regional Meeting American Chemical Society" (SERMACS) that will be held in Columbia, SC, October 23-26, 2016. ABSTRACT TITLE: "Synthesis of Zeolite Materials for Noble Gas Separation"

References

1. **Nishizawa, J., et.al. ,** "Adsorption by Zeolitic Composition", Jan 10. 1984, Patent # 4,425,143.
2. **Coe, C. G.,et. al.,** "Chabazite for Gas Separation", May 15, 1990, Patent # 4,925,460.
3. **Maroulis, P. J.,** "Selective Zeolitic Adsorbent and a Method for Activation Thereof" Dec. 15, 1987. Patent # 4,713,362.
4. **Meng,X., Xiao F.S.;** Chem. Rev., 2014, 114, 1521-1543.
5. **Aly, H. M.,** Moustafa E.M, Abdelrahman, E. A.; Advanced Powder Technology , 2012, 23, 757–760.
6. **Mignoni, M.L., et. al.,** Applied Clay Science , 2008, 41, 99–104
7. **Knight, C.L., et. al.,** Microbeam Analysis, 1989.
8. **Knops-Gerrits, P. P.; De Vos, D.E. e.t. al.** Microporous Materials, 1997, 8, 3-17.
9. **Fan, F., Feng, Z., Li, C;** Chem. Soc. Rev., 2010, 39, 4794-4801.
10. **Poborchii, V. V.; J.** Chem. Phys., 2001, 2707-2711.

Acronyms

XRD	X-ray Diffraction
SEM	Scanning electron microscopy
NMR	Nuclear Magnetic Resonance
MOR	Mordenite
LTL	Linde Type L

Hydrogen Isotope Separation by Nanosized Pd-Isoelectronic Rh-Ag Alloys

Project Team: K. L. Shanahan (Primary), S. Murph, G. Larsen, and K Coopersmith
Thrust Area: Non-Proliferation and Nuclear Deterrent
Project Type: Standard
Project Start Date: October 1, 2015
Project End Date: September 30, 2016

50/50 and 60/40 Rh-Ag nanoparticles have been reported to be candidate hydrogen storage materials. The claim is that they are isoelectronic to Pd, which SRS uses for hydrogen isotope separation. It is of interest to know if these new materials can also be used in that manner. Some Rh-Ag nanoparticles were synthesized and their hydrogen absorption/desorption properties measured.

FY2016 OBJECTIVES

- Synthesize 50/50 at% RhAg nanoscale alloy
- Obtain 1st preliminary isotherms
- Synthesize 60/40 and 40/60 Rh-Ag nanoscale alloys
- Characterize materials for at least two temperatures, determine thermodynamic properties (enthalpy, entropy)

INTRODUCTION

In 2010, Kusada, et al, (JACS 132, (2010), 15896) reported that 50/50, 60/40 and 30/70 alloys of Rh and Ag would absorb hydrogen reversibly (see Figure 1.). Subsequently, several more reports have been made on the hydrogen absorption capability of Rh-based nanoparticles. The explanation was given that these alloys, in particular the 50/50 Rh/Ag alloy, are isoelectronic to Pd and therefore should act similarly to Pd. Since Pd is used at SRS to separate and purify the tritium isotope from mixed hydrogen isotopes, it is of interest to know if these Rh/Ag nanoparticulate alloys could likewise be used for isotope separation. An alternative material for isotope separation would be of interest to the DOE and perhaps the DOD.

The intent of this project was to synthesize nanoparticulate Rh-Ag alloys of approximately 50/50 to 60/40 Rh/Ag composition and characterize their hydrogen isotope adsorption and desorption properties through the determination of isotherms.

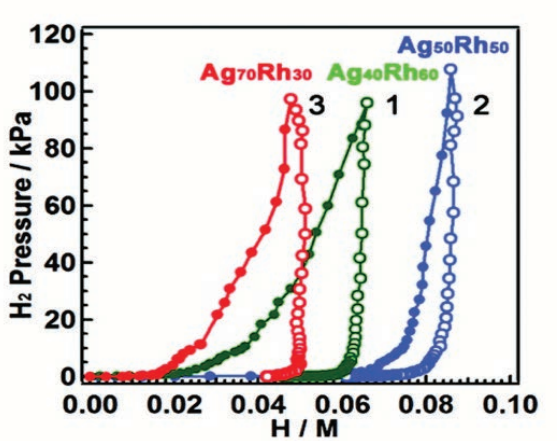

Figure 1. H_2 'Isotherms' of Isoelectronic Alloys (from Kusada, et al) (100 kPa ~ 1 atm.)

APPROACH

Nanoparticulate alloys were synthesized by co-precipitation methods and used either as unsupported or supported particles. Existing isotherm determination equipment was used to develop methods of isotherm measurement on milligram-sized samples in contrast to the normal 1-5 gram sample size. Control isotherms of nanoparticulate, microparticluate, and normal bulk Pd powders were obtained to demonstrate the measurement methodology.

Obtaining enough nanoparticulate alloy of a given composition was difficult, and required accumulating the products of multiple preparations. Because it was found that unsupported nanoparticulate samples could not be reliably contained in the test cells, subsequent samples were prepared on support materials. Both powdered kieselguhr (diatomaceous earth) and stainless steel (SS) coupons (cut into thin strips) were utilized. After several attempts, a 15 mg sample on SS appeared to give an adsorption/desorption isotherm indicative of metal-hydride-like chemistry. However, funding ran out before this could be confirmed.

RESULTS / DISCUSSION

A kieselguhr-based 7 milligram sample was tested and found not to show alloy hydrogen absorption (but it did show absorption onto the support material). A 15 milligram sample prepared by repeated preparation steps on SS strips was produced late in the year (Figure 2.) That sample appeared to show a hydride material-like absorption/desorption isotherm at ~60 °C in Figure 3 (following page), but insufficient time remained in the year to confirm this and determine if a Pd-like isotope effect existed.

The Pd control experiments produced the isotherms shown in Figure 4 (following page.) These are typical for bulk vs. nanoparticulate Pd as reported in the literature. Detailed examination of the pressure vs. time data underlying the isotherms indicated that the manifold valve tips were absorbing and desorbing hydrogen in addition to the samples. To eliminate this interference, an all-metal valve tip subassembly was constructed for further work.

Detailed examination of the pressure vs. time data underlying the isotherms indicated that the manifold valve tips were absorbing and desorbing hydrogen in addition to the samples.

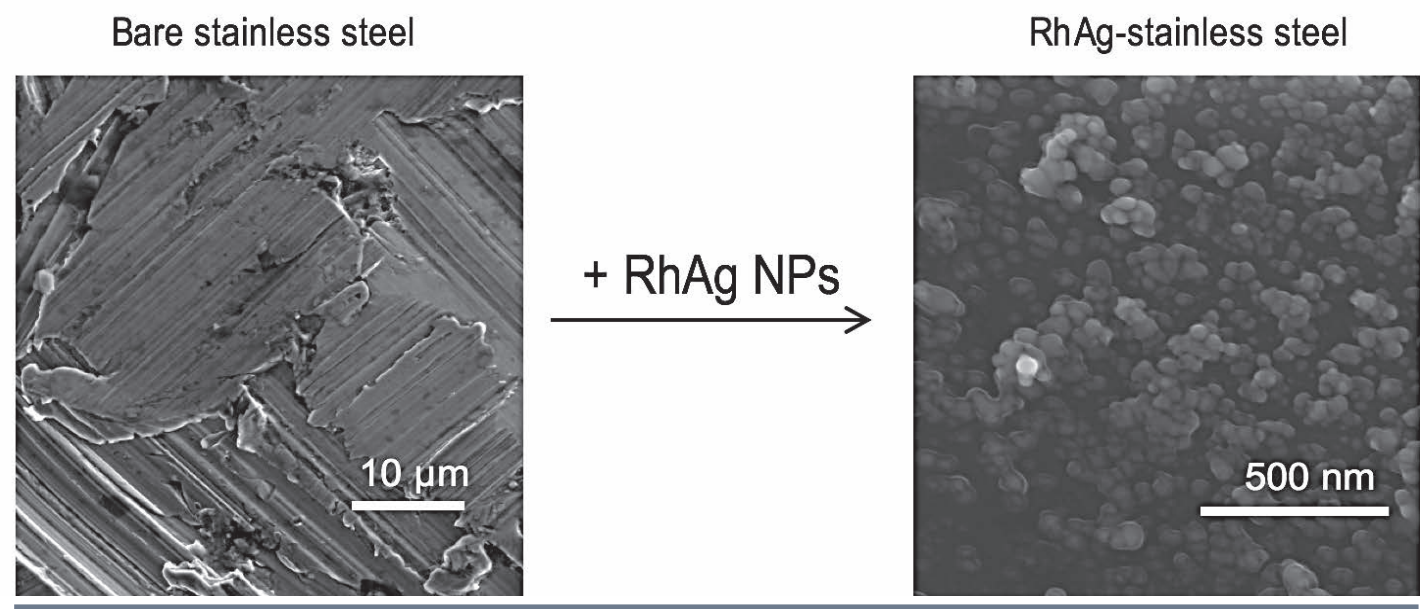

Figure 2. Before and after SEM images of SS support upon which nanosize RhAg alloy particles are deposited

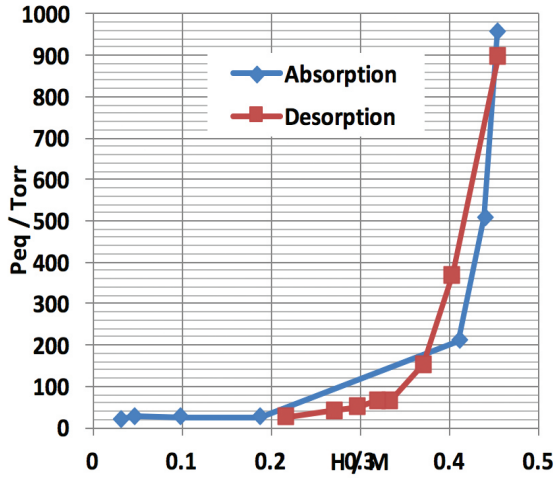

Figure 3. 15 mg ~60/40 Rh/Ag nanoparticles supported on SS strips; 60 °C isotherms using deuterium (D_2) after two protium activation cycles

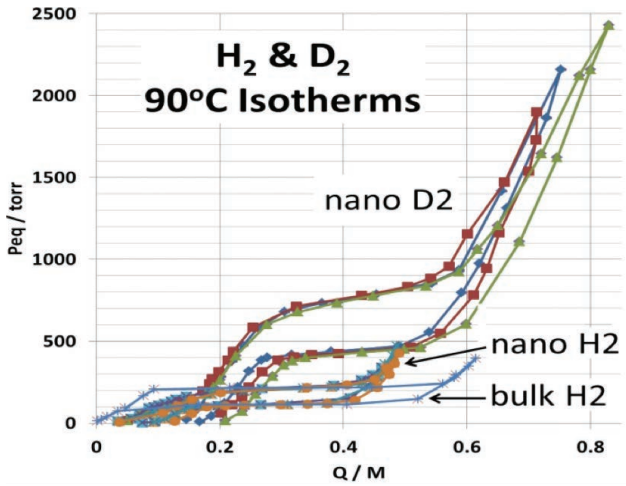

Figure 4. Pd control materials' 90 °C isotherms using protium (H_2) and deuterium (D_2) illustrating particle size and isotope effects

FY2016 ACCOMPLISHMENTS

- **Expanded the capability of existing equipment to allow milligram sample size use**
- **Determined that particulates should be deposited on support materials**
- **Prepared several nanoparticulate Rh/Ag alloy samples for testing.**
- **Determined approximately 15 mg of sample needed to observe hydride-like behavior for the Rh/Ag alloys**

FUTURE DIRECTIONS

- Indications are that this project is on the right track to accomplish its objectives. However, due to a starting material procurement delay and competing project requirements, limited unknowns were successfully examined this year. A request was made to continue the project for another year, but this project was not continued.

References

1. **K. Kusada, M. Yamauchi, H. Kobayashi, H. Kitagawa, and Y. Kubota,** "Hydrogen-Storage Properties of Solid-Solution Alloys of Immiscible Neighboring Elements with Pd", J. Amer. Chem. Soc., 132, (2010), 15896

Acronyms

SS	Stainless steel
Pd	Palladium
Rh	Rhodium
Ag	Silver

Total Number of Post-Doctoral Researchers

1. Kaitlin J. Coopersmith

2. George K. Larsen

Characterization of Environmentally Induced Chemical Transformations of Uranium Tetrafluoride

Project Team: M. Wellons, M. DeVore II, E.Villa-Aleman, M. Summer, R. Smith
Collaborators: C. Klug (NRL) T. Daroudi (Clemson University)
Thrust Area: Non-proliferation and Nuclear Deterrent
Project Type: Standard
Project Start Date: October 1, 2015
Project End Date: September 30, 2017

Technical nuclear forensics includes the chemical characterization of nuclear materials produced from various industrial uranium conversion processes where uranium oxides, fluorides, diuranates, and others are routinely produced. The characterization of the environmentally induced chemical and morphological changes for these uranium species is an emergent field of study, with most focus to date on the uranium oxides. The potential environmental factors include UV irradiation, temperature and water (i.e. relative humidity); with hydrolysis being the primary reaction responsible for chemical changes. This project's efforts have focused on uranium tetrafluoride (UF_4) hydrolysis chemistry because it is an intermediate in both the chemical processing of uranium ore to uranium hexafluoride, and the production of nuclear fuel post enrichment. Currently, published research on the hydrolysis of uranium tetrafluorides is rare; likely in part due to its assumed chemical inertness.

FY2016 OBJECTIVES

- **Testing of current hypothetical hydrolysis reaction pathway in correlation with different environmental conditions**
- **Establish bounding conditions for various rates of chemical transformation**
- **Investigation of surface morphology and internal structural changes**

INTRODUCTION

A key challenge with environmental sampling of particulate effluents is identification and attribution of the materials post release due to subsequent chemical changes. Uranium Tetrafluoride (UF_4) is of interest as it is an intermediate in both the upstream and downstream portions of uranium feedstock and metal production processes used in nuclear fuel production. Minimal published research exists relating to hydrolysis of UF_4 with previous efforts focused on bulk analysis, or hydrated UF_4 and pyro hydrolysis. There were conflicting studies of UF_4 as well.[1-4] One group reported decomposition of UF_4 in water in 24 hours; whereas another group reported no noticeable effect in boiling water for 72 hours. At the beginning of the effort the hypothetical hydrolysis induced chemical reaction pathway is as follows:

$$UF_4 \xrightarrow{H_2O} UO_2F_2 \cdot 2H_2O \xrightarrow{H_2O} UO_2(OH)_2 \cdot xH_2O$$

The pathway assumed a sequential hydrolysis reaction where U^{4+} oxidizes to U^{6+} forming a uranyl species (O=U=O) with fluorine and water species coordinated to a central uranium.[5] Previous work has shown the uranyl fluorides transition to hydroxides and eventually oxides with exposure to water in the form of relative humidity.[6,7] A similar reaction cascade was assumed for a system starting with UF_4. Instead, the FY16 effort has shown that although uranyl fluorides, hydroxides, and oxides are formed, they are not always present (dependent on reaction conditions), and that other species can be formed as well.

APPROACH

The experimental approach utilized in situ measurements in duration of < 2 weeks, longer serial measurements < 2 months, and multiple analytical tools. Starting UF_4 material was purchased from Bioanalytical Laboratories (Figure 2). Raman spectroscopy and powder X-ray diffraction techniques were employed to determine the phase changes of individual particles and the bulk material respectively using in-situ temperature and relative humidity chambers to determine the intermediate speciation changes. Simple hydrolysis experiments as well as long term exposure in relative humidity controlled salt baths, will also be undertaken to determine final progeny to oxides. All samples were evaluated for morphological and internal structures.

Figure 1. Commercially purchased UF_4 cast onto a carbon planchet; optical image at 1 kx magnification ***(left)*** and a UF_4 particulate approximately 10 µm in diameter; secondary electron image at 2.25 kx magnification ***(right)***

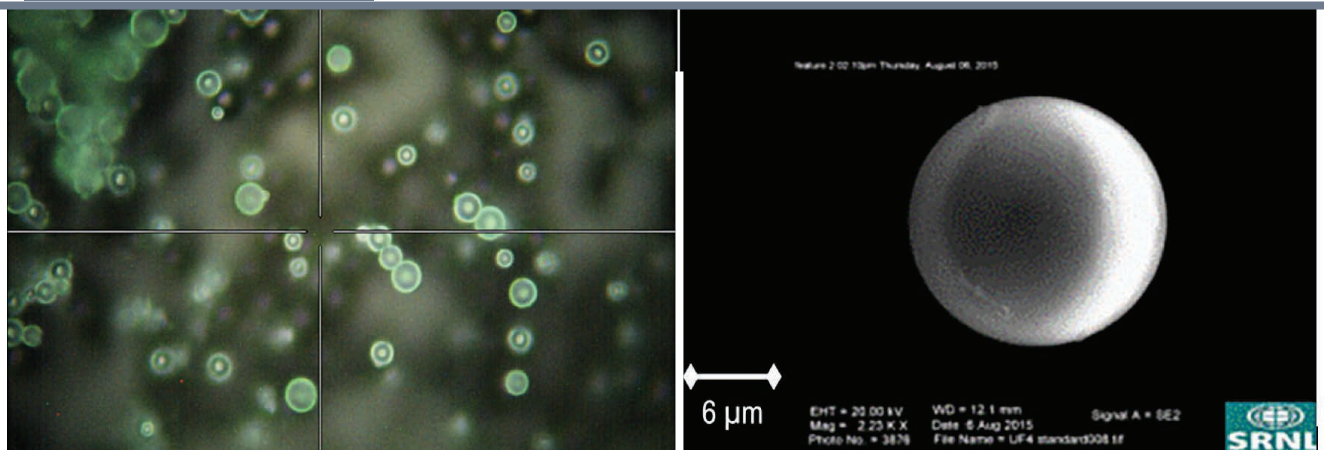

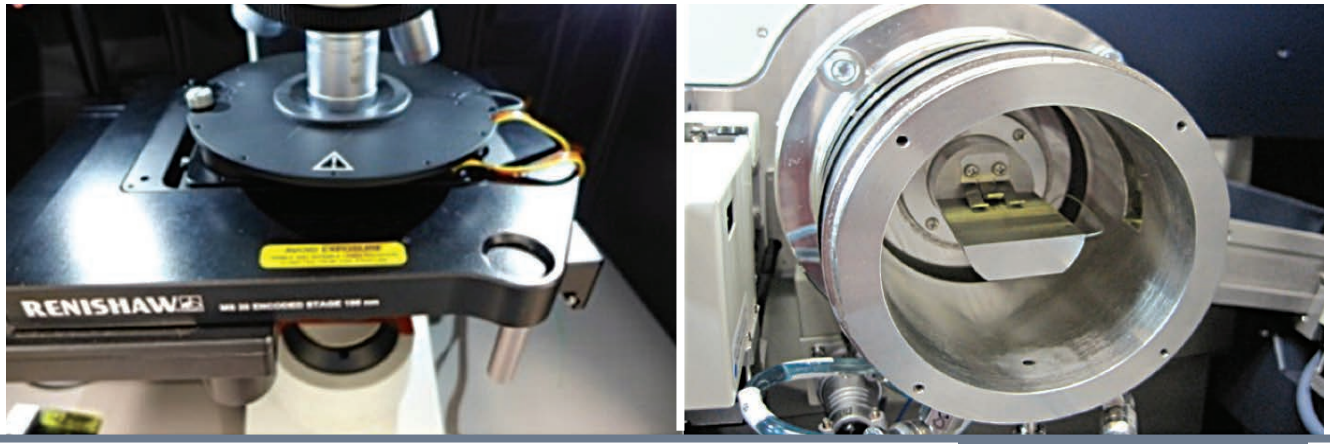

Figure 2. In situ environmental chamber couple to a Raman spectrometer ***(left)*** and in situ environmental chamber coupled to an X-ray diffractometer ***(right)***

Specific laboratory activities included:

>> Hydrolysis experiments within neat water (i.e. 100% RH)

>> In-situ characterization of both Raman Spectroscopy and XRD (Figure 2) at relative humidity for 50% and 85% RH

>> Long term serial measurements in salt bath RH controlled chamber (at 17, 35, 55, 75, and 87% RH)

>> SEM/EDS analysis for morphological and elemental characterization

RESULTS / DISCUSSION

The environmentally induced decomposition of UF_4 is more complex than initially theorized. Moderate RH conditions (50%) (designated below as experiment A) were consistent with the originally proposed environmentally induced decomposition pathway (i.e. UF_4 hydrolysis to form uranyl fluoride, then schoepite, and lastly oxides). However, elevated RH (85%) in-situ instead formed schoepite and oxide and from which the spectral signature of uranyl fluoride was not observed. A current hypothesis for these different chemical intermediates is that uranyl fluoride is a transient species, which does not accumulate to a detectable level within the experiment's measurement timescale, or instrumentation sensitivity. Additional reaction products were discovered via experiments using other methods to control relative humidity (designated experiment B and C). Experiment B used salt baths to control RH, and under at least one experimental condition led to the formation of studtite ($UO_2(O_2)\cdot xH_2O$). The formation of studtite was unexpected as the formation of a peroxo ligand is currently unexplained; future research will investigate and repeat these experiments. Lastly, a simple exercise (designated as experiment C) of mixing UF_4 in pure water was conducted and resulted in the formation of uranium tetrafluoride ($UF_4\cdot 2.5H_2O$). The updated hydrolysis schemes are represented as follows:

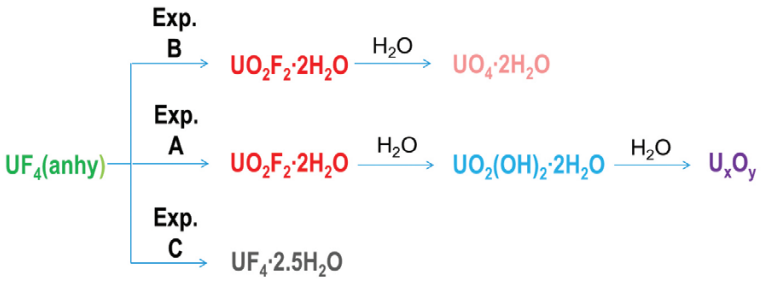

Figure 3. Updated UF_4 hydrolysis scheme for RH cond. A: In-situ measurements; RH cond. B: Salt bath RH chambers; RH cond. C: Neat H_2O

The chemical speciation identification within this effort relied on Raman spectroscopy but morphological characterization was also conducted via SEM. Experiment type A particles developed an uranium oxide shell and UF_4 core when exposed to higher relative humidity accompanied by a slowing of hydrolysis. Particles exposed to lower humidity appear to have a similar core/shell relationship, but are much less stable and deliquesce upon further exposure. The formation of studtite, within experiment type B, resulted in a third morphological change where cracks formed on the surface of the particle; extending a few hundred nanometers in depth. Further microanalytical measurements are needed to identify the spatial locations and relationships of the various phases. Further details of the three types of experiments are discussed below:

Experiment A. In-situ measurements were utilized to determine intermediate progeny, primarily via Raman spectroscopy. As shown in Figure 3, at 85% relative humidity (RH), an ingrowth of uranyl fluoride at 867 cm^{-1} was not observed as was expected; however the ingrowth of schoepite ($UO_2(OH)_2$) was observed after nine days and also UO_3 after eleven days. Unexpectedly, UF_4 Raman bands at 130, 167, 257, and 297 cm^{-1} were still observed in the spectrum throughout the two week study. Raman measurements at 50% RH (Figure 4) show the presence of uranyl fluoride with a peak at 867 cm^{-1} after 5 days, simultaneously with a schoepite peak. The schoepite dominates after 11 days. An oxide, tentatively identified based on Raman band structure to be U_3O_8, appears as well at the approximate seven day mark. Uranium tetrafluoride peaks disappear and are replaced by a sole uranyl fluoride peak at 174 cm^{-1} after seven days. The corresponding pXRD pattern, however, showed no change after seven days of exposure to 50% RH (not shown).

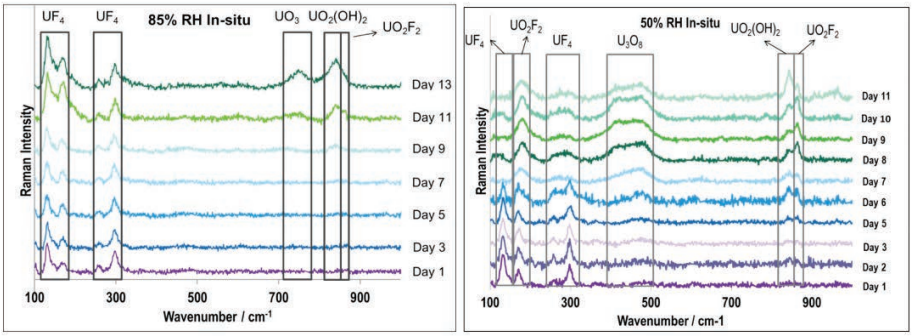

Figure 4. Raman spectra stack plot of measurements made over the course of two weeks for environmental conditions at 85% RT ***(left)*** and 50% RH ***(right)***

A variety of morphologies where observed including core/shell structures and collapsed particles. For example, energy dispersive X-ray spectroscopy mapping (Figure 5) shows the core of the particle consisted of uranium and fluorine (UF_4) and the shell was a mixture of uranium, fluorine, and oxygen. Other specimens demonstrated collapsed exteriors or roughened surfaces as shown in Figure 6. The nature of these morphological and structure features is linked to the environmental parameters but study is ongoing.

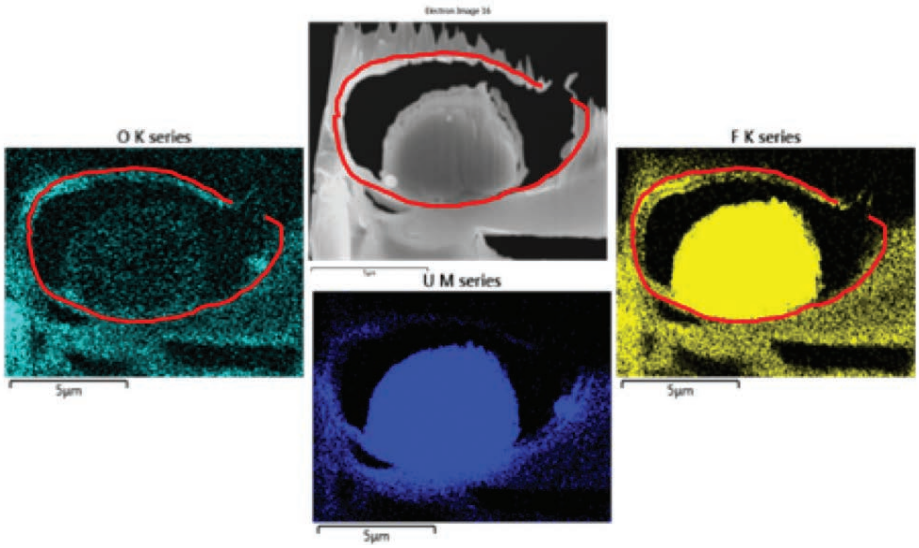

Figure 5. FIB and EDS mapping of a milled particle after exposure to 85% RH for two weeks; highlighted region denotes the outer shell of material (likely U oxide)

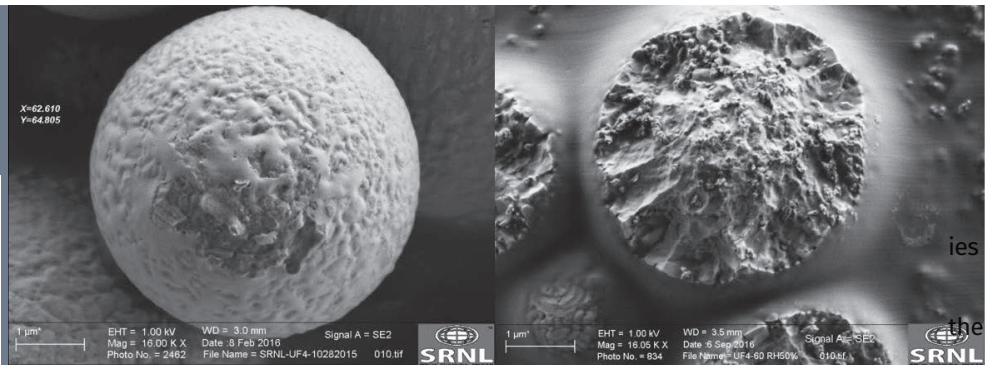

Figure 6. Secondary electron images of particles exposed to RH
(Left) 85% RH exposure
(Right) 50% RH exposure

Experiment B. Long duration studies utilizing salt baths to control the relative humidity resulted in the formation of studtite ($UO_2(O_2)$) at 57% RH ($Mg(NO_3)_2$ salt) and 77% (NaCl salt) RH while retaining UF_4 characteristic Raman bands (see Figure 7). While unexpected, reports of nuclear fuel corrosion and formation of studtite products due to seawater are published.[8] Studtite formation was not observed for 33% and 97% RH, but this maybe a nuance of the differing RH conditions. SEM imaging of particles subjected to 77% RH appear to have cracks throughout the surface, a morphology not observed in other experiments.

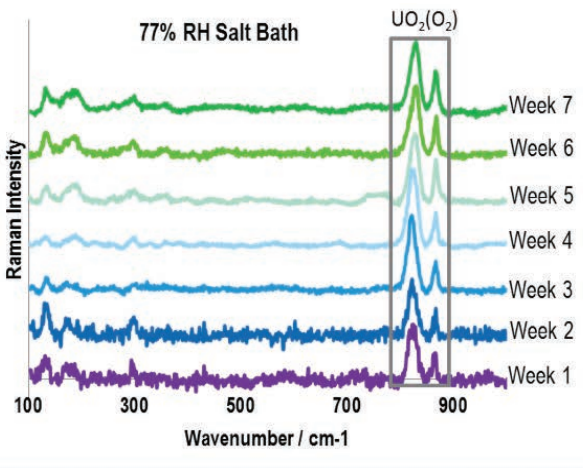

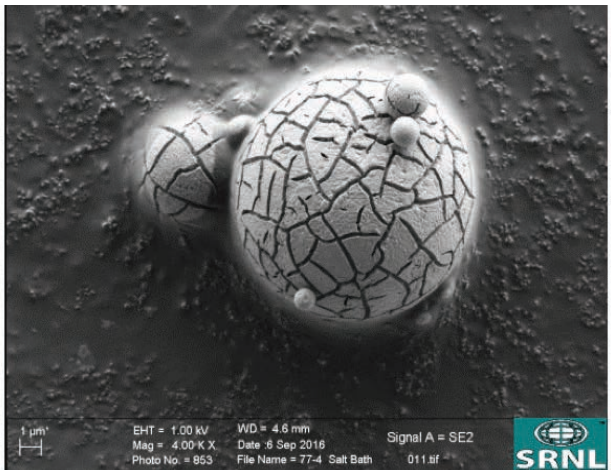

Figure 7. ***(Left)*** Raman spectra of particles exposed to 77% RH in a NaCl salt bath over 7 weeks. ***(Right)*** Secondary electron image of particles that were exposed to 77% RH NaCl salt bath

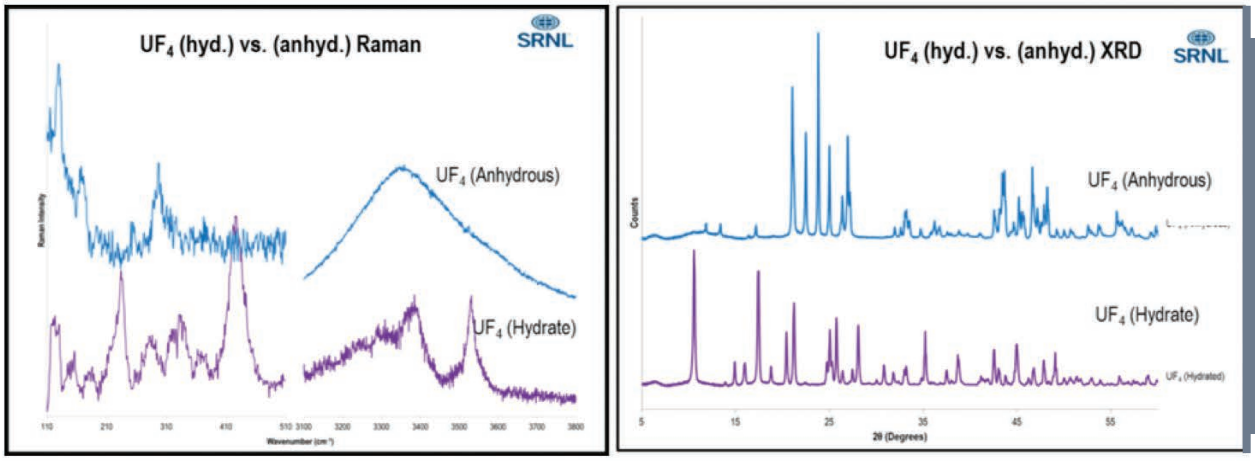

Figure 8. ***(Left)*** Raman spectra for comparison of UF_4 (anhydrous) and $UF_4 \cdot 2.5H_2O$. ***(Right)*** Powder XRD pattern comparison of the same materials.

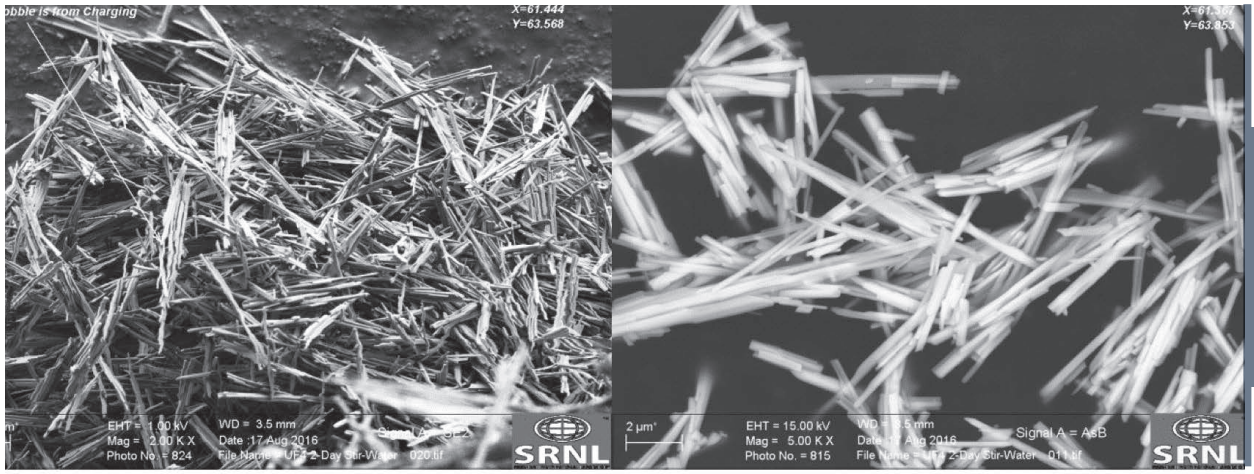

Figure 9. Secondary electron images of $UF_4 \cdot 2.5H_2O$ showing the needle like crystalline structures.

Experiment C. The simple hydrolysis experiments formed needle like crystals as shown in Figure 9. The presence of the intense Raman bands within the 3300-3600 cm^{-1} spectral region is consistent with hydrate moieties within the UF_4 crystal structure. Powder X-ray diffraction indicated that the material was $UF_4 \cdot 2.5H_2O$ as shown in a comparison to UF_4 (anhydrous) in Figure 8. A comparison of the hydrated and anhydrous Raman bands demonstrates the uniqueness of the fine spectral structure and that they are two different chemical species; the spectrum has been unpublished previously.

FY2016 ACCOMPLISHMENTS

Numerous experiments were executed, a variety of characterization techniques were employed, experimental equipment procured/installed, and used. Technical accomplishments have resulted in a more complete map of the various reaction pathways for UF_4 hydrolysis. Overall the hydrolysis of UF_4, within the context of environmental moisture was more complex than originally hypothesized with the formation of various uranyl species and uranium oxides. In particular, changes in humidity had markedly different chemical and structural effects as characterized by microanalytical and Raman spectroscopy methods.

FUTURE DIRECTIONS

- The characterization of UF_4 hydrolysis has demonstrated a complex series of potential reaction pathways and numerous chemically distinct progeny species. Efforts in FY17 will focus on NMR characterization techniques conducted at the Naval Research Laboratory in collaboration with Dr. Christopher Klug for additional spectroscopic characterization of hydrogen and fluorine containing species. The internal structural characterization of UF_4 material will continue in collaboration with Clemson University and focus on ion beam sample preparation techniques for subsequent Raman spectroscopy and potential electron energy loss spectroscopy. Additionally collaboration with the University of South Carolina is anticipated where two other forms of uranium tetrafluoride hydrates will be examined and compared with the $UF_4 \cdot 2.5H_2O$ material produced at SRNL in FY16.

FY 2016 Publications/Presentations

1. **"Structural Characterization of Hydrolyzed Uranium Tetrafluoride Solids"** M.DeVore II (presenter), Materials Research Society 2016 Spring Conference, Session EE13.10: Forensics, April 1, 2016, Presentation.
2. **"Advanced Microstructural Analysis Methods for Nuclear Materials Characterization and Technical Nuclear Forensics Applications"** M. Wellons (presenter), Materials Research Society Spring Conference, Session EE13.10: Forensics, April 1, 2016, Presentation.
3. **"Characterization of Hydrolyzed Uranium Tetrafluoride Solids by Raman Spectroscopy"** M.DeVore II, M. Wellons (presenters), External Review Commission, August 15, 2016, Poster.
4. **"Advancements in Particle Analysis for Nuclear Nonproliferation and Nuclear Forensics"** Jake Venzie, Matthew Wellons (presenters), Air Force Institute of Technology, July 29, 2016, Invited Lecture.
5. **"Structural and Spectroscopic Characterization of Hydrolyzed Uranium Tetrafluoride Solids"** M. DeVore II (presenter), American Chemical Society Fall Conference, Division of Nuclear Chemistry and Technology: Nuclear Forensics, August 22, 2016, Presentation.
6. **"Advancements in Microanalysis for Nuclear Nonproliferation and Nuclear Forensics"** Matthew Wellons (presenter), Characterization and Data Working Group (CDaWG) - Air Force Technical Applications Command, September 12, 2016, Invited Lecture.

References

1. **Cong, P. J.; Cao, S.; Sun, H.; Tan, X.; Wang, R. S. J.** Radioanal. Nucl. Chem. 1999, 242, 811.
2. **Dong, X.-y.; Zheng, X.-b.; Song, Y.-l.; Liu, Y.-x.;** Zhang, L. He Huaxue Yu Fangshe Huaxue 2014, 36, 181.
3. **Kang, S.; Zhao, J.** He Huaxue Yu Fangshe Huaxue 1998, 20, 202.
4. **Nikolaev, N. S.; Luk'yanychev, Y. A.** At. Energ. 1961, 11, 67.
5. **Lychev, A. A.; Mikhalev, V. A.; Suglobov, D. N.** Radiokhimiya 1990, 32, 7.
6. **Kips, R., Crowhurst, J., Kristo, M.J., Stefaniak, E., Hutcheon, I.D.** Micro-Raman Spectroscopy of Uranium Oxyfluoride Particulate Material for Nuclear Safeguards, Institute for Nuclear Materials Management Annual Meeting, 2010.
7. **Kips, R.; Pidduck, A. J.; Houlton, M. R.; Leenaers, A.; Mace, J. D.; Marie, O.; Pointurier, F.; Stefaniak, E. A.; Taylor, P. D. P.; Van den Berghe, S.; Van Espen, P.; Van Grieken, R.; Wellum, R.** Spectrochimica Acta Part B: Atomic Spectroscopy 2009, 64, 199.
8. **Guimbretiere, G.; Canizares, A.; Simon, P.; Tobon-Correa, Y. A.; Ammar, M. R.; Corbel, C.; Barthe, M. F.** Spectrosc. Lett. 2011, 44, 570.

Acronyms

EDS	Electron Dispersive Spectroscopy
FIB	Focused Ion Beam
NMR	Nuclear Magnetic Resonance
MAS-NMR	Magic Angle Spinning Nuclear Magnetic Resonance
pXRD	Powder X-Ray Diffraction
RH	Relative Humidity
SEM	Scanning Electron Microscope

Post-Doctoral Researchers

Two postdoctoral researchers:

1. Dr. Michael DeVore II

2. Dr. Robert Rogers.

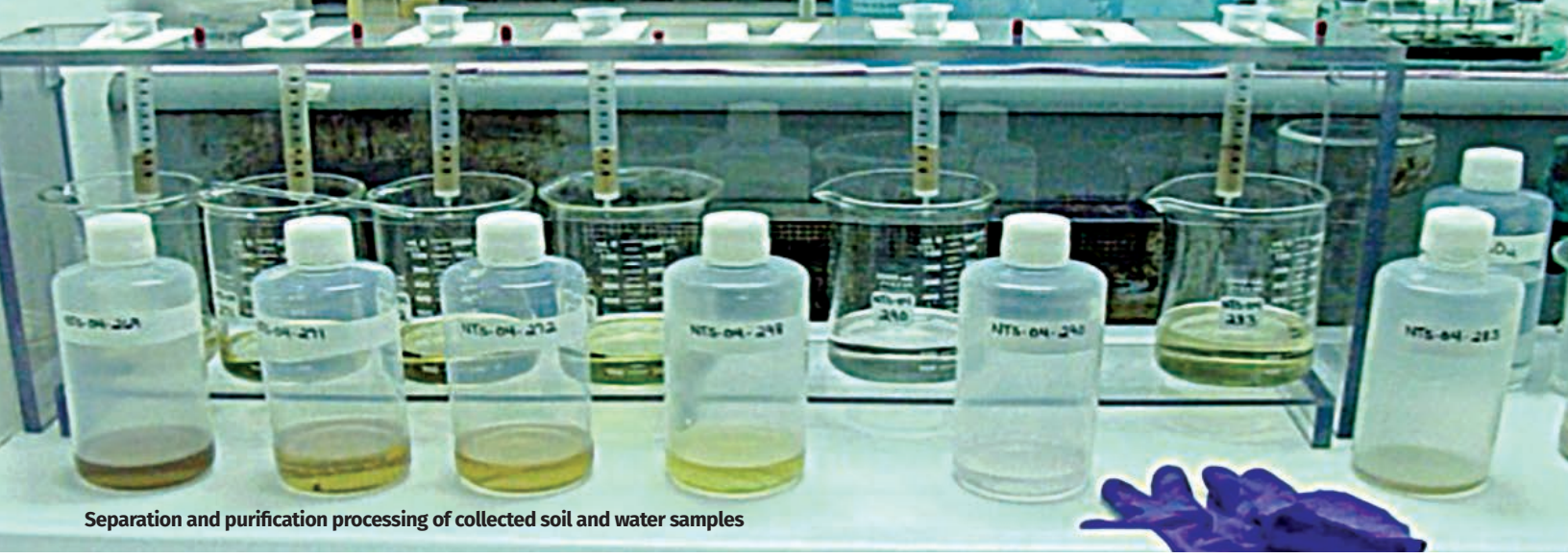

Separation and purification processing of collected soil and water samples

Understanding the Effect of Impurities on the Plutonium Ionization Efficiency with Thermal Ionization Mass Spectrometry (TIMS)

Project Team: C. Shick, Jr. (Primary), C. Armstrong, G. Hall, J. Hewitt, and R. Thomas

Thrust Area: Non-Proliferation & Nuclear Deterrent

Project Type: Standard

Project Start Date: November 16, 2015

Project End Date: September 30, 2016

Thermal ionization mass spectrometry (TIMS) is accepted as the benchmark method for precise and accurate isotopic determination of plutonium in collected environmental samples. TIMS has two major disadvantages. First, the ionization efficiency is less than 1% for plutonium samples. Second, extensive sample preparation is needed to separate and purify the plutonium from the sample matrix. This purified plutonium sample is needed to decrease isobaric interferences for the measured plutonium isotopes and to assist in better ionization efficiency of plutonium since the sample matrix elements are decreased. This project will determine which impurity elements are present in the purified plutonium samples and how these impurity elements affected the plutonium ionization efficiency. Identification of these impurity elements and their impact on the plutonium ion formation would allow the development of separation techniques aimed at reducing the concentrations of impurity elements that suppress the plutonium formation. Any enhancement in plutonium ion formation would result a gain in sensitivity when compared to current TIMS plutonium analyses.

FY2016 OBJECTIVES

Identification of the impurity elements present in two separation and purification methods used to prepare purified plutonium sample fractions from collected environmental samples

Identification of the impurity elements interfering with the plutonium ion formation by analyzing plutonium samples spiked with the impurity elements.

Identification of the impurity elements that negatively impact the plutonium ion formation so that refinements in the separation and purification methods could reduce their concentrations in the purified plutonium sample fractions

INTRODUCTION

Thermal ionization mass spectrometry (TIMS) has a long history in the measurement of isotope ratios in collected environmental samples. In thermal ionization, ions are produced by the interaction of the element of interest with a heated metal surface. Figure 1 is a thermal ionization schematic drawing. The open circles represent the elements of interest loaded onto a metal filament which is depicted by the solid line with "L"s underneath. The filament is slowly heated (400-2000°C) by passing an electric current through it. The element of interest loaded on the filament is evaporated, and a small fraction of the element of interest is ionized. Different filament materials and filament arrangements are used to find a balance between the work function of the filament material and the ionization potential of the element of interest. The overall goal is to maximize the ions generated for the element of interest. As an analysis technique, TIMS has two major disadvantages. First, the ionization efficiency is typically less than 1% for most elements. Second, extensive sample preparation is needed to separate and purify the element of interest from the sample matrix.

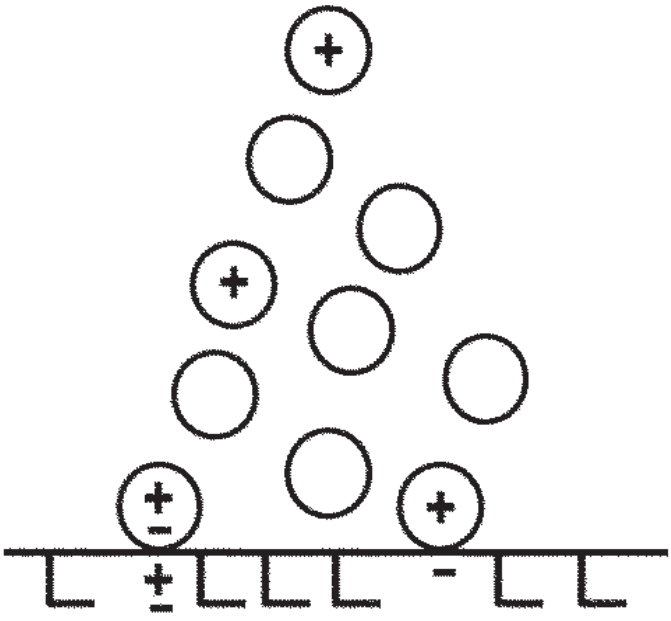

Figure 1. Thermal ionization schematic drawing

Over the years, the Nonproliferation Technology Section (NTS) at Savannah River National Laboratory (SRNL) has developed two different separation and purification methods that have been utilized for TIMS analyses of plutonium samples from collected environmental samples. While both methods have reasonable plutonium recoveries, little work has been done to determine what impurity elements are present in the purified plutonium sample fractions. The presence of impurity elements during TIMS analysis can lead to greatly reduced plutonium ionization efficiency due to complex chemical interactions. Sodium, potassium, and calcium are readily ionized and known to decrease TIMS ionization efficiency for actinide elements.[1] Additional studies have noted organic compounds can also interfere with TIMS ionization efficiency.[2-4] This work proposed here will be used to identify the impurity elements present in the purified plutonium sample fractions and to determine how these impurity elements affect the ionization efficiency of plutonium.

APPROACH

Process blanks, soil samples, water samples, and spiked swipe samples were prepared with both NTS separation and purification methods. These purified plutonium sample fractions were analyzed semi- quantitatively with a quadrupole-based inductively coupled plasma mass spectrometer (Q-ICP-MS) to identify what impurity elements are present in the purified plutonium sample fractions. Spiked solutions with individual impurity elements or groups of impurity elements were prepared in SRNL clean laboratories. These spiked solutions were to be added to TIMS quality control plutonium samples in F/H Laboratories. However, instrument priorities at F/H Laboratories did not allow any of these LDRD samples to be analyzed. Therefore, similar spiked impurity element samples were prepared and analyzed on the SRNL TIMS. By comparing the plutonium ionization efficiencies for the typical quality control plutonium (unspiked) samples and the spiked quality control plutonium samples, a better understanding of which elements are interfering with the formation of plutonium ions will be obtained. This project hoped to identify the impurity elements that have the most negative impact on plutonium ion formation so that modifications to the NTS separation and purification methods could be implemented to remove these impurity elements.

RESULTS / DISCUSSION

For both NTS separation and purification methods (Processes A and B), process blanks, soil samples, water samples, and spiked swipe samples were prepared. Three replicates for each sample type were combined to provide enough sample volume for the semi-quantitative Q-ICP-MS analysis. This technique entails the analysis of a NIST-traceable multi-element standard and the determined intensities for this standard are compared with the intensities for the other samples to yield approximate concentrations for selected elements. Table 1 reports the target impurity elements for both NTS separation and purification methods for Process A blank sample, Process A combined water sample, Process A combined soil sample, Process B swipe blank sample, Process B combined spiked swipe sample, and 5% nitric acid Q-ICP-MS rinse solution. Eighteen impurity elements were determined for the two NTS separation and purification methods for water, soil, and swipe samples.

Different solutions were prepared with the eighteen impurity elements, and different combinations of impurity elements and concentrations were spiked with plutonium quality control samples. These spiked plutonium quality control samples were analyzed with the NTS TIMS. Table 2 reports the single impurity element or group of impurity elements and the TIMS filament loading concentrations.

Table 1. Semi-quantitative Q-ICP-MS results determined eighteen impurity elements for the two NTS separation and purification methods for water, soil, and swipe samples

Target Impurity Elements	ICP-MS SQ Results for Process A Blk Sample (ppb)	ICP-MS SQ Results for Process A Combined Water Sample (ppb)	ICP-MS SQ Results for Process A Combined Soil Sample (ppb)	ICP-MS SQ Results for Process B Swipe Blank Sample (ppb)	ICP-MS SQ Results for Process B Combined Swipe Sample (ppb)	ICP-MS SQ Results for the CCB Set 1 (Blank) (ppb)
Li	1.1	1.1	0.73	0.27	4.9	0.16
B	556	246	65	37	1074	0.42
Na	1138	1407	635	75	2874	0.55
Mg	11	18	26	16	130	0.43
Al	4078	3979	2311	1876	8324	2.4
Ti	4.8	3.9	5.1	11	21	0.071
Cr	6.6	15	11	130	255	0.19
Mn	2.5	1.4	1.5	5.3	10	0.038
Fe	377	124	135	582	912	25
Ni	2.9	3.5	3.5	28	74	0.0085
Cu	3.9	5.9	4.4	22	35	0.042
Zn	37	34	99	11	36	0.075
Zr	1.7	2.1	1.9	5.9	24	0.0028
Sn	1.9	1.8	9.6	7.1	9.7	0.013
Ba	3.9	6.1	2.9	1.9	6.5	0.0078
Ce	10	9.4	6.1	0.28	1.2	<0.0011
Au	1.7	4.3	0.59	1.9	0.99	0.18
Pb	8.6	12	13	6.1	28	0.0069

For each studied matrix, ten TIMS filaments were prepared for TIMS analysis. In most cases, ten TIMS individual filaments were measured for each studied matrix combination; however, a couple of TIMS filaments were lost during TIMS analysis. By comparing the plutonium ionization efficiencies for the typical quality control plutonium samples (unspiked NBL CRM 128 solutions) and the spiked quality control plutonium samples, an understanding of which elements interfere with the formation of plutonium ions is gleaned (see Figure 2). While waiting on additional impurity element standards to arrive, duplicate samples with spike matrix A2 were also prepared and analyzed. Six of the impurity elements tested (Cr, Fe, Na, Pb, Sn, and Zr) were found to negatively affect the formation of plutonium ions. This project showed that additional efforts are needed to improve the NTS separation and purification methods to clean up these impurity elements to improve NTS TIMS plutonium detection limits.

Spike Matrix	Impurity Elements	TIMS spiked impurity element(s)
A	3	2 µg Cr, 5 µg Fe, 5 µg Sn
B	3	2 µg Cu, 2 µg Zn, 2 µg Mg
C	2	5 µg Pb, 5 µg Zr
D	1	5 µg Pb
E	1	5 µg Zr
F	2	10 µg Mn, 5 µg Li
G	2	10 µg Au, 5 µg Ni
H	1	2000 µg Na
I	1	1500 µg B
A2	3	2 µg Cr, 5 µg Fe, 5 µg Sn
J	1	5 µg Al

Table 2. The spike matrix relative to the number of impurity elements and TIMS filament loading concentrations

Figure 2. Plutonium ionization efficiencies for spiked quality control plutonium samples and unspiked quality control plutonium samples (Pu 128)

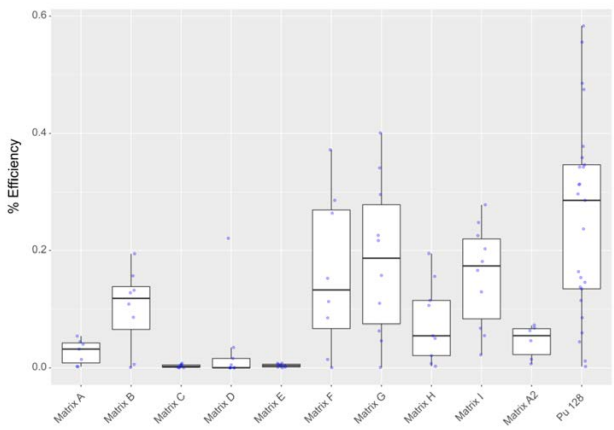

The elements in Matrices A/A2, C, D, E, and H were found to statistically decrease plutonium ionization efficiency.

FY2016 ACCOMPLISHMENTS

Eighteen impurity elements were determined for two NTS separation and purification methods for collected water, soil, and swipe samples

Spiked samples with the impurity elements were analyzed to determine plutonium ionization efficiency

Six impurity elements (Cr, Fe, Na, Pb, Sn, and Zr) negatively affect the formation of plutonium ions

FUTURE DIRECTIONS

- This work has shown that some impurity elements negatively affect the formation of plutonium ions; therefore, the four remaining impurity elements (Al, Ti, Ba, and Ce) should also be investigated as well.
- Refinements of the two NTS separation and purification methods to further reduce/remove contaminants in TIMS purified plutonium samples should be initiated.
- These refined separation and purification methods should to be tested to determine if the reductions in impurity element concentrations enhances the plutonium ionization efficiency.

Publications/Presentations

"2016 Savannah River National Laboratory Department of Energy (DOE) Network of Analytical Laboratories (NWAL) Activities," Charles R. Shick, Jr., Christopher R. Armstrong, Sheila S. Smalley, Gregory Hall, Joshua T. Hewitt, and James R. Cadieux, Jr., presented at the 2016 Annual DOE NWAL Technical Review Meeting, Washington, D.C., August 16-17, 2016

References

1. **Smith D.** (2000) "Thermal Ionization Mass Spectrometry" In: Barshick C., Duckworth D., and Smith D. (eds), Inorganic Mass Spectrometry: Fundamentals and Applications. Marcel Dekker (New York), 1- 30.
2. **Grate J., O'Hara M., Farawila A., Douglas M., Haney M., Peterson S., Maiti T., and Aardahl C.** (2011) Extraction Chromatographic Methods in the Sample Preparation Sequence for Thermal Ionization Mass Spectrometric Analysis of Plutonium Isotopes. Analytical Chemistry, 83, 9086-9091.
3. **Croudace I., Warwick P., Taylor R., and Dee S.** (1998) "Rapid Procedure for Plutonium and Uranium" Determination in Soils using a Borate Fusion followed by Ion-Exchange and Extraction Chromatography. Analytica Chimica Acta, 371, 217-225.
4. **Sahoo S., Yonehara H., Kurotaki K., Fujimoto K., and Nakamura Y.** (2002) "Precise Determination of $^{235}U/^{238}U$ Isotope Ratio in Soil Samples by using Thermal Ionization Mass Spectrometry" Journal of Radioanalytical and Nuclear Chemistry, 252, 241-245.

Acronyms

TIMS	Thermal Ionization Mass Spectrometry
NTS	Nonproliferation Technology Section
SRNL	Savannah River National Laboratory
Q-ICP-MS	Quadrupole-based Inductively Coupled Plasma Mass Spectrometer
DOE	Department of Energy
NWAL	Network of Analytical Laboratories

Total Number of Post-Doctoral Researchers

Joshua Hewitt, a postdoctoral research associate with NTS, worked on-site with this FY16 LDRD project.

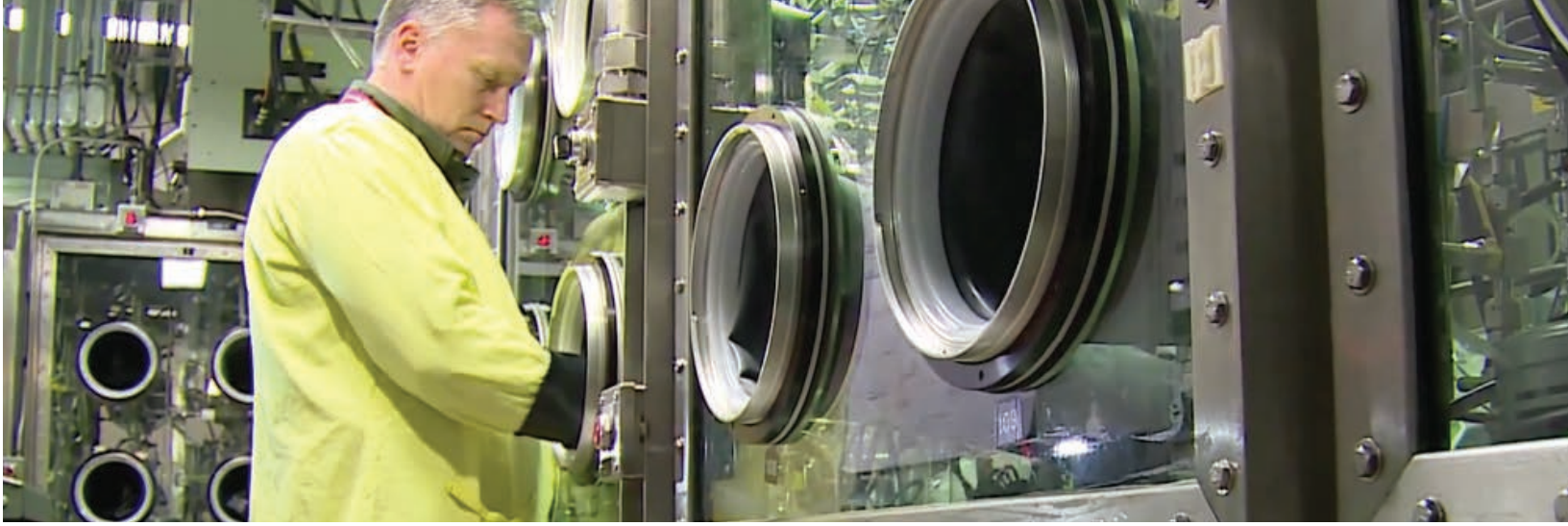

A Next Generation Digital Counting System for Low-Level Tritium Studies

Project Team: P. W. Bowman (Primary), P. P. Hughes, M. C. Maxwell, J. J. DeGange
Thrust Area: Nuclear Deterrent and Non-Proliferation
Project Type: Standard
Project Start Date: October 1, 2015
Project End Date: September 30, 2016

Since the early seventies, SRNL has pioneered low-level tritium analysis using various nuclear counting technologies and techniques. The electronics involved in performing the data acquisition changed dramatically from analog to the digital in 1999. Since then, SRNL has successfully performed routine low-level tritium analyses with counting systems based on digital signal processor (DSP) modules developed in the late 1990s. Each of these counting systems are complex, unique to the National Security Directorate at SRNL, and fully dedicated to performing routine tritium analyses of low-level environmental samples. To maintain the strong position we have had for decades in the low-level tritium analysis area, these counting systems must evolve due to advances in technology. The objective of this LDRD project was to design, build, and demonstrate a Next Generation Tritium Counting System (NGTCS), while not disrupting the routine low-level tritium analyses being performed in the Ultra-Low Level Counting Facility (ULLCF) on the legacy counting systems. The work involved (1) developing a test bed for building and testing new counting system hardware that does not interfere with our routine analyses, (2) testing a new counting system based on a modern state of the art DSP module, and (3) evolving the low-level tritium counter design to reflect the state of the science. The demonstrated system will help keep SRNL on the leading edge of low-level tritium counting.

FY2016 OBJECTIVES

To develop a test bed for evaluating counting system hardware without interfering with the routine analyses underway in the laboratory

To design, build and demonstrate a next generation digital counting system

To begin evolving the Low Level Tritium Counter design to maintain state of the science and reduce costs

INTRODUCTION

Transitioning the legacy counting systems to NGTCS technology is expected to lower the limit of detection, reduce system noise, increase system stability, lengthen counter longevity, and enhance efficiency of the detector manufacturing process.

Given the success of the low-level digital tritium counting systems at SRNL over the last 15 years, we anticipate that utilizing more modern DSP technology will work well for our application. We have identified a modern DSP module that we believe can replace the critical functionality of the legacy DSP modules and improve on the performance of the legacy systems. In particular, we are hopeful that the new DSP module combined with the expected advances in the design of the low-level tritium proportional counters will have the effect of increasing the overall sensitivity of the analyses with enhanced reliability and cost effectiveness.

The development of a test bed that is separate from the legacy counting systems will make it possible for us to evolve component design and evaluate modern DSP technology under carefully controlled conditions without adversely impacting the routine low-level tritium analyses being carried out on the legacy systems on our customer's behalf. The development of the test bed in the Ultra Low Level Counting Facility (ULLCF) will save money by avoiding the duplication of flammable gas services already available in the laboratory.

APPROACH

The basic approach was to design and build the test bed and then begin the development of the NGTCS in it. The electronics associated with the NGTCS was then brought into operation sequentially. The first element of the sequence was the installation of the anticoincidence circuit. This involved both the testing of the anticoincidence detectors and their associated signal chain. The second element was the testing of the low level proportional counter circuitry. This testing began with the fabrication of a typical low level tritium counter of the kind used successfully with the existing Low Level Digital Tritium Counting Systems. This counter became the first legitimate signal source for the NGTCS containing real signals with the full complement of typical noise. It was fully anticipated that there would be many difficult days of searching for a set of working parameters for the NGTCS. Once a working set of parameters was developed the slow process of optimizing the set of parameters could begin and the process of assessing new counter designs could move forward.

The new low level proportional counters were then manufactured, and assembled in preparation for installation in the NGTCS. This process was complicated by the mechanical differences in the materials used to manufacture the experimental end pieces for the new counters. Each counter had to pass a rigorous leak check under vacuum and pressure, and be evaluated for breakdown to be a candidate for installation in the NGTCS. The counters were installed in the test bed with their signals routed to one of the spare legacy DSP modules. In this arrangement we could begin to view the results of our forced evolution of the low level proportional counter design through a familiar lens. This approach was fruitful for investigating the results of evolving the low level proportional counter design, but without additional development of the data acquisition code for the NGTCS only limited testing with the NGTCS was possible.

Once a working set of parameters was developed the slow process of optimizing the set of parameters could begin and the process of assessing new counter designs could move forward.

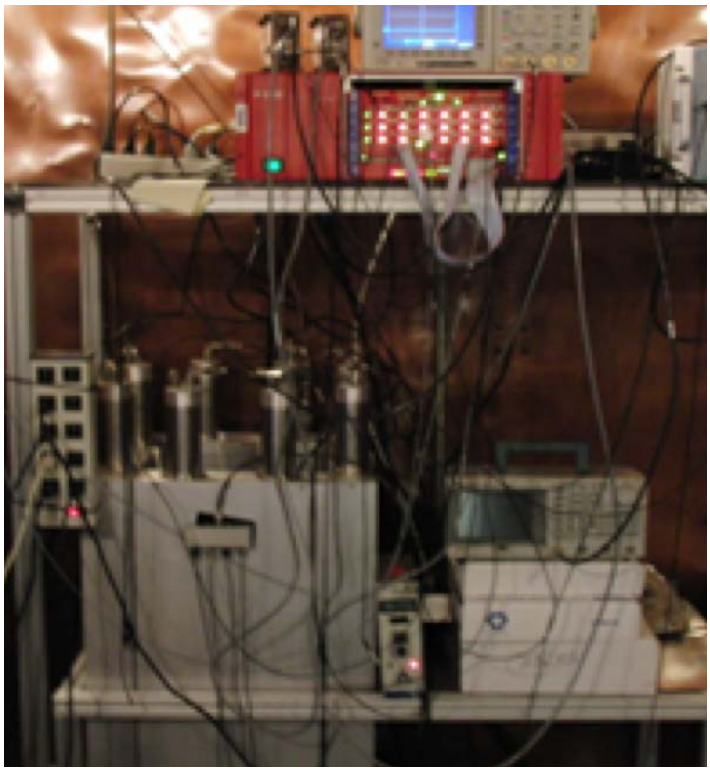

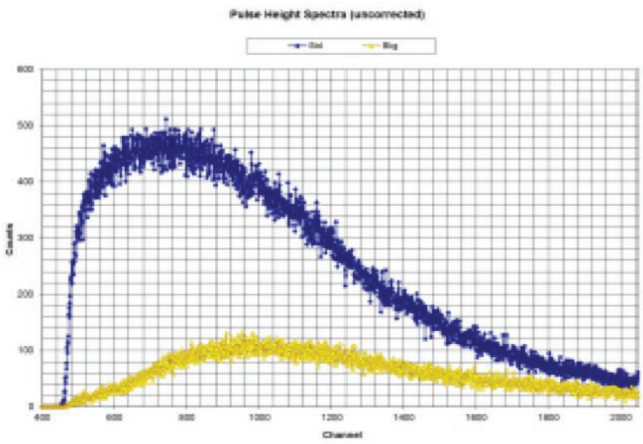

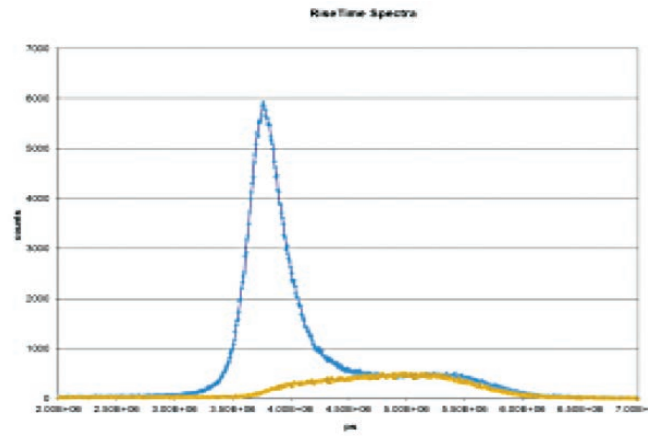

Test bed counting system ***(Above)*** as installed in the ULLCF. Pulse height ***(Top Right)*** and rise time ***(Bottom Right)*** spectra collected on system using a standard (blue line) and background (yellow line) gases

RESULTS / DISCUSSION

The test bed was completed and the NGTCS was designed, built and brought into operation with the skeletal data acquisition code (Rev. 0) shipped with the digital signal processing module. We expected the skeletal data acquisition code to provide us with only a crude set of tools for operating the NGTCS. As our experience with the new technology accumulated, it became clear that a document specifying the many expected details of the data acquisition code was needed. The skeletal data acquisition code is currently being rewritten using the document.

Two new low level proportional counter designs were tested using a counter of the legacy design as a control. The first trial design had end pieces that were longer than the legacy end pieces. The results with this lengthened proportional counter were so noisy in comparison to the legacy design that it was put aside for further testing. It was finally realized that the longer end pieces had more pick up from the larger portion of the sense wire outside the shielded region. The second trial featured the same overall length as the legacy counters, but a design that considerably reduces the process of preparing a counter from parts for a lifetime of operations. A set of 6 materials were selected for the end pieces of the set of 6 experimental counters, including Duratron, Tivar, Macor, Teflon, Kynar740-1000HD, Kel-F/PCTFE. The Macor parts have not arrived yet, but they are expected and they will be tested when they do. Unfortunately, the results from the Macor trials will certainly not be available for this report. The remaining experimental proportional counters were successfully brought into operation in the time since the midterm report. The new low level proportional counter design will continue to be tested in a number of ways all requiring more time than is left in this LDRD project. Of particular interest to us is the effect of the other materials on the counter's long term behavior. We have noted issues of conditioning long thought to be dependent on the materials from which the end pieces are constructed. This LDRD has been very helpful toward forming a less speculative model of the conditioning issues.

FY2016 ACCOMPLISHMENTS

The development of the test bed was completed, providing (1) gas and vacuum services for up to sixteen low level proportional counters, (2) a custom gas purged counter sprocket, (3) a multisegmented anticoincidence shield enveloping the sprocket, (4) a custom preamplifier shelf for reduction of microphonics, and (5) a heavy duty overhead electronics table (Such an arrangement was envisioned as being a flexible system for the likely modes of testing)

The test bed features the capability to work with both NIM and VME standard instrumentation either separately or at the same time (This greatly reduces duplication costs)

The modern digital signal processing module (VME) was installed in the test bed with the other electronics modules including one of our legacy DSP modules (This makes some important comparisons possible)

The multisegmented anticoincidence shield was successfully installed and tuned with both the legacy counting equipment (NIM gear) and the NGTCS (VME gear)

An initial set of working parameters has been successfully found for real pulses having noise that is typical of the low level proportional counters (The successful set of working parameters was then used as a starting point for working with the NGTCS hardware)

The NGTCS has clearly demonstrated the ability the acquire spectra over the range of activities the system is likely to see

The summation of our recent acquired experience with the NGTCS and the legacy counting systems was put into a form that would be used as a guide to write the revised version of the data acquisition code. It also featured a recommended firmware modification for the DSP module in the NGTCS

The NGTCS circumvents a myriad of issues associated with having the signals from the counters summed before being analyzed by a single DSP; Qualitatively, in the NGTCS each channel has its own DSP and associated field programmable gate array, as a result there appears to be excellent separation among the channels (The result is reduced coupling and noise; Ultimately, with a more complete data acquisition code a number could be extracted to describe the difference quantitatively)

Another benefit of the NGTCS over the legacy systems is the fact that we can have dissimilar signal sources in each channel of the modern DSP hardware (With the legacy systems a single FPGA and DSP served 16 similar channels; In the NGTCS, each counting channel has its own FPGA and DSP. This represents a significant cost savings over the lifetime of the NGTCS)

The circular buffering associated with the NGTCS hardware appears to have had a beneficial effect on the counting; Whether this is due to the buffering or the association of one channel with one pulse stream remains to be determined (This cannot be done without the firmware and data acquisition code revision)

The new low level counter design features end pieces whose construction greatly simplifies the process of preparing the counter for use; They feature improved seals, reduced axial travel, and less parts (More time and testing is required to determine the optimal material; It would be very useful to run the NGTCS hardware during this process)

The hope is to gain a more complete understainding of both the long- and short- term issues associated with the detectors and the low level counting electronics. With this knowledge we seek to improve the low level tritium analyses on behalf of our customers.

FUTURE DIRECTIONS

- The experimental counters will be run side by side with legacy counters in the NGTCS
- If such a thing exists and it is not cost prohibitive, we would like to select a more optimal material for constructing the end piece
- After the firmware and data acquisition code are modified the system should have the capabilities needed to continue the work of optimizing the working set of parameters for our application

References

1. **"Digital Acquisition Software for SRNL",** SRNL-TR-2016-00260.

Acronyms

SRNL	Savannah River National Laboratory
DSP	Digital Signal Processor
FPGA	Field Programmable Gate Array
NGTCS	Next Generation Tritium Counting System
ULLCF	Ultra Low Level Counting Facility

Advanced Atmospheric Ensemble Modeling Techniques

Project Team: R. L. Buckley (primary), S. R. Chiswell, R. J. Kurzeja, G. Maze, B. J. Viner, and D. W. Werth
Project Type: Standard
Project Start Date: October 20 2015
Project End Date: September 30, 2017

Ensemble modeling has become an essential tool for characterizing uncertainty in atmospheric model predictions. Airborne transport models are commonly driven by mesoscale atmospheric models, whose accuracy is reduced by model biases, limited available data to constrain the model solution, and natural variability. Ensemble modeling quantifies model uncertainty by providing a range of possible atmospheric end-states. Ensembles are still subject to underlying biases, however. We have used the first European Tracer Experiment as a testbed to compare standard ensemble modeling with two novel techniques: (1) a physics-based ensemble technique, which adapts models to specific geographical locations and time frames, and (2) data assimilation with an Ensemble Kalman filter. This research has demonstrated that transport accuracy can be substantially improved when a model is adapted to a particular location and time or when important local data is assimilated rigorously into the simulation.

FY2016 OBJECTIVES

Obtain data (meteorological and tracer) from Experiment #1 of the European Tracer Experiment (ETEX), conducted in October 1994, for testing of the ensemble techniques

Apply three sets of ensemble simulations to the ETEX tracer release: standard ensemble, Adaptive Programming, and Ensemble Kalman-filter techniques

Create statistical tools to evaluate each ensemble dataset by comparing it to the ETEX measurements. This includes both the meteorological and tracer concentration components.

Transport accuracy can be substantially improved when a model is objectively adapted to a particular location and time and through a dynamic and statistically optimized utilization of available local data.

INTRODUCTION

The assessment of emissions from known or suspected weapons facilities that release radionuclide, chemical, or biological materials is of great interest. Source emission estimates are often obtained by scaling downwind effluent measurements by atmospheric dilution rates estimated from airborne dispersion models. The latter are often forced by mesoscale meteorological models of limited accuracy. A more computationally robust solution is to use an 'ensemble' of model simulations, with a range of solutions. We seek to improve the standard ensemble approach through the development of two novel methods: (1) minimization of model error using adaptive (physics-based) programming techniques (AP, Roebber, 2015) and (2) application of a Kalman filter for assimilation of key local observations into the model prediction (EnKF, Evenson, 2003). Transport accuracy can be substantially improved when a model is objectively adapted to a particular location and time and through a dynamic and statistically optimized utilization of available local data.

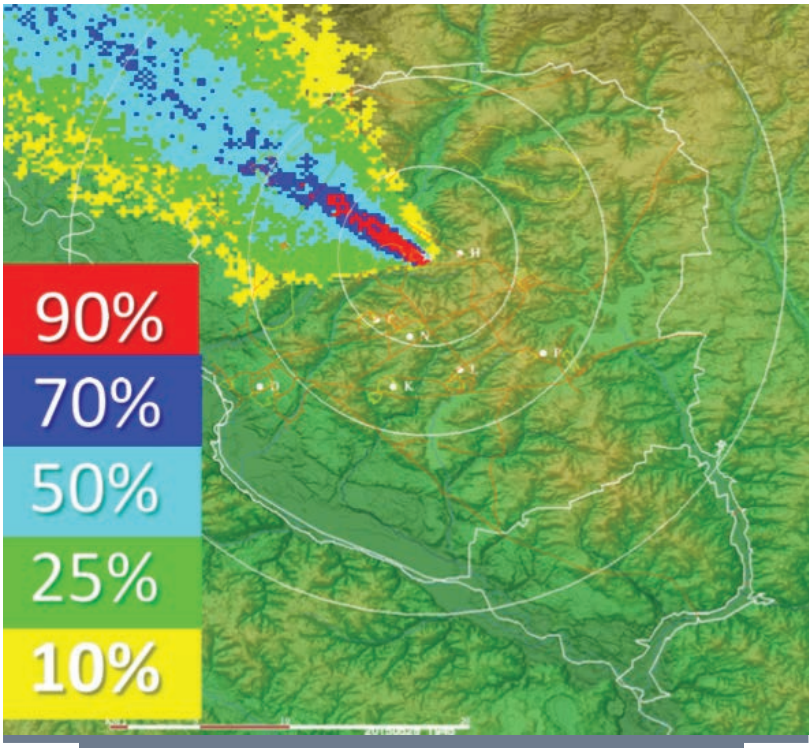

Figure 1. Confidence levels for ensembles run at SRS where contours represent the percentage of models agreeing on exceedance of a specified concentration threshold.

Ensemble modeling (EM)—the running of multiple simulations of the same event—has become the standard for quantifying uncertainties in atmospheric forecasts (Figure 1). EM accounts for uncertainty due to limited input data and for nonlinearities inherent in the Navier-Stokes equations, and has been shown to increase model forecast skill compared to single deterministic simulations (Galmarini et al., 2004). Unfortunately, ensembles based on a biased model will retain those biases, and the current practice is to perform EM with minimal consideration for the suitability or completeness of the ensemble (Stensrud et al., 2009). Improvements in ensemble modeling are important in applications related to atmospheric transport and dispersion, such as emergency response and non- proliferation. This research uses meteorological and concentration data collected during the European Tracer Experiment (ETEX, Girardi et al., 1998) to evaluate the quality of two novel ensemble modeling techniques. Demonstrating improvement in modeling by a more strategic selection of either method is illustrated.

APPROACH

The approach used in this research is to select a suitable modeling scenario and compare the standard EM approach with two novel ensemble techniques. Adaptive Programming (AP) accounts for errors due to the formulation of the model physics. Mesoscale models employ parameterizations to describe unresolved physical processes such as turbulence and cloud formation. A variety of parameterization settings are possible, each with a range of plausible values. Determining the appropriate parameter set is typically performed by trial and error, which is slow and less efficient due to the many simulations required to sample the entire parameter 'space'. AP is a more robust, iterative process in which we perturb the model parameters multiple times to generate an ensemble of members. The individual ensemble members are then run, and the best performing member is selected according to available observations. After a number of iterations the simulations should converge to an ensemble that is best suited (adapted) to the prevailing atmospheric conditions. The second novel approach uses an ensemble Kalman filter (EnKF) to examine the impact of assimilating selected observations into the simulation. The EnKF improves upon existing methods of data assimilation. Standard data assimilation affords equal weight to surface and above-ground winds, but the latter are much more representative of regional air flow, and should force a much broader scale adjustment to the model fields. The EnKF technique combines the model prediction and observations after weighting based on the error variance of each. Meteorological data from the ensemble techniques were ingested into the Hybrid Single Particle Lagrangian Trajectory (HYSPLIT, Draxler and Hess, 1998) atmospheric transport model to create three-dimensional, time-varying concentration fields.

Determining the appropriate parameter set is typically performed by trial and error, which is slow and less efficient due to the many simulations required to sample the entire parameter 'space'.

The research described here uses data from the internationally recognized European Tracer Experiment (ETEX, Girardi et al., 1998). ETEX provides a rich data collection over a large area, as well as an abundance of literature devoted to the data. This permits rigorous comparison of these approaches to many previous studies. In addition, reliable statistical techniques had to be used for the model evaluation. Metrics used in this study are taken from the Atmospheric Model Evaluation Study (ATMES II, Mosca et al., 1998).

RESULTS / DISCUSSION

The standard ensemble modeling (EM) approach is to perturb the initial meteorological conditions (fields of wind, temperature, etc.), assuming inherent uncertainty in the measurements used to develop them, and generate an ensemble of forecast solutions whose spread about the mean quantifies the forecast uncertainty. This is the baseline standard for comparing the two novel methods of EM. Twenty members were generated with the Weather Research and Forecast (WRF, Skamarock et al., 2008) model using a technique described in Berner et al. (2011) involving stochastic perturbation to the WRF simulations. Relative to tracer measurements from ETEX, the EM tended to transport the plume too quickly downwind, although the general direction of transport was good.

The AP ensemble technique perturbed 9 different model parameter inputs (including surface temperature, soil moisture, and turbulence length scale) of the Regional Atmospheric Modeling System (RAMS, Cotton et al., 2001). RAMS is used due to prior experience with AP at SRNL (O'Steen and Werth, 2009). The scoring of each AP ensemble member was based on upper-air observations at 7-10 locations both upwind and downwind of the ETEX tracer release location in western France, with the best result from a given "generation" saved for use in the next iteration. This was repeated for 80 generations. Dramatic improvement in predicted concentration magnitude and arrival time was demonstrated in meteorological and tracer concentration predictive skills due to slower plume migration. Preliminary results have already been presented at a recent conference devoted to atmospheric transport and dispersion. The EnKF technique used the WRF-Data Assimilation Research Testbed (DART) software (Anderson et al., 2009) and the original EM members as the starting point. In this case, all surface and upper-air data within the domain were used in the data assimilation process. Use of the EnKF technique resulted in a slowing of the plume due to the influence of the data assimilation (see Figure 2). By comparison, restricting EnKF assimilation to upper air observations without surface observations resulted in too much slowing of the plume migration indicating that surface wind data play a key role in the observed plume transport. Further testing of the EnKF technique is needed to fully optimize its usefulness.

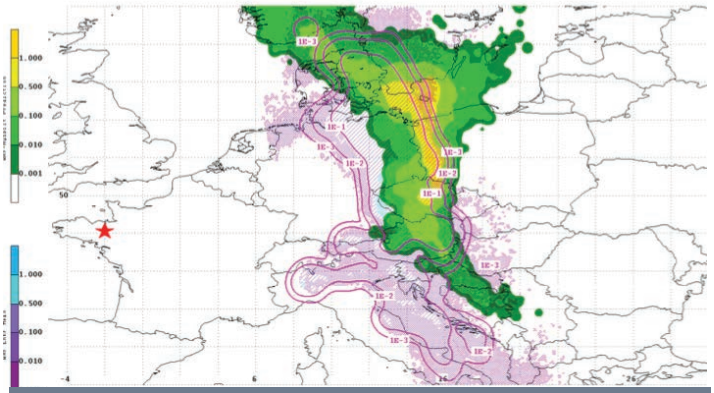

Figure 2. Plume location two days after release for the standard EM (green shading) and after applying EnKF (purple), indicating a slowing of plume migration. Shading and contours are concentration levels (ng/m^3)

FY2016 ACCOMPLISHMENTS

ETEX data were collected and organized for use in the ensemble modeling; This included assembling input gridded and observed meteorological data, as well as measured tracer concentrations

Statistical metrics and software were developed to assess ensemble model skill; Metrics can be applied to both meteorological results as well as the tracer data

A 20-member standard ensemble (using the WRF mesoscale model and running HYSPLIT for transport) was generated for ETEX

A 20-member EnKF ensemble (using WRF-DART platform and running HYSPLIT for transport) was generated for ETEX; Software was developed to allow for specific input of surface and upper-air meteorological data. Two different strategies were compared: 1) assimilation using all observations; and 2) assimilation using only upper air observations (Surface observations were found to significantly impact the model plume results.

A 10-member AP ensemble (using RAMS mesoscale model and running HYSPLIT for transport) was generated for ETEX; Relative to ATMES simulations, the initial simulation ranked 27th out of the 50 ATMES simulations, while the 80th generation ranked 14th out of 50

FUTURE DIRECTIONS

- Further testing of the AP technique: How much spread should be allowed when perturbing the input parameters?
- Further testing of the EnKF technique: Initial testing in this LDRD used all available upper-air and surface data. What specific observations should be used? How much weight should be given to surface versus upper-air data?
- How well do the novel ensemble techniques work on a smaller scale?
- Apply adaptive grid techniques (variable concentration grid resolution) to reduce computational burden.
- Explore running both AP and EnKF in an operational manner.
- An extension to this LDRD for FY2017 has been awarded to explore these topics, with an emphasis on application of the techniques at smaller spatial scales.

Publications/Presentations

1. **Werth, D. W., G. Maze, R. Buckley, S. Chiswell, R. Kurzeja, and B. Viner,** 2016: Novel Ensemble Atmospheric Modeling Techniques for the Simulation of Large-Scale Dispersion, 20th Annual George Mason University Conference on Atmospheric Transport and Dispersion, Fairfax, VA, June 2016.
2. **Buckley, R. L., S. R. Chiswell, R. J. Kurzeja, G. M. Maze, B. J. Viner, and D. W. Werth,** 2017: Novel Atmospheric Ensemble Modeling Techniques Applied to Long-Range Transport. 97th American Meteorological Society Annual Meeting (28th Conference on Weather Analysis and Forecasting/24th Conference on Numerical Weather Prediction). To be presented January 2017.
3. **Buckley, R. L., S. R. Chiswell, R. J. Kurzeja, G. M. Maze, B. J. Viner, and D. W. Werth,** 2017: Advanced Atmospheric Ensemble Modeling Techniques. Planned site report summarizing research results in greater detail, intended to be finalized within the next 6 months.

References

1. **Anderson, J., T Hoar, K. Raeder, H. Liu, N.Collins, R. Torn, and A. Avellano,** 2009: The Data Assimilation Research Testbed: A Community Facility, Bull. Amer. Meteor. Soc., 90, 1283-1296.
2. **Berner, J., S.-Y. Ha, J. P. Hacker, A. Fournier, and C. Snyder,** 2011: Model Uncertainty in a Mesoscale Ensemble Prediction System: Stochastic Versus Multiphysics Representations. Monthly Weather Review, **139,** 1972—1995.
3. **Cotton W. R., R. A. Pielke Sr., R. L. Walko, G. E. Liston, C. J. Tremback, H. Jiang, R. L. McAnelly, J. Y. Harrington, M. E. Nicholls, G. G. Carrio, and J. P. McFadden,** 2002: RAMS 2001: Current status and future directions. Meteorol. Atmos. Phys., **82,** 5-29.
4. **Draxler, R.R., and G.D. Hess,** 1998: An overview of the HYSPLIT_4 modeling system of trajectories, dispersion, and deposition. Aust. Meteor. Mag., **47**, 295-308.
5. **Evensen, G.,** 2003: The Ensemble Kalman Filter: theoretical formulation and practical implementation. Ocean Dynamics, 53, 343-367. Galmarini, S., R. Bianconi, W. Klug, T. Mikkelsen, R. Addis, S. Andronopoulos, P. Astrup, A. Baklanov, J. Bartnicki, J.C. Bartzis, R. Bellasio, F. Bompay, R. Buckley, M. Bouzom, H. Champion, R. D'Amours, E. Davakis, H. Eleveld, G. Geertsema, H. Glaab, M. Kollax, M. Ilvonen, A. Manning, U. Pechinger, C. Persson, E. Polreich, S. Potemski, M. Prodanova, J. Saltbones, H. Slaper, M. A. Sofiev, D. Syrakov, J. H. Sørenson, L. Van der Auwera, I. Valkama, R. Zelazny, 2004a: Ensemble dispersion forecasting—Part I: concept, approach and indicators. Atmos. Envir., **38,** 4607-4617.

References Continued:

6. **Girardi, F., G. Graziani, D. van Velzen, S. Galmarini, S. Mosca, R. Bianconi, R. Bellasio, W. Klug, and G. Fraser,** 1998: ETEX, The European Tracer Experiment. Joint Research Centre, EC, 107 pages.
7. **Mosca, S., R. Bianconi, R. Bellasio, G. Graziani, and W. Klug,** 1998: ATMES II – Evaluation of Long-Range Dispersion Models Using Data of the 1st ETEX Release. Joint Research Centre, European Commission. Luxembourg: Office for Official Publications of the European Communities (EUR 17756).
8. **NCEP/NCAR Global Reanalysis PREPBUFR input observations.** National Centers for Environmental Prediction/National Weather Service/NOAA/U.S. Department of Commerce. 1994, updated monthly. NCEP/NCAR Global Reanalysis Products, 1948-continuing. Research Data Archive at the National Center for Atmospheric Research, Computational and Information Systems Laboratory. http://rda.ucar.edu/datasets/ds090.0/. Accessed 14/Jun/2016.
8. **O'Steen, B.L., and D.W. Werth,** 2009: The Application of an Evolutionary Algorithm to the Optimization of a Mesoscale Meteorological Model. J. Appl. Met. and Clim., **48** (2), 317-329.
9. **Roebber, P. J.,** 2015: Evolving Ensembles. Mon. Wea. Rev., **143** (2), 471-490.
10. **Skamarock, W. C., J. B. Klemp, J. Dudhia, D. Gill, D. Barker, W. Wang, and J. G. Powers,** 2005: A description of the Advanced Research WRF Version 2. NCAR/TN-468_STR, 88 pp.
11. **Stensrud, D. J., N. Yussouf, D. C. Dowell, and M. C. Coniglio,** 2009: Assimilating surface data into a mesoscale model ensemble: Cold pool analyses from spring 2007. Atmos. Research, **93,** 207-220.

Acronyms

AP	Adaptive Programming
EM	Ensemble modeling
EnKF	Ensemble Kalman Filter
ETEX	European Tracer Experiment
HYSPLIT	Hybrid Single Particle Lagrangian Trajectory model IC: Intelligence community
LDRD	Laboratory Directed Research and Development
RAMS	Regional Atmospheric Modeling System
SRNL	Savannah River National Laboratory
WRF	Weather Research and Forecast model
WRF-DART	Weather Research and Forecast-Data Assimilation Research Testbed

Total Number of Post-Doctoral Researchers

1. **Dr. Grace M. Maze** served as a post-doctoral researcher on this project for much of FY2016 (through July 2016). Her post-doctoral work was directed by the Oak Ridge Associated Universities (ORAU).

Clean Energy

Multi-Component Separation And Purification of Natural Gas

Project Team: D. A. Tamburello (Primary), B. J. Hardy, and D. L. Anton
Subcontractors: P. Benard (UQTR), D. Sholl (GT), K. Walton (GT), and M. Sulic (SRC)
Thrust Area: Clean Energy
Project Type: Strategic
Project Start Date: October 1, 2014
Project End Date: September 30, 2016

It is proposed to prove the applicability of the multi-component potential theory of adsorption (MPTA) to a real world natural gas adsorbent system to properly characterize the adsorbent's selectivity for an individual gas component using only the single component isotherms. Thus, the real world gas separation/purification application of a specific adsorbent for a given gas stream can be obtained simply and effectively without the need for large experimental efforts or costly system modifications until after an initial computational screening of perspective materials has been completed. While the current research effort will use natural gas, which is the world's largest industrial gas separations application, to validate the MPTA, the tools gained through this effort can be applied to a gas separation effort, such as CO_2, H_2, deuterium, or tritium.

FY2016 OBJECTIVES

- Identify the adsorbent(s) and gas mixture composition(s) to be analyzed
- Complete the derivation of MPTA and apply it to specific adsorbent(s) for specific single-component and multi-component gas composition(s)
- Complete construction of a test stand for validation of the MPTA
- Demonstrate the utility of MPTA-predicted adsorbent selectivity for real-world gas separation/purification.
- Augment/update the MPTA for application to real-world gas separation/purification
- Explore in-situ growth of an adsorbent directly onto a heat exchanger surface for adsorption temperature control
- Explore novel AC pellet creation without adsorption losses from binders

INTRODUCTION

In 2010, nearly 24% of the world's energy demands were supplied by natural gas, which is an increase of 7.4% from the previous year[1].

Over the past decade, several technical developments (such as hydraulic fracturing) have led to an exponential increase in discovering new domestic natural gas reserves. In 2010, nearly 24% of the world's energy demands were supplied by natural gas, which is an increase of 7.4% from the previous year[1]. Raw natural gas composition can vary substantially from source to source. Typically, methane accounts for 75% to 95% of the total gas, with the rest of the gas containing ethane, propane, butane, other higher hydrocarbons, and impurities, with the most common including H_2O, CO_2, N_2, and H_2S. All natural gas requires some treatment, if only to remove H_2O; however, the composition of natural gas delivered to the commercial pipeline grids is tightly controlled. Natural gas processing is the largest industrial gas separation application in the world, with an estimated $5 billion natural gas separations equipment market in 2008[2]. Even with the economic and environmental incentives, as much as 20% of the worldwide natural gas reserves require extensive treatment (2008 estimate) and remain unusable due to high costs of purification and delivery to the commercial pipeline grid[2]. Sub-quality natural gas reserves—defined as fields containing more than 2% CO_2, 4% N_2, or 4 ppm H_2S—make up an estimated 50% of the world's natural gas volume[1]. The development of sub-quality, remote, and unconventional fields (i.e. landfill gas) can present new challenges to gas separation that require more efficient and economically viable approaches to the conventional CO_2 and N_2 removal processes[1]. Adsorbent technologies, such as the use of activated carbons, zeolites, or metal-organic frameworks (MOFs) are already widely used in the natural gas industry for separation of impurities[3]. "Central to the development and implementation of adsorption-based processes are the various selectivity mechanisms that give rise to the separation of components within the gas mixture."[1]

The selectivity of an adsorbent depends on the interactions between various components with the adsorbent surface, as well as on the intermolecular interactions between components themselves. For this reason, estimating the selectively and describing the thermal response and transport processes of a gas mixture in a given adsorbent requires much more than knowledge of single component adsorption isotherms; although the individual single-component isotherms do play a critical role in predicting the adsorbent-mixture behavior. There are several theoretical approaches to understanding and predicting mixture adsorption, such as DFT, IAST, RAST, VST, and CLM. While some of these approaches can describe the properties of mixture adsorption reasonably well, they typically describe ideal systems that behave very differently from actual adsorbents whose pore structures and surface areas generally vary significantly from ideality[4]. However, Dunbar et al. (2012) presented a very promising and versatile new approach for modeling the properties of non-ideal real gas mixture adsorption called MPTA. MPTA considers the mixture as a heterogeneous substance segregated in the external field of the adsorbent as shown Figure 1. A crucial advantage of MPTA is its capacity to accurately predict excess adsorption of various gases on adsorbents with very few fitting parameters due to the use of the same equations of state for both the bulk and adsorbed phases. For this and other reasons, MPTA and proving its capabilities in predicting real world gas separation/purification applications—specifically, natural gas adsorption—is the focus of the current research.

Through the results of this work, new adsorbents can be tested computationally in specific separation applications without the need for costly experimental efforts. In addition, existing gas separation technologies, such as PSA and TSA systems, will be improved through process intensification by accurately modeling these real world gas separation operations and testing new operating conditions, components, or adsorbent materials. Finally, the performance of new separation operations that combine existing technologies, such as a TAPSA system, can be modeled accurately to predict their performance without the need for excessive experimental efforts.

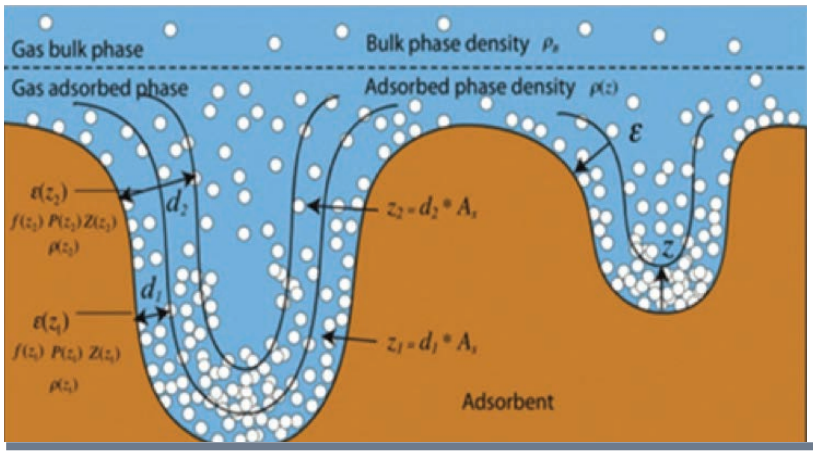

Figure 1. Basic principles of MPTA[4]

APPROACH

This program has two primary efforts: 1) theory derivation and adaptation and 2) experimental measurements and application. The first effort consists of an initial derivation of the MPTA and its adaptation to a specific gas composition. The mass and energy balances together with equations for the multicomponent isotherms and excess internal energy will be coupled to the real gas properties (compressibility, enthalpy, viscosity, etc.) to create a global model describing an ANG system. The second effort consists of adsorbent selection, gas composition selection, and experimental set-up. From the over fifty adsorbents currently in use by the petrochemical industry for natural gas separation, two to three will be chosen for analysis based on their availability, their ease of synthesis, and the availability of literature data.

These two efforts will merge together as the experimental data is taken and the models are validated. The remainder of the project will then consist of model validation and augmentation using both single-component and multi-component isotherm measurements. The single-component experimental data will then be fed into the MPTA model to predict and compare with the multi-component data for validation. As necessary, the MPTA model will be updated to correct for discrepancies and improve accuracy. By validating the MPTA model's viability to describe the adsorption selectivity of an individual component of a gas mixture using only single component isotherm data, this work will prove the predictive capability of using specific adsorbents for specific gas separation applications.

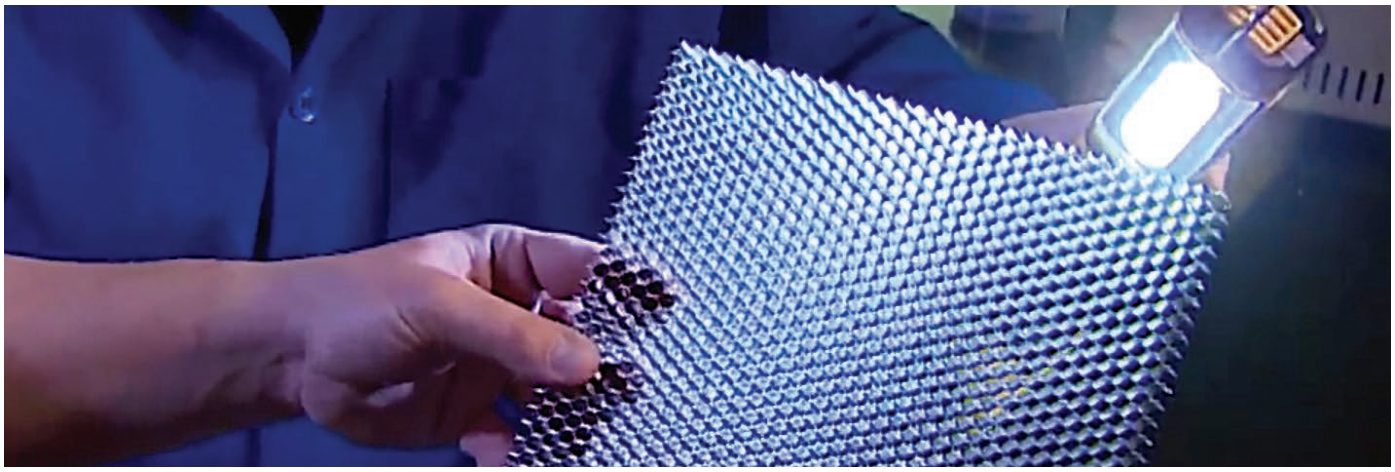

This project also includes a secondary effort aimed at improving adsorbents and their application in PSAs. Most adsorbents have extremely poor thermal conductivity, which can make the thermal control necessary for effective separation applications difficult. Growing an adsorbent directly onto a heat exchanger surface—dubbed in-situ adsorbent growth—minimizing thermal resistance with the heat exchanger surface and maximizes an adsorbent's thermal control. Additionally, many applications will use compaction to increase an adsorbent's thermal conductivity. However, many adsorbents cannot be compacted without either destroying adsorption sites or using a binder, both of which inhibit gas uptake and, thus, decrease adsorption capacity. To minimize these losses, another effort within this project seeks to create activated carbon compacts using another adsorbent as a binder.

RESULTS / DISCUSSION

We built a numerical implementation of the multicomponent potential theory of adsorption (MPTA) which is a two parameters thermodynamics model used to predict gas mixture adsorption using only pure gasses adsorption isotherms. Our implementation was written in Python3 and uses the NIST Refprop database to describe the thermodynamics properties of the fluids. NIST Refprop database is presumably the most accurate equation of state to describe pure fluids and mixtures. The MPTA model worked out-of-the-box in the supercritical regime, but it also worked great in the subcritical region by with minor changes of our implementation.

The constitutive equation of the MPTA is given by: $\mu_B(\rho_B) = \mu_{Ad}(\rho_{Ad}) - \varepsilon,$ where μ_B and ρ_B are the chemical potential and density of the fluid in the bulk phase, respectively, while μ_{Ad} and ρ_{Ad} are the chemical potential and density of the fluid in the adsorbed phase, respectively. ε represents the fluid-surface interaction potential. The bulk phase is defined as the region far from the surface, where the potential ε is negligible. Conversely, the adsorbed phase is defined as the region near the surface, where the fluid is significantly affected by the presence of the surface via the potential ε.

For our work, we modeled the potential ε using the well-known Dubinin-Radushkevich-Astakhov potential given by: $\varepsilon(z) = \varepsilon_0 \left(\ln \frac{z_0}{z}\right)^{\frac{1}{2}}.$

In the above equation, ε_0 is the characteristic energy of adsorption and z_0 is the limiting micropore volume. These are the fitting parameters of the model.

The equation for the potentials can be solved to get $\rho_{Ad}(z)$ and then the excess adsorption is evaluated using:

$$N_{ex}(\rho_B) = \int_0^{z_0} (\rho_{Ad}(z) - \rho_B) dz.$$

Figure 2 represents the adjustment of the model on experimental data[5] for pure CH_4, N_2 and CO_2 at 318.2 K on Calgon F-400 activated carbon. This is an example for supercritical fluids. In the subcritical region, the initial assumption of the root finding routines for the fluid density, in the adsorbed phase, must be carefully adjusted. Otherwise, the algorithm may fail to converge to the proper density. Figure 3 shows the results of the fit for a direct implementation of the model (red line) and of our implementation where the initial guess for density is finely tuned based on the fluid nature and phase (blue dashed line). To do this, we start with the bulk phase, where the fluid properties are well known, and then divide the adsorbed phase in small intervals (Δz). For each step Δz, we compute the fluid density using the density of the previous step as starting point. For supercritical fluids, this approach is enough because the fluid density is assumed to vary smoothly. For subcritical fluids, we also need to check the phase of the fluid and use a value greater than the liquid density as an initial assumption for the density. Here, we used experimental data for subcritical CO_2 at 298 K on Norit R1 activated carbon[6].

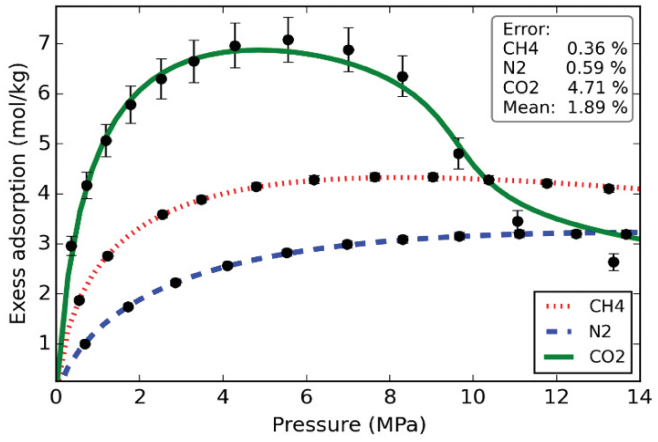

Figure 2. Illustration of pure CO_2, N_2, and CH_4 experimental data compared to model

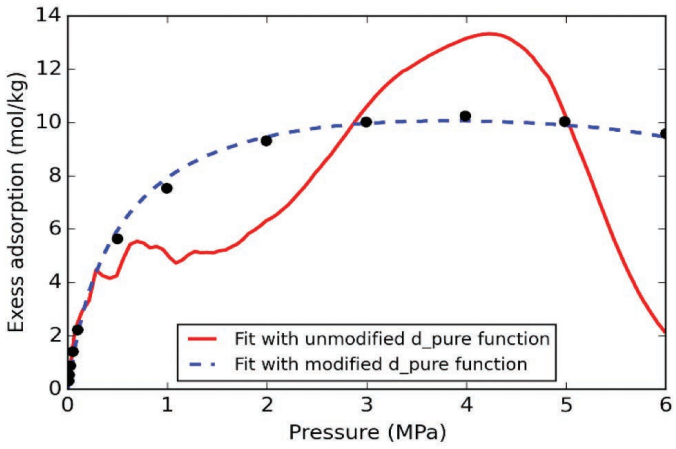

Figure 3. Fits to subcritical data for direct implementation (red) and finely tuned based on fluid nature and phase (blue) of the model

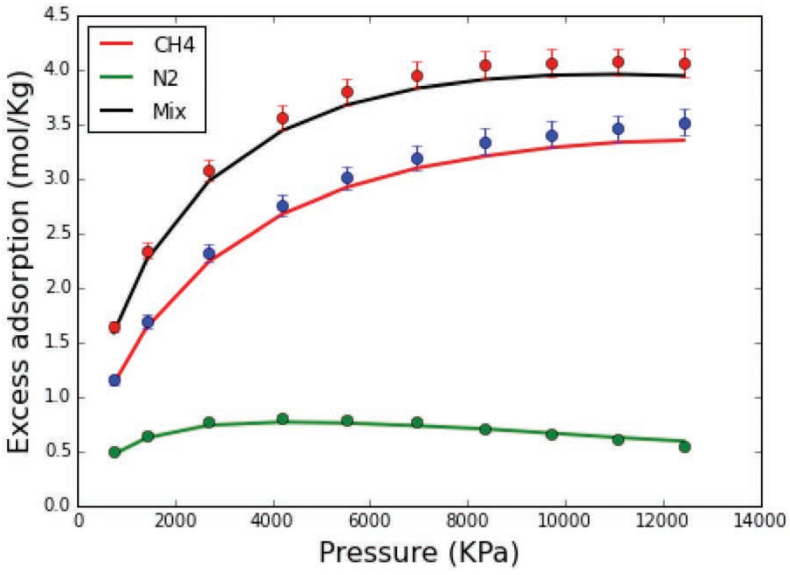

Figure 4. MPTA model and experimental data fit for fluid mixture constituting 60% CH_4 and 40% N_2 at 318.2 K

Once the model is properly fitted on pure gas isotherms (i.e. once the optimal parameters ε_0 and z_0 are founded), the model can be used to predict mixture adsorption. Figure 4 shows the agreement between the implementation of the MPTA model and experimental data for a fluid mixture constitute of 60% CH_4 / 40% N_2 at 318.2 K (Sudibandriyo et al., 2003). Table 1 provides the model mean error and experimental uncertainties of the data in Figure 4.

Table 1. The mean error between the implementation and experimental data and also the experimental uncertainties

	Model mean error	Experimental uncertainties
CH_4	4.63%	2.6%
N_2	3.56%	4.5%
Mixture	4.11%	2.5%

Previously reported, the robust metal-organic framework (MOF) UiO-66 was chosen as the parent adsorbent for this study due to its resistance to degradation in wet environments. Single component adsorption isotherms indicate a preferential for CO_2 as compared to CH_4 and N_2. To validate the MPTA multi-component adsorption model the MOF was also studied with a binary gas of CO_2/CH_4 with a 15/85 mixture in order to best simulate the average composition of natural gas (Figure 5). The multi-component isotherms differ from those of the single component, most notably for CO_2, due to the percent composition of the binary gas.

To further study the selective adsorption of the multi-component gas, additional UiO-66 based adsorbents were chosen. Alteration to the parent UiO-66 allows for potential improvement to the material's surface area, which in turn may enhance adsorption and selectivity. The additional MOFs synthesized, based on UiO-66, consisted of functionalized versions with either amine ($-NH_2$), nitrogen dioxide ($-NO_2$) and dimethyl (-DM) groups. Defective UiO-66 was also synthesized that created vacancies in the parent compound through additional work-up during the synthesis process. Table 2 list the UiO-66 based adsorbents and their related surface area as measured using the widely accepted Brunauer-Emmett-Teller theory (BET) including defective analogues that are ongoing.

Table 2. Surface area of UiO-66 based adsorbents tested for multi-component gas adsorption

Adsorbent	BET Surface Area (m^2/g)
Parent UiO-66	1329
UiO-66-DM	785
UiO-66-NO_2	914
UiO-66-NH_2	1501
Defective UiO-66_1	1690
Defective UiO-66_2	1922
Defective UiO-66_3	1654
Defective UiO-66_4	1617
Defective UiO-66_5	Ongoing
Defective UiO-66_6	
Defective UiO-66_7	
Defective UiO-66_8	

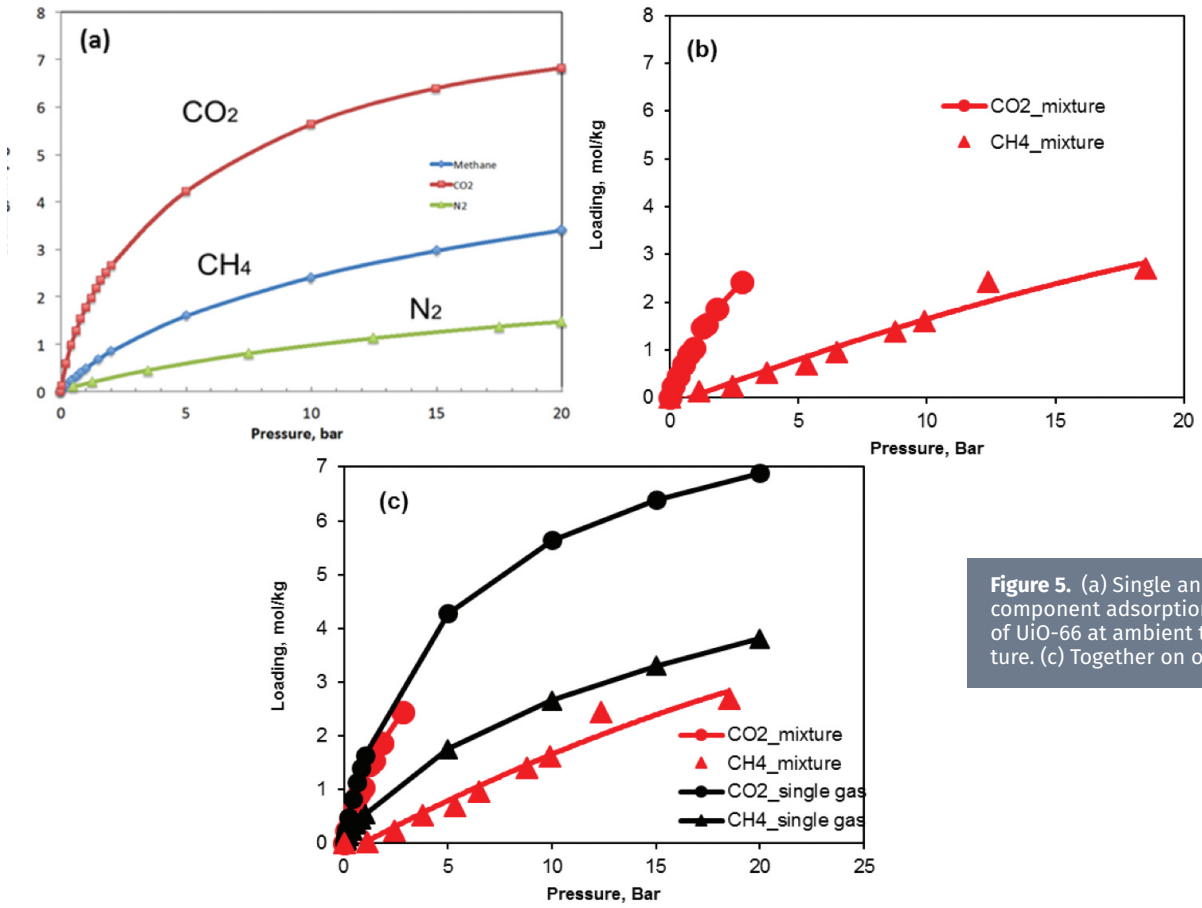

Figure 5. (a) Single and (b) multi-component adsorption isotherms of UiO-66 at ambient temperature. (c) Together on one graph

Multi-component isotherms have also been collected for -DM, -NO_2 and -NH_2 (defective UiO-66 ongoing) for the same gas composition (15% CO_2: 85% CH_4). Figure 6 shows the single component isotherms and the multi-component equivalent.

As the main focus of this project was to study the separation of gases on an adsorbent and to validate the MPTA model, it is important to examine the isotherm adsorption data of UiO-66 and its derivatives for selectivity. As with any natural gas stream the ideal scenario is to capture undesirable gases and allow the desired gas (methane) to continue.

To more closely compare the adsorbents studied and their selectivity of CO_2 over CH_4 we considered the equation at right where i = CO_2, j = CH_4, x = composition in adsorbed phase, and y = composition in the gas phase.

$$\alpha_{ij} = \frac{x_i}{y_i} \times \frac{y_j}{x_j}$$

The above equation for selectivity is used by the membrane industry to determine the optimum membrane required for a separation process where the selectivity, α_{ij}, is defined as the ratio of permeability of species i with relation to species j. It was modified for this project due to the two phases that occur during solid-state adsorption. Figure 7 shows the preferential selectivity for CO_2 of the UiO-66 adsorbents that have been studied thus far. Note that the data for original UiO-66 does not follow the trend shown for its variants. This is believed to be a data acquisition error and the data will be retaken to prove/disprove this belief. Also note that the –DM variant shows a higher selectivity than the other versions, which was an unexpected result. At this time, no explanation is available without additional study.

Figure 6. Methane and carbon dioxide single and multi-component isotherms of UiO-66 functionalized with (a) -DM, (b) -NO_2, and (c) -NH_2

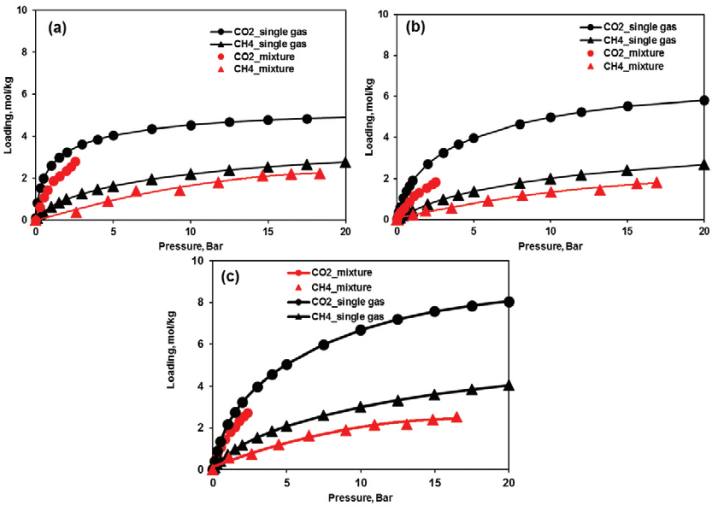

Figure 7. Preferential selectivity ($\alpha_{i,j}$) for CO_2 over CH_4 of the variants of UiO-66.

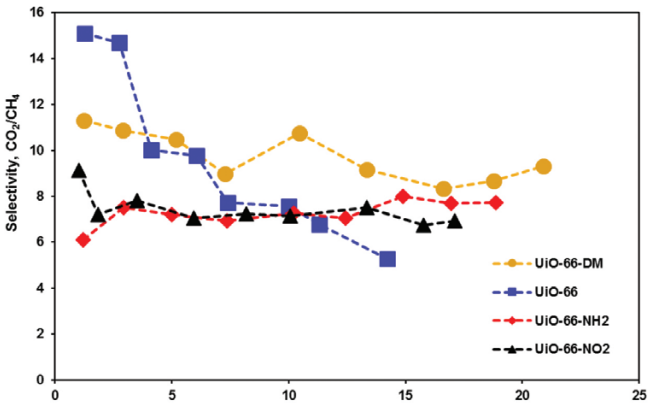

FY2016 ACCOMPLISHMENTS

Completed derivation of the MPTA model to account for multi-component gas streams. (Written in Python3 utilizing the NIST Refprop database to describe the thermodynamic properties of the gases; Consideration of the subcritical gas region proved to paramount as without careful initial adjustment the model would not converge on the proper density)

Completed validation measurements of single-component excess adsorption isotherms of CH_4, N_2, and CO_2, on UiO-66, UiO-66-DM, $-NH_2$ and $-NO_2$.

Completed validation measurements of multi-component excess adsorption isotherms of CH_4 and CO_2 on UiO-66, UiO-66-DM, $-NH_2$ and $-NO_2$

Determined the selectivity of CO_2 over CH_4 for the studied metal-organic frameworks

Synthesized 16 derivatives of the parent adsorbent UiO-66

Retrofitted high pressure Sieverts apparatus with gas chromatograph for gas mixture measurements

Devised experimental techniques to quantitatively determine the concentration of a gas mixture in the adsorbed and gas phase after equilibrium is achieved

FUTURE DIRECTIONS

- Improvement of the MPTA using single-component adsorption isotherms
  - >> Validate/Refine the MPTA derivation based on experimental data
  - >> Develop a method to overcome potential field limitations—such as pore condensation—wherever possible
- Improvement of the MPTA using multi-component mixture adsorption isotherms
  - >> Validate/Refine the MPTA derivation based on experimental data
  - >> Quantify differences based on static and flowing mixture adsorption
  - >> Alter/improve single-component potential fields for increased accuracy
- Validate measurements of single component excess adsorption isotherms of CH_4, CO_2 and N_2 on defective UiO-66
  - >> Up to 20 bar initially with addition measurements up to 100 bar
- Validate measurements of multi-component excess adsorption isotherms of CH_4/CO_2 (85:15) on defective UiO-66 adsorbents
- Validate measurements of multi-component excess adsorption isotherms of CH_4/N_2 (85:15) on UiO-66, UiO-66-DM, $-NH_2$, $-NO_2$ and defective MOFs
- Techno-economic analysis of TAPSA vs. PSA vs. TSA
- Build a functional PSA / TSA system to examine real-world operation

References

1. **Rufford, T.E.; Smart, S.; Watson, G.C.Y.; Graham, B.F.; Boxall, J.; Diniz da Costa, J.C.; May, E.F.** "The removal of CO2 and N2 from natural gas: A review of conventional and emerging process technologies" Journal of Petroleum Science and Engineering 2012, 94-95, 123.
2. **Baker, R.W.; Lokhandwala, K.** "Natural Gas Processing with Membranes: An Overview" Ind. Eng. Chem. Res. 2008, 47, 2109.
3. **Furukawa, H.; Ko, N.; Go, Y. B.; Aratani, N.; Choi, S. B.; Choi, E.; Yazaydin, A. O.; Snurr, R. Q.; O'Keeffe, M.; Kim, J.; Yaghi, O. M.** "Ultrahigh Porosity in Metal-Organic Frameworks" Science 2010, 329, 424.
4. **Dunbar, E.; Zacharia, R.; Chahine, R.; Benard, P.** "Modified potential theory for modeling supercritical gas adsorption" International Journal of Hydrogen Energy 2012, 37, 9137.
5. **Sudibandriyo, M.; Pan, Z.; Fitzgerald, J.; Robinson, R.L.; Gasem, K.** "Adsorption of Methane, Nitrogen, Carbon Dioxide and their Binary Mixtures on Dry Activated Carbon at 318.2 K and Pressures up to 13.6 MPa" School of Chemical Engineering 2003, 19, 5323.
6. **Dreisbach, F.; Straudt, R.; Keller, J.U.** "High pressure Adsorption Data of Methane, Nitrogen, Carbon Dioxide and their Binary and Ternary Mixtures on Activated Carbon" Adsorption 1999, 5, 215

Acronyms

AC	Activated Carbon
ANG	Adsorbent Natural Gas
ARPA-E	Advanced Research Projects Agency – Energy
CLM	Corrected Langmuir Model
DFT	Density Functional Theory
GT	Georgia Institute of Technology
IAST	Ideal Adsorption Solution Theory
MOF	Metal Organic Framework
MPTA	Multi-component Potential Theory of Adsorption
PSA	Pressure Swing Adsorption
RAST	Real Adsorbed Solution Theory
SRC	Savannah River Consulting
TAPSA	Temperature Assisted Pressure Swing Adsorption
TSA	Temperature Swing Adsorption
UQTR	Université du Québec à Trois-Rivières
VST	Vacancy Solution Theory

Intellectual Property

Invention disclosure SRNS-15-014 (SRNS-85-S) entitled In-situ Adsorbent Growth onto a *Heat Exchanger Surface* was submitted to the Technology Transfer department at SRNS in June of 2015.

Total Number of Post-Doctoral Researchers

Two post-doctoral researchers (one at GT and one at UQTR) are being funded through this work.

Selective Adsorption/Purification Of Natural Gas Using Tunable Adsorbents

Project Team: Bruce Hardy-PI (SRNL), Theodore Motyka (SRC), Martin Sulic (SRC), Claudio Corgnale (SRC), Natalia Shustova (USC), Donna Chen (USC)
Subcontractor: SRC and USC
Thrust Area: Clean Energy
Project Type: Strategic
Project Start Date: October 1, 2015
Project End Date: September 30, 2017

The proposed research effort consists of the systematic development of adsorbent based natural gas purification systems. The project will focus on MOFs, but can readily be extended to other adsorbents. The effort is distinct from prior work in that it evaluates adsorbent based separation from fundamental adsorbent properties and synthesis to performance of the MOFs in a separation system. MOFs will be designed to have separation factors and distribution coefficients suitable for removal of commonly occurring impurities in natural gas using techniques established at USC for producing "tunable" surface properties. The MOFs will be synthesized and characterized for selectivity via analytical methods that examine the in situ binding energies of the adsorption sites. Multicomponent isotherm models, that utilize single component data, will be incorporated into mathematical simulations for adsorbent based separation on a system level. The system models will be used to design large-scale separation processes and evaluate them in terms of economic and exergetic efficiency.

FY2016 OBJECTIVES

Develop isotherm models describing multicomponent selective adsorption. (Multicomponent models will use single component isotherm data to predict multicomponent adsorption; Validate models against binary data)	For existing adsorbents, use the isotherm models to demonstrate proof of concept for pressure swing separation	Implement multicomponent isotherms in preliminary system models for industrial scale separation	Simultaneously, USC is to design, synthesize and evaluate new selective adsorbents for target gas species	Adsorbents developed by USC to be sent to SRNL for isotherm measurement (along with other required properties)

INTRODUCTION

Worldwide, there are significant reserves of sub-quality natural gas, defined as containing >2% CO_2, >4% N_2, >4 ppm H_2S. It is estimated that 50% of known reserves have > 2% CO_2. Adsorption-based purification processes have high potential for energy and capital investment savings over conventional CO_2 amine scrubbing and cryogenic distillation N_2 rejection unit technologies.

This LDRD project, which comprises the first year of a proposed 2 year effort, consists of the systematic development of adsorbent based natural gas purification systems. The project focuses on the use of metal organic frameworks (MOFs), which are a new class of adsorbent materials that can be designed to selectively bind to specific gases. In partnership with the University of South Carolina (USC), MOFs will be engineered and synthesized to have "tunable" surface properties suitable for removal of commonly occurring impurities in natural gas. As such, MOF based purification processes, designed to specifically take advantage of the performance of these adsorbents, have the potential for significant improvement over currently used adsorbents. In this effort, adsorbent based gas separation is evaluated from fundamental adsorbent properties and synthesis to performance of the MOFs in a separation system. Although this effort is applied to separation of methane from wellhead natural gas, the underlying methodology can be readily applied to other gas purification processes.

MOF synthesis will occur over several generations, the first of which has been produced and delivered to SRNL and will be characterized for its selectivity at the beginning of the second year of the project. The characterization data will be used in mathematical models, developed by SRNL, that predict the performance of process systems. The models will be used to design large-scale separation systems and evaluate them in terms of economic and exergetic efficiency. The MOFs will be synthesized and then characterized for selectivity via unique analytical methods that examine the in-situ binding energies of the adsorption sites. Results from the models will identify needed improvements in MOF performance which will be used to guide the design and synthesis of the successive generations of MOFs for this project.

APPROACH

The goal of this LDRD is the design and techno-economic evaluation of an adsorbent based separation system for natural gas; this part of the effort will be conducted by SRNL. The basis of the separation process will be novel adsorbents, synthesized by USC, to have high affinity for gas species comprising wellhead natural gas. For tractability within the timeframe of a strategic LDRD, the focus will be restricted to metal organic frameworks (MOFs). To maintain practical cycling rates, the system will operate as a pressure swing adsorption (PSA) process. System design will thus focus on PSA operation, although the operating temperature will be allowed to vary within practical limits, to identify optimal conditions for performance.

The combination of intrinsic porosity with adsorption selectivity is necessary to achieve the rational design of new selective adsorbents or materials with high gas separation efficiency. MOFs are a class of crystalline hybrid materials that satisfy both criteria. MOFs also offer unprecedented tunability, thereby enabling very high adsorption selectivity based on either: pore aperture or geometry, composition, and ensemble sizes of the metal active sites. Therefore, enhanced selectivity to gas separation or adsorption could be achieved by systematic alteration of the metal sites and variation of MOF surface area through the ligand design. Moreover, MOF metal nodes can include a least two distinct metals, which provides a pathway for tandem selectivity (i.e., selectivity for two or more adsorbates simultaneously).

RESULTS / DISCUSSION

The technical approach to this project requires the development of mathematical models for the behavior of the adsorbent in a pressure swing system and the design and synthesis of species selective MOFs that are durable in the presence of gases in the process stream.

At this point of the project, multicomponent isotherm models that determine the degree of separation have been developed and tested against a known MOF. With SRNL characterization data for MOFs provided by USC, the models can be used for general MOF/gas compositions.

Starting from Cu_3BTC_2 (HKUST), which is a known and durable MOF, USC has designed and synthesized "first generation" selective MOFs. USC evaluated these MOFs for suitable properties and selectivity by using: X-ray photoelectron spectroscopy for surface elemental composition; powder X-ray diffraction for phase transitions and crystallinity; Fourier transform-infrared spectroscopy to identify chemical compounds and molecular bonds; energy dispersive X-ray spectroscopy with a scanning electron microscope for elemental analysis; and inductively coupled plasma mass spectrometry which detects very low concentrations of metal and non-metal elements. Two generalized synthesis methods were developed and 10 MOFs were successfully synthesized and are being characterized (more MOF formulations were attempted). The MOFs were delivered to SRNL for measurement of properties required for the adsorption system models.

FY2016 ACCOMPLISHMENTS

Specialized experimental apparatus in place to measure single and multicomponent isotherms as adsorbents become available (future capability for SRNL)

Software required to develop multicomponent isotherm models has been acquired, tested and used for surrogate calculations

Developed modeling framework for multicomponent isotherms. (Developed theoretical and numerical formulation of models; Developed Isotherm models using MPTA and IAST for system models)

Isotherm models were used with MOF-5, as test, to demonstrate that the pressure swing concept is viable for N_2/CH_4 separation. (Isotherm measurements were performed at SRNL)

System (global) models for large-scale processing are in preliminary form. (Future use in FY2017 for design of separation systems, scale-up, optimization and evaluation of concepts as well as to determine economic and exergetic efficiency

USC has designed and synthesized "1st generation" selective MOFs (They were evaluated at USC using PXRD, FT-IR, ICP-MS, EDX and XPS; and deliveredto SRNL for measurement of isotherms and other properties required for separation system design)

FUTURE DIRECTIONS

- SRNL will perform property measurements and selectivity characterization to obtain data for model input
- SRNL models will be used to design and evaluate a pressure swing adsorption system for methane purification from wellhead natural gas
  >> Models will be used to perform a techno-economic evaluation and evaluate the exergetic efficiency of the separation system
  >> Results of the models, with sensitivity analyses, will provide guidance on improved MOF characteristics
- Results from the models will identify needed improvements in MOF performance which will be used to guide the design and synthesis of the successive generations of MOFs for this project
  >> MOF synthesis will occur over several generations, the first of which has been produced and delivered to SRNL

Publications/Presentations

Preparations for papers and presentations at both MOF-2016 and SERMACS are in progress.

References

1. **Rufford, T E, et al., et al. "**The removal of CO2 and N2 from natural gas: A review of conventional and emerging process technologies" 94-95, s.l. : Elsevier, 2012, Journal of Petroleum Science and Engineering, pp. 123-154.
2. **Myers, A L and Prausnitz, J M.**"Thermodynamics of Mixed-Gas Adsorption" 1, 1965, AIChE Journal, Vol. 11, pp. 121-127.
3. **Yang, Ralph T.** "Gas Separation by Adsorption Processes. ISBN-10 1-86094-047-1. 1987 (Repr 2008)"

Acronyms

EDX	Energy Dispersive X-ray Spectroscopy
FT-IR	Fourier Transform-infrared Spectroscopy
ICP-MS	Inductively Coupled Plasma Mass Spectrometry
MOF	Metal Organic Framework
PXRD	Powder X-ray Diffraction
XPS	X-ray Photoelectron Spectroscopy

Exploring Innovative Chemistry for Natural Gas Conversion to DME (Dimethyl Ether)

PI:: Steve Xiao
R&D Team: Anthony Thompson (ORAU/SRNL), Patrick Ward (Greenway Energy/SRNL), Elise Fox (SRNL), Salai Ammal (USC), Libin Lei (USC), Andreas Heyden (USC), Donna Chen (USC), Frank Chen (USC)
Subcontractor: University of South Carolina (Columbia, SC)
Project Type: Strategic
Project Start Date: October 1, 2015
Project End Date: September 30, 2017

A new method for conversion of natural gas into dimethyl ether (DME) is being explored. The process involves the use of a proton-conducting membrane to keep oxygen separated from methane, avoiding their direct reaction which typically results in combustion to byproducts that have no value as fuels. The method is akin to a direct methane fuel cell, where methane is partially oxidized to DME instead of being fully combusted. In year 1 we have computationally predicted a series of catalysts with good theoretical performance and developed methods to synthesize these catalysts in the laboratory. Materials were selected for cathode, anode, and electrolyte for the membrane and tested for compatibility with the catalyst. The membrane materials and the catalyst samples were fully characterized by several methods. Capabilties are being established to build and test a membrane electrochemical reactor as well as a fixed bed reactor for catalyst and combatibility testing.

FY2016 OBJECTIVES

- **Fabrication of high performance solid oxide membrane with proton conducting electrolyte**
- **Catalyst design and reaction engineering**
- **Reaction mechanism, *ex situ* and *in situ* catalyst characterization**

INTRODUCTION

Natural gas shows promise as a potential alternative to petroleum and is currently abundantly available in the United States{O'Reilly, 2011 #14}. Unfortunately, a significant portion of the natural gas in the U.S. is stranded, or located in remote areas. Since methane, the main constituent of natural gas, cannot easily be compressed into a liquid, transportation costs per unit energy are very high, especially in these stranded areas, and natural gas is often vented into the atmosphere or flared in order to save costs{McFarland, 2012 #13}. Direct conversion of methane to liquids has been sought after for decades with few successes. One issue with this chemistry is that the liquid products (e.g. methanol) are more reactive than methane itself and tend to undergo further oxidation under the reaction conditions, eventually leading to CO_2, which has no energetic value as a fuel{Xu, 2003 #15}.

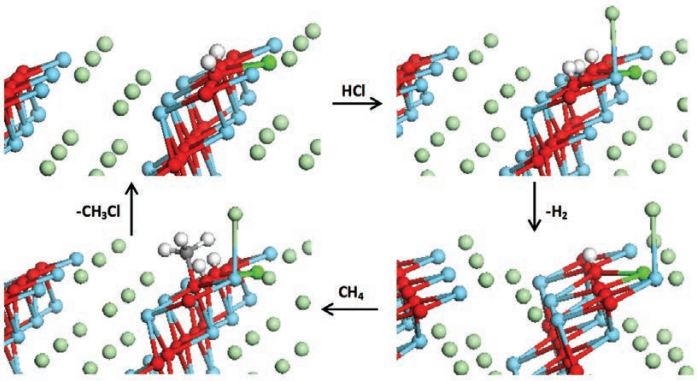

Figure 1. Catalytic cycle obtained from a computational study on methane activation over a catalyst surface

In this work we have designed a system to convert methane into dimethyl ether (DME), a gas that is easily compressed into a liquid at room temperature. DME can be mixed with existing diesel fuels and has a high cetane number. With a revamp of the fuel system to accommodate pressurized fuel, DME has been used by itself in current diesel engines. Because of the lack of C-C bonds in the chemical structure of DME, it also produces less soot than conventional fuels such as gasoline{Szybist, 2014 #16}. To produce DME from methane, an oxidant is required ($CH_4 + O_2 = CH_3OCH_3 + H_2O$). However, oxygen- methane mixtures tend to combust at high temperatures into less useful products such as CO_2. We have designed a system that should circumvent this issue by ensuring that oxygen and methane are never in contact with each other.

APPROACH

The method used here relies on a catalytic membrane, which oxidizes methane to DME without allowing oxygen and methane to come into contact. A schematic illustration and the accompanying chemical reactions are shown in Figure 2. On the anode side, methane reacts with a LaOCl catalyst to form chloromethane. This is a known reaction that has been studied previously with the same catalyst{Peringer, 2009 #2;Peringer, 2008 #10;Podkolzin, 2007 #1}. The oxygen and chlorine needed for the reaction are supplied by the LaOCl surface. The oxygen is later replaced with oxygen from water molecules that are fed in with the methane, and the chlorine is replaced with hydrogen chloride resulting from the subsequent reactions, so that the catalyst is not lost during the reaction. Chloromethane and water then react to form methanol and hydrogen chloride, and methanol and chloromethane react to form hydrogen chloride and DME. These are known reactions that have been studied previously{Khaleel, 2011 #7}. The membrane assembly will be synthesized and electrical contacts and flow tubes will be made using standard fuel cell methodology. The reaction will take place at 400-500 °C.

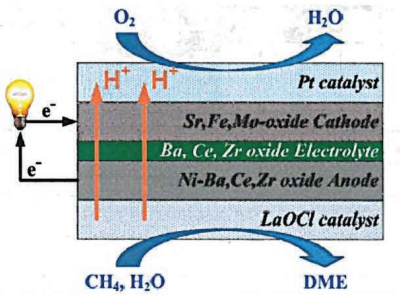

$$2CH_4 + 2HCl + O_2 \xrightarrow{LaOCl} 2CH_3Cl + 2H_2O$$

$$CH_3Cl + H_2O \longrightarrow CH_3OH + HCl$$

$$CH_3OH + CH_3Cl \longrightarrow CH_3OCH_3 + HCl$$

overall: $2CH_4 + O_2 \longrightarrow DME + H_2O$

ΔH=-231.2 kJ/mol, ΔG=-158.3 kJ/mol (650K)

Figure 2. Selective methane conversion over solid oxide membrane and catalyst assembly

RESULTS / DISCUSSION

First Principles Investigation of LaOCl Surface Models

In the first phase of this study, we used DFT and constrained ab initio thermodynamics simulations to identify the nature of the LaOCl surface that would be present under experimental reaction conditions. All calculations have been performed using the VASP program with the PBE functional. We first examined the most stable (001) termination of the LaOCl surface by constructing a (3×3) surface slab composed of 3 molecular layers and a 15 Å vacuum gap. The interaction of H, Cl, and O on the surface as well as the presence of O or Cl vacancies were examined under reaction conditions and the results are summarized in Table 1. The calculated free energies of adsorption of H, Cl, and O atoms with reference to the corresponding gas molecules are positive and the formation of O and Cl vacancies on the surface are highly endergonic which suggested that the stoichiometric LaOCl (001) surface is not reactive.

Table 1. Calculated reaction energies (ΔE) and free energies (ΔG, T=600 K; Pgas = 1 atm) for the adsorption/desorption of O, Cl, and H on the LaOCl (001) surface

Reaction	ΔE (eV)	ΔG (eV)
$LaOCl \leftrightarrow LaOCl_{1-x} + \frac{1}{2} Cl_2$	4.22	3.55
$LaOCl \leftrightarrow LaO_{1-x}Cl + \frac{1}{2}O_2$	6.65	6.07
$LaOCl + \frac{1}{2}O_2 \leftrightarrow LaOCl\cdots O$	0.49	1.08
$LaOCl + \frac{1}{2}Cl_2 \leftrightarrow LaOCl\cdots Cl$	0.71	1.38
$LaOCl + \frac{1}{2} H_2 \leftrightarrow LaOCl\cdots H$	2.35	2.73

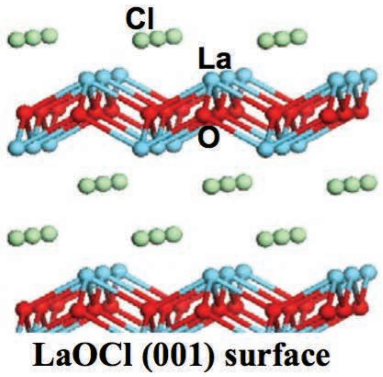

The activity of p-doped LaOCl (001) surfaces were then examined by replacing a surface La^{3+} ion by alkaline earth metals such as Ba^{2+}, Sr^{2+}, and Ca^{2+} ions. This study was motivated by reported experimental studies{Peringer, 2009 #2;Podkolzin, 2007 #1} which suggested that the chlorination of methane in the presence of oxygen on a LaOCl surface occurs via a Mars-van Krevelen like mechanism and that the Cl atom that goes into the product CH_3Cl originates from the LaOCl surface. Since doping with lower valent cations can facilitate removal of surface Cl atoms, we examined the activation of CH_4 on the doped LaOCl surface models. As shown in Table 2, we found that removing a surface Cl atom is energetically favorable in the presence of a dopant. However, the reaction free energies calculated for CH_4 activation, where a surface Cl atom is removed to form CH_3Cl and the H atom from CH_4 is adsorbed on the LaOCl surface, are still above 2 eV. These results suggest that the H adsorption is not favorable on the LaOCl (001) surface both in the presence and absence of dopants and consequently this surface is most likely not active for CH_4 activation in the absence of gas phase oxygen. When gas phase oxygen is present, CH_4 dissociation becomes feasible by transferring the H atom to the adsorbed O atom.

Table 2. Reaction free energies (ΔG) for the formation of a Cl-vacancy and activation of CH_4 on the doped LaOCl(001) surface

Reaction	ΔG (eV) T = 600 K; P_{gas} = 1 atm			
	M=La	M=Ba	M=Sr	M=Ca
$La_{1-x}MOCl \leftrightarrow La_{1-x}MOCl_{1-x} + \frac{1}{2} Cl_2$	3.55	-0.11	-0.15	-0.09
$La_{1-x}MOCl + CH_4 \leftrightarrow La_{1-x}MOCl_{1-x}\cdots H + CH_3Cl$	3.23	2.34	2.25	2.14

Next, we examined the activity of LaOCl (111) surface models for which the energy to form a Cl vacancy was found to be lower than the (001) surface by an earlier theoretical study{Chrétien, 2012 #17}. Our calculations also revealed that the reaction free energies for Cl vacancy formation and H adsorption on the (111) surface are 1.1 eV and 2.3 eV lower than that of the (001) surface, respectively. We further discovered that the co-adsorption of a Cl atom on a surface La and an H atom on its neighboring oxygen is highly favorable on the (111) surface and activation of CH_4 in the presence of HCl is energetically not favorable. The effect of p-doping on the (111) surface was then examined by replacing a surface La^{3+} by Ca^{2+}. Our calculations suggested that the effect of doping with lower valent cation on this surface is preferably compensated by reducing the neighboring oxygen (forming –OH) rather than forming a Cl vacancy. When a single Ca dopant is present on the surface, the calculated reaction free energies and activation barriers for CH_4 activation were found to be above 2 eV suggesting that the activity would still be low. Thus, we replaced two surface La atoms by Ca which corresponds to approximately 20% surface doping and examined the reaction mechanism.

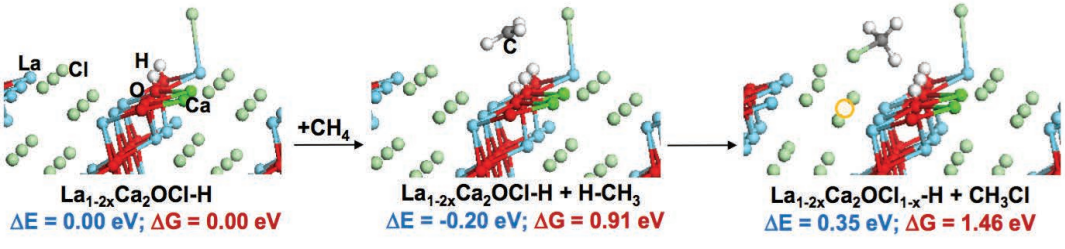

Figure 3. Relative energies (ΔE) and free energies (ΔG) calculated for CH_4 activation on Ca-doped LaOCl (111) surface model

The CH_4 activation mechanism (Figure 3) occurs via transferring an H atom to the free oxygen atom next to the Ca dopant (E^{act} = 0.41 eV) and the CH_3 radical reacts with the surface Cl to form CH_3Cl leaving a surface Cl vacancy (E^{act} = 0.83 eV). Dissociation of HCl can replenish the Cl vacancy and the surface H atoms can be removed through the proton conducting membrane. Although this pathway seems to be feasible, the complete catalytic cycle and a microkinetic analysis need to be performed to identify the activity of this material. This work is in progress.

Proton-conducting membrane material development

Selection of $BaZr_{0.1}Ce_{0.7}Y_{0.1}Yb_{0.1}O_{3-\delta}$ (BZCYYb) ceramic proton conductor. Following the discovery of high temperature proton conduction of the perovskite-type ceramics, proton-conducting ceramic membranes have received great attention due to their potential application in hydrogen separation and membrane reactors. The ceramic proton conductors typically have a ABO_3 perovskite-type structure, where A=Ba and B=Ce/Zr. Oxygen vacancy in the perovskite-type ceramic is generated through aliovalent doping on the B-site, as shown in the Kröger–Vink notation $2Ce^{X}_{Ce} + O^{X}_{O} + Y_2O_3 \rightarrow 2Y'_{Ce} + V^{\bullet\bullet}_{O} + 2CeO_2$ in an example of $BaCeO_3$ doped with Y_2O_3. If there is moisture present in the environment, then proton defects are formed through the equation $H_2O + V^{\bullet\bullet}_{O} + O^{X}_{O} \rightarrow 2OH^{\bullet}_{O}$. Proton conductivity is determined by the two major factors: proton defect concentration and mobility of the proton defects. Figure 4 shows the bulk proton conductivity of typical proton conductors of various oxides as a function of temperature. It can be seen that proton conductivity first increases with temperature due to increase in the mobility of proton defects, and then decreases with temperature due to reduced concentration of the proton defects. The highest bulk conductivity is found in $BaZrO_3$-based ceramic. However, $BaZrO_3$ has high grain boundary resistance. Therefore, the most-studied proton conductor is $BaCeO_3$-based ceramics.

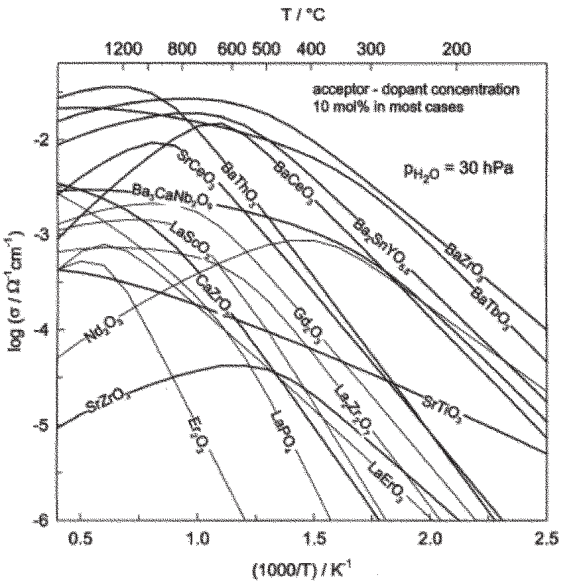

Figure 4. Bulk proton conductivity of different oxides as a function of temperature{Kreuer, 2003 #18}

Figure 5 shows the temperature dependence of ionic conductivity for some ionic conductors. It can be seen that $BaZr_{0.1}Ce_{0.7}Y_{0.1}Yb_{0.1}O_{3-\delta}$ (BZCYYb) shows relatively high proton conductivity at temperature below 600 ºC. Consequently, BZCYYb has been selected as the condidate membrane material for this study.

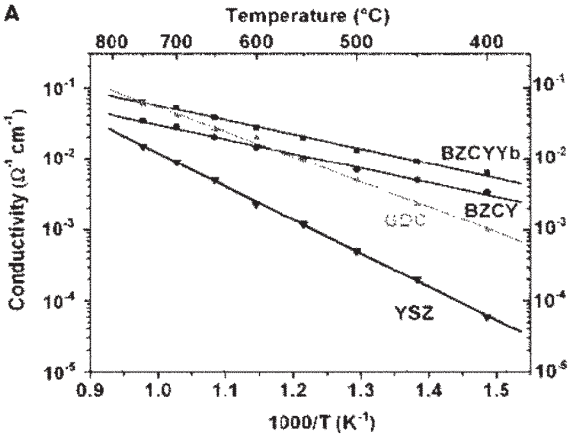

Figure 5. Ionic conductivity of some selected oxides as a function of temperature{Yang, 2009 #19}

Preparation of (BZCYYb) ceramic proton conductor. BZCYYb powders were synthesized by a sol-gel combustion method. $Ba(NO_3)_2$ (Alfa Aesar 99%), $Ce(NO_3)_3{\cdot}6H_2O$ (Alfa Aesar 99.5%), $ZrO(NO_3)_2{\cdot}xH_2O$ (Alfa Aesar 99.9%), $Y(NO_3)_3{\cdot}6H_2O$ (Alfa Aesar 99.9%), and $Yb(NO_3)_3{\cdot}6H_2O$ (Alfa Aesar 99.9%) were dissolved in distilled water and titrated by an ethylenediaminetetraacetic acid (EDTA) titrimetric method. Stoichiometric amounts of metal nitrate solution were mixed in a beaker and heated at 80 °C under stirring. EDTA and citric acid were added as complexation agents, with the molar ratio of EDTA/citric acid/total metal cations setting at 1:1.5:1. The pH value of the solution was adjusted by ammonia to around 8. Appropriate amount of ammonium nitrate was then added as a trigger for combustion. The solution was heated under stirring for 2 hours followed by heating in a microwave oven until automatic ignition to obtain a white ash. The ash was then calcined at 1100 °C for 5 h to obtain single phase BZCYYb powder. XRD result in Figure 6 shows that the obtained BZCYYb has pure perovskite structure.

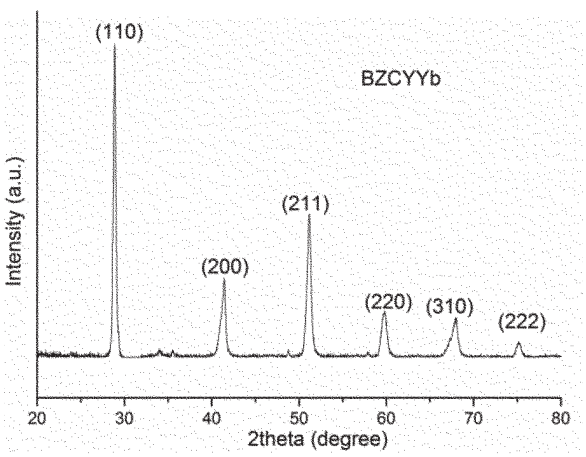

Figure 6. XRD result of the BZCYYb powders

Catalyst Development

Several different methods were screened for lanthanum oxychloride catalyst synthesis {Lee, 2001 #8;Peringer, 2008 #10;Podkolzin, 2005 #12} and the resulting materials were characterized to determine purity. Care was taken to exclude air during all syntheses, as CO_2 is known to react with oxides of lanthanum to form a carbonate species{Bakiz, 2010 #21}. The method that gave the most favorable results (no undesired carbonate in the final product, good O:Cl ratios, pure XRD patterns) was the solid-phase synthesis method{Lee, 2001 #8}. Equal molar ratios of lanthanum chloride heptahydrate and lanthanum oxide were reacted in a ball mill with ZrO_2 jars. The samples were then calcined at 500 °C under CO_2-free air. Using this method, lanthanum oxychloride samples were synthesized along with two alkaline earth metal-doped LaOCl samples (Calcium and Barium, 10 mol% doping).

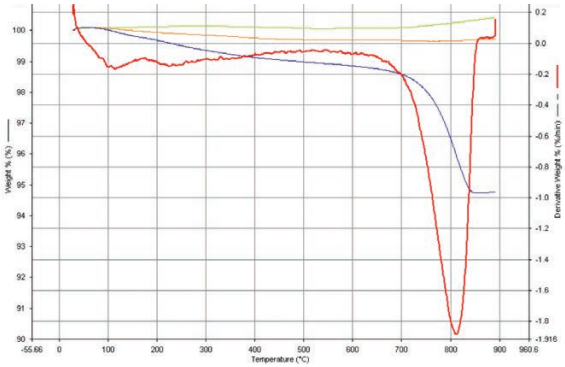

Figure 7. XRD result of the BZCYYb powders

Thermal Gravimetric Analysis (TGA) of the synthesized LaOCl catalysts shows thermal stability up to 900 °C for catalysts not containing the carbonate species. TGA/RGA (residual gas analysis) also provides a method for determining if the catalyst contains carbonate species as shown by the weight loss and CO_2 signal in Figure 7 below. The weight loss in the beginning is likely due to residual solvent from the synthesis whereas the significant weight loss at 700 °C (shown by the peak in the first derivative) is due to CO_2 loss from the carbonate. The carbonate species only occurs on samples that were prepared using a wet synthesis method. Since these samples were prepared in an inert atmosphere, the carbonate most likely occurs because of residual traces of organic solvent present in the pores of the material before calcining.

Calcium and Barium doped LaOCl in the amount of 10 mol % of Ca and Ba were synthesized by mechano-chemical and calcination methods. Figure 8 displays the TGA curves of Ca and Ba doped samples which display thermal stability up to 900 °C and no presence of carbonate species. This demonstrates their thermal suitability for the dimethyl ether (DME) synthetic strategy proposed and theoretical calculations predict a lower energy pathway for the mechanism of the reaction. Powder X- ray diffraction (XRD) patterns for the carbonate-free LaOCl, 10 mol. % Ca doped LaOCl, and 10 mol. % Ba doped LaOCl confirm that the crystalline lattice contains the tetragonal lattice structure with slightly different unit cell distances. Figure 9 below displays the XRD pattern for these materials. Rietveld refinement of the XRD patterns demonstrate a slight increase in the unit cell size as the atomic size of the dopant is increased from Ca to La to Ba. This is consistent with the replacement of La atoms with Ca and Ba within the lattice structure.

Figure 8. TGA data for the BaLaOCl (green), CaLaOCl (orange), and the carbonate containing LaOCl (blue)

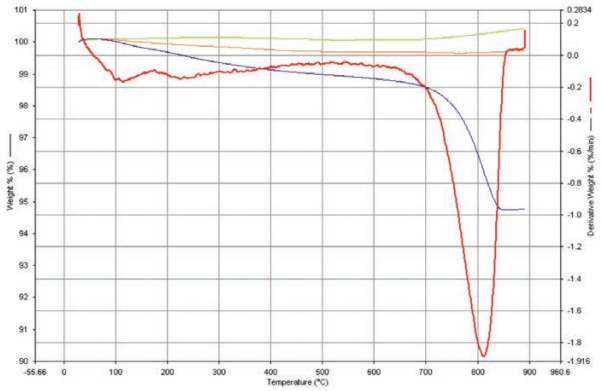

Figure 9. XRD patterns for LaOCl (blue), LaCaOCl (red), and LaBaOCl (black)

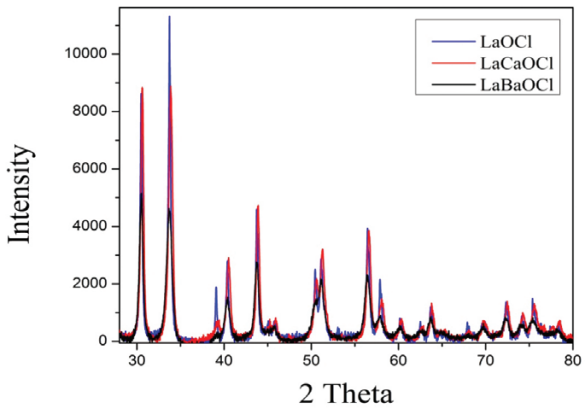

Catalyst and membrane characterization

X-ray photoelectron spectroscopy (XPS) studies were carried out on LaOCl, as well as doped $Ba_{0.1}La_{0.9}OCl$ and $Ca_{0.1}La_{0.9}OCl$ catalysts, prepared by the dry synthesis method. Data for the La(3d) region is shown in Figure 10. For all three samples, there is a doublet observed for the La($3d_{5/2}$) peaks around 833.6 eV and another doublet observed at 838 eV for the La($3d_{3/2}$) peaks. The La(LMM) Auger features also contribute to the background rise with increasing binding energy, and a distinct Auger peak is found at 865 eV. The splitting of the La(3d) peaks is typical of La^{+3} and attributed to final state effects.[1] In the case of the Ba-doped LaOCl, the shape of the La$(3d)_{5/2}$ peak is nearly identical to that of pure LaOCl. However, a shoulder appears for the La$(3d)_{5/2}$ peak for Ca-doped LaOCl, and this suggests that there is a greater electronic perturbation of the La^{+3} environment for the Ca-doped catalyst compared to the Ba- doped catalyst. XPS spectra were also collected for the O(1s) region (Figure 11). For all three catalysts, two oxygen species are observed at 528.5 eV and 531.2 eV. The lower binding energy peak is assigned to lattice oxygen,[2] whereas the higher binding energy peak is attributed to a CO_3^{-2} species, given that previous studies have shown that CO_2 reacts on the surface of LaOCl to form carbonates.[2,3] For the two doped catalysts, the surface concentration of the carbonate oxygen is comparable to lattice oxygen, but for pure LaOCl, the intensity from CO_3^{-2} is roughly half that of the lattice oxygen. Furthermore, the C(1s) spectra are consistent with the formation of surface carbonate, which has a binding energy of 289 eV;[3] according to the integrated C(1s) signals, the concentration of CO_3^{-2} is lower on LaOCl compared to the doped catalysts (Figure 12). Note that the large feature at 284.8 eV is assigned to adventitious carbon on the surface.

The next phase of this work will be to study the decomposition of methane on these three catalysts in order to understand if the doping of LaOCl promotes activity for C-H bond scission in methane. We anticipate that $Ca_{0.1}La_{0.9}OCl$ is more likely to have greater activity than $Ba_{0.1}La_{0.9}OCl$ and LaOCl because there is evidence of greater electronic perturbation with Ca doping. For this study, the catalysts will be initially heated in vacuum or in oxygen to remove the adventitious carbon species, and then exposed to methane at 800 °C. The concentration of carbon observed on the surface after methane decomposition will be investigated by XPS and used as measure of methane activity on the surface.

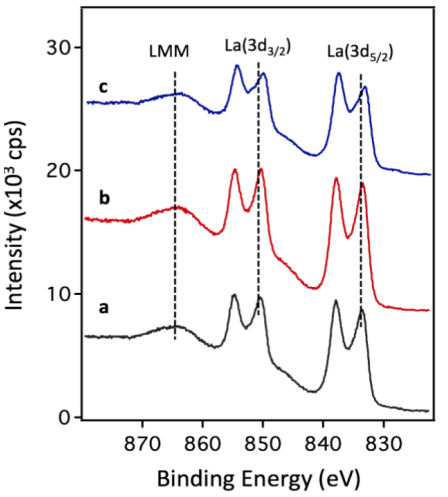

Figure 10. XPS data for the La(3d) region for: a) LaOCl; b) $Ba_{0.1}La_{0.9}OCl$; and c) $Ca_{0.1}La_{0.9}OCl$

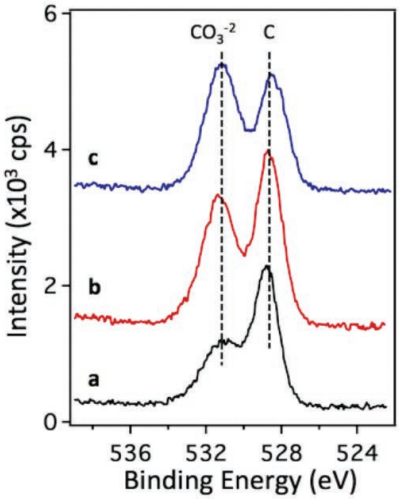

Figure 11. XPS data for the C(1s) region for: a) LaOCl; b) $Ba_{0.1}La_{0.9}OCl$; and c) $Ca_{0.1}La_{0.9}OCl$

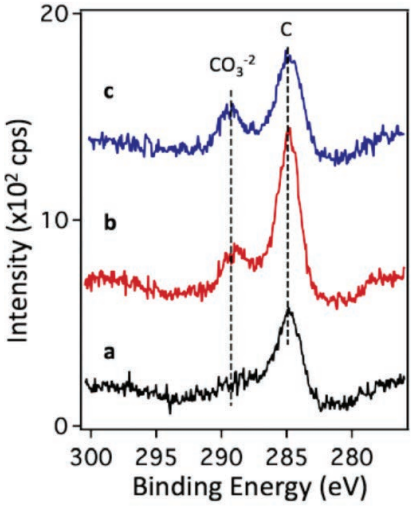

Figure 12. XPS data for the C(1s) region for: a) LaOCl; b) $Ba_{0.1}La_{0.9}OCl$; and c) $Ca_{0.1}La_{0.9}OCl$

FY2016 ACCOMPLISHMENTS

- **Performed theoretical calculations to determine candidates for catalytic materials**
- **Selected and synthesized materials for the electrolyte, cathode, and anode of the proton-conducting membrane**
- **Developed methods to synthesize pure and doped catalyst powders**
- **Characterized a range of catalyst samples to verify purity and gain chemical information**

FUTURE DIRECTIONS

- Test pure and doped catalyst samples for oxidative chlorination of methane{Podkolzin, 2007 #1}
- Test compatibility of membrane materials with pure and doped LaOCl catalysts
- Test stability of membrane materials under desired reaction conditions
- Begin assembly of membrane reactor
- Catalyst testing and performance evaluation

References

1. **O'Reilly, D.J., D.L. Foshee, and M.W. Nichols, "**Prudent Development: Realizing the Potential of North America's Abundant Natural Gas and Oil Resources," D.o. Energy, Editor. 2011, National Petroleum Council: Washington, D.C.
2. **McFarland, E.W.,** "Unconventional Chemistry for Unconventional Natural Gas," Science, 2012. **338**(6105): p. 340-342.
3. **Xu, Y., X. Bao, and L. Lin, "**Direct Conversion of Methane Under Nonoxidative Conditions," Journal of Catalysis, 2003. **216**(1–2): p. 386-395.
4. **Szybist, J.P., S. McLaughlin, and S. Iyer, "**Emissions and Performance Benchmarking of a Prototype Dimethyl Ether-Fueled Heavy-Duty Truck," D.o. Energy, Editor. 2014, Oak Ridge National Laboratory: Oak Ridge, TN.
5. **Peringer, E., et al., "**Modified Lanthanum Catalysts for Oxidative Chlorination of Methane," Topics in Catalysis, 2009. **52** (9): p. 1220-1231.
6. **Peringer, E., et al., "**On the synthesis of LaCl3 Catalysts For Oxidative Chlorination of Methane," Applied Catalysis A: General, 2008. **350**(2): p. 178-185.
7. **Podkolzin, S.G., et al., "**Methyl Chloride Production from Methane over Lanthanum-Based Catalysts," Journal of the American Chemical Society, 2007. **129**(9): p. 2569-2576.
8. **Khaleel, A., I. Shehadi, and A. Al-Marzouqi, "**Catalytic Conversion of Chloromethane to Methanol and Dimethyl Ether Over Mesoporous Y-alumina," Fuel Processing Technology, 2011. 92(9): p. 1783-1789.
9. **Chrétien, S. and H. Metiu, "**DFT Study of the Electronic Properties of LaOCl Surfaces," The Journal of Physical Chemistry C, 2012. **116**(1): p. 681-691.
10. **Kreuer, K.D., "**Proton-Conducting Oxides," Annual Review of Materials Research, 2003. **33**(1): p. 333- 359.
11. **Yang, L., et al., "**Enhanced Sulfur and Coking Tolerance of a Mixed Ion Conductor for SOFCs: BaZr0.1Ce0.7Y0.2–xYbxO3-δ," Science, 2009. **326:** p. 126-129.
12. **Lee, J., Q. Zhang, and F. Saito, "**Mechanochemical Synthesis of LaOX (X=Cl, Br) and Their Solid State Solutions," Journal \ of Solid State Chemistry, 2001. **160**(2): p. 469-473.
13. **Podkolzin, S.G., O.V. Manoilova, and B.M. Weckhuysen, "**Relative Activity of La2O3, LaOCl, and LaCl3 in Reaction with CCl4 Studied with Infrared Spectroscopy and Density Functional Theory Calculations," The Journal of Physical Chemistry B, 2005. **109**(23): p. 11634-11642.
14. **Bakiz, B., et al., "**Carbonatation and Decarbonatation Kinetics in the La2O3-La2O2CO3 System under CO2 Gas Flows.," Advances in Materials Science and Engineering, 2010. **2010:** p. 6.
15. **Deasha, A. M.; Nix, R. M.** "Oxidation of Lanthanum Overlayers on Cu(111)," Surface Science 1995 322, 41-50.
16. **Wei, Z. X.; Wang, Y.; Zhang, X. J.; Hu, C. W.** "Combustion Synthesis and Effect of LaMnO3 and LaOCl Powder Mixture on Hmx Thermal Decomposition," Thermochimica Acta 2010 499, 111-116.
17. **Marsal, A.; Rossinyol, E.; Bimbela, F.; Tellez, C.; Coronas, J.; Cornet, A.; Morante, J. R.** "Characterisation of LaOCl Sensing Materials Using CO2-TPD, XRD, TEM and XPS," Sensors and Actuators B-Chemical 2005 109, 38-43.

Acronyms

BZCYYb	Barium Zirconium Cerium Yttrium Ytterbium Oxide
BZY	Barium Zirconium Yttrium Oxide
CH3Cl	Chloromethane
CH4	Methane
DME	Dimethyl Ether (CH3OCH3)
EDTA	Ethylenediaminetetraacetic Acid
LaOCl	Lanthanum Oxychloride
LDRD	Laboratory Directed Research and Development RGA – Residual Gas Analysis
SRNL	Savannah River National Laboratory
TGA	Thermogravimetric Analysis
USC	University of South Carolina, Columbia
XRD	X-Ray Diffraction

Total Number of Post-Doctoral Researchers

1

Develop High Activity, Low Cost Non-PGM Fuel Cell Electrocatalyst and Stable Supports

Project Team: H.R. Colón-Mercado, M.C. Elvington, B. L. Garcia-Diaz, J.B. Gaillard
Subcontractor: Savannah River Consulting, LLC
Project Type: Standard
Project Start Date: October 1, 2015
Project End Date: September 30, 2017

A unique approach has been developed to probe the non-PGM catalyst active site for the Oxygen Reduction Reaction (ORR) for PEMFC. Iron based functionalities have been engineered into Metallic Organic Framework (MOF) catalysts to evaluate their impact on activity for the ORR. A series of FePhen@MOF catalysts have been synthesized with varying [Fe] to investigate the effect on electrochemical and electrocatalytic properties. The magnitude of the $Fe^{II/III}$ redox couple and the electrochemical surface area are analyzed to determine if there is a correlation between [Fe] and the ORR onset potential and/or the relative number of active sites.

FY2016 OBJECTIVES

- Synthesize a series of FePhen@MOF catalysts
- Physical characterization (bulk composition, surface composition)
- Electrochemical characterization (CV, RRDE)

INTRODUCTION

Worldwide efforts to produce durable, highly active non-PGM electrocatalysts have resulted in slow, incremental improvements in activity as well as a partial understanding of the catalytically active site. To achieve a breakthrough in activity, a more complete understanding of the nature of the non-PGM ORR active site is needed. The composition of the active site is currently under debate, which has received heightened attention recently. In particular, the role of iron and/or Fe-N_4 complexes have in catalyzing the ORR is central to the debate. Most evidence suggests either iron has a direct role in the ORR catalysis or it influences the formation of the active site. This work focuses on developing a better understanding of the role iron has in the ORR.

A series of FePhen@MOF catalysts have been synthesized with varying [Fe] to investigate the impact, if any, on the electrochemical and electrocatalytic properties. The FePhen@MOF catalyst type was chosen for this work because it has excellent activity for the ORR and is easily synthesized with varying iron content. Elemental and surface analysis of the FePhen@MOF catalysts shows the incorporation of iron in a targeted and controlled manner. In conjunction with the electrochemical results, insight into the nature of the ORR active site and the role iron plays can be gained. This work has the potential to impact future catalyst development by improving the active site knowledge base.

APPROACH

FePhen@MOF catalysts consist of a MOF that is formed of the ZIF-8 type with Fe and phen (phen=1,10-phenanthroline) in situ, resulting in encapsulation of FePhen complexes. ZIF-8 is a zeolitic imidazole framework (ZIF) synthesized from 2-methylimidzaole and zinc(II) nitrate, has a cage structure with the SOD net with a cage diameter of 11.6 Å, which is of sufficient size to encapsulate Fe(phen)2 complexes. The initial encapsulated FePhen@MOF is formed at room temperature followed by two high temperature heat treatments, first under argon for 1 hour at 1050 °C, and the second under ammonia for 30 min. at 900 °C, resulting in the catalytically active material.

RESULTS / DISCUSSION

Elemental analysis, including inductively couple plasma atomic emission spectroscopy (ICP-AES) and CHN analysis, show iron incorporation in the FePhen@MOF catalysts in a predictable and controlled manner.

Electrochemical investigations, including cyclic voltammetry (CV) and rotating ring disk electrode (RRDE), show several trends relative to [Fe]. First, increasing iron content, resulted in decreasing electrochemical surface area, likely due to increased carbon degradation caused by the iron content during the heat treatments. Second, the redox couple at ~650 mV vs. RHE, suspected to be the $Fe^{II/III}$ couple, increases in magnitude with increasing iron content, with one exception. The Fe(5)Phen@MOF catalyst initially shows a significant redox couple at the same potential but rapidly degrades upon potential cycling. Most importantly are the findings relating iron content with the ORR data. As indicated by the Fe(0)Phen@MOF catalyst, no iron results in poor onset potential for the ORR, confirming the original hypothesis that either iron has a direct role in the ORR catalysis or it influences the formation of the active site. The series of catalysts that include Fe(0.1)Phen@MOF, Fe(0.5)Phen@MOF, and Fe(1)Phen@MOF, indicate that a certain amount or iron is needed to form the optimal catalyst material, but once this minimum amount is reached, additional iron does not further increase the onset potential or number of active sites. This is evident comparing the Fe(0.5)Phen@MOF and Fe(1)Phen@MOF catalysts which show approximately the same onset potential and number of active sites. This may indicate that iron does not have a direct role in catalyzing the ORR, that instead, it only influences the formation of the active site, and that only a minimum amount is needed for this purpose. Another possibility is that only some of the iron is incorporated into active sites that have a direct role in the ORR catalysis and that excess iron does not contribute to additional active site formation. The electrochemical results for the Fe(5)Phen@MOF material suggests that not only does excess iron not contribute to the formation of additional active sites, it has a detrimental effect, resulting in poor electrochemical surface area (ESA) and poor activity, due to the formation of unstable surface species that rapidly degrade upon potential cycling.

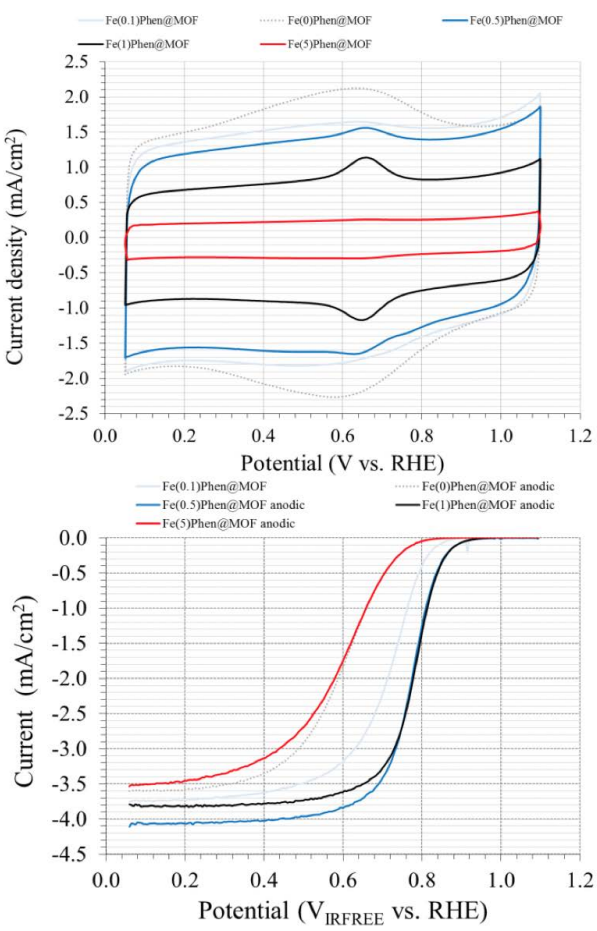

Figure 1. Cyclic Voltammetry (top) and RRDE (bottom) for a series of FePhen@MOF catalysts showing the effect of varying Fe content.

FY2016 ACCOMPLISHMENTS

Synthesized a series of FePhen@MOF catalysts with varying [Fe]

Physical characterization (bulk composition, surface composition) of MOF catalysts consisting of ICP-AES and CHN analysis. Bulk compositions for iron content range from 0.03 % to 11.00 % while nitrogen content ranges from 6.92 % to 1.96 %

Electrochemical characterization (CV, RRDE) of FePhen@MOF series of ORR electrocatalysts. Fe(0.5)Phen@MOF and Fe(1)Phen@MOF match state-of-the-art activity performance

FUTURE DIRECTIONS

- Continue the development of non-PGM catalysts, using SRNL's unique approach
- Finalize publication focusing on the iron effects on non-PGM ORR activity
- Apply for funding opportunity announcements from DOE-EERE

FY 2016 Publications/Presentations

1. **M.C. Elvington, H.R. Colon-Mercado,** "Fe redox couple in ZIF-8 based non-PGM electrocatalyst and its relation to ORR", article under preparation.
2. **M.C. Elvington, H.R. Colon-Mercado,** "Fuel Cell Catalyst Concepts", internal presentation to FCTO, DOE-EERE managers, July 2016.

Acronyms

CHN	Carbon Hydrogen Nitrogen
CV	Cyclic Voltammetery
ESA	Electrochemical Surface Area
ICP-AES	Inductively Couple Plasma Atomic Emission Spectroscopy
MOF	Metallic Organic Framework
NET	Three Letter Zeolite Network Code
non-PGM	Non Platinum Group Metal
ORR	Oxygen Reduction reaction
PEMFC	Proton Exchange Membrane Fuel Cell
Phen	1,10-phenanthroline
RHE	Reversible Hydrogen Electrode
RRDE	Rotating Ring Disc Electrode
ZIF	Zeolitic Imidazole Framework

Intellectual Property

Invention disclosure initiated

Post-Doctoral Researchers

Dr. Mark C. Elvington, Savannah River Consulting, LLC

On-Line Underground Cable Diagnostic System

Project Team: K. W. Burkes (Primary), R. B. Barnett
Project Type: Standard
Project Start Date: October 1, 2015
Project End Date: September 30, 2017

The health of the nation's underground distribution cable network is widely unknown throughout the utility system. Typically, utility companies have policies which state that if a cable fails they can splice the failed location up to three times and then must remove the cable. The problem is this is done after the cable has caused a fault and has been de-energized. This on-line diagnostic system can detect and monitor the degradation of the insulation in underground cables before they fail and allow for better asset management for the utility industry. FY 16, we proved that performing TDR on branching cables is possible through using the leading and lagging cable reference platform to identify termination reflections.

FY2016 OBJECTIVES

- Perform Electromagnetic Transient Simulation
- Perform Multiphysics Simulation
- Test Branching Cables Experimentally With Real Cable
- Compare Electromagnetic Transient Simulation, Multiphysics simulation, and experimental results of monitoring branching cables

INTRODUCTION

The increasing practice of underground residential distribution (URD) cables being installed in the power system requires utility companies to know the health of these cables. Since the health of URD cables cannot be determined by visual methods like overhead lines, a better understanding of the power cable and its aging process is needed. Insulation of medium voltage URD power cables age from a phenomenon called water treeing Figure 1. Water trees are important to utility companies because they cannot be detected using traditional protection methods. Also, they can be growing in cables without any effect on the voltage or current. They are the main reason for URD cable failures. These water trees can grow across the insulation and not cause the cable to fault [1]. Also, they do not produce partial discharge [2], a common cable diagnostic tool. Because of these two facts detecting them becomes very difficult and expensive.

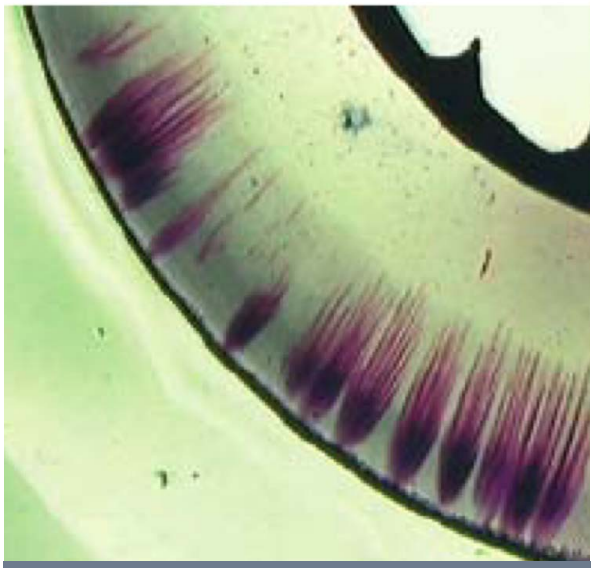

Figure 1. Water trees growing from the outside of cable [3]

Time Domain Reflectometry (TDR) is a traveling wave based method to determine whether water trees are present within the cable. TDR can be performed off-line or on-line. When a traveling wave is sent down a cable, it will have a reflection when it reaches the end of the cable or an element with different impedance. This can be used to locate water trees in a cable since the water treed region will change the impedance in that section. An early reflection may indicate water trees in the cable [3].

In this project work was done to better understand how TDR voltage pulses travel through the insulation of an underground cable, and what affect a water treed region has on the reflection of that pulse. Also, a platform for distinguishing between branching cables' reflection pulses was developed. This information is vital for developing the hardware needed to autonomously monitor a distribution network's health.

APPROACH

Two different software were used to simulate the branching cable network and also a water tree located within the cables. An electromagnetic transient software PSCAD was compared to a finite element analysis software COMSOL. When a water tree is represented the electric permittivity is change and is modeled in [4].

The Leading/Lagging Cable Referencing Platform is a unique method for monitoring the insulation degradation of underground cables within a distribution network. The system takes advantage of the well-known concept of traveling wave theory, where an injected pulse will travel through a medium at a specific speed until reaching a mismatch in properties, at which a reflection occurs. Traditional systems inject a pulse into a network and record a reference response. Any deviation from the reference response indicates a change in network health. However, due to the topology of the network determining the location of the change in network health is very difficult. This platform now does this by using branching cables within the network as reference signals for each other to isolate any changes in insulation health; by utilizing a leading or lagging reflection pulse, the change in insulation health can be pinpointed to a specific cable. The leading or lagging reflection is utilized because of the configuration with which cables are connected to a bus. When a reflection pulse returns to the beginning of a cable, it is transmitted into all of the cables connected at that bus. This is what normally causes difficulty in traditional methods, but because each cables' sending ends are being monitored and the injected pulse is very fast. There is a time delay between when the reflection is measured in the corresponding cable and in the other cables connected at the bus. Therefore, when looking at all the measured signals at a single bus, the cable's signal with a measured reflection which is leading the others, is the cable which created the reflection. The signals which are lagging are understood to not be related to the cable of interest.

RESULTS / DISCUSSION

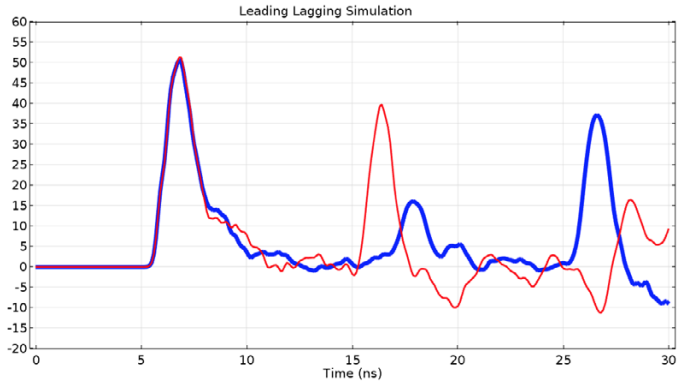

Figure 2. COMSOL simulation of branching cables

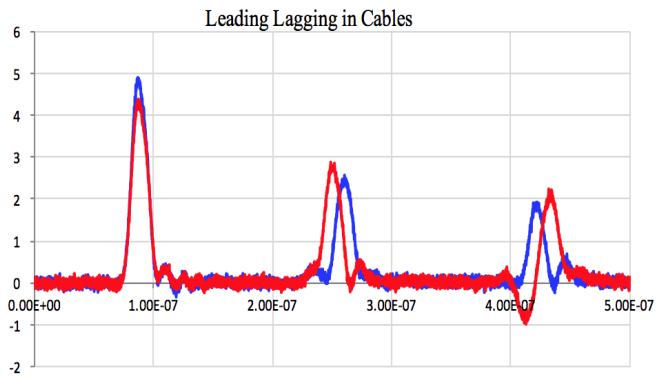

Figure 3. Experimental setup of branching cables

An example of Leading/Lagging behavior is shown in Figure 2 and Figure 3. Figure 2 is a Multiphysics simulation of the experimental setup, and Figure 3 is this concept shown in real cables. The first measured pulse is the injected pulse on the cables, which is seen at arriving at the same time from another cable. This pulse is similar in magnitude because of the similar construction and connection of cables. The first set of reflection pulses show a clear time delay between the moments when they were measured. The red pulse is leading the blue pulse, indicating that the first reflection pulse is from the termination of the cable measured by the red signal. The second set of reflection pulses also show the same amount of time delay due to the distance between the measurement points doesn't change. This time the blue pulse is leading the red pulse, indicating that the final set of reflections is due to the termination of the cable measured by the blue signal.

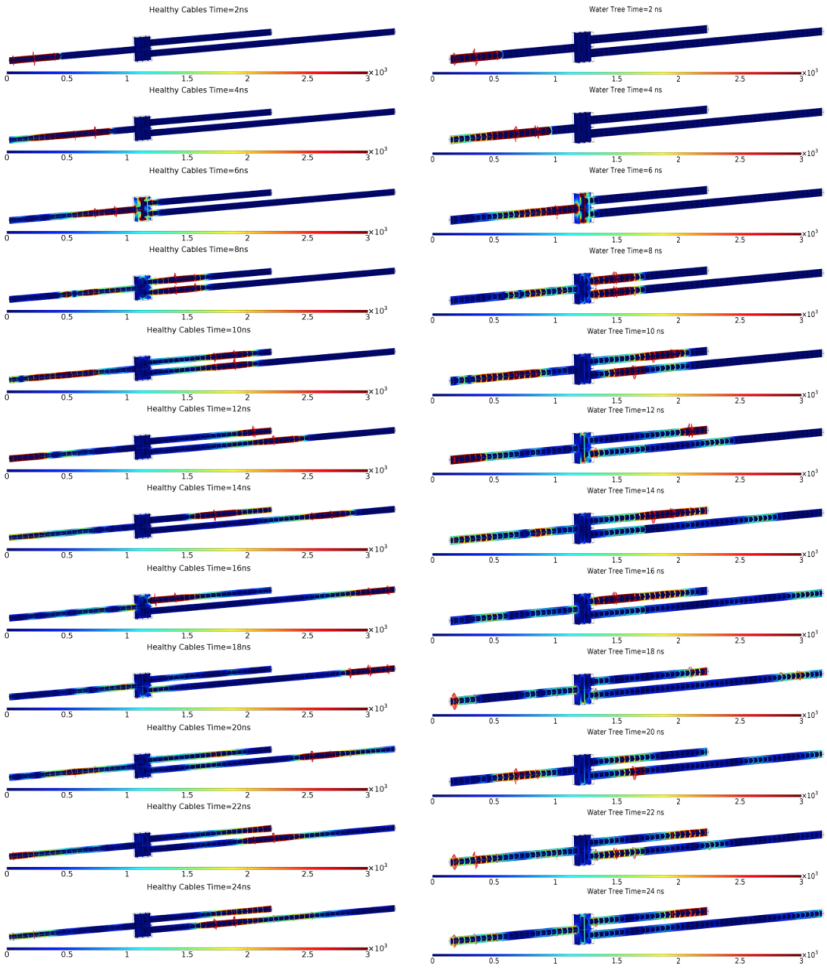

Figure 4. COMSOL simulation of branching network without and with a water tree

When a water tree is located inside a cable a reflection is produced due to the change in impedance at that location. This is visually shown in Figure 4. The electric field traveling through the two simulations is the same until it reaches the water tree in the longer branching cable at a quarter of the length. This occurs between 8 and 10 nanoseconds. At this point it can be seen that most of the energy is reflected back and a small amount passes through.

FY2016 ACCOMPLISHMENTS

Current technology can determine that degradation is located in a cable, but cannot isolate it without having a person testing both cables. The developed Leading/Lagging Cable Referencing Platform is different than current methods, and it will allow for a standalone, autonomous system to be able to monitor all cable in a distribution network without human involvement. We accomplished:

- **Validated water tree models in COMSOL & PSCAD in a single cable**
- **Developed accurate Multiphysics models of underground cables**
- **Compared experimental TDR in Coaxial Cables with the COMSOL Simulations**
- **Created the Leading/Lagging Cable Reference Platform to distinguish return reflections measured in different branching cable, allowing for the development for an on-line cable network to be monitored in a standalone mode**

FUTURE DIRECTIONS

- FY2017 work is funded to develop a specialized pulse generator and sensor, which connects onto the capacitive test point of a standard cable elbow. It will produce an exponential voltage pulse, large enough to generate reflections from insulation degradation. The pulse generator will produce a mono-polarity pulse with a pulse width less than 20 nanoseconds, and the circuit will be coupled with a high speed sensor for monitoring at the location of the pulse. A test network will be developed and tested here at SRNL de-energized, and then it will be tested at the Duke Energy Electrical Grid Research Innovation and Development (eGRID) center by energizing it to electric distribution voltage/current levels to perform on-line monitoring. Finally, the effect on the power quality will be analyzed due to the injection of high speed pulses into the cable to perform the monitoring of the cable's insulation health.

Publications/Presentations

K. Burkes, "Time Domain Reflectometry of a Water Tree inside an Underground Cable," in COMSOL Conference, Boston, 2016.

References

1. **W. A. Thue,** "Treeing," in Electric Power Cable Engineering, Boca Ranton, FL, Taylor & Rancis Group, 2012, pp. 367-384.
2. **J. Densley,** "Ageing mechanisms and diagnostics for power cables—an overview," IEEE Electrical Insulation Mag. vol. 17, pp. 14-22, Jan/Feb 2001.
3. **V. Dubickas,** On-Line time domain reflectometry diagnostic of medium voltage XPE power cables, Stockholm, Sweeden: Royal Institute of Technology, 2006.
4. **K. Burkes,** "Time Domain Reflectometry of a Water Tree inside an Underground Cable," in COMSOL Conference, Boston, 2016.

Intellectual Property

Invention Disclosure titled "Leading/Lagging Cable Referencing Platform for Monitoring the Health of Underground Cable Networks"

Metal Hydride Thermal Energy Storage Material Development for Dish-Stirling and other Thermal Storage Applications

Project Team: Theodore Motyka, Ragaiy Zidan, Patrick Ward
Project Type: Standard
Project Start Date: October 1, 2015
Project End Date: September 30, 2017

The development of low-cost, renewable, continuous power concentrated solar power (CSP) plant relies heavily on the development of a suitable thermal energy storage (TES) system. Metal hydrides have the advantage of providing high energy densities and a low cost TES system if an appropriate hydride material is selected. This work aims at developing Ca_xSi_y and Ca_xAl_y materials as low-cost high temperature metal hydrides for thermal energy storage. Previous work has shown that these metal hydrides can approach DOE cost targets. The suitability of $CaAl_2$ as a high temperature metal hydride has been demonstrated as well as methods for enhancing the thermal conductivity of these materials. Custom reaction vessels were also developed which outperform commercial vessels.

FY2016 OBJECTIVES

- Synthesis and characterization of high temperature metal hydride materials
- Material modification and enhancement
- Cycle and performance testing
- Develop methods for scaling up the material to multi-gram or kilogram quantities
- Preliminary evaluation of alternative TES materials

INTRODUCTION

The development of renewable energy technologies to replace existing fossil fuel power plants has been of increasing interest over the last few decades due to the realization of global warming and fossil fuel depletion. Since sunlight is the largest carbon-neutral energy source available on Earth, its utilization to generate electricity on a large scale is key in the realization of fossil fuel replacement. While photovoltaics play a large role in the harnessing of solar power, these devices are limited to the utilization of the visible and UV portion of the solar spectrum and require expensive battery banks for the storage of electricity for night time use. On the other hand, concentrated solar thermal power (CSP) plants are designed to absorb > 90 % of the solar irradiance spectrum and have the capability of producing power continuously with the incorporation of a suitable thermal energy storage (TES) system. CSP power plants utilize focused solar irradiance to generate large amounts of heat which can be used to generate electricity by conventional turbine engine based methods. Unfortunately, the solar irradiance is not always available and, in order to maintain electricity generation, a method for storing large amounts of heat is required.

Three of the major areas for TES system improvements are in lowering their costs, reducing their full charging time to less than 6 hours and increasing their temperature of operation to improve the CSP overall production efficiency. Metal hydride TES systems have the ability to enable all of these improvements. In addition, many of the high and even the new lower temperature metal hydrides are fairly inexpensive. Preliminary calculations indicate that existing metal hydride TES systems can approach $15-$25/kWh. [1] Only 3-4 kg of material would be needed per kWh. Because of their very high thermal capacity (approximately 20 times that of current systems), the size of the overall TES system can be substantially reduced leading to additional capital cost savings. Metal hydride TES systems can also be made to be self-regulating, thereby simplifying their design and lowering not only their capital but their operating costs as well. Because of their high energy capacity and reasonable kinetics many metal hydride systems can be charged rapidly. This coupled with high heat of reaction allows metal hydride TES systems to produce very high thermal power rates (approx. 1kW per 6-8 kg of material). Our group extensively researched the use of metal hydride thermal energy storage systems [2-5] and has been successful in developing the highest temperature low-cost metal hydride for TES applications.

APPROACH

The enthalpy of CaH_2 is -181.5 kJ/mol, which demonstrates a promising potential for thermal energy storage. Unfortunately the equilibrium pressures of CaH_2 are quite low (~ 1 bar) even at very high temperatures (750 °C). Furthermore, CaH_2 is highly corrosive in the molten state which creates significant challenges and increased cost in the construction of containment vessels for this material. In this work, we utilize additives which alloy with the Ca after dehydrogenation to alter the thermodynamic properties of the material and prevent corrosion. The addition of Si or Al to the material results in the formation of Ca_xSi_y and Ca_xAl_y alloys upon dehydrogenation.

Figure 1. Example of a Sterling engine CSP dish system

RESULTS / DISCUSSION

In order to study the isothermal absorption of Ca_xSi_y materials at 750 °C, commercial reaction vessels were purchased and found to develop small leaks after several uses. Therefore, two custom reaction vessels were developed to circumvent the limitations of commercially available vessels. (Figure 2) Ca_2Si was scaled up to multi-gram quantities (>50g) with the use of an attiritor mill. In this process CaH_2 and Si were milled in the desired stoichiometric amounts and annealed at 600 °C under vacuum. Isothermal absorption of this material demonstrated 1.4 wt. % H_2 uptake at 750 °C starting at 14.2 bar in less than 15 minutes as shown in Figure 3. The sample temperature profile of the absorption, shown in Figure 4, suggests that this is a multi-step absorption process with at least 3 steps which requires further study to determine the exact mechanism.

$CaAl_2$ was also investigated and demonstrated excellent reversibility and reasonable hydrogen uptake at lower pressures (20.5 bar) and 600 °C. Figure 5 (following page) shows the XRD pattern of the $CaAl_2$ material in the dehydrogenated and hydrogenated state. Upon dehydrogenation of the $CaAl_2$ material, a pure phase of $CaAl_2$ is regenerated. Upon full hydrogenation (92 bar at 600 °C) the material completely converts to CaH_2 and Al. When the material is cycled at 20.5 bar H_2 and 600 °C a cycling capacity of ~1.2 wt. % can be achieved in 30 minutes. Figure 6 (following page) shows a slight increase in capacity after cycling from 1.1 wt. % to 1.3 wt. % over 14 cycles. This is commonly observed with many complex metal hydrides and is likely due to the material reaching a “steady state” in which the particles equilibrate in their respective positions to each other. The temperature profile for the cycling of the material demonstrates significant temperature increases and decreases over the cycling of the material. Modification of the Ca_2Si material with the incorporation of 3 mol. % $TiCl_3$ and 5 wt. % Al led to an increased overall capacity of 2.2 wt. % H_2 as shown in Figure 7 (following page.)

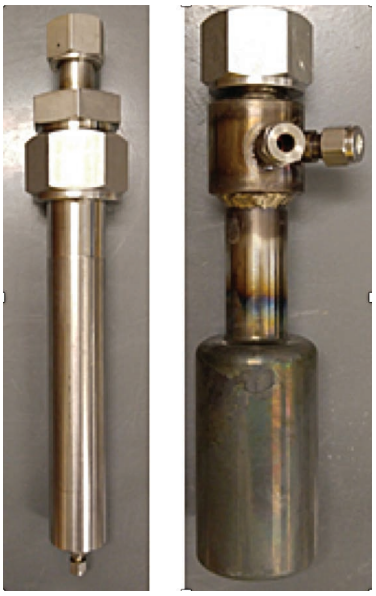

Figure 2. Custom designed reaction vessels for operation at 800 °C and 100 bar H_2 (made of Haynes 230 alloy and Inconel 625)

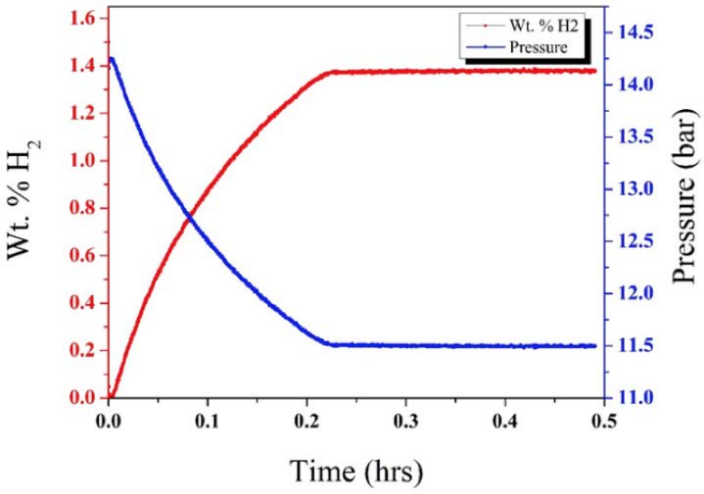

Figure 3. Isothermal absorption of Ca_2Si at 750 °C and starting at 14.2 bar H_2

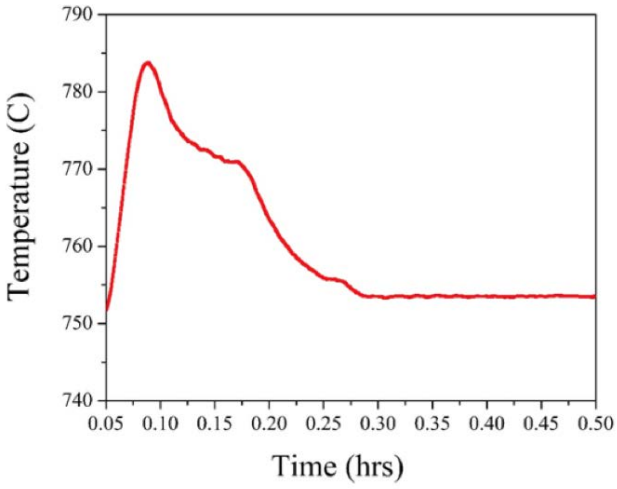

Figure 4. Sample temperature profile of Ca_2Si during absorption process

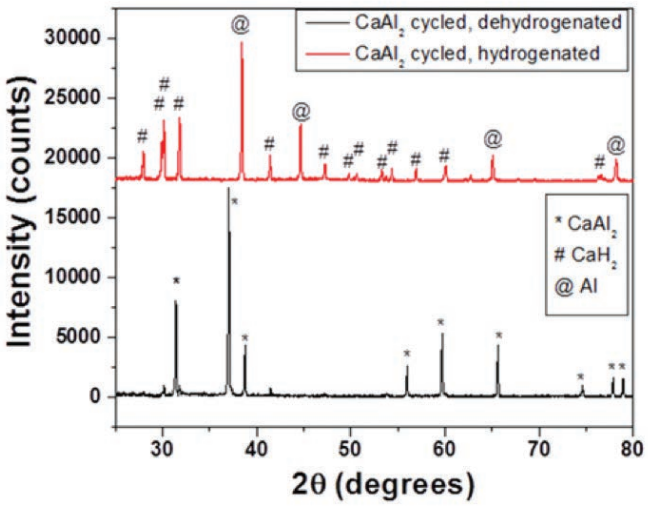

Figure 5. XRD diffraction pattern of the hydrogenated and dehydrogenated $CaAl_2$

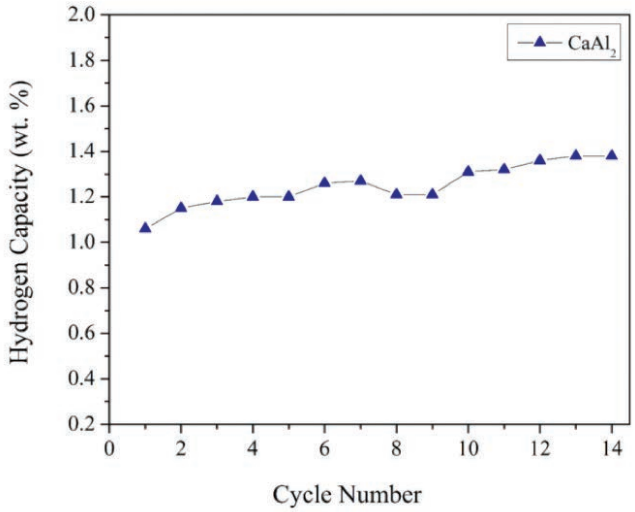

Figure 6. Hydrogen capacity of $CaAl_2$ over 14 cycles

Enhancement of the thermal conductivity of the Ca_xSi_y materials was carried out by the incorporation of expanded natural graphite (ENG). Laser flash thermal conductivity measurements were carried out at Clemson University and required innovative sample preparation techniques to introduce a sensitive materials into the instrument. In order to conduct the measurements, the sample pellets were gold sputtered (40 nm) and graphite coated. The gold layer prevented oxidation of the sample while the graphite layer reduced the reflection of the surface to allow for accurate measurements. It was determined that the ENG addition significantly increase the thermal conductivity of the Ca_2Si material by nearly an order of magnitude (0.35 W/mK at 200 °C without ENG) with the addition of 20 wt. %. Figure 8 displays the thermal conductivity at temperatures up to 750 °C. The discrepancies between the heat up and cool down measurements are believed to be due to sintering of the material at high temperatures. Further measurements on preheated samples are required to confirm this hypothesis.

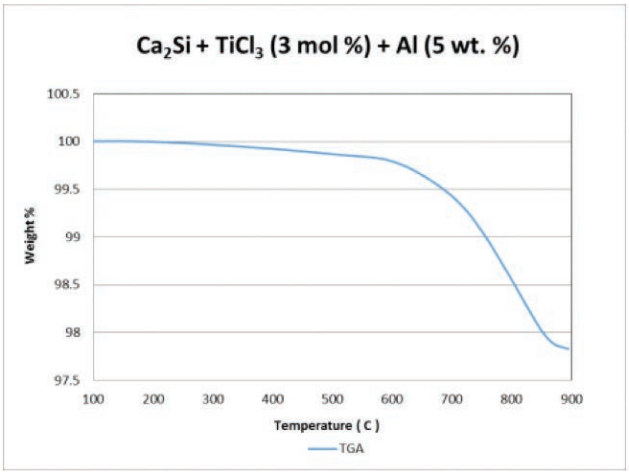

Figure 7. TGA of hydrogenated Ca_2Si with added $TiCl_3$ and Al

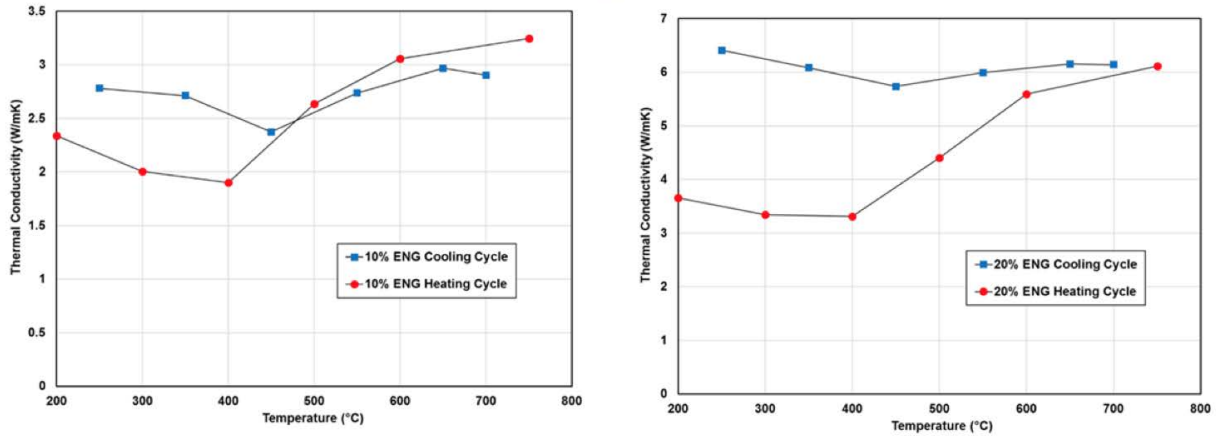

Figure 8. Thermal conductivity of Ca_2Si with 10 wt. % ENG (left) and 20 wt. % ENG (right)

FY2016 ACCOMPLISHMENTS

Successfully demonstrated 2.2 wt. % H_2 uptake in the modified Ca_2Si material via TGA

Successfully demonstrated scale up of the Ca_2Si material to multi-gram quantities (> 50 grams) with no foreseen issues of approaching 500g or acquiring larger equipment for further scale up

Demonstrated the feasibility of using $CaAl_2$ as a highly reversible stable TES material for operation at 600 °C

Demonstrated a significant enhancement in the thermal conductivity of Ca_2Si with the incorporation of ENG

FUTURE DIRECTIONS

- Development of catalyst for the Ca_xSi_y system to increase hydrogen capacity improve desorption kinetics
- Determine long term stability of thermal conductivity enhancers and catalysts
- Conduct spectroscopy studies to determine the underlying mechanism of the storage
- Demonstrate methodology to scale up materials with enhancer and catalysts in a low cost manner
- Demonstrate material operation at temperature required for steam methane reformation

References

1. **C. Corgnale, B. Hardy, T. Motyka, R.Zidan, J. Teprovich, B. Peters,** "Screening Analysis of Metal Hydride Based Thermal Energy Storage Systems for Concentrating Solar Power Plants," Renewable & Sustainable Energy Reviews, 2014,38,821-833.
2. **P. Ward, C. Corgnale, J. Teprovich, B. Hardy, T. Motyka, B. Peters, R.Zidan** "High performance metal hydride material based thermal energy storage systems for concentrating solar power plants" Journal of Alloys and Compounds, 645(1),2015,S374-S378.
3. **Ward, P.A., Corgnale, C., Teprovich, J. A., Moytka, T., Hardy, B., Sheppard, D., Buckely, C., Zidan, R.** Technical challenges and future direction for high efficiency metal hydride thermal energy storage systems. Appl. Phys. A, 2016, 122, 462.
4. **D. A. Sheppard, M. Paskevicius, T. D. Humphries, M. Felderhoff, G. Capurso, J. Bellosta von Colbe, M. Dornheim, T. Klassen, P. A. Ward, J. A. Teprovich Jr., C. Corgnale, R. Zidan, D. M. Grant, C. E. Buckley.** Metal hydrides for concentrating solar power energy storage. Appl. Phys. A, 2016, 122, 395.
5. **C. Corgnale, B. Hardy, T. Motyka, R. Zidan.** Metal hydride based thermal energy storage system requirements for high performance concentrating solar power plants. Int J Hydrogen Energy, 2016, in press.

Acronyms

TES	Thermal Energy Storage
CSP	Concentrated Solar Power
ENG	Expanded Natural Graphite

Intellectual Property

R. Zidan, "Storing High Exergetic Thermal Energy Based on Reversible Alloying and High Enthalpy Hydrides", July 14, 2014, Patent Disclosure No. SRS-14-021 (patent being filed).

Post-Doctoral Researchers

1. Patrick A. Ward
2. Martin Sulic

Solid State NMR evaluation of Carbon Dots (CD) and fluidic $LiBH_4$ on C_{60}

Project Team: Joseph Teprovich, Patrick Ward, Aaron Washington, Ragaiy Zidan
Subcontractor: California Institute of Technology (Prof. Son-Jong Hwang)
Thrust Area: Clean Energy
Project Type: Exploratory
Project Start Date: May 2016
Project End Date: September 2016

Multi-nuclear solid state NMR analysis will be performed on two different sample types. This information will then be used to pursue additional funding in energy and storage applications including hydrogen storage, solar cells, and solid ionic conductors for batteries. There is a need to understand the type and quantity of oxygen defects (hydroxyl, carboxyl, epoxy, etc.) in a carbon dot (CD) system to determine what type of defects lead to the observed photoluminescent properties. This information can then be utilized to fine tune and control the absorption and emission properties of these materials for various applications (i.e. photovoltaics). NMR will also be able to determine if the presence of C_{60} evokes the formation of fluidic-like BH_4^- anions in the solid matrix. This information could allow for the development of novel ionic conductors for battery applications as well as for reversible hydrogen storage at temperatures applicable for vehicular storage.

FY2016 OBJECTIVES

- **Synthesize carbon dots (CD) with various degrees of oxygen defect**
- **Perform multinuclear NMR analysis to examine oxygen defects in CD**
- **Determine if C_{60} can induce fluidic-like motion in MBH_4-C_{60} composites**

INTRODUCTION

The EERE program within DOE is very interested in material development that will enable more energy efficient and conversion devices. This includes the development of novel ionic conductors for solid state batteries (Vehicle Technologies), hydrogen storage (Fuel Cell Technologies Office), and photovoltaics (Solar Energy Technologies Office). Composite materials of metal hydrides and carbon nanomaterials have many of properties needed for the next generation of energy storage and conversion devices. However, these composite materials have a large amorphous content which makes there analysis difficult by common spectroscopic techniques. Multinuclear NMR provides an opportunity to understand these interactions and potentially design new materials based on this information.

APPROACH

CDs have been prepared at SRNL by exposing $LiBH_4$-C_{60} (70-30 wt%), annealed at 300°C, to air and allowing the material to passivate. The air passivation treatment that resulted in the fluorescence is not well understood. Structural changes during the passivation process were followed by multinuclear NMR measurements on samples with various exposure times. All NMR spectra were obtained using a Bruker DSX-500 spectrometer and a Bruker 4 mm magic angle spinning (MAS) probe at Caltech.

All samples were handled inside of an Ar-filled glovebox. Samples that were received in powder form were loaded into 4 mm ZrO_2 rotors and capped with air-tight kel-F caps. Note that the mother sample, a physical mixture of $LiBH_4$ and C_{60}, that was highly dielectric to prevent from probe tuning, was diluted by grinding with quartz powder (1:1 in volume) before loading to a sample rotor. Dry N_2 gas was used for spinning samples for MAS NMR experiments. The operating frequencies at a 11.7 T magnet are 500.23, 125.4, 160.5, 190.5 MHz for ^1H, ^{13}C, ^{11}B, ^7Li nuclei, respectively. MAS NMR signals were recorded after single pulse (4 μs-π/2 pulse for ^1H and ^{13}C or 0.5 μs-π/12 for ^{11}B and ^7Li) under samples spinning at 14 kHz. ^{13}C cross polarization (CP) MAS NMR was recorded at sample spinning rate of 8 kHz and with strong ^1H decoupling pulse. NMR spectra are reported in part per million (ppm) with reference to external standards: TMS for ^1H and ^{13}C, $BF_3(OEt)_2$ for ^{11}B, and 1 M LiCl aqueous solution for ^7Li nucleus. Probe tuning varies wildly because of the presence of C_{60} that is highly dielectric. This prohibits quantitative evaluation of NMR signals among different samples. Therefore, normalized NMR spectra were not used in this presentation, but vertical scale adjustments were made to display spectra in the similar height. Do note that, however, a consistent scale was used for 3 samples (exposed to air for 5 min, 30 min, and 60 min) for changes as a function of the exposure time.

RESULTS / DISCUSSION

Task 1: NMR studies of Fluorescent Carbon Dots (CDs)

Except the water washed sample, ^1H, ^{11}B, and ^7Li NMR spectra of the rest of the samples shown in Fig. 1 are very similar to NMR signature of bulk $LiBH_4$ in major part. This observation supports that only a small part of $LiBH_4$ is reacting with C_{60}. -40 ppm resonances in ^{11}B NMR represent BH_4^- groups that are dominating in most of samples even after exposure to air. After washing with water, BH_4^- is no longer present and the majority of boron atoms are replaced by BO_4 units as 0 ppm peak appears.

To the contrary, there is no sign of the presence of neat C_{60} that is supposed to render a sharp signal at 143 ppm as we have reported in the past[1]. This indicates that majority of C_{60} reacted with $LiBH_4$. ^{13}C CPMAS NMR of exposed three samples shows broad resonances both at the aromatic region (120-150 ppm) and the aliphatic region (10-80 ppm). For the as-mixed sample, it was not possible to get good signal reception due to the small amount used. There appear to be two broad peaks around the aromatic and the aliphatic regions while their presence cannot be convincingly clarified.

In Figure 2, ^{11}B and ^{13}C NMR spectra of passivated samples are plotted again with those obtained for the $^{13}C_{60}$-$LiBH_4$ sample. Strong ^{13}C signal from the $^{13}C_{60}$-$LiBH_4$ composite is useful in revealing the hydrogenation reaction of C_{60} by $LiBH_4$ for the as-prepared sample. Note that our previous analysis for the $^{13}C_{60}$-$LiBH_4$ system showed about 1/5 of C_{60} was reduced to CH groups (12 carbons). Our current ^{13}C spectrum would not allow us to estimate what portion of carbons were reduced in the as prepared and not exposed CD sample. ^{11}B MAS NMR is rather more effective in showing the aftermath of the mixing process (vide supra). It is only possible to speculate that a composite [$Li_xH_xC_{60}$-BH_{4-x}] might have formed in the as-prepared sample.

Interestingly, ^{13}C CPMAS NMR signal became observed after passivation for 5 min, suggesting that some change in the oxidation state of [$Li_xH_xC_{60}$-BH_{4-x}] took place. This could involve an electron transfer to transform NMR invisible state, let's say paramagnetic, to NMR visible state (diamagnetic). ^{13}C CPMAS spectra of passivated sample are similarly composed of aromatic and aliphatic carbons as was in the case of $^{13}C_{60}$-$LiBH_4$ sample.

From the comparison of ^{13}C resonances shown in Figure 2, however, the detailed change in C_{60} is slightly different for both as prepared samples. For example, the strongest resonance at 50 ppm from $^{13}C_{60}$-$LiBH_4$ is not present for the CDs samples. The location of the aromatic peaks is further up-filed for the CDs samples. For the $^{13}C_{60}$-$LiBH_4$ sample, the conversion of BH_4^- units is revealed as the -20 ppm resonance in ^{11}B NMR that is newly appeared as relatively sharp peak. From ^{11}B NMR signal integration, we have estimated the -20 ppm resonance to be about 4 % of total BH_4 used. BO_4 and BO_3 species were also present in about 3 mol% level for the sample.

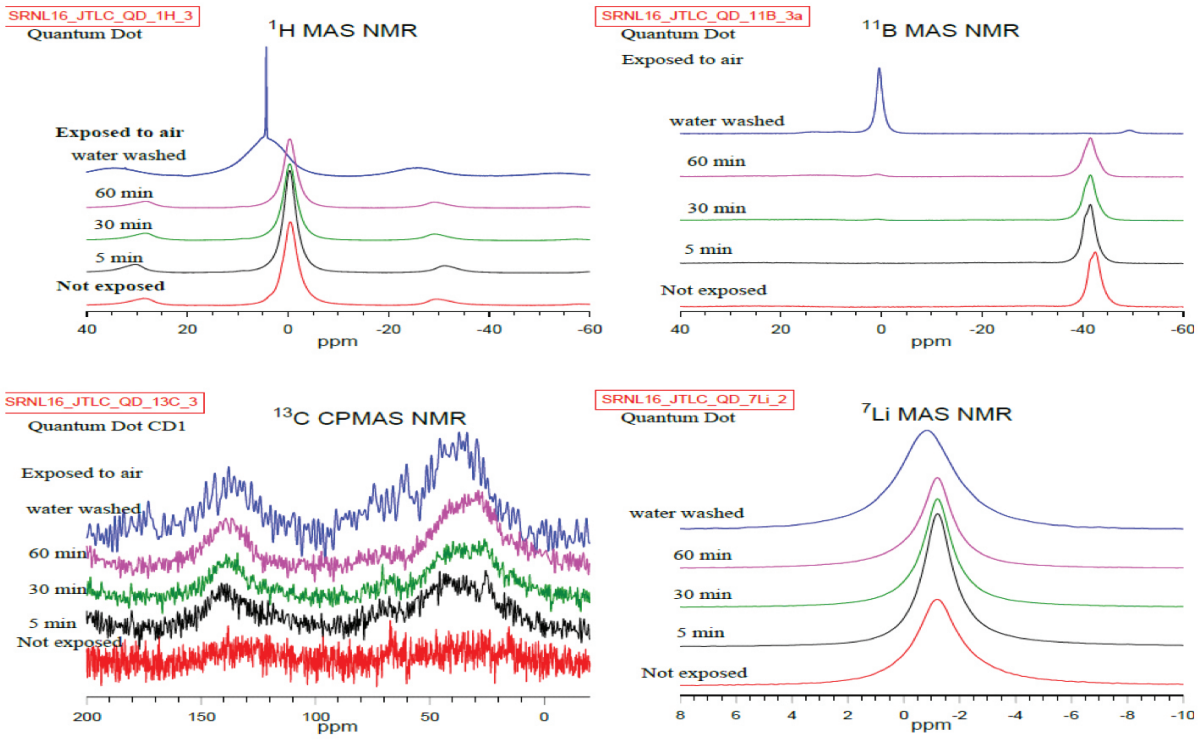

Figure 1. Multi-nuclear NMR spectra from 5 different samples. Note that NMR spectra were displayed at the similar vertical height. When normalized scale is applied, the washed samples shows about 1/5 of magnitude of the unwashed air exposed samples

NMR spectra of CDs shown in Figure 2 show noticeable differences from those of $^{13}C_{60}$-$LiBH_4$ composite. The unexposed sample is characteristic with broad ^{11}B MAS NMR resonances at 20 ppm and -30 ppm (marked with arrows in Figure 2) instead of the relatively sharp -20 ppm. The broad components accounts about 30% of total boron species. More accurate quantitative ratio will be presented after peak fitting of spectra. At this moment, the molecular structure responsible for the broad resonances are not yet characterized. There is no sign of BO_x species formed before air exposure. Air exposure produced BO_x species (20-0 ppm range) as the 30 min sample clearly shows ^{11}B signal for oxide species. As expected, we observe most production of BO_x from the 60 min sample. At the same time, BH_4 resonance at -40 ppm was the smallest for the 60 min sample while the broad peak at 20 ppm did not change noticeably. The experimental observation supports that oxidation consumed BH_4^- to produce BO_x species. When both ^{11}B and ^{13}C CPMAS NMR were considered, there is no strong correlation between the BO_x species formed and the change on ^{13}C resonances although the aliphatic peaks for the 60 min sample looks slightly stronger. If the passivation strengthen the illumination power of quantum dots, we can conclude that the amount of BO_x species matters while the change on structure of C_{60} may stop at air exposure time of 5 min.

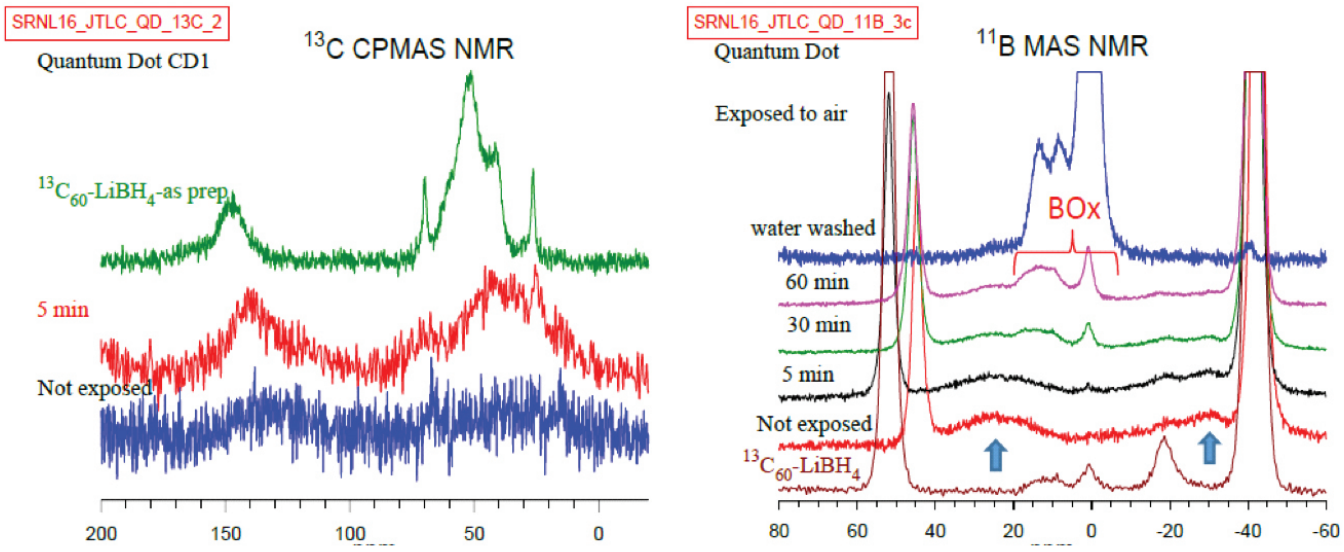

Figure 2 ^{13}C CPMAS and ^{7}Li MAS NMR spectra of $LiBH_4$-C_{60} mixtures after various treatments. The $^{13}C_{60}$-$LiBH_4$ has not been exposed to air, serving as a reference for ^{11}B NMR of $LiBH_4$ reacting with $C_{60.}$ ^{11}B NMR spectra are displayed to unveil the formation of species after mixing and passivation as shown with broad lines at ~ 20 ppm and -20 and -30 ppm

There is no clear peak resolution in ^{7}Li MAS NMR to reflect the state of [$Li_xH_xC_{60}$-BH_{4-x}]. There was no far upfield peak observed as an indication for Li@C_{60}. When compared for as prepared samples, seen in ^{7}Li NMR is the presence of broader component in the CD sample. The dispersive component is expected to be associated with Li motion and/or dispersive structure (more amorphous) nature of [$Li_xH_xC_{60}$-BH_{4-x}]. Passivation treatment did not produce any noticeable change as shown in Figure 1. ^{6}Li NMR or variable temperature NMR may be more informative.

^{11}B NMR analysis of the washed sample: 0 ppm of ^{11}B NMR signal shown in Figure 1 for the washed sample is consistent with BO_4 unit. Spinning sideband of ^{11}B NMR was further used to estimate the quadrupole interaction of the ^{11}B (I=3/2) nuclei. The parameters are consistent with BO_4 in tetrahedral geometry. B_2O_3 like oxide was found as a minor component with its concentration is less than 10 %. For the washed sample, ^{1}H NMR shows sharp peak at 4.3 ppm, which is due to the presence of H_2 gas that might be trapped inside of $C_{60.}$ The major ^{1}H signal is the broad resonance at ~ 2 ppm, which is due to CH protons.

Task 2: Systematic studies of $LiBH_4$:C_{60} mixtures and annealed samples with variable composition

Physical mixtures of $LiBH_4$:C_{60} were prepared with three different mixing ratios, followed by annealing at 300 °C. Multinuclear solid state NMR measurements were performed in the same way described in Task I. ^{1}H MAS NMR spectra are shown below for 6 samples of which spectra were divided into two groups, as-prep and annealed, and further distinguished with color coding for variation of $LiBH_4$:C_{60} ratio. ^{1}H signal of the as-prep samples is composed of sharp and broad components. Broad resonance at -0.5 ppm is representing BH_x species of which identity will be better addressed from ^{11}B NMR. The sharp component is due to the formation of CH_4 as further confirmed by ^{13}C NMR. CH_4 molecules are in gas phase as highly averaged ^{1}H line indicates although there is not enough information about how the molecule stays with C_{60} molecules. The JT-LC1 (30:70) sample shows the strongest CH_4 signal and the strength decreases progressively as the C_{60} content decreases. The intensities of broad peak grow as the $LiBH_4$ concentration increases.

Figure 3. ^{1}H NMR spectra of as-pre and annealed $LiBH_4$-C_{60} composite (All three as-prep samples show sharp peaks at ~ 0 ppm as shown more eminently in the center-band only plot ***(right side);*** Spinning side bands are marked by and samples were spun at 14 kHz. reacting with C_{60}; ^{11}B NMR spectra are displayed to unveil the formation of species after mixing and passivation as shown with broad lines at ~ 20 ppm and -20 and -30 ppm)

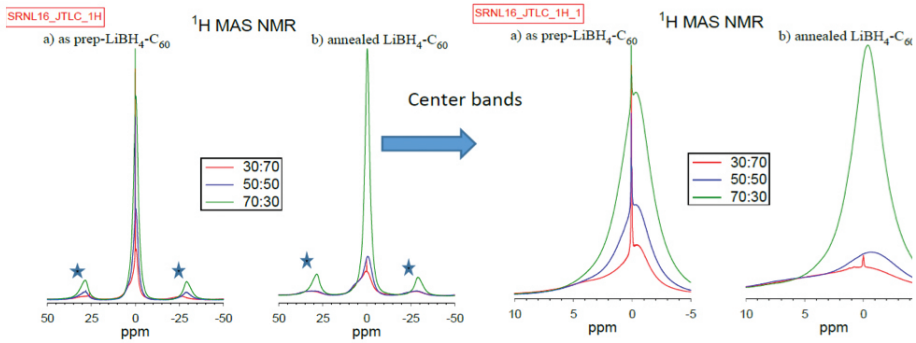

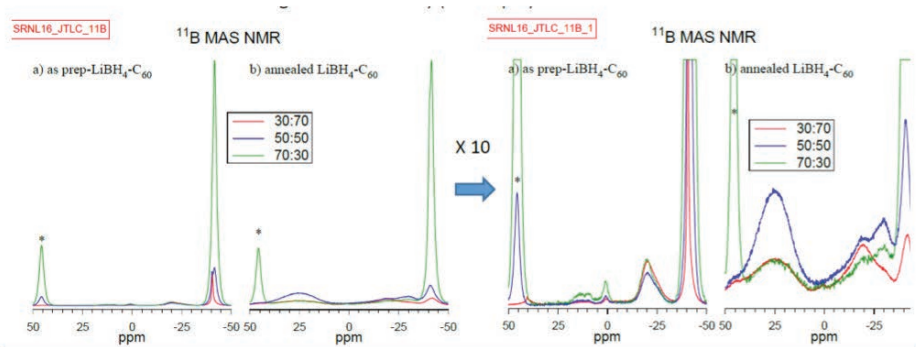

Figure 4. MAS NMR spectra of as-prep and annealed samples. The same plot was scaled up by 10 times in the right side in order to show the broad components

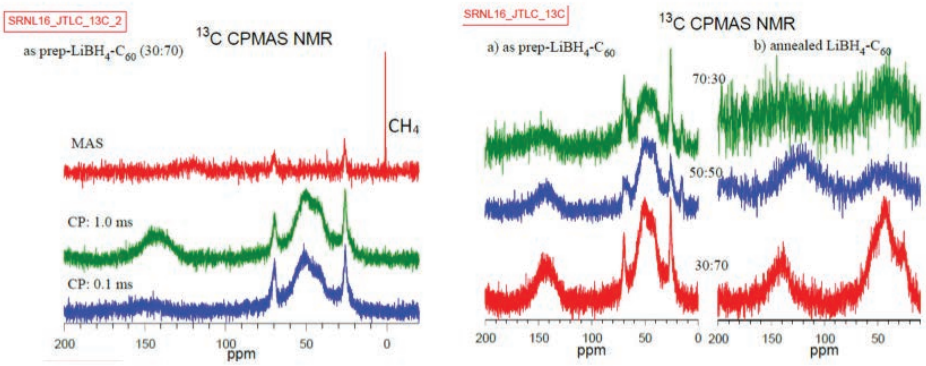

Figure 5. ^{13}C NMR from JT_LC1_JTLC3 series. ^{13}C CPMAS NMR was recorded with contact time of 1.0 ms unless otherwise noted; Sample was spun at 8 kHz. As-prep samples show two sharp peak for solvent THF

Most of the boron species produced from these composites appear in chemical shifts ranging from - 50 to 50 ppm. Intact $LiBH_4$ or BH_4 units interacting neighbor molecules are seen at -41 ppm. Resonances at the downfield then obviously represent boron atoms in chemically modified forms such as $B_xH_yC_z$ or $B_xH_yO_z$, etc. Peak fitting is now in progress to estimate the species in a quantitative manner. As briefly mentioned above, resonance at -20 ~ -25 ppm peak is characteristic for the as-prep sample while the residual BH_4 units are seen at ~-40 ppm. ^{11}B NMR clearly shows that $LiBH_4$ in the bulk crystalline phase in the first two samples (30:70 and 50:50). The JT-LC3 (70:30) only show strong -40 ppm peak for the $LiBH_4$ in the bulk phase. After the annealing treatment, a broad resonance at 25 ppm appears as the one of the major species. The species gains its maximum partition for the JT-LC2 sample (50:50). Interestingly, the amount decreases noticeably when more $LiBH_4$ molecules are added, i.e. 70:30 sample. The probable candidate for the resonance require boron atoms interacting with the $H_xLi_yC_{60}$ fragments with possible B-C bond formation, and in trigonal geometry. Boron atoms in tetrahedral geometry appear at the negative chemical shifts[2]. For example, $LiB(CH_3)_4$ gives a resonance at ~-20 ppm in the literature. On the other hand, trimethylboron, $(CH_3)_3B$ yields a resonance at 86 ppm. There are two other peaks at -20 and -30 ppm that are associated with boron atoms in BH_{2-} or BH_{3-} moieties.

From ^{11}B NMR results, we have learned that the 50:50 mixture induced the highest amount of $LiBH_4$ that underwent transformation. When $LiBH_4$ concentration is raised, the majority of $LiBH_4$ remain in the bulk phase as seen for the 70:30 sample. ^{13}C MAS and CPMAS NMR spectra from the series of samples are presented in Figure 5. For all as prep samples, the formation of CH_4 was observed as evidenced by 0 ppm peak and its ^1H J coupling pattern. As expected, we see strong ^{13}C CPMAS signal at the aliphatic region (30-70 ppm) for all samples and they are the consequence of reduction of part of C_{60} carbons by BH_4 after the mixing. Some aromatic carbons around the reduced carbons are also detected in ^{13}C CPMAS spectra. Both aliphatic and aromatic carbons appeared to be affected by annealing treatment as their peak shapes changed, again the change was most intense for the 50:50 sample. As for the CD sample, the annealed sample of 70:30 mixture lost resolution and generated dispersive resonances with no specific features for both aromatic and aliphatic carbons.

FY2016 OBJECTIVES

A series of carbon dots were synthesized with various exposure times to the atmosphere including immersion in water

Multinuclear NMR experiments identified unique species formed upon air exposure leading the formation of carbon dots

NMR also showed the formation of CH_4 which is unexpected and possibly physisorbed on the surface of C_{60}

FUTURE DIRECTIONS

- Pursue additional funding through the Material Science and Engineering program of the Office of Science - Basic Energy Science (BES)
- Examine other possible energy storage and conversion devices that can be based on this technology

References

1. **Nano Letters** 2012, 12, 582.
2. **NMR Basic Principles and Progress,** 1991; Vol. 23.

Acronyms

CD	Carbon Dot
NMR	Nuclear Magnetic Resonance

Post-Doctoral Researchers

1. Patrick Ward